EXPERIMENTAL INVESTIGATIONS ON MAGNETIC ABRASIVE FINISHING PROCESS

A THESIS
SUBMITTED IN FULFILMENT OF THE REQUIREMENT FOR
THE AWARD OF THE DEGREE

OF

DOCTOR OF PHILOSOPHY

IN

MECHANICAL ENGINEERING

BY

SHADAB AHMAD

(Roll no. 2K16/PhD/ME/03)

Under the supervision of

Dr. RANGANATH M. SINGARI
(Professor)

Dr. R. S. MISHRA
(Professor)

DEPARTMENT OF MECHANICAL ENGINEERING
DELHI TECHNOLOGICAL UNIVERSITY
(Formerly Delhi College of Engineering)
Bawana Road, Delhi - 110042, India

MAY 2021

CERTIFICATE

This is to certify that the work embodied in this thesis entitled, **"Experimental Investigations on Magnetic Abrasive Finishing Process"** being submitted by **Shadab Ahmad (Roll No-2K16/PhD/ME/03)** for the award of Doctor of Philosophy (Ph.D.) Degree in Mechanical Engineering at Delhi Technological University, Delhi is an authentic work carried out by him under our guidance and supervision.

It is further certified that the work is based on original research and the matter embodied in this thesis has not been submitted to any other university/institute for award of any degree to the best of our knowledge and belief.

Prof. Ranganath M. Singari
Professor,
Department of Mechanical
Engineering (DTU, Delhi)
Head, Dept. of Design (DTU, Delhi)

Prof. R. S. Mishra
Professor, Dept. of Mechanical
Engineering (DTU, Delhi)
Dean, Outreach & Extension Activities
(DTU, Delhi)

ACKNOWLEDGEMENTS

This thesis has been written during my position as a doctoral candidate at Delhi Technological University, Delhi. First of all, I am thankful to the Almighty, most beneficial and merciful who blessed me with strength and patience to acquire knowledge and learning.

I would express my deeply-felt gratitude to my PhD supervisors, **Prof Ranganath M. Singari** and **Prof R. S. Mishra** for their valuable guidance to carry out this research work. I thank them for the scholarly inputs which I received throughout the research work. I sincerely treasure their precious remarks about academic writing, research and future perspectives, and I am honoured to acknowledge their mentoring along the way. I would also like to thank the unknown reviewers of our research papers for their valuable suggestions and comments which gave me insight into the areas which we never thought of venturing into.

I would like to express my sincere gratitude to the members of the dissertation committee. I am extremely grateful for the member's willingness to take part in my doctoral examination, as well as for the precious comments and insightful questions they provide on the present research work. I also wish to express my gratefulness to "**Department of Mechanical Engineering, Delhi Technological University, Delhi"** for facilitating the progress of my research work by providing the necessary facilities in the department. I would also thank the **"Council of Scientific and Industrial Research (CSIR) - Government of India,"** for financial support in the form of JRF and SRF.

My heartfelt appreciation also extends to **Prof. G. C. Maheshwari (DTU, Delhi), Prof. Nand Kumar (DTU, Delhi), Prof. D. K. Singh (MMMUT, Gorakhpur), Dr. Harish Kumar (NIT, Delhi)** and **Dr. Swati Gangwar (NSUT, Delhi)**, for their time-to-time guidance and moral support during my research study. Also, for encouraging my passion for learning, and whose truly inspiring example turned me towards teaching and academics. I am extremely grateful for their wisdom in pushing me further than I thought I could go.

PhD is not a lonely task. I would express my deep appreciation to my Ph.D. colleagues Dr. Sumit Chaudhary, Mr. M. J. Akhtar, Mr. M.G. Mustafa, Mr. H. Sadique, Mr. Pradeep Mouria for helpful discussions and priceless moral support which helped me in accomplishing my work. I am also thankful to Mr. Sunil (Senior Mechanic) for helping me in the experimentation part. It is a pleasure to convey my gratitude to all the good people who came across, whose contributions in various ways helped me in my research and they deserve special thanks.

Afterwards, I am thankful to my parents for their uncountable support and faith in me. I would like to express my deep sense of gratitude to my sisters, brother-in-law and friends for their invaluable encouragement, suggestions, support, care and countless calls. I especially thank all my family and friends for their faith, encouragement, understating, and unfailing support.

Shadab Ahmad

ABSTRACT

Magnetic abrasive finishing is a prevalent advanced method which by applying gentle forces using flexible magnetic abrasives for removing surface irregularities, provides a micro/nano range of defect-free surface finish. During magnetic abrasive finishing, magnetic forces allow the flexible magnetic abrasive particles to shear off the material from the surface in the form of microchips. In industries, MAF is highly recommended where zero or negligible post-process surface defects are an obligatory requirement. During the finishing of a material having high hardness value such as titanium alloy, nimonic alloy, and ceramics, etc., it is necessary to choose a proper magnetic abrasive considering the rate of improvement required in the surface finishing. Owing to the exceptional mechanical properties of Ti-6Al-4V, it is widely utilized in numerous critical mechanical parts for the uncompromised factor of safety. However, performing machining operations on this alloy in close tolerance is a challenging task. Moreover, establishing a process for its efficient finishing has become the interest of researchers. In the same context, process optimisation is essential for making it commercially viable. This research work mainly presents three phases of study considering the gaps found from the extensive literature survey.

In the first phase a new magnetic abrasive has been developed, which is suitable for finishing of Ti-6Al-4 V. The sintering method was used to develop the magnetic abrasive, and hence the developed magnetic abrasive has been named as sintered magnetic abrasive (SMA). A mixture of abrasive powder of aluminium oxide and silicon oxide (Al_2O_3-SiO_2) with carbonyl iron particles (ferromagnetic material) has been taken as components of sintered magnetic abrasive. The authors have studied the morphology of the sintered magnetic abrasive by scanning electron microscopy (SEM), energy dispersive spectrum (EDS), and X-ray diffraction technique. The findings reveal that the abrasives were uniformly and tightly rooted in the carbonyl iron particles. Also, magnetic abrasive finishing roughness studies on the Ti-6Al-4 V workpiece were carried to evaluate the performance of SMA. Change in the surface roughness from Ra = 1.14 μm to Ra = 0.85 μm were observed and atomic force microscopy (AFM) of the finished surface confirms an excellent finishing effect by the developed sintered magnetic abrasive on Ti-6Al-4 V during magnetic abrasive finishing.

The second phase of study comprises a novel a robust modelling and optimisation tool i.e., artificial neural network and genetic algorithm (ANN-GA) that is applied to scrutinise and improve the performance of the magnetic abrasive finishing of stainless steel SS302 which focuses to find

its applicability on MAF process. In addition, the results from ANN-GA modelling and optimisation have been compared with conclusions drawn from conventionally used Taguchi-ANOVA analysis. An L27 non-orthogonal array design has been opted for as per machining set-up restriction. Abrasive size, voltage, machining gap, and rotational speed were the design variables considered in the present research work. It was found that the parametric design used in this study provides a straightforward, methodical, and proficient method of modelling and optimisation of change of surface roughness or finishing behaviour during theme process. Modelling and optimisation done with ANN-GA show a maximum value of change of surface roughness equal to 0.256 μm, which is 7% better than the result obtained from Taguchi-ANOVA analysis.

In the third phase of this research study, the magnetic abrasive finishing process (MAF) has been studied using the ANN-GA approach, where ANN has been used for modelling of input–output relations, and GA has been used to optimize the MAF process. The experiments were conducted on a pulsating DC sourced MAF set-up, and SiC-based loosely bonded magnetic abrasive media was used for material removal. During experimentation, the current, machining gap, speed of rotation, abrasive composition, and finishing time were taken as input parameters being arranged in an array of L16orthogonal. In contrast, output parameters were changed in surface roughness, change in the microhardness, and change in the modulus of elastic indentation. ANN-GA approach provides a set of optimal solutions for obtaining suitable output values. Furthermore, loosely bound SiC-based magnetic abrasive media and its composition is found to be a very critical factor for the performance of the finishing quality on Ti-6Al-4V.

CONTENTS

NOMENCLATURE

ε_0	permittivity of the vacuum (F/m)
ε	permittivity of the medium (F/m)
μ_0	relative magnetic permeability in vacuum (Wb/(A-m))
μ_{FP}	relative magnetic permeability of ferromagnetic particle (Wb/(A-m))
ρ	charge density (A/m^2)
H_s	source magnetic field intensity (T)
H	magnetic field strength in the working zone (A/m)
J	electric current density (A/m^2)
E	electric field intensity (V/m)
B	magnetic flux density (T)
B_a	magnetic flux density in air gap (T)
B_w	magnetic flux density in work piece (T)
B_{avg}	average magnetic field density (T)
P	magnetic pressure (Pa)
n	number of turns in coil
φ	magnetic scalar potential (A)
α	volume ratio of iron in magnetic and abrasive mixture
R_a	Average Surface Roughness
ΔR_a	Change in surface roughness
ΔHV	change in the Microhardness
ΔEIT	change in the Modulus of Elastic Indentation
S/N	Signal to noise ratio

ABBREVIATION

SR	Surface Roughness
MRR	Material Removal Rate
DDMAF	Double Disk Magnetic Abrasive Finishing
RSM	Response Surface Methodology
ANFIS	Adaptive Neuro-Fuzzy Inference System
MAP	Magnetic Abrasive Polishing
UAMAP	Ultrasonic Assisted Magnetic Abrasive Polishing
MFGA	Magnetic Finishing with Gel Abrasives
MA	Magnetic Abrasives
SMA	Sintered Magnetic Abrasives
MAF	Magnetic abrasive Finishing
ANOVA	analysis of variance
OA	Orthogonal Array
DC	Direct Current
FMAB	Flexible Magnetic Abrasive Brush
ANN	Artificial Neural Network
GA	Genetic Algorithm
HV	Vickers Hardness
EIT	Modulus of Elastic Indentation
UMAPs	Unbonded Magnetic Abrasive Particles

LIST OF FIGURES

LIST OF TABLES

Chapter 1

INTRODUCTION

In this chapter, the discussion converges on the importance of superfinishing in modern industry for quality products, after understanding the traditional and non-traditional machining processes and their classifications. The specifics of the traditional Magnetic Abrasive Finishing process, as well as its advantages, disadvantages, and applications, are discussed. Later on, the MAF working, classifications, elements, tooling method, and abrasive types were elaborated.

1.1 An Overview

A part made by any of the fundamental manufacturing procedures (e.g., casting, forging and machining etc.) is usually finished as a final process [1]. The finishing process will cost approximately 10% to 15% additionally of the overall manufacturing cost. Furthermore, choosing the accurate machining conditions is crucial for controlling surface and sub-surface defects like micro-macro cracks, micro structural changes, heat affected zone, and surface hardening. For certain parts, the final surface quality is critical, such as the texture that allows lubricating oil to be retained, which can be achieved using the EDM method [2]. The fatigue strength of the component decreases after such machining operations, such as electrochemical machining and chemical machining. The aesthetic appearance of a machined surface may carry a lot of weight in some cases. As a result, before placing a component in an assembly or, sub-assembly it is imperative to enhance the surface characteristics to meet the part's functional requirements as well as safety and aesthetic requirements. As a result, rather than focusing solely on the planned dimensions and tolerances, it's often important to understand different aspects of a finished surface [3].

The strategies for improving surface characteristics can be divided into the following categories:

a. Techniques for refining the surface finish (lowering the value of surface roughness).
b. Methods for deburring.
c. Methods for enhancing bulk properties (heat treatment, shot peening, etc.).
d. Strategies for improving corrosion resistance and aesthetics (painting, electroplating, etc.).

There are two types of techniques for improving the finish on a surface: Traditional finishing methods (e.g., Grinding, Lapping, Honing or micro-Honing), and Advanced finishing processes e.g., Magnetic Float Polishing, Magnetorheological Finishing, Abrasive Flow Machining, Magnetorheological Abrasive Flow Finishing, Elastic Emission Machining, and Chemo Mechanical Polishing [4].

The shape, profile and dimensions of a part that can be finished by each of the conventional processes are severely limited. Honing, for instance, is best for cylindrical surfaces, while lapping is best for flat surfaces. But these methods often lack control of the forces that act on the workpiece during the finishing operation, resulting in a low degree of control over the finish. Unless the finishing conditions are designed appropriately and managed precisely, ample heat generation, especially during grinding, results in a variety of defects (thermal residual stresses, micro-cracks, etc.) [5], [6].

Traditional methods are incapable of finishing complex formed workpieces, three-dimensional parts, finishing of microchannels, internal finishing of complex and narrow geometry e.g., cooling holes in turbine blades with diameters less than 2 mm. As a result, a deterministic type of finishing processes are needed, which can control the forces externally that is acting on the workpieces, can finish complex formed workpieces, also capable of delivering a better surface finish than conventional finishing processes [7], [8]. As a result of these expectations, the second group of finishing processes, i.e., advanced finishing processes (AFPs) developed.

The abrasives a tool medium whose rheological properties can be regulated externally by a magnetic field in some of these AFPs. magnetic float polishing, magnetorheological finishing process, and magnetorheological abrasive flow finishing are some of the finishing processes accessible [9]. The magnetic field controls the process but as the magnetic field changes the rheological properties may or may not if desired as a rheological medium can be customized according to the purpose. Abrasive flow machining, chemo-mechanical polishing and elastic emission machining are all-important finishing processes that do not rely on magnetic fields to power the operation.

However, conventional finishing methods are still used as mainstream finishing operations on the shop floor. As a result, it has been suggested that recent advances be used to improve the capabilities and overcome some of the innate complications of these conventional finishing methods. For example, Dressing and de-clogging a grinding wheel, are necessary steps in the

grinding method rather than being inefficient and costly. ELID (electrolytic in-process dressing) is a low-cost solution towards this issue [10]. As a result, hybridization of these conventional finishing methods has been undertaken to advance the basic capabilities and this step also broadens the variety of applications for these processes. Electrochemical grinding (ECG) and electro-discharge abrasive grinding are two of the hybridized methods (EDAG)[11]–[13].

In the actual environment, Surface Roughness is the main key to affect the performance of the fabricated component, so inevitably these engineering industries are compelling to develop new and advanced methods of manufacturing [14], [15]. For instance, in the integrated circuit manufacturing industry, there is a high demand for silicon wafer planarization to meet stringent non-uniformity and surface polishing specifications [16].

1. As we know that the surface roughness value always has a consequential effect on functional properties of any component such as frictional power losses, wear and tear and its fatigue life. As the expeditious advancement in various industries (optical, electronic, medical equipment, atomic energy, military components, aerospace etc.) requires significantly high quality and integrity of precision in surface finish.
2. Because of the advancement of the materials field, the latest materials with properties high toughness, high roughness, fragility, and high strength to weight ratio are now become worthy of attention in present applications in various industries (as mentioned above). These significant and advanced properties of such materials are making them more demandable for diverse applications. Despite that, the processing of these materials by using conventional processes is now a great challenge for manufacturing industries.
3. Surface finishing of material having advanced properties. Conventional process like lapping, honing and grinding creates surface cracks, micro/nano burrs, residual stress, subsurface damages, increases susceptibility to corrosion because of high surface stress, loss of magnetic properties of ferromagnetic materials, high grinding temperatures may add a thin martensitic layer.
4. The conventional process also, cannot be used for fragile materials like fiber cement sheets, glass, etc. Acquiring the nano-level surface finish value through a conventional process is uneconomical and very difficult. For obtaining such finishing of these materials there are some unconventional finishing methods like magnetic abrasive finishing (MAF), magnetic float

polishing (MFP), magnetorheological finishing (MRF), chemo-mechanical polishing (CMP) and abrasive flow machining (AFM).

1.2 Classification of material removal processes

Material removal or machining techniques are divided into two categories.

a. Traditional machining and,
b. Non-traditional machining processes.

These methods are further subdivided into different divisions depending on the method of machining operation and the applications they are used for. The general description of substance removal processes is seen in Figure 1.1.

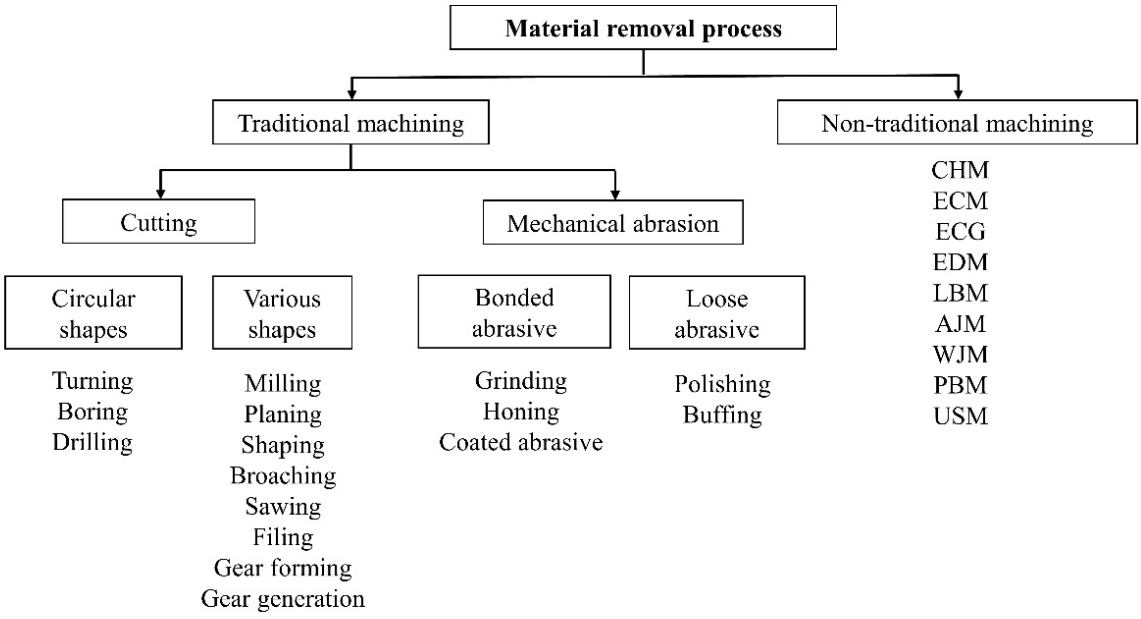

Figure 1.1 Classification of material removal processes [17].

1.3 Need of advanced machining and finishing processes

Numerous components produced by conventional method, require additional post-processing before they are final ready for functional use. Parts must be interchangeable in many engineering applications in order to work correctly and consistently over their intended service lives; therefore, dimensional accuracy and surface profiles of the components and parts must be controlled during manufacture. The machining process requires removing a certain amount of material from the

workpiece in order to achieve a precise geometry with a high level of precision and surface uniformity. The need for high dimensional accuracy, improved surface finish, and a high production rate of produced components drives researchers all over the world to dig out the solution to face challenges of conventional manufacturing. Advanced, non-traditional, or unconventional manufacturing methods developed in such situations. They offer an improved surface finish, tighter tolerances, lower tool wear, and a higher metal removal rate. These unusual methods can machine those materials which are hard and challenging to machine, such as carbide materials, glasses, and other high temperature-resistant materials. [18].

Manufacturing of precise parts is still a matter of concern due to its most essential, labor-intensive, and inconvenient existence. High precision finishing methods are critical in the age of nanotechnology and are a requirement of today's manufacturing environment. Manufacturers all over the world were feeling the pressure to increase manufacturing precision in order to boost part interchangeability, efficiency, and fatigue life.

Advanced machining is useful especially in the cases where there's a dire need to create parts with small features, tight tolerances, complex geometries, and challenging materials or finishes. Some common hurdles/drawbacks/caveats faced by engineers in a typical manufacturing scenario, along with how they may be overcome by advanced machining, are given below -

In parts with a small tolerance for the entrance hole, factors like the tool length, tool angle, and thermal fluctuations during manufacturing can make it significantly harder to maintain the desired tolerance. Techniques like Advanced microfabrication and high-speed rotary forming can create minuscule parts to their exact specifications, while the correct set of tools and jigs may be used to hold parts in place for a smooth surface finish.

Advanced machining tools like end mills, with minimum diameters down to 0.01 mm, can efficiently and consistently perform milling, hole drilling and S0.5 (0.5-mm diameter) thread cutting—even for hole entrance tolerances of ±5 μm or less. These tools can also meet a thickness tolerance of 0.15 ± 0.01 mm and maintain a surface roughness of R_a 0.1 μm. These specifications are challenging and difficult for most manufacturers to emulate.

Though a traditional press may be considered as a reliable process for the manufacturing of miniature steel parts with thin walls, a lot of heat is generated in this process which can create residual stresses in the workpiece. This achieves a precise wall thickness, without distortion, a challenging task in terms of the additional time, effort and money required. Despite these caveats,

one may be tempted to use a traditional press, but the machining alternative offers many advantages in terms of the precision and cost involved.

For a round, cylindrical part like a stainless-steel motor housing, the typical wall thickness requirement is 0.2 ± 0.05 mm. This requirement is easily achievable in the scope of advanced machining - which can manufacture parts with walls as thin as 0.035 mm while maintaining precise geometric tolerances for roundness and concentricity.

Top-tier applications often demand materials like stainless steel be contorted into complex shapes while maintaining certain standards of surface roughness. These parts require their surfaces to be contoured in multiple axes and hence require the latest machining technology. For instance, stainless steel valves used in fuel cell vehicles demand scratch- and burr-free internal passages. Such tasks are ideal for the kind of precision and quality finishes expected of advanced machining.

Advanced machining, for example, may be used to create miniature parts with external diameters less than Ø160 to strict geometric tolerances. In addition, it has the ability to provide concentric groove machining and four-axis grinding, plus a wide array of surface finishes like a seal- and mirror-surface finishes.

Machining titanium and superalloys like Hastelloy is challenging for traditional part-makers. In addition to the difficulty in machining, as they are often used in critical applications, impeccable accuracy and quality are often demanded by the equipment manufacturers.

For the machining of hard-to-cut materials e.g., nimonic alloys, titanium and carbides etc., there is a need for companies to collaborate with specialist machinists that use high-performance machine tools and have a thorough knowledge of machine tool technology and metallurgy. They understand the latest chucking and cooling technologies, cutting speeds and cutting tools, and have the dexterity to assemble several parts and machine them to the precise surface roughness demanded. Companies like Aomi Precision have developed extensive databases of the processing requirements and conditions required for the machining of hard-to-cut materials. This has helped them to expedite the process and deliver the most optimal machining method for all kinds of parts.

When faced with a challenging part design, it is easy for designers to revert to conventional production methods. Familiarity with traditional methods can be a hurdle for many designers to move adopt advanced machining methods. In addition, the production of a small batch of such specialized products may render it difficult for designers to justify the additional setup costs involved. But for a number of small, intricate and hard-to-manufacture products, parts and

prototypes, there isn't a more suitable time to explore the advantages, capabilities and efficiency offered by advanced machining.

According to Tsuyoshi Aomi (Chairman and CEO of Aomi Precision), advanced machining can prove to be a golden opportunity for specialized machining companies as the miniature prototype market expands and gains more traction. These companies have the technological experience and metallurgical knowledge to manufacture many hard-to-make parts with challenging specifications. They also have the ability to keep costly third parties at bay and make special tools in-house, expediting the process from prototype to production and delivery.

1.3.1 Applications

Figures (1.2, 1.3, and 1.4) demonstrate few applications of non-traditional manufacturing methods.

Figure 1.2 Parts produced using advanced machining techniques (courtesy: Aomi Precision).

Figure 1.3 Advanced machining can accurately produce turned parts with thin, small features, as seen in these examples (courtesy: Aomi Precision).

Figure 1.4 Parts produced using advanced machining techniques. a) Complex parts may be machined out of titanium and other difficult-to-machine materials as a sample (courtesy: Aomi Precision).

Taniguchi looked back over the last century to see how much machining precision had progressed. He had also generalized the likely future advances in micro and nanotechnology. Figure 1.5 shows how machining operations are categorized based on the precision which can be accomplished, namely conventional machining, precision machining, and ultra-precision machining. Processes that accomplish or have accomplished the maximum possible dimensional

accuracy at a given moment in time are referred to as ultra-precision machining. It is a subjective concept that changes over time.

Machining accuracies in traditional processes were expected to exceed 1 µm by 2000 AD, while precision and ultra-precision machining category would reach 0.01 µm and 0.001 µm (1 nm), respectively [19]. His forecasts, which he made nearly two decades ago, are still accurate today thanks to developments in industrial technology. These ultra-precision machining precision targets cannot be reached simply by extending conventional machining processes and techniques. Figure 1.5 shows achievable machining accuracy by different processes. Table 1 shows a comparison of these unusual processes. The table clearly shows that the surface finish attained through unconventional machining processes is significantly better than that attained through traditional machining processes.

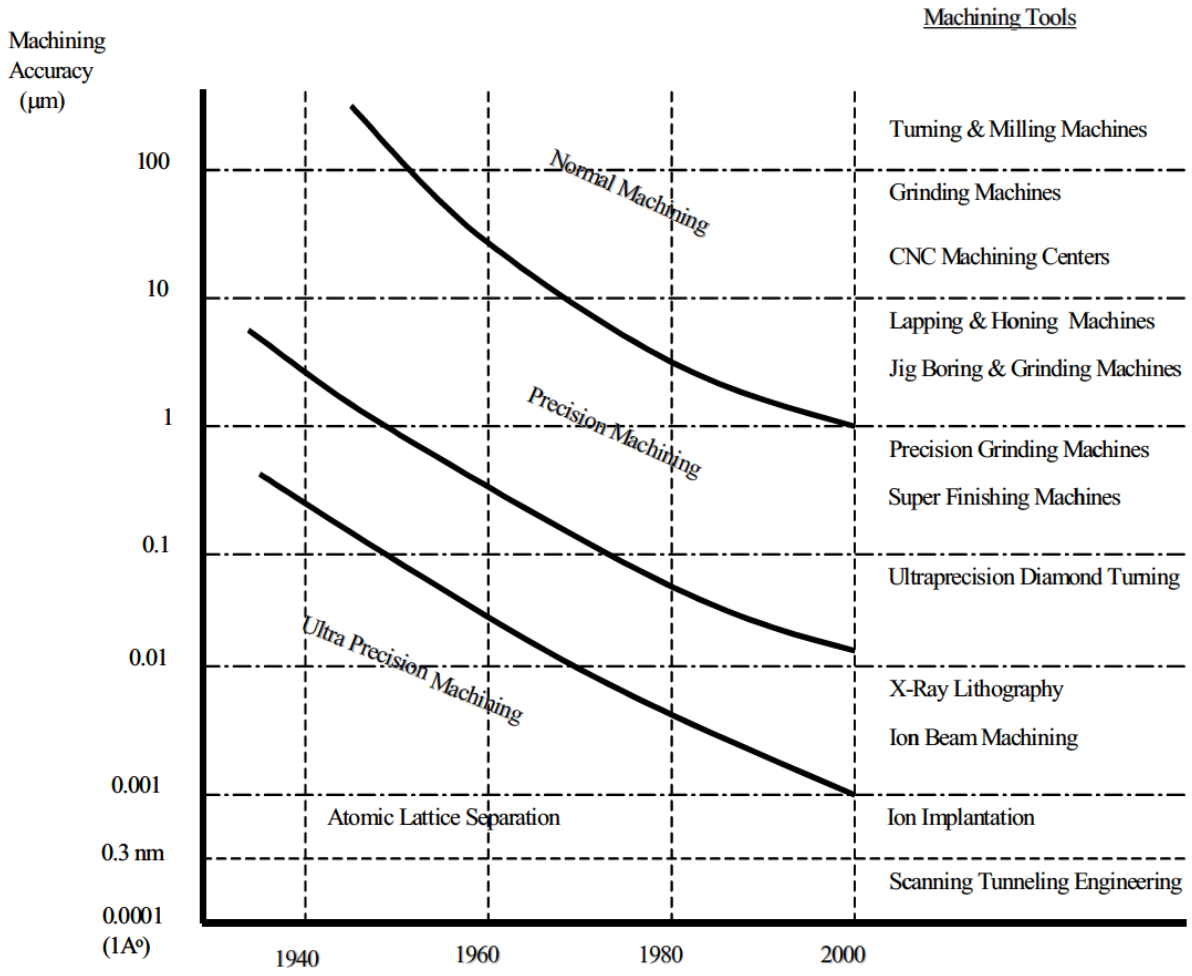

Figure 1.5 Achievable Machining Accuracy [6]

1.4 Traditional finishing processes

Before we get into the details of advanced finishing processes like magnetic abrasive finishing, Abrasive flow finishing and Rheological finishing etc., it's important to comprehend how common finishing processes such as grinding, lapping, and honing work. Both of these methods use multipoint cutting tools in the form of abrasives for material removal, that might or might not be bonded. Because of their ability to manufacture even surfaces with tight tolerances, these processes have been used since the dawn of time. Abrasive particle hardness is a significant qualification for processing. When it is used appropriately, these abrasive machining methods can produce a superior surface finish with controlled surface roughness, a pleasing residual stress distribution, and no surface or subsurface damage. The hardness of abrasive particles is a critical criterion for processing. When performed correctly, these abrasive machining processes will result in a high-quality surface with balanced surface roughness, satisfying residual stress, and no surface or sub-surface damage [3].

1.4.1 Grinding

Of all the traditional manufacturing methods, grinding is the most widely used abrasive finishing method. The material is removed from the work piece surface during the grinding process by the relative motion of a cylindrical wheel with abrasive particles embedded on its border. A porous spinning body is formed by the abrasive particles being bonded together which when coming in contact with the workpiece results in material removal. In general, grinding can be divided into two types: stock removal grinding (SRG) and form and finish grinding (FFG). The primary goal of SRG is to eliminate excess material from the soil, while the primary goal of FFG is to improve the surface quality. A grinding wheel's abrasives are tightly bonded with an effective binder while still having the opportunity for grain fracture to renew cutting edges. Since abrasive grain wears out quickly when grinding harder materials, a weakly bonded wheel is suitable for use [3]. The porosity of the grinding wheel is a variable that can be regulated to provide spaces for chips to be contained. Glass-bonded wheels are the strongest and toughest, while organic bonds are weaker. The size distribution of grits, as well as the wheel arrangement, all play a significant role in the grinding process. It is important to choose the right wheel for the job based on the finishing specifications. Grinding is mostly used for basic geometries such as cylindrical or plane surfaces, where size is limited by grinding wheel movement [5], [20].

1.4.2 Lapping

To finish the surface, lapping employs erratic abrasives. It operates on a three-body abrasive wear theory, in which abrasion by hard particles enthralled between the workpiece surface and a comparatively soft counter formal surface known as lap completes the finishing process. The workpiece is seized against the lap and pushed in undifferentiating ways under tension after an abrasive slurry is introduced between the workpiece and the lap surface. A compliant lap can be used to finish simple three-dimensional forms and rounded surfaces (convex, concave, etc.). The amount of material extracted is negligible since this procedure is primarily used to improve surface finish and precision. [4], [9].

1.4.3 Honing

Honing is an abrasive finishing technique that is widely used to smooth inner curved surfaces. To produce a random cross-marked surface with a good finish, abrasives in the form of grain or brushwood are carried in an increasing and oscillating mandrel. Stick pressure on the workpiece surface is higher than lapping pressure. Because of the oil retaining ability in the cross-hatched outline, the surface created after honing has self-lubricating properties [6], [8].

1.5 Advanced finishing processes (AFPs)

Many advancements are being made in the finishing of materials with fine abrasives, including that of the techniques, the abrasives, and their bonding, that all allow it for nanometer order of surface finish. Traditional manufacturing methods often fail to produce products in a variety of shapes and sizes. Non-traditional or modern production methods must be used since it is now possible to obtain nanometer surface finishes and dimensional tolerances using abrasives. Ion beam Machining (IBM) and Elastic Emission Machining (EEM) remove atoms and molecules from the surface directly. Other abrasive particle wear processes kill them in clusters. Mechanical, thermoelectric, electrochemical, and chemical processes are all forms of AFPs. This section covers advanced fine finishing techniques such as Abrasive Flow Machining (AFM), Thermal Additive Centrifugal Abrasive Flow Machining (TACAFM) [21], Magnetic Abrasive Flow Machining (MAFM), Magnetic Float Polishing (MFP), Magnetic Abrasive Finishing (MAF), and Magneto-Rheological Abrasive Finishing (MRAF) [9], [17].

Advances in materials synthesis have made it possible to produce ultra-fine abrasives with sizes in the nanometer scale. For manufacturing components of different shapes, sizes, consistency, finish, and surface integrity, abrasives are used in many ways, including loose abrasives (polishing, lapping), bonded abrasives (grinding wheels), and coated abrasives [22]. The electronics and computer industries are always in demand of higher and higher precision for large devices and high data packing densities [19]. To finish nanometer-scale surfaces, material in the at the level of atoms or molecules must be removed discretely or in groups. Some AFPs such as Ion Beam Machining (IBM) [23] and Elastic Emission Machining (EEM) [24] works by eliminating atoms and molecules from the workpiece surface, while other processes based on abrasives finishing, remove atoms and molecules in bunches [25].

Advanced machining processes (AMP) can be divided into different broad categories based on the specific energy used viz: mechanical, chemical, electrochemical, and thermoelectric. The material properties of the workpiece and the component's functional specifications influence the process choice. Mechanical AFP necessitates a high level of precision in finishing forces. Recently developed many AFPs use a magnetic field to monitor finishing forces operating on abrasive particles from the outside. To name a few, magnetic field-assisted finishing processes include Magnetic Float Polishing (MFP), Magnetic Abrasive Finishing (MAF), Magnetorheological Abrasive Flow Finishing (MRAFF) and Magnetorheological Finishing (MRF) [26]–[29].

Chemo Mechanical Polishing (CMP) utilizes both mechanical wear and chemical etching to achieve a surface finish in the nanometer range and a high level of planarization CMP is the most common method for finishing and planarizing silicon wafers in the semiconductor industry. Since the amount of material removed in fine abrasive finishing processes is so limited, they can be used to achieve nanometer surface finishes with very low dimensional tolerances. Advanced abrasive finishing processes are a subset of ultra-precision finishing processes that are designed to achieve nanometer-level surface finishes [30]. A comparison of surface finish obtainable from different finishing processes is given in Table 1.1. Surface finishes of less than 1 nm can be achieved using methods that extract material in the form of atoms or molecules. The following is a discussion of the working theory and some recent developments in these processes.

1.5.1 Types of finishing operation

Table 1.1 Surface finish achievable by different finishing processes [4], [19], [20].

S. No.	Finishing Process	Workpiece	Ra value (nm)
1	Grinding	-	25–6250
2	Honing	-	25–1500
3	Lapping	-	13–750
4	Superfinishing	-	12-800
5	Buffing	-	50-3200
6	Tumbling	-	50-400
7	Electroplating	Nickel and WC	4500-6700
8	Abrasive flow machining (AFM)	Hardened steel	50
9	Magnetic abrasive finishing (MAF)	Stainless steel	7.6
10	Magnetic Float Polishing (MFP)	Si_3N_4	4.0
11	Magnetorheological Finishing (MRF)	BK7 Glass	0.8
12	Elastic Emission Machining (EEM)	Silicon	<0.5
13	Ion Beam Machining (IBM)	Cemented carbide	0.1

However, due to the unique properties of materials, CNC machine tools have a difficult time automating the production of complex micro curved surfaces. This is due to the difficulty of conventional machining equipment entering the manufacturing site [31], [32]. Several advanced finishing processes have been developed in recent decades to achieve precision finishing of complicated micro component surfaces. According to their processing principles, advanced abrasive finishing processes can be classified into two classes. The first one includes Abrasive Flow Finishing (AFF) [33], Chemical Mechanical Polishing [26] Elastic Emission Machining (EMM) [24], where external forces interacting on the workpiece during the finishing are

impossible to control. The second one includes MRAFF, MRF [34], MFP [35] and (MAF) [36] etc., where the forces acting on the workpiece can be controlled by the magnetic field.

The MAF process has gained popularity in industrial applications because it can be used to finish both ferromagnetic and non-ferromagnetic products. Use gentle forces and versatile abrasives to remove surface defects to achieve nanometer range finishing. Magnetic forces cause the flexible magnetic abrasive particles to shear off the material from the surface in the form of microchips during magnetic abrasive finishing (MAF). Since polishing tools (magnetic brush) made of fine magnetic particles are versatile and simple to closely follow the finished surface, this process is considered a promising precision finishing technique for flat surfaces, complex curve surfaces, and inner surfaces of tubes. Furthermore, MAF has numerous advantages over traditional finishing processes such as grinding, including self-sharpening, high adaptability, controllability, and the ability to easily attach to numerically operated machine tools and robots, making finishing automation simple to implement. Magnetic field-assisted finishing processes are now being developed for a broad range of applications, including medical components, electronics, optics parts, dies and molds, fluid systems, and microelectromechanical systems [16], [37], [38].

1.6 Magnetic abrasive finishing (MAF)

The use of magnetic fields in the regulation of manufacturing processes has caught the interest of both industry and researchers in recent years. Each of the advanced finishing processes mentioned above has both advantages and disadvantages, particularly in terms of the surface finish and the shape and size of the workpiece that can be achieved. The processes addressed so far do not qualify to produce a nano-level surface finish on flat, large-size workpieces made up of difficult-to-machine materials. The process of magnetic abrasive finishing (MAF) is being developed to finish such workpieces efficiently and with precision [39]–[42]. In this process, ferromagnetic particles are mixed with fine abrasive particles and these particles are called magnetic abrasive particles (MAPs). Figure 1.6 and Figure 1.7 shows a schematic diagram of a MAF process respectively for bonded MAP and loosely bonded MAPs.

In these figures, it is clearly can be seen that magnetic field lines across the machining gap i.e., between the workpiece's top surface and the rotating electromagnet pole's bottom face the working or machining gap is the space between the top surface of the workpiece and the bottom surface of the electromagnet. Figures 1.6 and 1.7 provide an expanded view of the MAF process's

machining zone, workpiece, and electromagnet. The resolved components of the magnetic force acting on the work surface to extract material in the form of tiny chips are seen in the expanded view of the machining gap/finishing zone. It is shown in the center and right of the schematic diagram presented, where we can see the magnetic lines of forces and other information [28].

Magnetic abrasive is retained in the machining gap by the magnetic field, which serves as a binder, allowing the MAPs to be forced against the surface to be finished. The usual force (F_{mn}) caused by the magnetic field causes abrasive penetration onto the very workpiece, while tangential or cutting force is caused by rotation of the magnetic abrasive brush (MAB) that is intact to the north pole (F_c). The resultant of these forces is responsible to remove material in the form of tiny chips [37], [43], [44]. The magnetic abrasive particles join each other magnetically due to dipole-dipole contact between the magnetic poles (into the machining gap) along the lines of magnetic force as shown in Figure 1.6, forming a flexible magnetic abrasive brush (FMAB) which is usually (1–3 mm thick) [44].

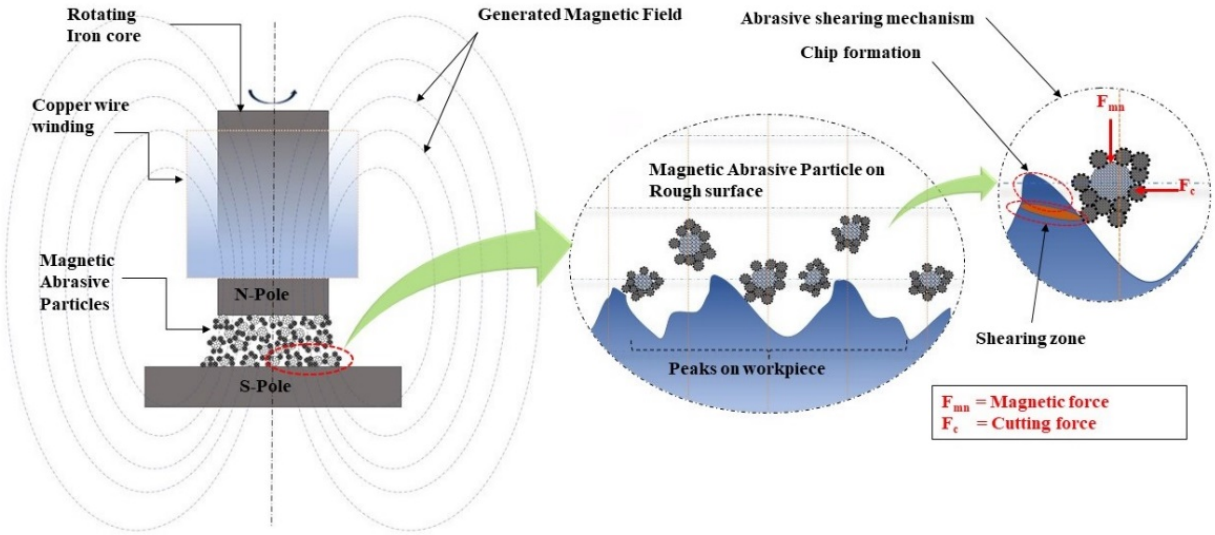

Figure 1.6 Schematic diagram of the magnetic abrasive finishing process.

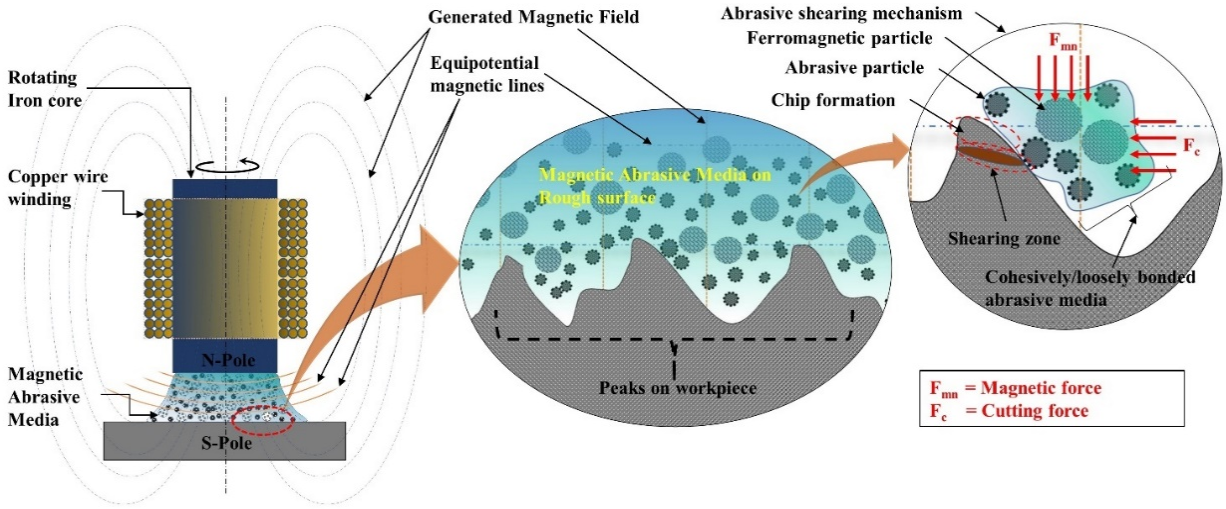

Figure 1.7 Schematic diagram of the magnetic abrasive finishing process [28].

In the case of unbounded (un-sintered) or loosely bonded, magnetic abrasive particles are made up of mixing (homogeneously), the abrasive particles get intertwined amid the chains [44], [45]. This FMAB is used by MAF for surface and edge finishing. This FMAB has many cutting edges and works as a multi-point cutting tool to separate material from the workpiece as tiny chips. Since the magnetic field's machining force is small but controllable, a mirror-like surface finish (Ra value in the nanometer range) can be achieved, and its acceptance is determined by the mesh of abrasive particles.

MAF can also be used for tasks like polishing and removing thin oxide films from high-speed rotating shafts. MAF has been used to finish the external and internal surfaces of cylindrical workpieces such as shafts, vacuum tubes, and sanitary tubes, as well as mould inserts, by researchers [46]–[48]. The workpiece surface is finished quickly and precisely owing to the controllable relative motion between the abrasive particles and the workpiece surface. A cylindrical workpiece, like ceramic bearing rollers, is rotated between the magnetic poles. Axial vibratory motion is also introduced into the magnetic field by the oscillating motion of the magnetic poles/workpiece, allowing for faster and better surface and edge finishing [49]–[51]. The workpiece circumferential speed, magnetic flux density, working gap, workpiece material, and abrasive size, type, and volume fraction decide the surface roughness, material removal and finishing rates. The magnetic coil's exciting current precisely controls the machining force

transferred by magnetic abrasive particles on the workpiece. According to the paper, the MAF process was used to finish stainless steel rollers [52].

The presence or absence of a slot in the magnet also affects the process performance [53], [54]. Finishing of stainless-steel rollers using the MAF process to obtain a final R_a of 7.6nm at an average finishing rate of 7.08 nm/s has been reported [30], [52]. MAF is capable of producing mechanical and electronic components with high precision and a very low surface roughness value, with few surface defects. This method has also been used to deburr micro-holes using a permanent magnet instead of an electromagnet. [55].

It can be used in a variety of other fields;

a. It can be used to polish fine components such as printed circuit boards (PCB).
b. Oxide layer removal and protective coatings
c. Intricate form polishing by machine.
d. Flat surface polishing.
e. Gear and cam chamfering and deburring

1.7 Magnetic Abrasives

Natural abrasives like Diamond, Garnet, Corundum, and Quartz can be found as minerals or rocks in the earth's crust. Artificial abrasives, also known as synthetic abrasives, are made of a variety of materials and have a high hardness. Artificial abrasives such as carborundum, aluminium oxide, silicon carbide, and others are examples. When these abrasives are combined with ferromagnetic materials, magnetic abrasive is formed. Few important magnetic abrasives are-

a. Diamond
b. CBN
c. Alumina
d. Silica
e. Silicon carbide etc.

There are two types of abrasives:

(a) Unbonded Abrasives or loose magnetic abrasives
(b) Bonded or Synthetic

Figures 1.8 and 1.9 depict unbonded or loose magnetic abrasives, while Figure 1.10 depicts bonded magnetic abrasives. While magnetic abrasives are broadly categorized into two groups, there are several ways to prepare magnetic abrasives, including:

i. Sintered magnetic abrasives

It is a technique for forming solid objects from powder using heat and pressure. In a sintering furnace, powder materials are heated below their melting point until the particles bind to each other. It is widely used in the production of ceramic items.

ii. Plasma-based magnetic abrasives

This approach involves introducing material in the form of powder or wire into the plasma jet as it passes through the plasma torch. The substance melts in the jet and begins to flow onto a substrate. As molten droplets come into contact with the ground, they flatten out and quickly solidify into a deposit that sticks to the target material.

iii. Mechanical alloyed magnetic abrasives

It is a two-stage process, firstly the alloy materials are combined in a ball mill and converted into a fine powder. Then, a hot isostatic pressing (HIP) processes applied simultaneously to compress and sinter the powder.

iv. Adhesive based magnetic abrasives

In this method, the ferromagnetic and abrasive components are mixed with an adhesive material. The quantity of adhesive in a mixture of abrasive and ferromagnetic components was decided in `such a way that the adhesive completely wets the mixture and at the same time the mixture should be semifluid.

v. Loosely bonded magnetic abrasives

MAPs are prepared this way by combining ferromagnetic and abrasive particles without adding any bonding material. Ferromagnetic particles are thought to be sandwiched between abrasive particles. The combination of iron and abrasive particles induces abrasion on the workpiece surface when a magnetic field is applied.

Figure 1.8 Prepared magnetic media [56].

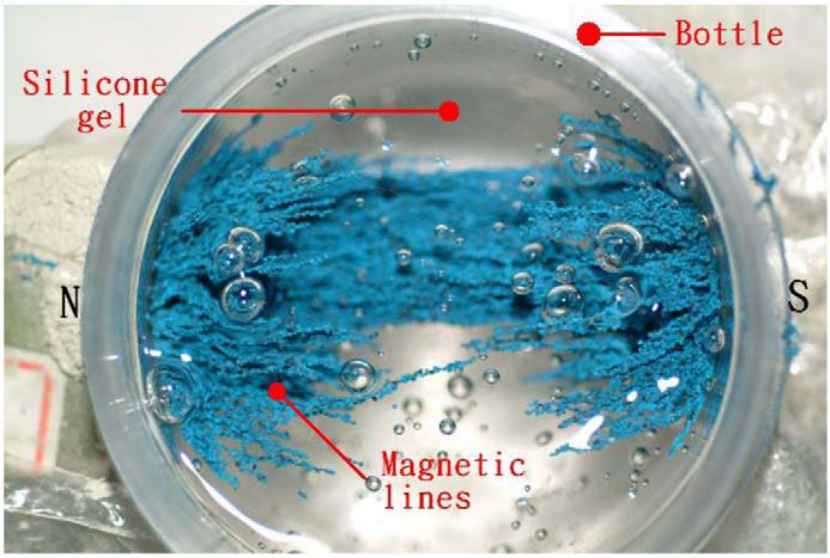

Figure 1.9 Magnetic lines of steel grits in the silicone gel [57].

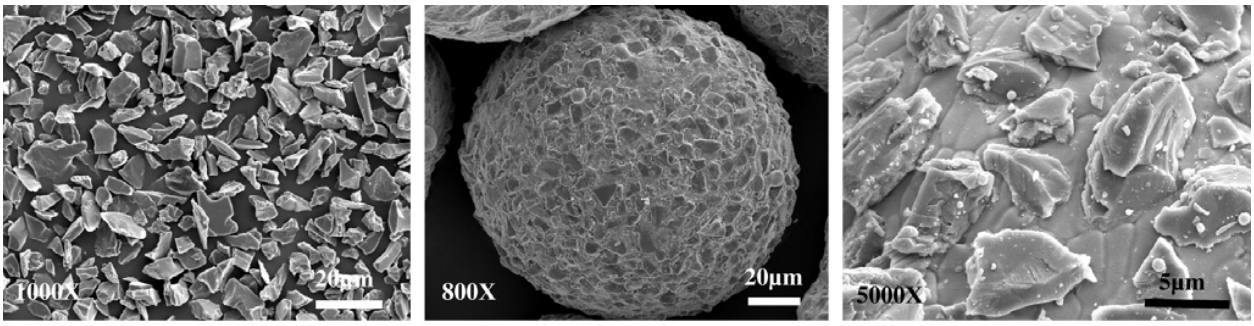

Figure 1.10 SEM micrographs of WA micro powder and spherical composite magnetic abrasive: (a) WA micro powder; (b) low-magnification SEM micrograph; (c) high-magnification SEM micrograph [58].

In this research work, it has been tried to introduce MAF operation for the finishing of Ti-6Al-4V. A novel approach to model and optimize the process. Development of Sintered magnetic abrasive and loosely bonded abrasive and its performance during MAF process. The experimentation has been conducted based on literature studies with parameters. The broad idea of this present work can be drawn using a flow diagram of the plan of research work represented in Figure 1.11.

1.8 Organization of the thesis

Chapter 1: In this chapter, the discussion converges on the importance of superfinishing in modern industry for quality products, after understanding the traditional and non-traditional machining processes and their classifications. The specifics of the traditional Magnetic Abrasive Finishing process, as well as its advantages, disadvantages, and applications, are discussed. Later on, the MAF working, classifications, elements, tooling method, and abrasive types were elaborated.

Chapter 2: This chapter begins with a comprehensive review of the literature available with the conventional Magnetic Abrasive Finishing process and its hybrid forms. Studies related to experimental research, analytical research, recent advancements have been done. Parameters affecting material removal, surface finish, surface roughness, and microhardness have also been reviewed. In the last section, Magnetic Abrasive Finishing process optimization techniques are discussed and reviewed followed by pointing out the research gaps.

Chapter 3: In this chapter, various MAF components with their working are elaborated. This chapter discusses the design, fabrication of the developed set-up for the MAF process. The parts and arrangements used in this process are thoroughly explained. Further, their working and specifications are also elaborated.

Chapter 4: In this chapter, an attempt has been made to prepare composite magnetic abrasive through the sintering process, which combines high-pressure compaction, crushing, and sieving for appropriate particle size using ferromagnetic carbonyl iron powder with alumina and silica as abrasive. Analysis of the elemental/phase composition analysis of the samples was used to describe the composite magnetic abrasive morphology and phase composition. Also, the development of loosely bonded magnetic abrasive is discussed and their rheology Characteristics is explained.

Chapter 5: This chapter introduces the Design of the experiment for the proper planning of experiments. Further, the ANN Modelling and Genetic Algorithm Optimization were studied to obtain the optimum response in the developed process.

Chapter 6: In this chapter the basic parameters of the MAF method, as well as the workpiece material and geometry used for experimentation, are described. In addition, the response characteristics chosen for this study are described in detail. Experiments were conducted according to Taguchi's orthogonal array and non-orthogonal array. Variable parameters such as current or voltage to the electromagnet, machining gap, rotational speed, working gap, and finishing time etc with their levels were selected to optimize the parameters for the responses, such as a change in surface roughness, change in microhardness, Change in modulus of elastic indentation. Precisely, this chapter discusses experimental investigations, parameters, responses, material and testing methods.

Chapter 7: This chapter discusses finite element analysis of the designed electromagnet using the magnetostatic module of ANSYS 2020 workbench, to predict the capacity of production of magnetic field density.

Chapter8: This chapter contains the important results of the study during the present investigation. It includes the morphology study of the sintered magnetic abrasive and its performance during magnetic abrasive finishing. It also includes ANN-GA, a modelling and optimisation tool to scrutinise and improve the performance of the magnetic abrasive finishing. Further, the best combination of the parameters was found to improve the process efficiency. At last, the surface topography has been analysed to study the microstructure of the sample using a Scanning Electron Microscope.

Chapter 9: This chapter contains salient conclusions. Important conclusions of the investigation regarding modelling along with the selection of optimum process parameters have been presented. Significant findings have been drawn from performed experimentation.

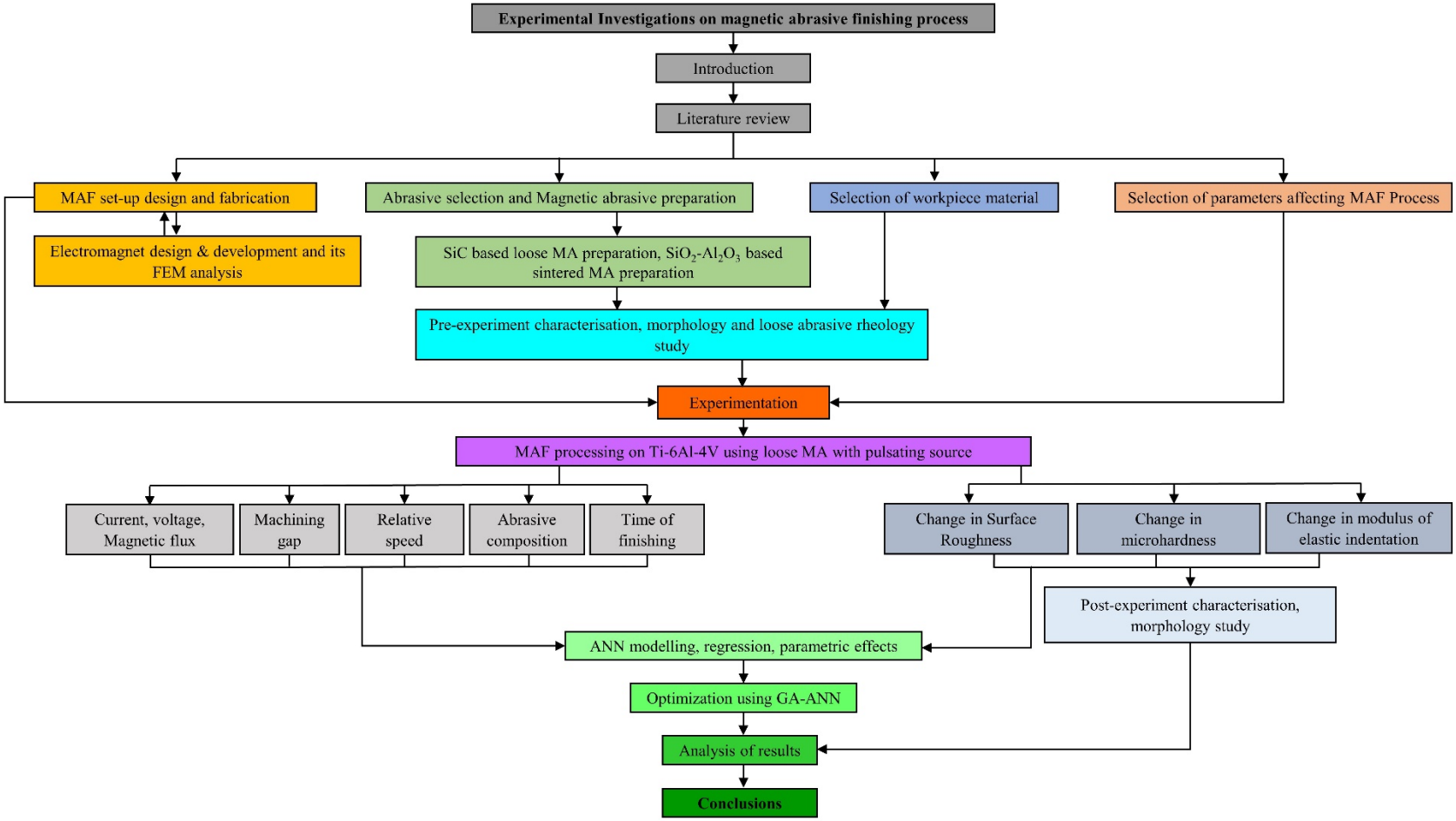

Figure 1.11 Flow diagram of the plan of research work.

Chapter 2

LITERATURE REVIEW

This chapter begins with a comprehensive review of the literature available with the conventional Magnetic Abrasive Finishing process and its hybrid forms. Studies related to experimental research, analytical research, recent advancements have been done. Parameters affecting material removal, surface finish, surface roughness, and microhardness have also been reviewed. In the last section, Magnetic Abrasive Finishing process optimization techniques are discussed and reviewed followed by pointing out the research gaps.

Introduction

An incredible study was conducted to examine the impact of MAF variables on process efficiency. Abrasives-based parameters, in addition to these process parameters, have a major impact on the finishing procedure. With a thorough understanding of all of these variable parameters, there is a greater range of variables from which to choose for improved process efficiency. Some research projects have been identified that have led to a better understanding of the impact of various MAF parameters on different quality characteristics for various finishing requirements.

The advancements in the field of technology and sciences have embarked the requirement of high surface finish of products along with very tight tolerances and surface integrity. The parts now-a-days are subjected to conditions which have never been so harsh along with being efficient in terms of energy and Weight. Thus, the requirement of a process that can produce very high finish surfaces without affecting its integrity due to thermo-mechanical damage, has made Magnetic Abrasive Finishing, a highly sought-after surface finishing technique. As my present study focusses on development of machinery for exploiting and characteristics of the limitations of MAF process. The following chapter thus presents a detailed analysis of the development, variations and different applications of the MAF process, available in literature.

The finishing processes are the most time and expense intensive in the current metalworking industry. Furthermore, complex finishing procedures necessitate manual handling, which is time-consuming, and these repetitive tasks may be harmful to workers' health. Modern difficult-to-machine products, as well as their manufacturing and complex precision component

designs, present unique machining and finishing challenges. The MAF method is capable of meeting the aforementioned challenges. Many manual finishing processes have been replaced by the MAF process, resulting in improved component standardization. Magnetic abrasive finishing and its composite forms with other production methods have been studied extensively since the 1980s. The main areas of MAF research are explored in greater depth.

The following three basic research patterns in the MAF method can easily be distinguished.

a. **Experimental Research:** Magnetic field strength parameters (magnetic flux, voltage, current, etc.), relative motion, machining or working gap, abrasive grain size, magnetic abrasive media composition, magnetic abrasive media thickness, media viscosity, material and geometry of work piece are just a few of the variables that affect the output of the MAF method. The effect of critical process parameters on material removal, surface roughness improvement, modulus of elastic indentation adjustment, and micro hardness was investigated in this study, and an attempt was made to optimize the process parameters.
b. **Analytical Research:** Mathematical and computational modelling of variable parameters are part of analytical analysis (i.e., magnetic flux, relative motion, machining or working gap, magnetic abrasive media composition, magnetic abrasive media volume, Viscosity of media, Material and Geometry of work piece. etc.). This study is done to improve process management.
c. **Evolution and recent advancements in MAF:** A lot of research is being done to hybridize the basic MAF process with other traditional and non-conventional machining processes in order to boost its performance. A lot of research is also going on to increase the consistency of finishing and the reliability of the process by making various changes in the process.

2.1 Experimental research in MAF

Jain et al. [59] in 2001 studied the effect of working gap and circumferential speed on the performance of magnetic abrasive finishing process. In which they designed an experimental setup for finishing cylindrical workpiece and used loosely bounded powder as the abrasive mixture which consists magnetic powder, abrasive powder (Al_2O_3, 600 mesh size), current and lubricant. Parameters selected by them Ire abrasive particle size, amplitude of vibration, Applied Voltage, Ferromagnetic Particles, Finishing Time, Frequency of vibration. According to the findings, raising the working distance or decreasing the circumferential speed of the workpiece reduces

material removal, whereas increasing the circumferential speed of the workpiece increases change in surface roughness. Jain et al. investigated the finishing of the exterior surface of a cylindrical workpiece and discovered that the working distance and circumferential speed of the workpiece are the parameters that have a major impact on material removal and surface roughness adjustment.

In another study, Jain et al. [60] studied In the magnetic abrasive finishing process, the effect of pulsating direct current The study's parameters were duty cycle, on time, off time, and pulse time. They discovered that using a pulsating DC supply improves the surface finish, owing to the creation and destruction of FMAB during the on-time and off-time of the pulsating power supply, respectively.

Singh et al. [61] used the Taguchi method to optimise the parameters of a magnetic abrasive finishing process. The work piece was made of steel alloy, and the statistical programme MINITAB was used to design the experiments. Material removed and surface roughness value were the two process outputs that were optimised. He discovered that the machining distance and magnetic flux density are the two most critical parameters that influence surface roughness and material removal. Furthermore, a microscopic examination of the work piece prior to and after machining showed that it was free of cracks and other defects.

Yin et al. investigated the effect of ultra-high-speed magnetic abrasive machining (UHSMAM) on the AISI machined surface's plastic strain and strain energy. They also looked at the residual strain in the AISI 304 bars that had been plastically deformed. The UHSMAM method significantly improved the surface roughness, micro-diameter, and removal weight of the bars, while the plastic strain did not adjust after machining, according to the researchers [62].

Bhagavatula and Komanduri [30] explained that, because of the high temperature and pressure produced by frictional heat while finishing the surface, a solid-phase reaction occurred between the abrasive and the workpiece. This solid-phase reaction produces a chemical substrate on the finished surface, compromising the workpiece's surface integrity.

Singh et al. used aluminium 6060 as a workpiece to perform an experimental investigation of surface temperature on the workpiece-FMAB interface during the MAF operation. Surface temperature is directly related to voltage, abrasive particle weight, and working gap, according to the findings [63].

Magnetic Abrasive Finishing is primarily used to finish ferrous alloys due to the low magnetic permeability of non-ferrous materials, which makes the process inefficient and yields no

appreciable results using the typical MAF process. As a result, a number of researchers have attempted to overcome this shortcoming by using double electromagnets, which combine a permanent magnet with an electromagnet.[64], [65] etc.

The characteristics of a magnetic abrasive finishing of cylindrical pipes using sintered magnetic abrasives were identified by Palwinder Singh et al. (mixture of Al_2O_3 and ferromagnetic particles). The surface finish was measured in percentage improvements (PISF). The maximum PISF obtained was 95%, and the minimum surface roughness (R_a) was 0.05 µm [66].

According to Jae Seob Kwak [67], traditional magnetic abrasive polishing is ineffective on non-magnetic materials. As a result, a device with an electro-magnetic array table may be placed underneath the non-magnetic material's working field. It may aid in the enhancement of magnetic force.

MAF is an advanced finishing technique in which the magnetic field is used to guide the cutting force. Due to low forces acting on abrasive particles, it reduces the likelihood of microcracks on the workpiece's surface, particularly in hard brittle materials [37]. On flat surfaces, as well as internal and external cylindrical surfaces, this process can produce surface roughness in the nanometer scale. [59]. The MAF method has a number of benefits, including self-sharpening, adaptability, and controllability, and the finishing tools do not require compensation or dressing. [45].

The workpiece is kept between the two poles of a magnet during MAF. Magnetic abrasive particles made up of ferromagnetic particles and abrasive powder fill the working distance between the workpiece and the magnet. Magnetic abrasive particles are available in two forms: bound and unbound. Typically, ferromagnetic particles are sintered with fine abrasive particles (Al_2O_3, sic, CBN, or diamond) in this phase, and these particles are referred to as ferromagnetic particles [58], [68].

According to (Lin et al., 2007) [69], the material removal weight can be adjusted depending on the size of the magnetic abrasives, and the workpiece materials can be magnetic (e.g., steel) or non-magnetic (e.g., ceramics). As a result, MAF is a multi-functional precise finishing process that can be used to effectively achieve high-quality surface finishes.

2.2 Analytical research in MAF

The use of the Finite element approach for modelling and simulation of magnetic forces had a significant effect on material removal and surface roughness, according to previous literature.

To study the theoretical aspects of magnetic abrasive process, Jayswal et al. [70] proposed a mathematical model for material removal mechanics and a model for surface roughness. They created a finite element code to determine the distribution of magnetic forces, with the key parameters being magnetic flux density, form and size of magnetic abrasive particles, and the working gap. Jayswal et. al. tried to model the material removal taking place in the MAF process, and the ensuing surface roughness obtained by assuming a uniform surface profile, lacking any variation in its surface. The whole space within the working gap was divided into 2-dimensional mesh around which the governing equations are solved using the Glarekin's method of finite element analysis as shown in Figure 2.2. Number of different assumptions regarding the constancy of magnetic field with time, homogeneity of working brush, and zero leakage of magnetic flux etc. Ire made in order to simplify the problem. The shearing model of material removal was used by assuming the MAP to be perfect spherical in shape. An experiment was also carried out on SUS304 using Silicon Carbide based magnetic abrasives, by them to check the accuracy of the model. Appreciable conformity between the experimental and predicted results was obtained at 4 minutes of machining time. The same methodology was extended to non-uniform surface profiles, assuming a statistical distribution of surface topology in order to improve the accuracy of predictions, and a reduction in % error between the predicted and experimental results are achieved.

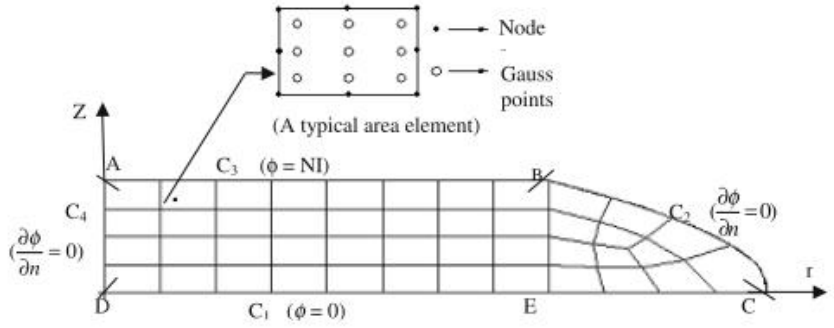

Figure 2.1 Finite element mesh of working gap

A finite element model of a rotating magnetic field was developed by J. D. Kim et al. [71] in his paper "Development and finite element analysis of the finishing system using rotating magnetic field".

By considering the Gaussian distribution of the ordinates of the surface profile, Jain et al., [72] modelled and simulated the surface profile obtained after MAF. This model predicts centre-line average surface roughness value (R_a) obtained after MAF. Literature survey indicates that there are little contributions toward the simulation of the magnetic abrasive finishing process.

Singh et al. used a semiempirical dimensional model using the Buckingham π-theorem for evaluating the effect of various process parameters on the rise of temperature of the target surface. It was found that MAF is a low-temperature finishing process and makes the finishing material thermally-stable. Furthermore, the voltage and abrasive weight in the magnetic abrasive brush are found to be the most influential factors with regards to the response parameter of 'rise in temperature' [73].

Mishra et al. [55] in 2014 analysed the work brush interface temperature in magnetic abrasive finishing process. In the study, they performed transient analysis of workpiece to predict temperature rise due to magnetic flux. During the transient analysis current in the coil was in between 0.45 to 0.91 Ampere, number of turns are 480, and volume ratio of iron was 43-70. The results of the transient study stated that magnetic flux density was 0.10-0.223 T for the coil current in range of 0.45-0.91 A and the maximum rise in temperature occurred at 450 rpm and 0.23 T magnetic flux.

Kim and Choi [74] have developed a mathematical model to assess the magnetic field gradient that generates the attractive force between the abrasives, as well as the machining pressure in the air-gap. The magnetic flux density increases as the air-gap length decreases, according to the model and simulation of the MAF method for finishing cylindrical workpieces developed.

Mulik and Pandey [75], [76] designed and built an experimental setup to perform experiments and evaluate the effect of process variables on the surface finish obtained using unbonded Fe and SiC magnetic abrasive particles during the MAF process. In their research, they used a different electromagnet design that produced a better surface finish at lower magnetic forces. They assessed the sur-face finish by rotating the electromagnet between 180 and 450 rpm and measuring the magnetic flux density between 0.02 and 0.2 T.

Kumar and Yadav[77] used a finite element model to estimate temperature rise in a Si_3N_4 workpiece, with Cr_2O_3 as the abrasive (unbonded). The temperature rise was determined to be between 150°C and 800°C, depending on the magnetic flux density and tool rpm. The magnetic flux density was between 0.8 and 1.0 T, and the electromagnet rotation was between 5305 and 6366 rpm.

According to Mulik and Pandey [78], In the MAF phase, the temperature on the work piece–brush interface was calculated experimentally when the maximum magnetic field was 0.2 T and the rotation of the magnet was 180–450 rpm. They discovered that the temperature was between 31 and 42 degrees Celsius, but they have yet to create a process physics-based model to predict the temperature. The MAF process is very complex in nature due to the large number of cutting surfaces present inside the flexible magnetic brush at any time. The interaction of all the maps in the brush is also very difficult to study and model using mathematical or numerical techniques but still a number of commendable attempts have been made in the past to perform such herculean task.

2.3 Evolution and recent advancements in MAF

2.3.1 Vibration assisted MAF

The traditional MAF process has major advantage that the brush used to machine workpiece may become blunt after some time of operation, as the cutting edges of all the abrasive particles present in the region of brush that is in contact with the workpiece and actually carrying out the cutting, fades down. To overcome this shortcoming a number of different approaches Ire employed by researchers. One such commendable technique is to impart vibrations to either the workpiece or the tool. The vibrations help to replenish the cutting edges by moving the abrasive particles in contact with the workpieces to the non-cutting zone and vice versa.

K. B. Judal et. Al. [79] developed a novel approach to improve the efficiency of magnetic abrasive finishing process of cylindrical workpieces by applying longitudinal vibrations to magnetic poles. A U-shaped electromagnet setup having 1,000 turns of copper wire having 1 mm diameter was wound per coil, around a 40 mm diameter core. A 0-5A DC supply was used as the power source, and the workpiece material was selected as aluminium. 60:40 ratio of steel grit and Al_2O_3 powder was used as the abrasive material and the finishing operation was performed for 300

seconds. The change in Ra values was studied and it was found that the frequency of vibrations applied to the electromagnet and the size of abrasive particles are crucial for the change in S.R. and the MRR, because the vibrations help to resharpen the magnetic brush by removing the worn-out abrasives and supplying fresh abrasives from the magnetic brush. He also concluded that the rotational speed of the workpiece has profound effects on the output characteristics and as the size of abrasives reduces the resulting surface finish improves.

Shaohui Yin et. al. [80] in their paper titled "Vertical vibration-assisted magnetic abrasive finishing and deburring for magnesium alloy", explored the use of vertical vibration assisted MAF process for finishing and deburring of Mg alloy-based materials. Vertical vibrations of 1 mm magnitude Ire imparted to the workpiece in order to enhance the efficiency of the process, by replenishing the working surface of the flexible abrasive brush with new cutting surfaces. Therefore, the time required for deburring the holes to a desired value decreased heavily by employing vibrations during the MAF process. An increase in Ry value was obtained when using vibrations with the process, due to the increased normal pressure on the surface. The vibrations occurring in the workpiece produces a pulsating effect of the pressure due to which the peak and mean pressure rises heavily, resulting in an increased MRR but with rougher finish obtained.

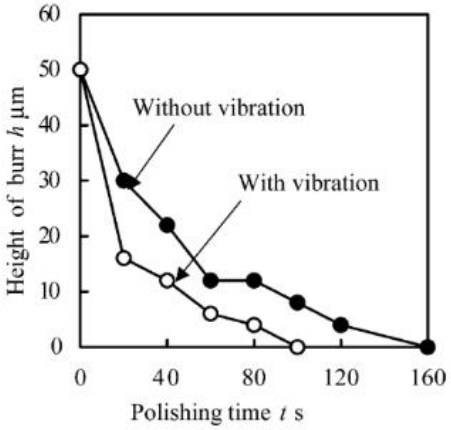

Figure 2.2 Effect of vibrations on deburring of holes [80].

2.3.2 Ultrasonic Assisted MAF

Rahul S. Mulik et. al. [81] in his paper he developed a numerical model using Buckingham Pi theorem to develop a relationship between the worksurface temperature and the various parameters present in an ultrasonic assisted MAF process. The vibrations imparted during the finishing process are of the range between 5 µm- 12 µm, 20 kHz frequency. Unbonded magnetic abrasive

particles consisting of 300 mesh size iron particles and 800 mesh size sic particles are used to finish the surface with 1.5 mm working gap, for 5-minute-long machine runs. Because of the ultrasonic vibrations a net increase in the maximum working temperature of the work-brush surface was observed, as it changed to 46^{o} C from 41^{o} C, which was measured with the help of K-type temperature sensors, installed below the workpiece surface. It was also concluded that a net increase in the temperature during the finishing process takes place with increase in the applied voltage, Weight of abrasives, and the pulse on time duration. The model thus formed was in good agreement with the experimental results.

One such noticeable attempt was successfully made by P. Kala et. al. [51]. In his paper "Polishing of Copper Alloys using Double Disk Ultrasonic Assisted Magnetic Abrasive Polishing", he placed a disk made out of perpex, so that the workpiece rests between it and the electromagnet, to increase the intensity of magnetic field through the workpiece. The electromagnet used was made of 4 sets of coils, designed such that each pole produces a maximum of 0.25 T magnetic field at peak operation. In order to study the effects of imparting ultrasonic vibrations to the workpiece, he carried out 2 sets of experiments, one without vibrations and other with it. Voltage, rotational speed, pulse on time of the vibration horn and mesh number of the maps are selected as the input parameters and each workpiece was machined for 5 minutes. A 16 point % change was obtained by using the ultrasonic assisted MAF compared to the typical MAF process.

2.3.3 Other modifications and hybridization of MAF

Wu et. al. [82] proposed an ultraprecision MAF process using low frequency alternating magnetic field which promotes the dispersion of micro magnetic particles and enhance the stability of tool used for grinding. In this study, the investigation of impact of alternating magnetic field on magnetic field distribution, force of finishing and abrasive behaviour was carried out. A design of experiment was developed for finishing the SUS304 stainless steel plate. The effect of different process parameters namely grinding fluid, rotational speed of pole and current frequency on the surface geometry and material removal was studied. The surface roughness of SUS304 stainless steel plate was improved from 240.24 nm to 4.38 nm, with the increase of magnetic particle diameter, the size and variation of amplitude of force are increased. The surface geometry and the material removal enhance with increase in rotational speed.

Kim et. al. [83] proposed a new finishing process called magneto-electrolytic abrasive polishing. By combining the Lorentz force effect to the traditional electrolytic finishing process, the process was developed to notice the high efficiency and enhance the surface geometry. This work provides a theoretical explanation behind the modification of motion of electrolytic ion caused by magnetic field, the effect of magnetic field was studied by analysing the results of model test. Th magnetic field affects the movement of electrolytic ion and changes the linear path to curved path by accelerating the ions. It enhances the finishing efficiency. For the higher efficiency the optimum magnetic flux density exists and it was 0.6 T for gap of 1mm. The correlation between the flux density, the working electrode gap and potential determines the optimal value for optimal value for optimum efficiency of surface finish.

K. B. Judal et. al. [84] presented the performance of machining on cylindrical electrochemical MAF to get the enhanced efficiency of machining. A list of experiments was conducted on AISI 304 stainless steel workpiece based on rotational design technique of response surface methodology. The effect of different process parameters (viz. Workpiece rotational speed, current to electromagnet, electrolytic current and frequency of vibration) is studied on processed variables i.e., Surface roughness and material removal. After conducting analysis of model, it was found that rotational speed and electrolytic current have a noticeable influence on the output variable i.e., MR and Ra. Increase in these variables results in increasing material removal and lowering Ra due to synergic working effect of abrasive assisted passivation and passivation assisted abrasive. After carrying out multiple response optimization for maximizing MR and minimizing Ra, the optimal input processing variables are working rpm, electrolytic current and 6Hz frequency of vibration.

El A -Taveel [85] proposed a hybrid process of Electrochemical Turning and MAF that enhances the material removal rate and lower down the surface roughness of 6021 Al/Al2O3. This study focuses on the characteristics of development of empirical mathematical models based on RSM for comparing the interactive relationships of processing parameters i.e., Magnetic flux density, applied voltage, tool feed rate and workpiece rotational speed. The effect of these machining parameters was studied on the MRR and SR. This also highlights on validity and correctness of models developed for in depth analysis of processing parameters on MRR and SR. To maximize MRR and minimize SR, these parameters are optimized. Increasing both voltage and feed rate leads to enhancing the machining efficiency and surface roughness. Assigning ECT with

MAF improves surface geometry of material. The formed mathematical model was found to be flexible and if shows the optimized effects of processing parameters.

G.Y. Liu et. al. [86] proposed a complex hybrid model combining electrochemical machining and magnetic abrasive finishing. A suitable tool which is capable enough to work under two different processes of different characteristics was designed and list of experiments was carried out on Al-6061 to investigate the impact of EMAF process. The results obtained after conducting experiments showed that EMAF help to obtain the better surface finish and higher metal removal rate compared to traditional MAF process. The surface roughness Ra of material lowered down to range of 0.2 μm to 1.3 μm by EMAF technology. To obtain the enhanced surface quality in the hybrid process, the ECM must be kept in passivation status. A limit of surface quality exists with spindle type tools due to non-uniform distribution of magnetic and abrasive.

N. Sihag et. al. [87] devised a new process combining the chemical oxidation and magnetic field assisted abrasion for fast processing of material and by combining CMP and MAF, and is termed as Chemo Assisted Magnetic Abrasive Finishing (CMAF). A list of experiments was conducted on tungsten workpiece and the effect of machining parameters like percentage Weight of abrasive, oxidizing agent concentration, rotational speed of magnet and working gap on the surface geometry are investigated. The planned design of experiment designed by using Taguchi L9 orthogonal array was analysed by ANOVA to study the contribution of individual parameter on the surface geometry. To study the surface morphology of material SEM micrographs ire obtained. A model was developed to study the change in surface roughness of material. It was found that in CMAF process, the surface geometry i.e., Ra was affected by rotational speed of magnetic disk (37.71%), percentage Weight of abrasive (27.74%), working gap (16.12%) and concentration of H202 which is used to form oxide layer. The maximum peak to valley height in geometry profile is approximately $1/5^{th}$ of same of unfinished sample.

2.3.4 Optimization and data analysis review

In the MAF process application of gentle forces by using flexible magnetic abrasives brush (FMAB) for removing surface unevenness has been a great idea. During MAF, the magnetic forces are allowing the FMAB to shear-off the material from the surface in the form of microchips [1, 7-10]. Many authors have studied various control factors, and optimization techniques to accomplish the better surface finish on different advanced material using the MAF manufacturing processes.

But these optimization techniques lack intelligent iterative optimization methodology for better performance of the process.

Yamaguchi et al. [89] used diamond paste for the Finishing of an uncoated carbide tool (UCT) surfaces using MAF to get better tool-wear characteristics. Finishing-time, Pole tip feed, Spindle speed, Machining Gap, Steel grits mean-dia, diamond Abrasive, Lubricant, were chosen as control factors. It was reported that Roughness less than 25 nm could be achieved. Tool life of MAF processed UCT had been doubled compared to MAF unprocessed UCT when it was used in turning of Titanium (Grade 5) rods. It is vital for coated tool finishing to use different sizes of the abrasive particle simultaneously adjust magnetic force for desired finishing and less material removal, [90].

Amineh et al. [91] utilized the MAF to remove the recast layer formed by wire electro-discharge machining (WEDM). The MAF was able to shear off the recast layer generated during WEDM without any micro crack. It was found that increasing abrasive particle causes higher recast layer removal, and better would be the surface roughness.

In another study Amnieh et al.[92] examined the effectiveness of finishing parameters such as Tool rotational speed, abrasive mesh number, and finishing. Jiang Guo et al. [93] found that the MAF was an effective finishing operation for Flat workpiece of Polyamide 12 (PA12) 3-D Printed parts under constant magnetic field. The process leaves no visible chemical change within the 10μm subsurface level.

Jiang Guo et al. [94] investigated the tribological performance of RSA-905 after finishing the surface by magnetic field-assisted finishing (MFAF). Magnetic abrasive (SiC, Al_2O_3, Carbonyl Iron Powder) was used for finishing and achieved desired finish without any post-process subsurface defect. Tribological performance was improved, and surface residual stresses were released. However, a little decrement in hardness was noticed.

Yuewu Gao et al. [95] studied various process variable's influence on the polish quality and compared the surface roughness of Cu-27400 and SS316 flat workpiece. Al_2O_3 based atomized magnetic abrasive tool was selected for processing under the control of permanent magnet (Nd-Fe-B).

Shadab Ahmad et al. [36] examined the consequence of sintered magnetic abrasive (SMA) on the MAF process. The process parameters considered were voltage, machining gap, and rotational speed. There were three experimental arrays designed according to the L_9 orthogonal array. The Taguchi-ANOVA method was used to find the optimized surface roughness change and

corresponding values of the parameter with their quantitative effect. The most influential parameter was voltage followed by machining gap and rotational speed, respectively and it was found that the Abrasive size has a significant role in the MAF process [18-20].

The application of different optimization methods like Taguchi, Response Surface, Fuzzy Logic, Genetic Algorithm, Moth Flame Algorithm, and Particle Swarm Algorithm for the effective utilization of the MAF process, are increasing [21, 22]. The influence of voltage, machining gap, abrasive size, and rotational speed on surface roughness during the MAF process was studied by employing various methods by many researchers. Table 2.1 shows the Finishing parameters and optimization techniques employed in the research.

Vahdati and Rasouli evaluated the effect of the various parameters of MAF on the surface finishing of Al-alloy and compared the RSM simulation of the same with the experimentally obtained results. The gap, spindle rpm and feed rate are found to be significant parameters. The difference between the simulated and experimental models varies between 15% and 26% as the simulation overestimates the magnetic flux density. The gap was found to have the highest influence on the change of surface roughness. Lower feed rate, higher cutting speed and less gap produced the best result [98].

Singh et al. used the moth-flame optimization (MFO) algorithm and ANN to make a multi-objective optimization model of the processing conditions of MAF for the AA6060 alloy. The responses were surface roughness, temperature of workpiece during the finishing operation and hardness of finished surface with respect to the input parameters of working gap, abrasive weight, voltage and rotational speed. The hybrid ANN-MFO model provided effective and accurate predictions [97].

Yadav et al. used ANN-NSGA-II approach for the modelling and optimization of hybrid machining process of electrical discharge diamond face grinding (EDDFG). ANN was used for the modelling while NSGA-II was used to optimize the control parameters of the machining process. The wheel speed, pulse current, pulse on-time and duty factor were taken as input for the corresponding output parameters of material removal rate and average surface roughness [77].

Pasandideh and Niaki elaborated on the use of DFF-GA to solve multi-response statistical optimization problems. They underlined four methods for the same, including different randomness conditions of the problem [99].

Recently, Singh et al. had developed a hybrid multi-objective optimization technique by joining the Artificial neural network with Moth flame optimization. Their new methodology had successfully optimized the MAF process. they key findings were voltage and the working gap should be kept at a minimum to achieve a better surface finish and hardness [97].

Ahmad et al. used ANN-GA for the modelling and optimization of MAF of stainless steel SS302 and compared it with the Taguchi-ANOVA analysis of the same. The abrasive size, voltage, machining gap, and rotational speed were considered as the input parameters for studying the response parameter of surface roughness; a 7% improvement in the results was observed with the hybrid ANN-GA approach [42].

Ali-Tavoli et al. used group method of data handling (GMDH)-type neural networks-GA and NSGA-II with Pareto-based optimization to construct a multi-objective optimization model of abrasive flow machining processes for brass and aluminium samples' material removal and surface finish. Such a combined application has led to the discovery of useful and interesting design relationships [33].

Table 2.1 Finishing parameters and optimization techniques

S. No.	Authors	Workpiece /Abrasive	Type of Magnetic Source	Voltage or current supply	Machining Gap (mm)	Rotational Speed (rpm)	Abrasive Size	Surface Roughness Range or effect	Remarks
1.	T. C. Kanish et al.[96]	SS316L/ SiC	-	15-20V	1.5-2	270-540	400-1200mesh	35-50%	Taguchi optimization and fuzzy modeling used to predict SR
2.	Prateek Kala et al.[64]	Copper/ Alumina	Permanent	-	1.5-2.5	200-400	800mesh	-	Taguchi optimization and analysis of finishing force and torque involved in DDMAF done
3.	K. B. Judal et al. [79]	AISI-304/ SiC	DC Supply	0.5-2.5A	1-3	150-1200	10-180µm	(0.28µm,0.32µm) - 0.039µm	RSM optimization techniques were used. Rotational speed and Electrolytic current lead significant improvement in MRR and SR.
4.	Yi-Hsun Lee et al.[50]	SUS304/ SiC	Permanent	-	1-2	100-1000	1000-8000mesh	0.13-0.03µm	Taguchi optimization done and 77% improvement found in SR
5.	Amer A Mosa.[100]	Brass/ Quartz	DC supply	1.5-3.5A	1-2	175-525	150µm	-	ANFIS used for mapping and optimization of experimental results
6.	Prateek Kala et al.[51]	Copper Alloy C70600/ Al2O3	DC supply	70-100V	2	112-224	600-1200mesh	62%(MAP), 76%(UAMAP)	Taguchi method is applied for process optimization, and this study concludes that UAMAP is an improved technique than MAP.
7.	A. Cheng Wang et al.[101]	SKD11/ AL2O3, SiC	-	1-3A	-	700-1300	4000-8000mesh	0.029µm	Claimed that MFGA is better over MAF, because of gel-based MA. Optimization of the process done by the Taguchi method.
8.	Nitesh Sihag et al.[102]	Tungestun Alloy/ Al2O3	Permanent	-	2	150	1200mesh	0.34-17µm	86% improvement in SR with chemical oxidation RSM and ANOVA was used to design the experiments and analyze the results

2.4 Research Gap

The literature review on the Magnetic Abrasive Finishing (MAF) process revealed that, despite extensive experimentation to better understand the MAF process and related parameters, there is still a gap in providing adequate data for the creation of a comprehensive process model. Due to a wide factor of space and a number of MAF applications, this is the case.

a. In MAF, material removal in this process is very low comparative to other finishing techniques. A lot of research work has been conducted to enhance the material removal by hybridized MAF with others non-conventional processes but there are still needs to develop new techniques which remove more material in comparison to the other conventional and hybrid processes developed so far.
b. Several mathematical and empirical models have been developed pertaining to prediction of material removal and surface finish, however most of them are specific and can't be generalized. Hence, comprehensive modelling and simulation of newly developed MAF is necessary.
c. The optimization of process parameters from component quality point of view.
d. Detailed study on Magnetic abrasive properties by various combinations of different abrasive and ferromagnetic material developed are still untouched.
e. On thorough analyzing the research work on Magnetic Abrasive finishing it has been observed that the geometry of finishing surface is mainly cylindrical and flat shaped. Intricate or complex shape are not touched extensively.

2.5 Problem formulation

This segment explains the Magnetic Abrasive Finishing process and how it works. The complexity of the problem and the goals of the current study have been formulated and addressed in this chapter of problem formulation after a critical analysis of the literature. This chapter explains the problem formulation, or what the problems were that needed to be solved through our work, as well as the goals that were set after the problem was identified.

Advances in materials science have followed the production of harder and more difficult-to-machine materials, posing challenges to existing technologies in terms of processing time, cost, and energy consumption. Because of recent technological advances, precision component

manufacturing must become more accurate and effective. Many precision processes, on the other hand, are unable to meet the finishing criteria of higher quality and surface finish.

In the present investigation, an electromagnet has been designed and developed and tested with the aim to efficiently control the magnetic field. Also, novel magnetic abrasives are developed of both types bonded as well as unbonded discussed in chapter 4. These steps will help MAF process to overcome with, Low MRR, longer finishing time, huge energy consumptions. In MAF process a smooth surface is required by the abrasive particles from a very hard surface in general. This requires developing such a process which can overcome these difficulties. The basic concept of present investigation is to achieve the synergetic machining action by developing electromagnetic tool and magnetic abrasive further a novel approach of process modelling and optimization will be done.

Studies on the MAF process have primarily focused on the process's growth and expansion of its capabilities and applications. This technology was able to achieve excellent process capabilities. Device performance, surface finish, surface hardness, and elastic indentation modulus all benefit from the new technology.

Following are the problems in the MAF Process which are being observed through literature review.

a. Providing engineering engineers with alternative strategies for addressing unique manufacturing problems.
b. Cost-effective operations by technological advancements in the current finishing method.
c. Process management that is consistent, as well as computational modelling to propose a process mechanism.
d. The MAF process has a long processing time, which can be reduced using the established method. It extracts a comparable amount of content in a shorter amount of time.

2.6 Research Objectives

From the above-mentioned research gaps, the present investigation aims to develop a new MAF Setup with following objectives-

a. Development of new magnetic abrasive for MAF process and investigation of process behaviour.
b. To study the effect of various process parameters (i.e., Voltage (DC), Voltage (PC), Magnetic abrasive size, Magnetic abrasive quantity, Machining gap, Rotational speed, finishing time, type

of abrasive etc.) Of MAF on the response such as material removal and surface roughness of different workpiece material.

c. Multi-response optimization of MAF.
d. Modelling of developed MAF process.

2.7 Research Methodology

To achieve the required MAF processing and develop its reputation, the following research methodology was used.

a. Choosing MAF parameters, main process parameters, and quality attributes.
b. Creating the MAF process and putting in place the required facilities, equipment, and resources.
c. Use Design of Experiments principles such as Taguchi orthogonal array to plan and perform the experiments.
d. To use a multi-response optimization strategy to find a balance between the chosen quality characteristics and thereby find the best solutions.
e. Verifying the findings using experimental observations and evidence from the literature.

Chapter 3

MAGNETIC ABRASIVE FINISHING - SETUP

This chapter discuss about the design, fabrication of the developed set-up for MAF process. The parts and arrangements used in this process are thoroughly explained. Further their working and specifications are also elaborated.

Introduction

The MAF process setup has been developed in the Metal cutting Laboratory, Department of Mechanical Engineering, Delhi Technological University, Delhi, India.

The arrangement of the developed experimental setup of MAF process is shown in Figure 3.1 and Figure 3.2. The experimental setup included a fixture for holding the work piece and electromagnetic tool for guiding the magnetic abrasive media or magnetic abrasive particle onto the workpiece. Power supply unit to control the magnetic flux generated by electromagnet to the face of solid cylindrical core by altering the voltage or current. Also, this power supply was capable of providing static or pulsating power supply during Direct Current (D.C) mode as wells as Alternating current source.

In this experimental set up a radial drill machine tool has been considered to work for MAF system. The function of the radial drill machine is to provide rotational motion to the core placed in electromagnet. Also, the core sleeve was attached to the machine tool spindle, and spindle also have translatory motion which maintains the working gap between workpiece surface and electromagnetic tool surface. The electromagnet was divided mainly into five parts as shown in Figure 3.3. It included core rod, bearings, spool, coil and sleeve. The wooden and nylon made fixture was used to hold the workpiece and also to absorb the minute vibration due to eccentricity between sleeve, spool, and core of the electromagnet. Along with these merits it also provides a barrier to the ferromagnetic character of machine tool fixture which would affect the magnetic field generated from tool face of electromagnet. For pulse power supply manual type of analogue controller (25 Ampere) was used. The function of the controller is to supply the current whenever the gap is maintained between both the surface for producing the magnetic field.

3.1 MAF System

In this section various MAF components such as Radial drill machine, Electromagnetic tool, power supply unit, fixture and necessary tooling systems with their working are elaborated.

3.1.1 Introduction

A radial drill machine has been considered to work for MAF system. The function of the Radial Drill machine is to provide Rotational motion to the core placed in electromagnet. Massive and rigid construction.

- Ergonomically grouped controls for operating convenience.
- Light centering of spindle.
- Precise depth release.
- Electrohydraulic clamping provided for drill head, arm & sleeve.
- Shock-free engagement of taps through clutch and spindle reverse for withdrawals.
- Machine with vertical motion capacity of 100 mm.

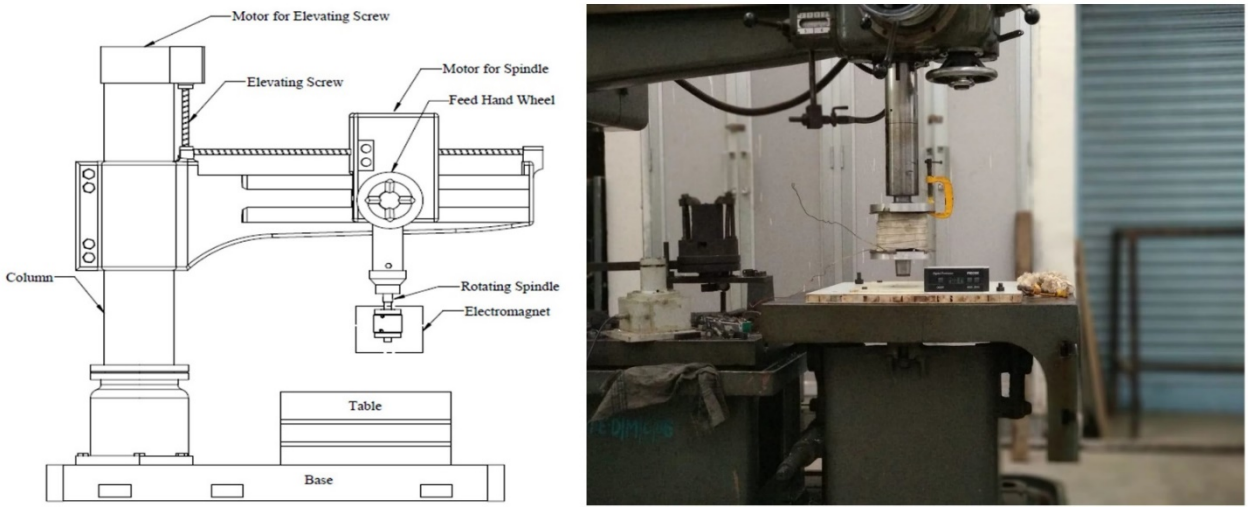

Figure 3.1 Shown Radial Drill machine as structure for MAF set-up (a) schematic (b) physical

3.1.1 Electromagnetic tool

At first, rare earth permanent magnets were used to generate magnetic field in MAF process. When MAPs were placed in the machining gap due influence of magnetic flux, MAPs get aligned according to the magnetic lines of flux and formed a FMAB. Abrasive particles get stuck in between iron particles creating a chain in the FMAB. Advantage of using permanent magnet was

that, it gave constant magnetic flux and limitation that the strength of magnetic brush could not vary according to need.

Figure 3.2 MAF setup

Initial studies conducted on MAF by using permanent magnetic field showed that it had certain limitations. To overcome the limitation, magnetic field generated by static-direct current was evolved which help in better controlling of magnetic flux and it enhanced the performance of MAF process. By using it, strength of magnetic flux could be regulated by current and voltage of electromagnet and helps in superior finishing of the surface of workpiece. Recently, work had started to maximize the scattering effect of MAPs in the magnetic abrasive brush with assistance of alternating magnetic field, produced by feeding alternating current. This new mechanism provided reciprocating motion to the abrasive particles to enhance the utilization rate of MAPs that led to higher finishing efficiency of MAF process.

Therefore, for the effective use of FMAB, a stronger magnetic field generating electromagnet design is essential part to focus on before any MAF study to carry forward. In this present study, an electromagnet is designed to use static-direct current with and without pulsating form.

3.1.1.1 Development of Electromagnetic tool

After an extensive literature survey, and various trial a final CAD model is presented in Figure 3.3 and Figure 3.4. The electromagnet was divided mainly into five parts as shown in Figure 3.4. It included core rod, bearings, spool, coil and sleeve. Figure 3.5 shows Electromagnet front view with dimension. The distorted layers of winding may produce non-uniformity in magnetic flux. Figure 3.6 represents layer by layer copper wire winding on spool during the fabrication.

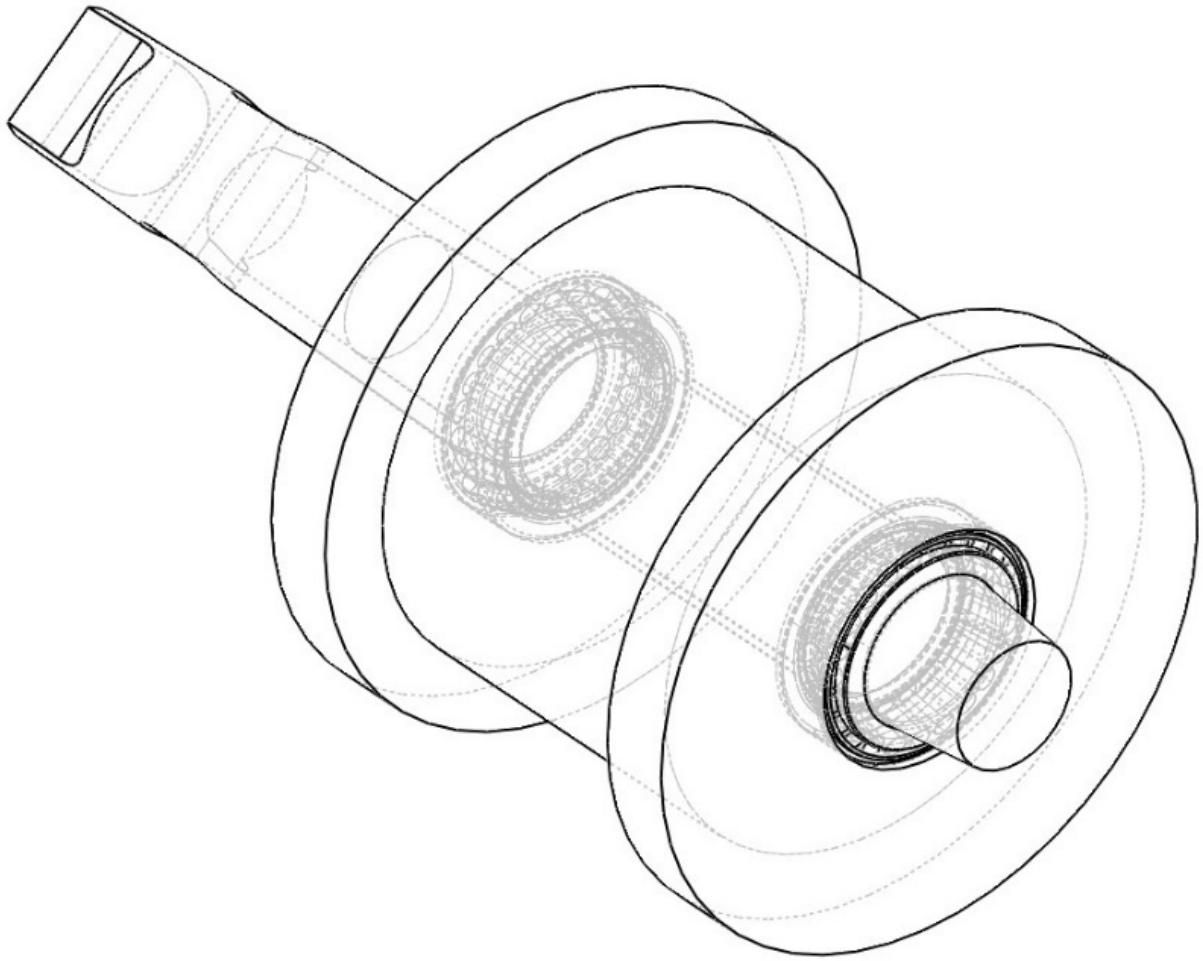

Figure 3.3 Electromagnet CAD model Isometric view

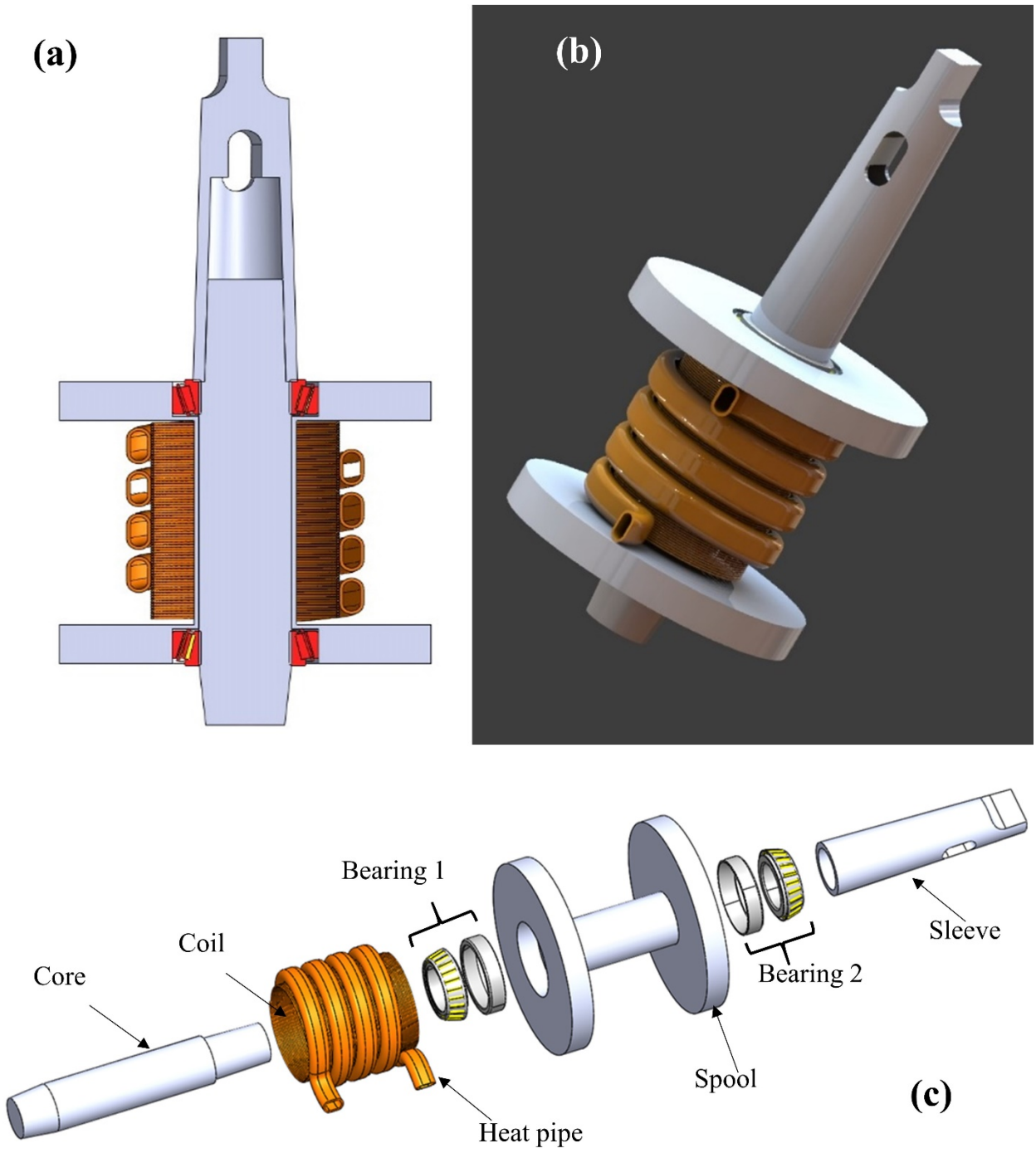

Figure 3.4 Proposed electromagnet CAD model (a) cross sectional view (b) Full rendered view (c) Electromagnet CAD model exploded view

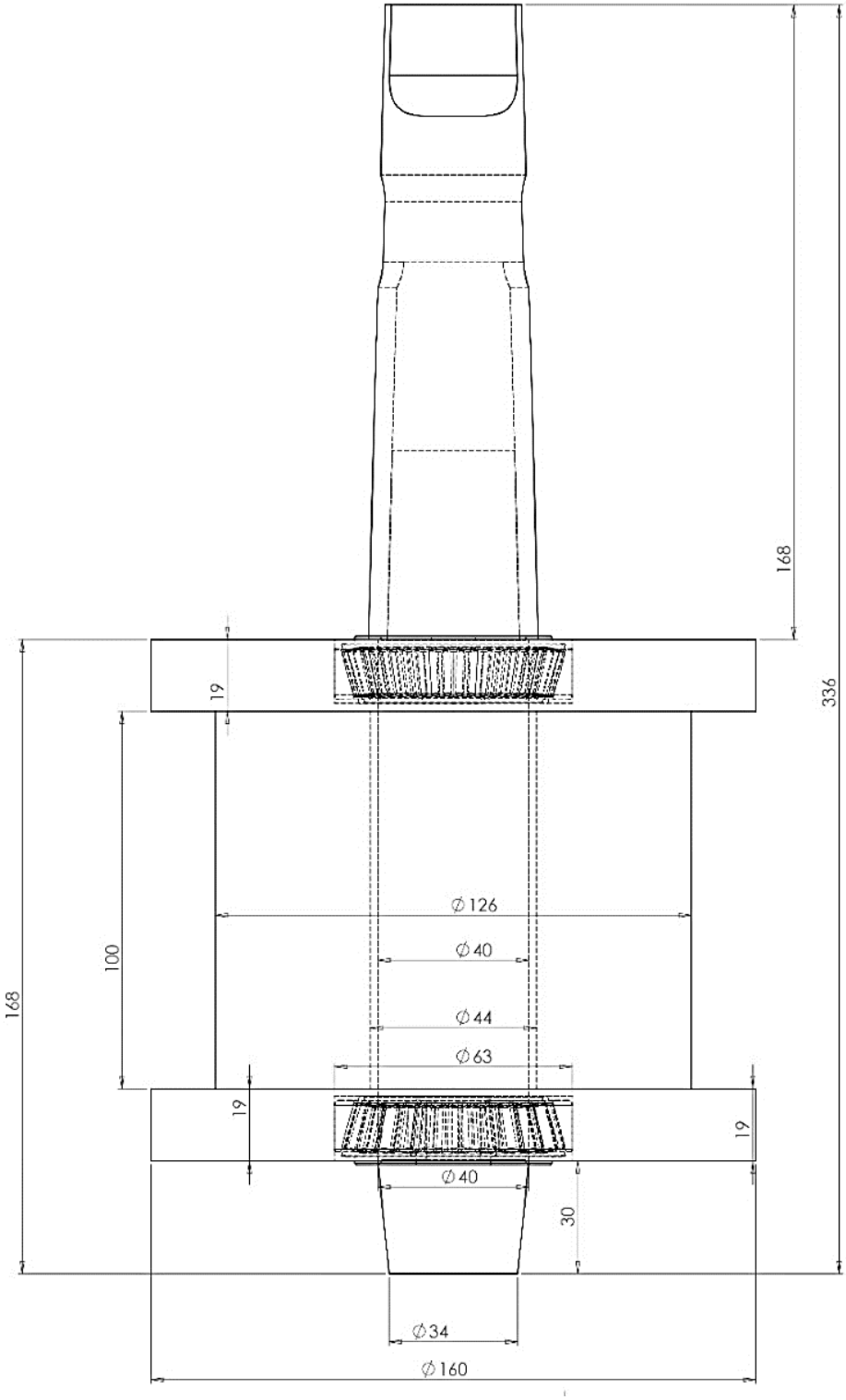

Figure 3.5 Electromagnet front view with dimension

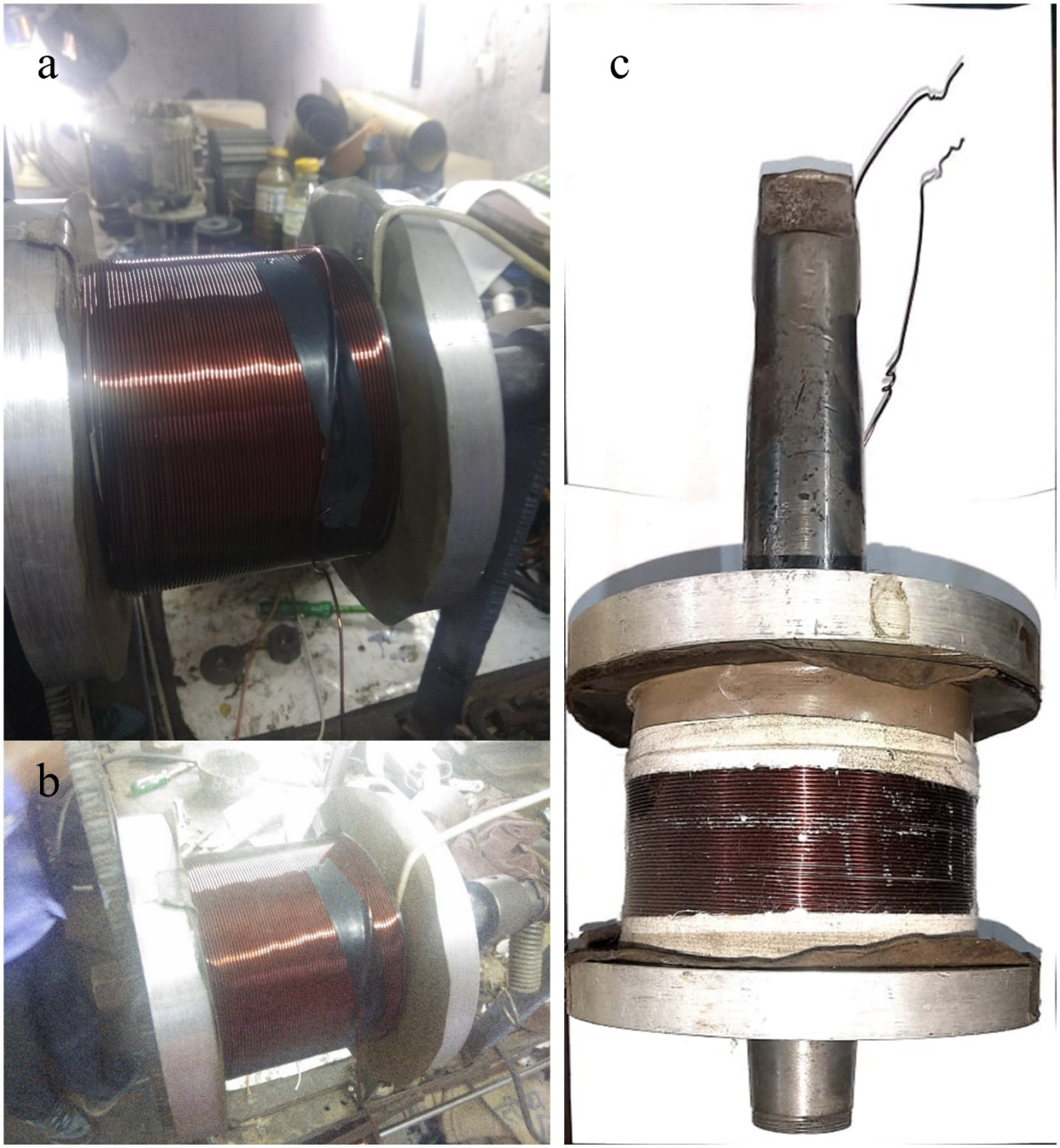

Figure 3.6 (a, b) Copper wire winding on spool, (c) Fabricated Electromagnetic tool.

3.1.2 Power Supply Unit

For pulse power supply manual type of analogue controller (25 Ampere) was used. The function of the controller is to supply the current whenever the gap is maintained between both the surface for producing the magnetic field. Figure 3.7 shows DC supply unit to control current and voltage and Figure 3.8 Arduino controller to generate pulsating power source. Figure 3.9 Digital display

of Arduino controller unit mounted on Arduino controller which displays on-off time of pulse generated.

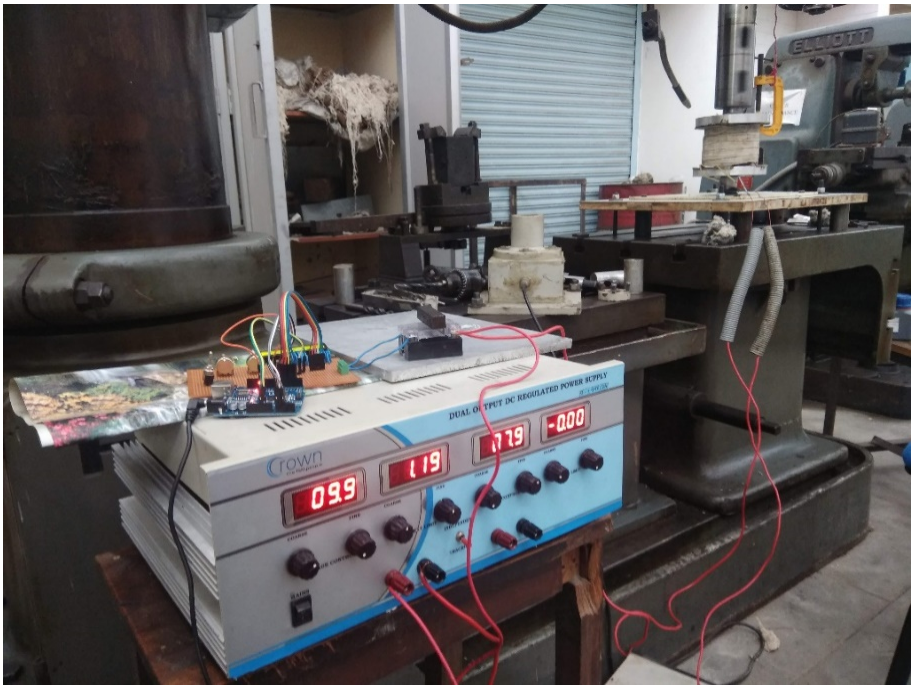

Figure 3.7 DC supply unit to control current and voltage

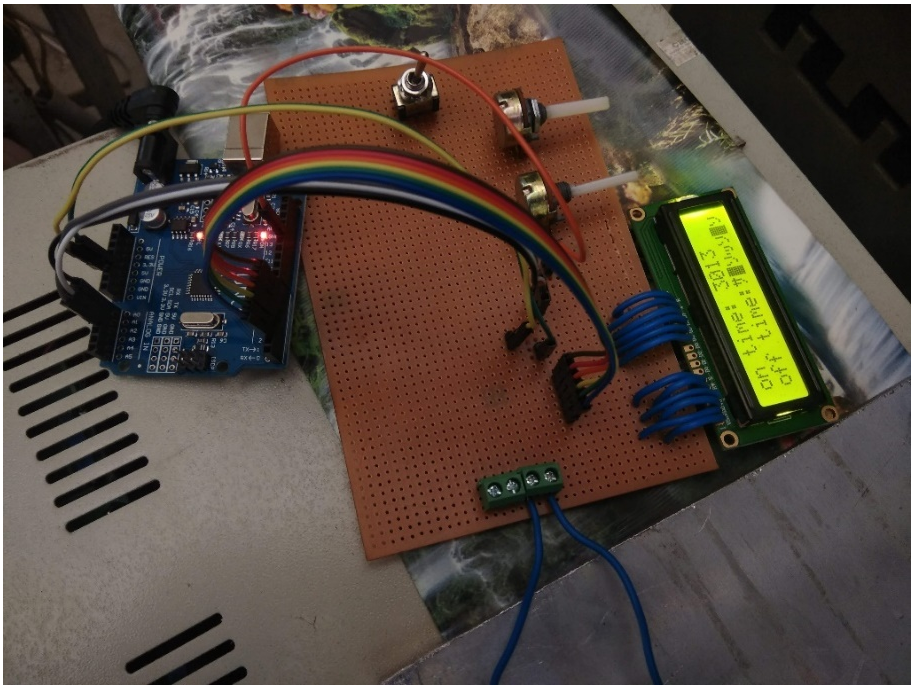

Figure 3.8 Arduino controller to generate pulsating power source

Figure 3.9 Digital display of Arduino controller unit

3.1.3 Fixture and Tooling

The function of the fixture is to hold the work piece and to maintain its position horizontally to face its surface towards tool face just over it. Square Plate made of Nylon material fixed with square wooden board piece and fixed horizontally. Digital protractor was used to maintain the fixture position at Horizontal condition. The fixture is made of Nylon because it has good wear properties. In this developed MAF Setup fixture is made in three parts containing the wooden board, nylon plate. These materials are good for Vibrational isolation and absorb majority of machine and electromagnetic tool vibration during the processing which was transferred from FMAB to workpiece. The arrangements of fixture parts and their design are shown in Figure 3.10.

Figure 3.10 Fixture

Chapter 4

DEVELOPMENT OF MAGNETIC ABRASIVE

In this chapter, an attempt has been made to prepare composite magnetic abrasive through the sintering process, which combines high-pressure compaction, crushing, and sieving for appropriate particle size using ferromagnetic carbonyl iron powder with alumina and silica as abrasive. Analysis of the elemental/phase composition analysis of the samples was used to describe the composite magnetic abrasive morphology and phase composition. Also, development of loosely bonded magnetic abrasive is discussed and their rheology characteristics is explained.

Introduction

The manufacturing of fluid systems, medical components, optical instruments, electronic components, dies and molds, electromechanical systems, and mechanical components require significantly better surface finished for critical applications [1-3]. For example, Liquid piping systems in food industries, gas tubes, vacuum tubes, and pharmaceutical containers and piping entail a smooth finished inner-surface of pipes or hollow chambers to avoid the contamination of liquid and gas [4, 5]. To achieve the surfaces mentioned above it involves high cost and sophisticated manufacturing techniques [6, 7]. Thus, advanced manufacturing and finishing processes are increasingly being developed to meet market requirements.

4.1 Magnetic Abrasives

Magnetic Abrasive Finishing (MAF), is one of the solutions which employs magnetic force to control magnetic abrasive particles for finishing of the surfaces [8, 9]. A Flexible Magnetic Abrasive Brush (FMAB) is used as a cutting tool in MAF, which consists of magnetic abrasives (ferromagnetic particles with abrasives, bonded, or unbonded) is used [37], [45], [65], [68], [81]. This flexible brush forms on the influence of the applied magnetic field as the ferromagnetic core of magnetic abrasive align themselves along the magnetic field. Also, the strength of the flexible brush depends on the intensity of the magnetic field [11, 14, 15].

S. Ahmad, R. M. Singari & R.S. Mishra (2021) Development of Al_2O_3-SiO_2 based magnetic abrasive by sintering method and its performance on Ti-6Al-4V during magnetic abrasive finishing, Transactions of the IMF, 99:2, 94-101, DOI: 10.1080/00202967.2021.1865644 (Impact Factor- 1.052)

The MAF process successfully applied for finishing, cleaning, deburring, and burnishing of metal and advanced materials [104]. For the improvement of the MAF process efficiency, various methods are employed, such as improvement in the machining setup capacity, process hybridization, parametric optimization, and by using new magnetic abrasives [16–19].

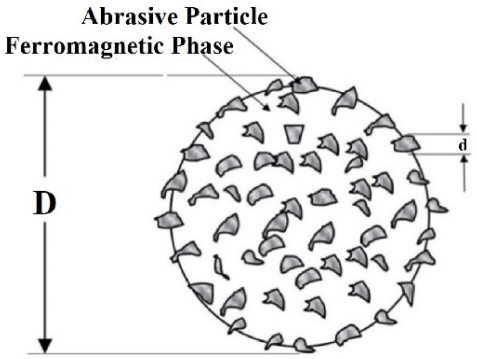

Figure 4.1 Ideal magnetic abrasive grain morphology.

Magnetic Abrasive Particles (MAPs) behave as a micro-cutting tool as well as a carrier of removed material. Thus its critical importance cannot be ignored in the MAF process [9, 12, 16]. The magnetic abrasive particles should possess the following characteristics [8, 9]: high permeability, significant susceptibility (magnetic), simple handling, and stung bonding between phases of the carbonyl iron matrix and high hot hardness of magnetic abrasive grains. The magnetic abrasive's service life depends on the material characteristics and the level of desired surface finish [9]. It also requires ease of manufacturing, low cost, and uniform shaped magnetic abrasives. Figure 4.1 demonstrates the typical single grain morphology of the MAPs where 'd' is abrasive particle size, and 'D' is the average grain size of MAPs. However, loosely bonded or unbounded magnetic abrasives can also be considered as an option due to its easy preparation process, but loosely bonded or unbonded was always ineffective when it is compared to bonded abrasive [52].

4.2 Development of bonded magnetic abrasive

4.2.1 Sintered magnetic abrasive

Bonded magnetic abrasive is a composite in the form of powder, which consists of the ferromagnetic material and ceramic hard abrasive grains [18, 19]. However, several methods have been reported for the preparation of magnetic abrasives in the open literature, based on bonded or unbonded nature [17], for example., gel-based, mechanically alloyed, adhesive-based, plasma

spraying, atomized, etc. These methods of preparation are usually time-consuming, complicated, expensive, or inefficient [13, 20, 23–25].

The level of surface roughness that can be achieved is determined by magnetic abrasive particles [19, 21, 22]. With relief, the average surface roughness (R_a) values ranging from 200 μm to 1 nm, and MAF can achieve this, representing the degree of flexibility available for a MAF setup [8]. The size of magnetic particles in the FMAB maintains the finishing forces, which was controlled by the applied magnetics force. Yet, the only particular particle size in the brush has some undesirable effects, such as the inability to grab tiny abrasives and the existence of air gaps as a consequence of a comparatively better packing [21, 10, 22].

Mixing the small magnetic particles with large abrasive particles in the FMAB can solve these issues by covering the voids present in the brush [56]. The smaller abrasive particles effectively surround the larger particles, inside the string of particles. Also, the smaller abrasive particles continuously remove the material when surface roughness decreases. A selection of the proper abrasive size and relative speed, i.e., the rotational speed of electromagnetic tool in the discussed scenario, can alter the near authority of surface quality and roughness [36]. Moreover, the shape of the magnetic abrasive is also unusual, with reduced processing capacity and low processing performance. Through existing methods, it is hard to meet the demand for mass production for commercial applications.

In this research, an attempt has been made to prepare composite magnetic abrasive through the sintering process, which combines high-pressure compaction, crushing, and sieving for appropriate particle size using ferromagnetic carbonyl iron powder with alumina and silica as abrasive. Analysis of the elemental/phase composition analysis of the samples was used to describe the composite magnetic abrasive morphology and phase composition. Also, for the confirmation of the performance of developed SMA, the MAF process has been performed on Ti-6Al-4V.

4.2.2 Materials and method

4.2.2.1 Abrasive and workpiece material

In this research work, the fabrication of alumina-silica (Al_2O_3-SiO_2) based composite magnetic abrasive or sintered magnetic abrasive (SMA) has been done by sintering of Al_2O_3-SiO_2 powder and carbonyl iron particles (CIPs). Abrasive and iron particle with their particle sizes are shown

in Figure 4.2, and the material purpose, composition, and particle size are shown in Table 4.1. Also, magnetic abrasive finishing has been performed on Ti-6Al-4V (Titanium alloy - Grade 5) workpiece. For workpiece composition, the XRF test was done. With considerable impurities, it was found that workpiece material comes under the grade 5 category of Titanium. Table 2 confirms the material composition of the workpiece material.

Table 4.1 Material purpose, composition, and particle size

S. No.	Component	Purpose	Composition (% by weight)	Particle Size (µm)
1	Al_2O_3	Abrasive	25	90
2	SiO_2	Abrasive	15	90
3	Carbonyl Iron Powder	Ferromagnetic Material	60	90, 150, 300
4	Cold Polyvinyl Acetate	Bonding Agent	5-10 of total	-

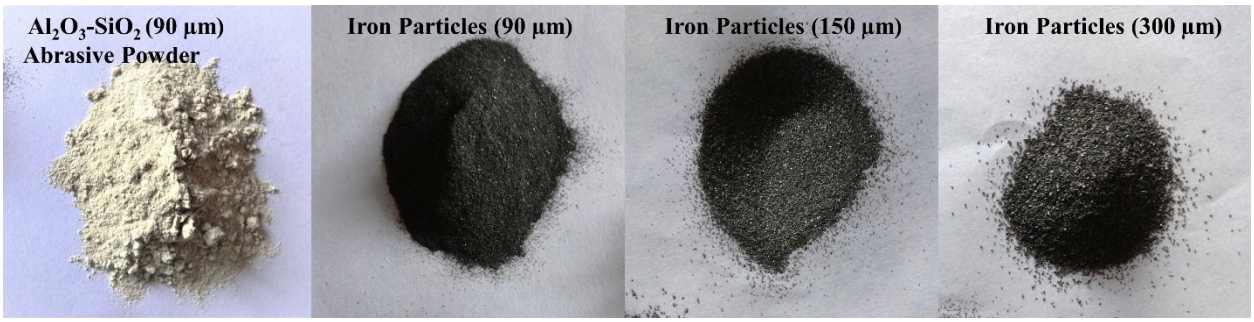

Figure 4.2 Abrasives and iron particle with their particle sizes

4.2.3 Experiment detail

The development of SMA involves the five easy steps, as shown in Figure. 4.3 and details are shown in Figure. 4.4 The first step of the process was Mixing/blending of alumina-silica (Al_2O_3 and SiO_2) powder keeping 25% and 15% by weight ratio, respectively, of total compact weight with Carbonyl iron powder (Ferromagnetic part of magnetic abrasive) keeping 60% weight ratio and cold polyvinyl acetate (PVA) solution as a bonding agent for compacts (5-10% by weight). The second step was the compacting of the mixture in a cylindrical mould, which underwent up to 200 kPa pressure. The third step includes annealing of the compacts reaching up to 1100^0C and keeping this temperature static for 2-3 hours; then, compacts were set to cool down the ambient

temperature in the same furnace, followed by Crushing of compacts in a ball mill for 1 hour and sieving into the desired size.

Figure 4.3 The stepwise procedure of SMA preparation.

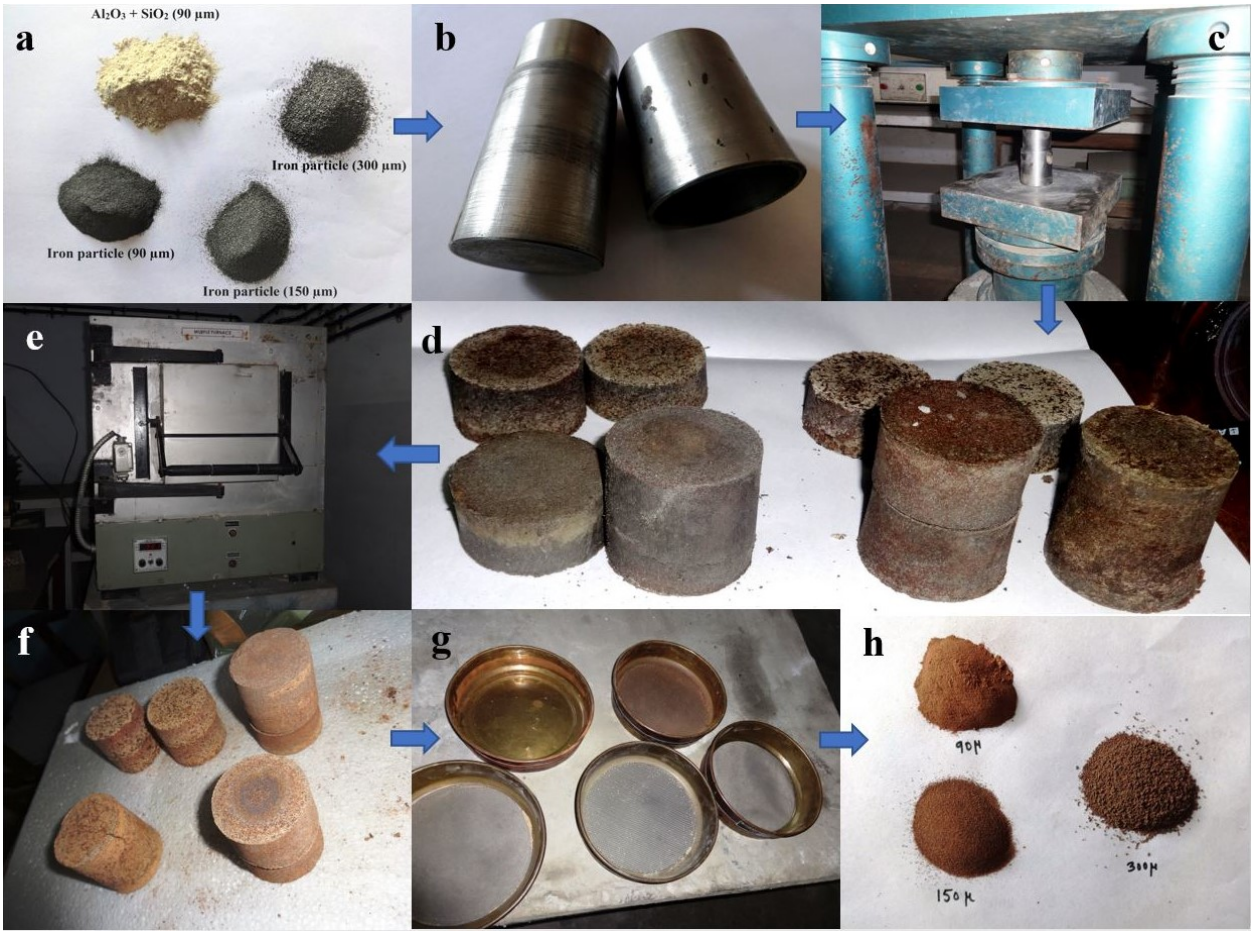

Figure 4.4 Images show sequential preparation of sintered magnetic abrasive (a) iron and alumina powder (b) piston-cylinder mould (c) compacting process, (d) raw compacts of the mixture, (e) muffle furnace, (f) sintered compacts of the mixture, (g) different sizes of sieve (h) different size of magnetic abrasives.

4.2.4 Results and Discussion

Morphology

The successful production of SMA, as shown in Figure. 4.5, which confirms the ideal magnetic abrasive grain morphology form of magnetic abrasive is mainly because of the following reasons; Appropriate control of the pressure involved in compacting and controlled annealing temperature. The larger size of the ferromagnetic particle allows a higher percentage of the abrasive particle to cover it from all sides, and in a similar fashion entire matrix was formed. There is no chemical or metallic affinity between abrasive-to-abrasive particles during the annealing process. When compacts underwent annealing process, the higher intermetallic bond affinity between ferromagnetic particles with abrasive particles allowed them to form individual magnetic abrasive. The shape of individual magnetic abrasive depends on the shape of the ferromagnetic particle chosen; hence alteration of shape from random to the ideal can be controlled easily. Appropriate

amounts of Al_2O_3 and SiO_2 can significantly influence the adequate hardness of magnetic abrasive. Active oxides of Aluminum and Silicon can decide the wedge angle of the cutting points of SMA working as a cutting tool that affects the machining action during the abrasive finishing process since carbonyl iron powder has been taken as a ferromagnetic particle for magnetic abrasive, which avoids the ploughing effect as it breaks due to its brittleness, when any impurity of targeted workpiece comes between, during the action. CIP's brittleness can be easily controlled by alloying carbon into carbonyl iron, depending upon the hardness of the workpiece. Hence useful customization could be done just by choosing the appropriate carbon percentage in the ferrous phase. Therefore, sintered magnetic abrasive (SMA) with optimized strength, hardness, and toughness, with excellent magnetic properties, high processing capacity was obtained due to the above-mentioned factors.

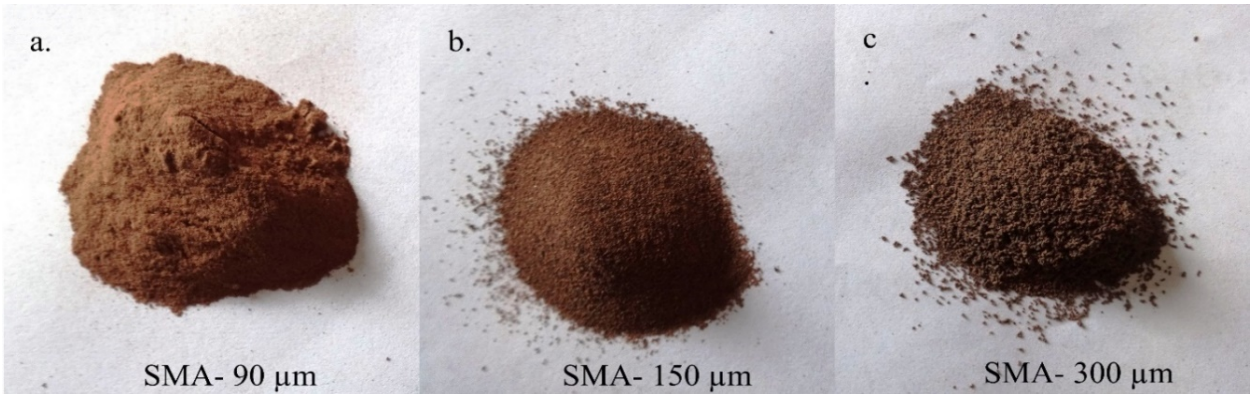

Figure 4.5 Sintered magnetic abrasives.

4.2.4.1 SEM and EDS Analysis

Figure. 4.6 represents the basic morphology of developed Sintered Magnetic Abrasive (SMA) in this experiment; Figure. 4.6a and 4.6b show SEM images of the developed SMA, which was produced by the sintering method incorporating high-pressure compaction, crushing, and sieving, respectively, at low and high magnification. Certainly, it is noticed that the prepared SMA has a good shape, and the Alumina-Silica particles are distributed evenly on the ferromagnetic core surface (see Figure. 4.6a and 4.6b). Alumina-Silica micro powder grains have not been found to form lumps. Figure. 4.6c shows that the Alumina-Silica micro-powder has excellent bonding with a ferromagnetic layer, and the abrasive grains are well integrated into the ferromagnetic matrix where powerful bonds are established between them.

The Alumina-Silica abrasive grain in Figure. 4.6b retains its original shape during this cycle compared to the morphology shown in Figure. 4.6a, and consequently, its processing potential

remains. The SMA's structure and morphology prepared by this approach suit the ideal, as shown in Figure. 4.1. In this research, any suitable alloy materials for magnetic abrasives can be easily added all through compaction, ensuing the uniform chemical composition of the magnetic abrasive. The SMA powder particles formed by this sintering process combining high-pressure compaction, annealing, crushing, and sieving have been finely-grained, have good strength and packed density with excellent soft magnetic properties, and were resistant to corrosion (due to 33.48% of oxygen as shown in Table 4.2 involved in the oxidation of aluminum, silicon, and ferrous elements). This method is relatively easy and inexpensive (the only considerable cost is the cost of fine-grained raw, abrasive particles), and is therefore very suitable for commercial production on a large scale.

Figure. 4.6a shows the low magnification SEM image of the SMA, which was prepared after the compaction, annealing, crushing, and sieving of the particles. The abrasive grains Al_2O_3 and SiO_2 are firmly embedded in the matrix of ferromagnetic cast iron is shown in Figure. 4.6b. From the Energy-dispersive spectrum (EDS) mapping of the elements shown in Figure. 4.6c, 4.6d, 4.6e, 4.6f confirms the presence of Oxygen, Ferrous, Aluminum, and Silicon only. Figure. 4.7 is about the energy-dispersive spectrum of SMA incorporating high-pressure compaction, annealing, crushing, in which the peaks of Fe, Al, and Si are clearly visible, and furthermore, it indicates that the SMA consists mainly of carbonyl iron, Alumina, and Silica.

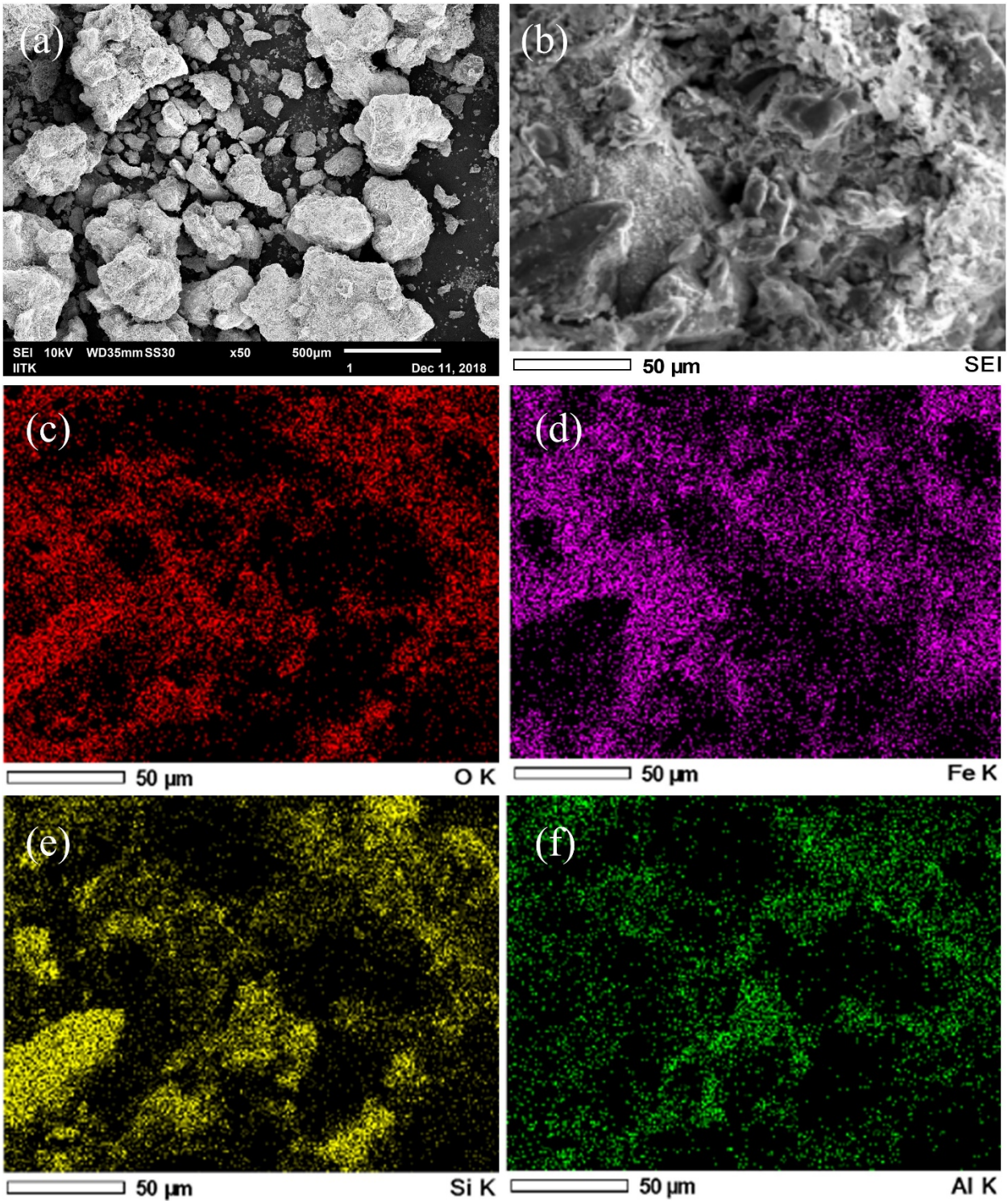

Figure 4.6 (a) Low-magnification SEM micrograph (b) High-magnification SEM micrograph (c) EDS map of element Oxygen(O) (d) EDS map of element Ferrous (Fe) (e) EDS map of element Silicon (Si) (f) EDS map of element Aluminum (Al)

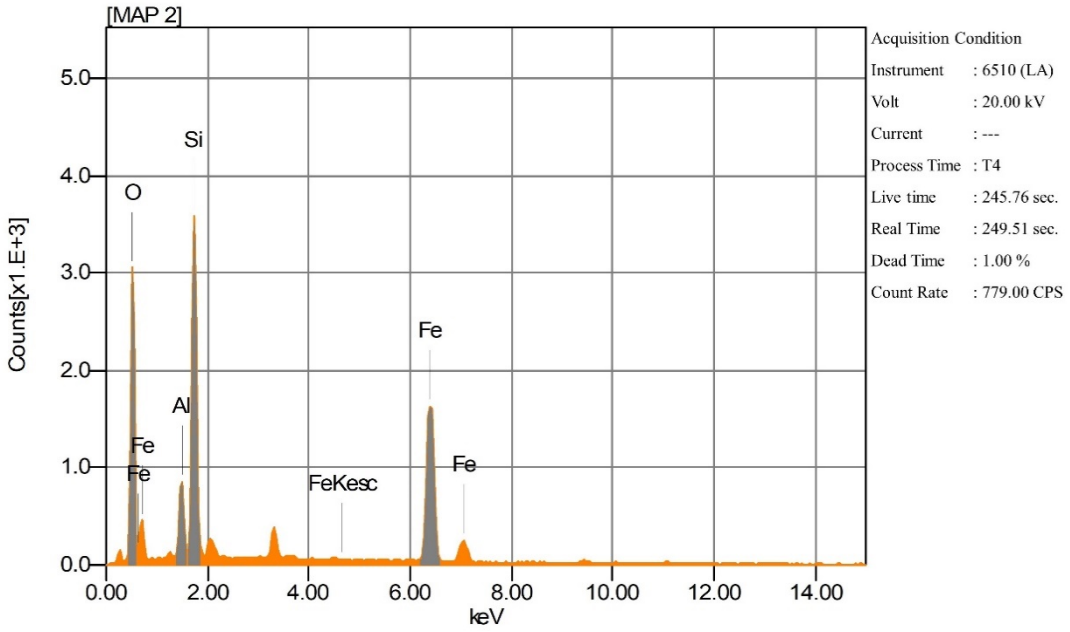

Figure 4.7 Energy dispersive spectrum of SMA (experimental)

Table 4.2 Details of the alloying element in SMA

Chemical Formula	Mass%	Atom %	Sigma	Net	K ratio	Line
Oxygen	33.48	56.13	0.08	79823	0.0271329	K
Aluminum	4.28	4.26	0.05	25298	0.0027598	K
Silica	20.44	19.53	0.10	132174	0.0161406	K
Ferrous	41.80	20.08	0.14	113947	0.0496041	K
Total	100.00	100.00				

4.2.4.2 XRD Analysis

X-ray analysis for sintered magnetic abrasive powder was conducted to examine the structural changes during the annealing process. X-ray diffraction of the SMA has been expressed in Figure.4.8. The Alumina (Al_2O_3) peaks of abrasive powder are collected in a mixture of carbonyl iron powder along with fine Al_2O_3 and SiO_2 particles, and SiO_2 peaks are covered in the background due to the presence of a marginal amount of SiO_2 particles. In addition to the prominent ferrite peaks, the X-ray diffraction of the SMA, i.e., composite powder, reveals that minor peaks of cementite, hematite, cohenite, magnetite, α- Fe-iron, and β- Fe-iron are obtained.

A part of carbon particles found in carbonyl iron powder is thought to result in the formations of iron carbides during annealing. Therefore, the formation of Fe_3O_4 is observed, suggesting that the presence of oxygen in the chamber oxidizes the composite material.

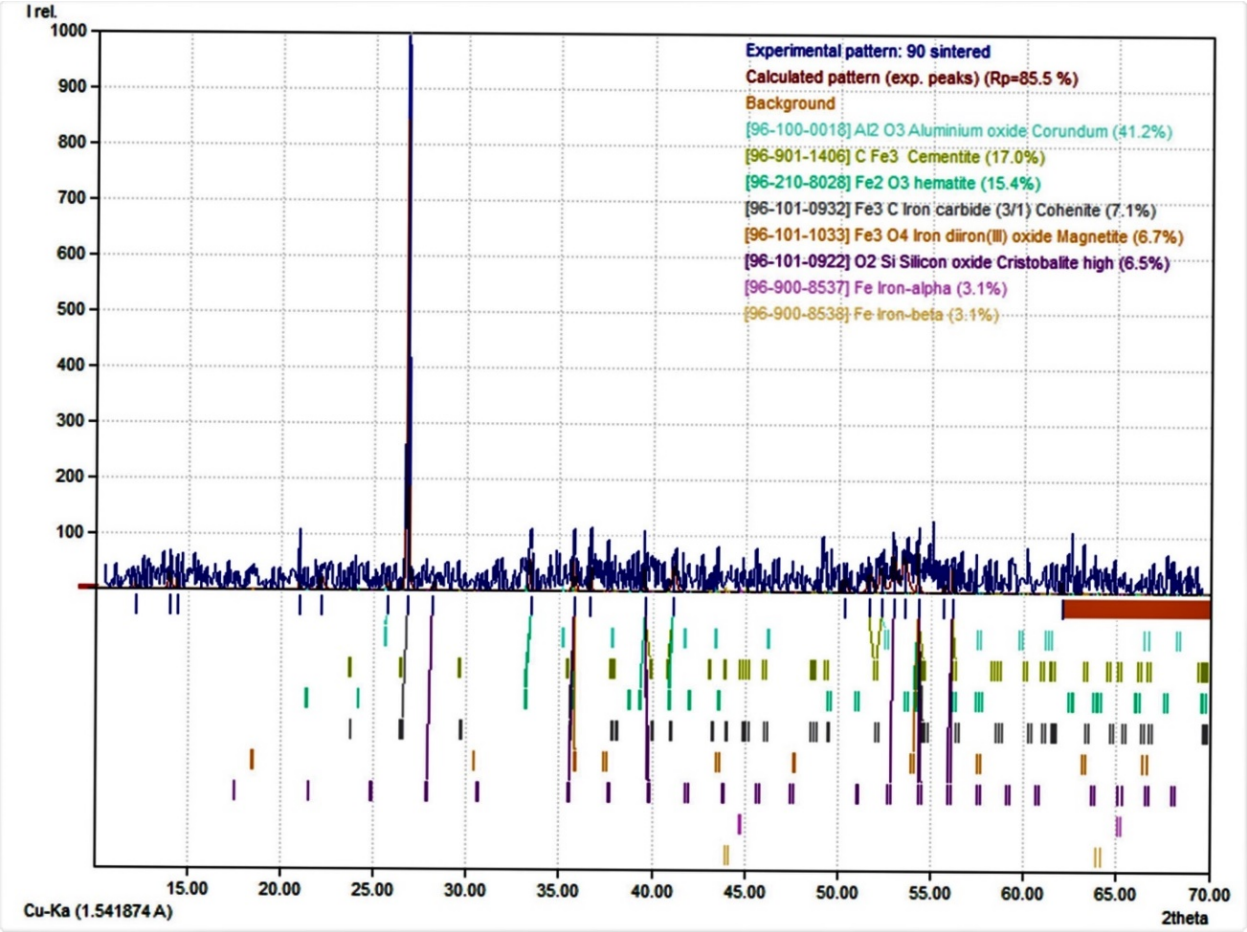

Figure 4.8 X-ray diffraction of iron-based composite sintered magnetic abrasive with Al_2O_3-SiO_2 particles.

4.3 Development of loosely bonded magnetic abrasive

Silicon Carbide and Iron particles with a lubricant mix were used as magnetic abrasive media [3]. This abrasive media comprises iron powder (300 mesh, a ferromagnetic material), Silicon Carbide (400 mesh), and lubricant (5W30, engine oil) to hold them together. SiC based loosely magnetic abrasive samples are shown in Figure 4.9. Shear stress vs Shear rate and viscosity vs shear rate plots for various compositions of iron and abrasive respectively as mentioned in Table 4.3, for 5%, 10%, 15% of lubricants are shown in Figure 4.10, Figure 4.10, Figure 4.10, Figure 4.10.

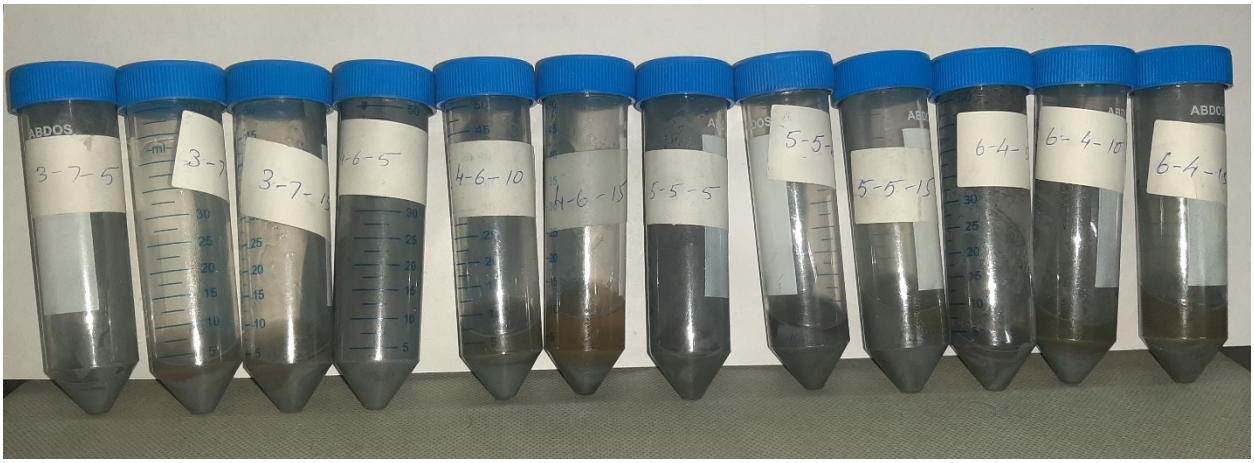

Figure 4.9 SiC based loosely magnetic abrasive samples.

Table 4.3 Sample compositions

S. No.	Iron powder 300 mesh	Abrasive (SiC), 400 mesh	Lubricant percentage
1	3	7	5
2	3	7	10
3	3	7	15
4	4	6	5
5	4	6	10
6	4	6	15
7	5	5	5
8	5	5	10
9	5	5	15
10	6	4	5
11	6	4	10
12	6	4	15

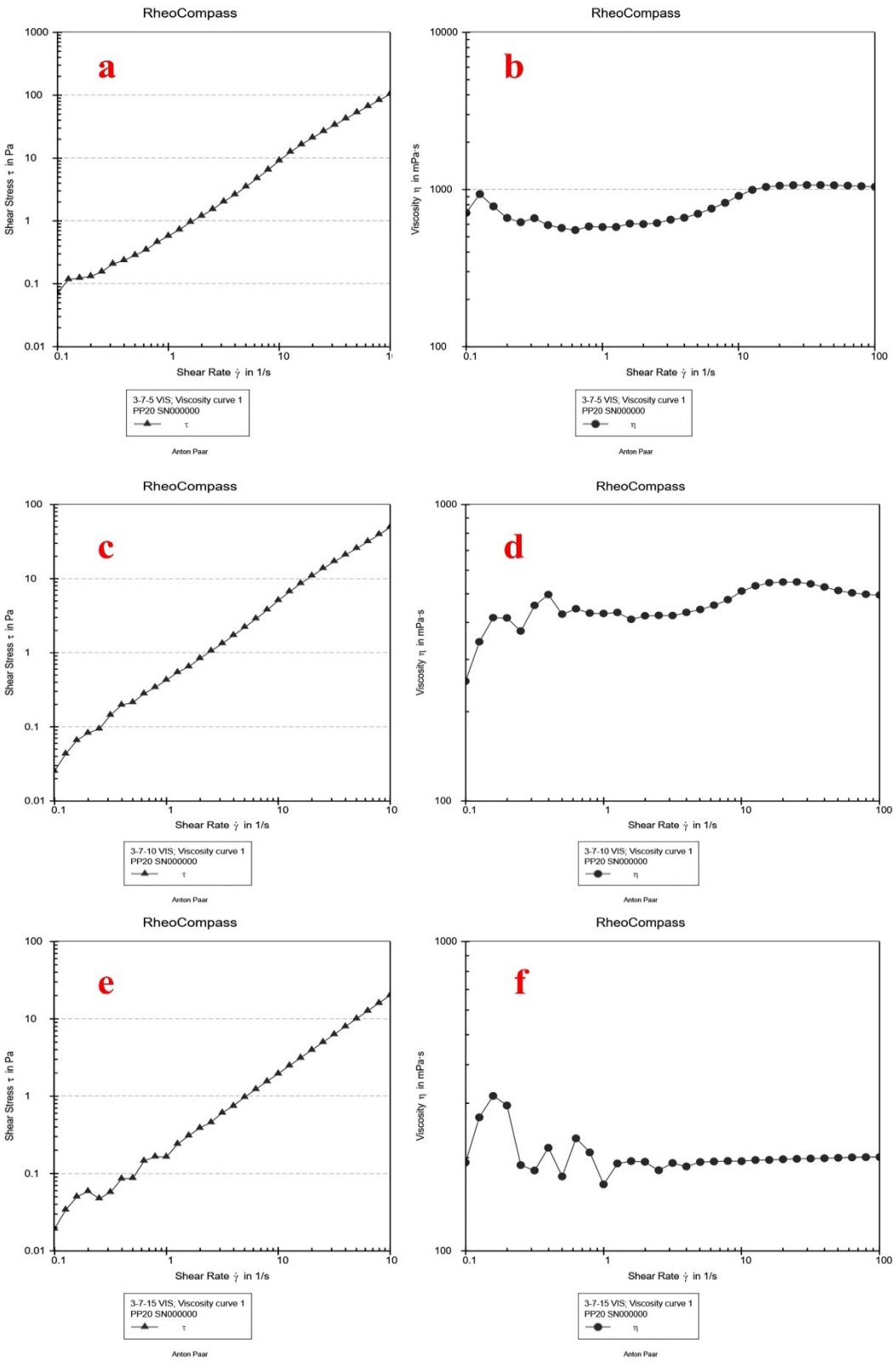

Figure 4.10 Shear stress vs Shear rate and viscosity vs shear rate plots for 3:7 ratio of iron and abrasive respectively for 5%, 10%, 15% of lubricants.

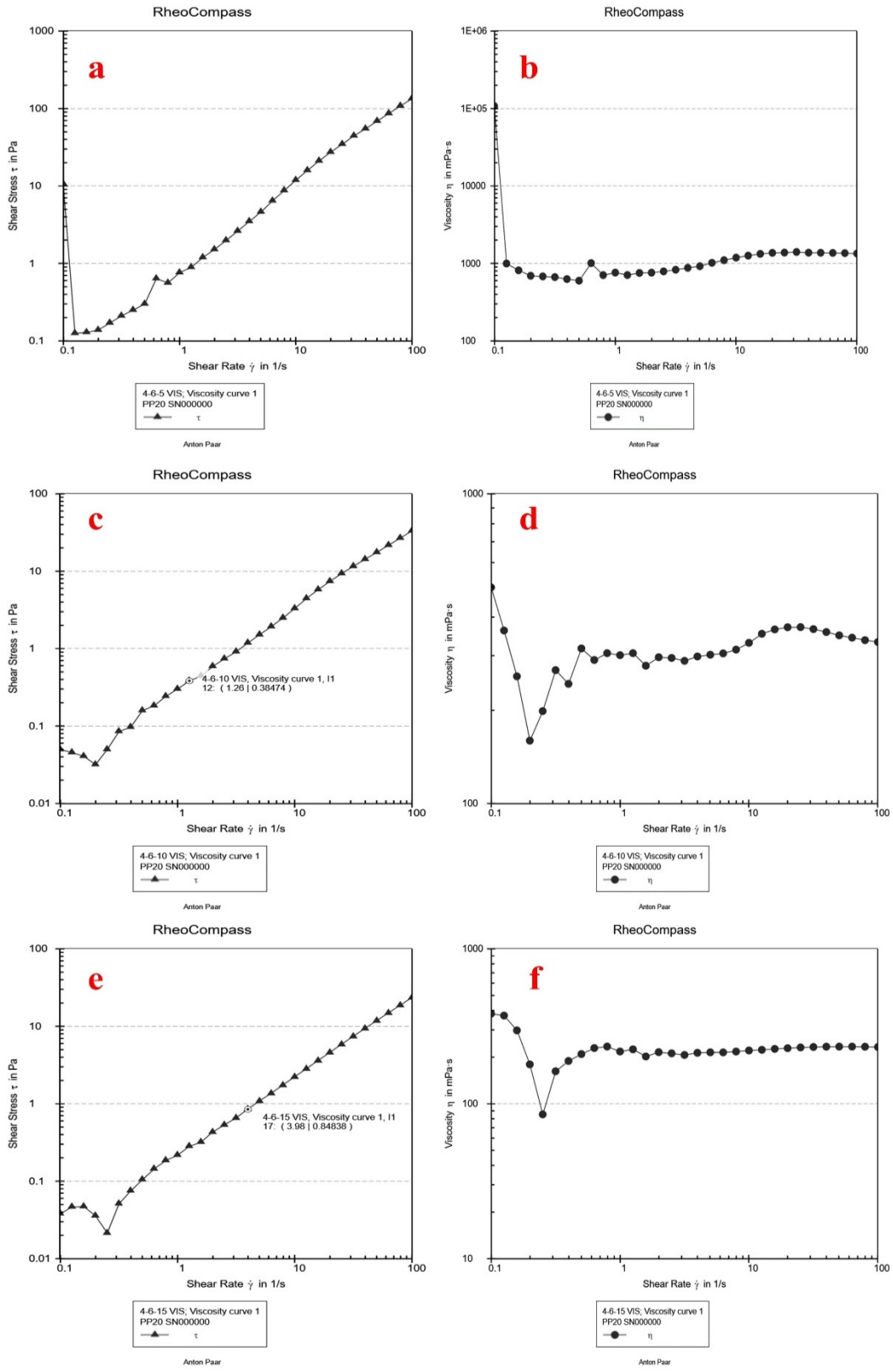

Figure 4.11 Shear stress vs Shear rate and viscosity vs shear rate plots for 4:6 ratio of iron and abrasive respectively for 5%, 10%, 15% of lubricants.

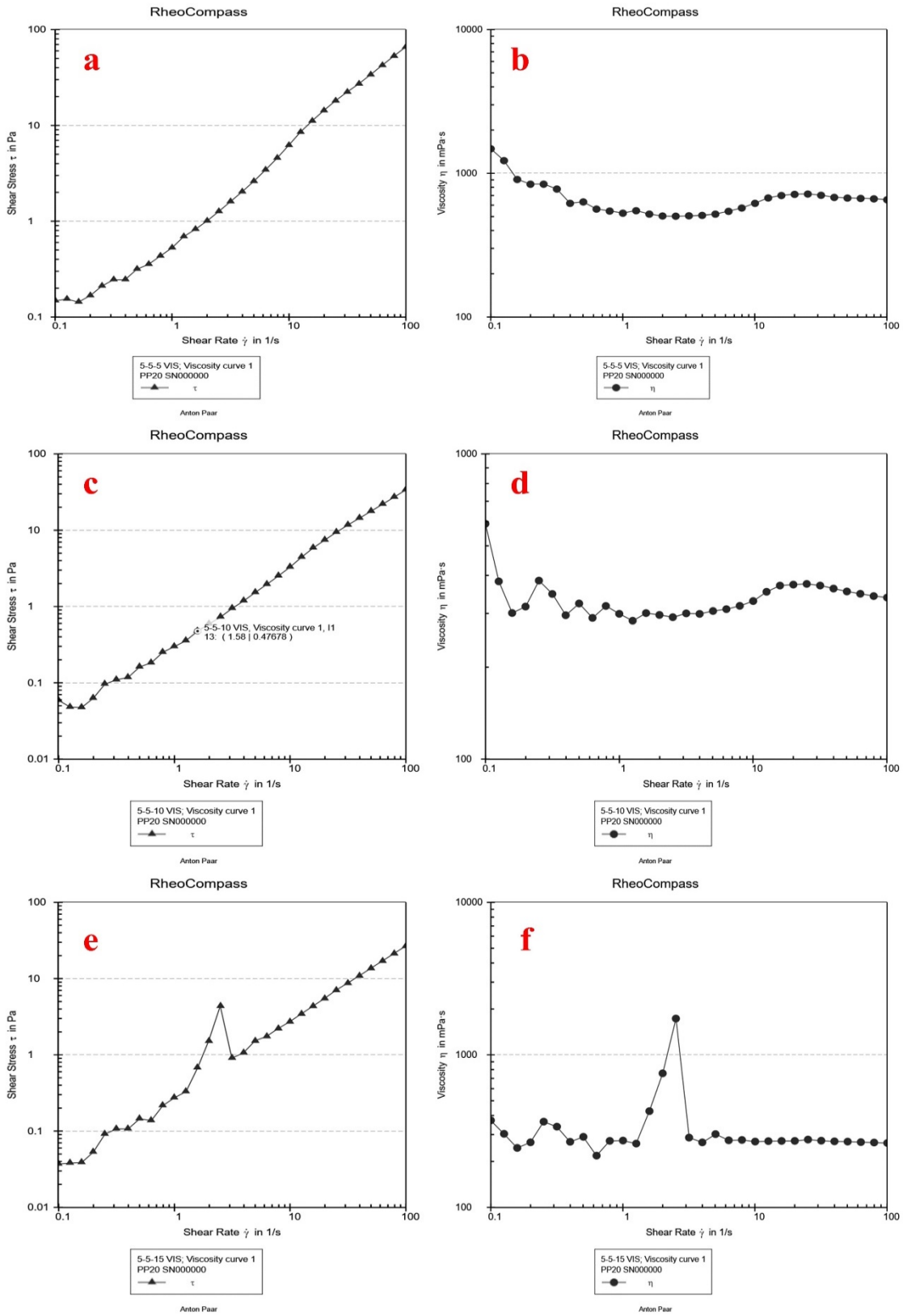

Figure 4.12 Shear stress vs Shear rate and viscosity vs shear rate plots for 5:5 ratio of iron and abrasive respectively for 5%, 10%, 15% of lubricants.

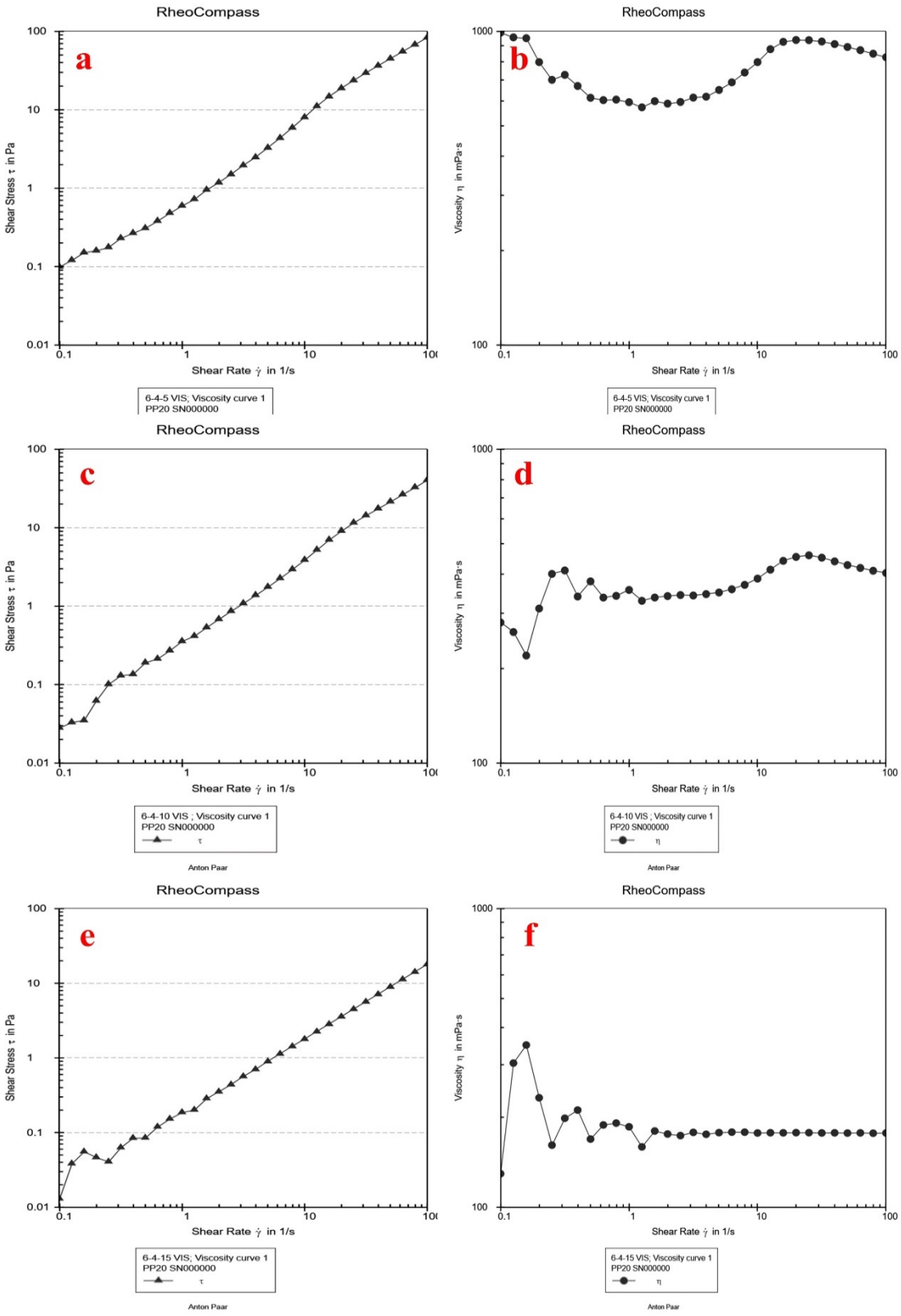

Figure 4.13 Shear stress vs Shear rate and viscosity vs shear rate plots for 6:4 ratio of iron and abrasive respectively for 5%, 10%, 15% of lubricants.

Chapter 5

EXPERIMENTAL DESIGN AND COMPUTATIONAL STATISTICS

This chapter introduces the Design of experiment for the proper planning of experiments. Further the ANN Modelling and Genetic Algorithm Optimization was studied to obtain the optimum response in the developed process.

Introduction

A well-planned and designed experiment is crucial for the derivation of cogent and accurate experimental results. Design of experiments is One such technique to accomplish this task. Essentially, the methods establish processes that facilitate deriving inferences from observations even when they are subject to some variation and are not exact. It also specifies the suitable methods which should be applied for recording experimental data. In this chapter, furthermore, the methods for proper interpretation of the recorded results have been studied. For the present investigation Artificial Neural Network and Genetic Algorithm, modelling and optimisation technique was used for the parametric study and process optimization.

The following are some of the benefits of preparing experiments for experiment design:

a. Identifies critical decision variables that monitor and improve product or process efficiency
b. Significantly decreases the number of trials
c. The best parameter settings can be discovered.
d. The experimental error may be calculated.
e. Inferences about the impact of parameters on process characteristics can be made.

5.1 Taguchi orthogonal array

It is a complex learning model which trains on a set of data, analyses and learns the pattern followed in it, and then predicts the result of a similar dataset. Dr Taguchi of Nippon Telephones and Telegraph Company, Japan has developed a method based on " Orthogonal Array (OA) " experiments which give a significantly less ‘variance’ for an experiment conducted at the optimum settings of the control parameters. Thus, the Design of Experiments optimized values of control

parameters resulted in the best experimental observations in the Taguchi method. OA provided a set of minimum, well-balanced experiments to achieve this.[111].

The concept of orthogonality has been central to the development of design theory, even in those situations where it was, deliberately, avoided. It is essential to examine the importance of orthogonality in present-day conditions. There are precisely two reasons why orthogonality might be considered important.

(a) Orthogonal structures imply a simple form of analysis in which the effects of each orthogonal factor or classification may be calculated independently of other factors: there is an associated simplicity of presentation of results.

(b) The interpretation of the effects of different orthogonal factors may, similarly, be made independently of other factors. I have already argued that the benefits of simpler forms of calculation have been substantially diminished by the power of modern computing. F or interpretation we must ask how much does non-orthogonality matter? At one extreme effect may become completely confounded and then non-orthogonality is unacceptable unless deliberately chosen. However, in general, statisticians accept that multiple regression can provide useful information when there is a non-zero correlation between parameter estimates and that some non-orthogonality is acceptable. The important question is 'How much non-orthogonality can we accept without unacceptable ambiguity of conclusions?'. The answer is sure 'None' and It is suspected that most simple and sensible non-orthogonal designs do not approach the critical level (if only we knew how to define that) except possibly for relatively low priority effects.

5.2 Regression Analysis

Many problems involve multiple, inter-related variables and the study of such multi-variate models is often of interest to the researchers. The yield of a chemical operation, for example, is proportional to the operating temperature. The chemical engineer could create a model that relates yield to temperature and use it for prediction, process optimization, or process control. Assume there is a single dependent variable or response y that is influenced by k independent or regressor variables, such as x_1, x_2, . . ., x_k. A regression model is a mathematical model that describes the relationship between these variables. A collection of sample data is used to match the regression

model. In certain cases, the experimenter is aware of the precise nature of the true functional relationship between y and x_1, x_2, . . ., x_k.

In most cases, however, the true functional relationship is uncertain, so the experimenter selects a function to approximate it. Approximating functions based on low-order polynomial models are commonly used. The design of experiments and regression analysis are inextricably linked. To promote comprehension, analysis, and implementation, researchers have stressed the importance of expressing the effects of an experiment quantitatively, in terms of an empirical model. The foundation for this is regression models.

Regression models help in the analysis of unplanned analysis, like the ones arising from uncontrolled phenomena or historical records. They are also handy in designed experiments where something might have 'gone wrong.'

5.3 Artificial neural network

In industrial science and machining technology, there are difficult problems with general principles that can be understood but are not yet amenable to scientific care. It is also stated that good engineering is responsible for achieving goals in a cost- and time-effective manner. As a result, any model that only addresses a small portion of the necessary technology is unlikely to be treated with consideration. Neural network analysis is a form of regression or classification modelling that can assist in resolving these issues when pursuing long-term solutions [112].

Despite the fact that there are simple trends that seasoned metallurgists identify and understand, there has been little progress in predicting machining activity due to their reliance on a large number of variables. It is well known, for example, that steel's hardness can be increased by making its microstructure more chaotic, causing propagating cracks to be deflected more often. Although it is unclear how much toughness is likely to increase, the qualitative relationship has been well founded via numerous studies.

In situations where the complexity of the problem is daunting for other standard models and any simplification of the problem would result in unsatisfactory results, neural network models are useful. The aim of this analysis is to show how NN methodology can be used to integrate such complex problems into quantitative models.

Artificial Neural Networks, or ANN, is a data processing model based on how the biological nervous system, such as the brain, processes data. It is made up of a large number of closely

connected processing elements (neurons) that work together to solve a problem [113]. It uses a connectionist approach to process the data in the datasets, and several functions are run on it at the same time. Neurons are linked by synapses, which each have a weight factor. ANNs are data processing models that are used to explain convoluted capacities in various applications by evaluating the nonlinear relationship between the involved, powerful determinants and the output(s). The model is made up of three layers: input, secret, and output. Many of the input variables are used in the input layer. Data is processed via one or more hidden layers through the input layer, and the corresponding output vector is computed in the final layer. The backpropagation algorithm is one of the most widely used learning algorithms. Choosing an appropriate network framework, which includes the activation mechanism and the number of neurons in the hidden layer, is one of the most difficult aspects of building an ANN model.

Deep learning is the most efficient and exciting branch of machine learning. It's a method for teaching computers to do what humans do naturally: learn by example. Deep learning is a key component of self-driving vehicles, allowing them to identify a stop sign or differentiate between a pedestrian and a lamppost. It enables voice control in consumer electronics such as phones, tablets, televisions, and hands-free speakers [114]. Deep learning has gotten a lot of press recently, and for good reason. It's producing outcomes that were previously unattainable.

A computer model learns to perform classification tasks directly from pictures, text, or sound in deep learning. Deep learning models can achieve state-of-the-art precision, even surpassing human output in some cases. Models are trained using a wide collection of labelled data and multilayer neural network architectures. Deep Learning models can be applied to a wide range of complex tasks, including:

- Regression and classification - Artificial Neural Networks (ANN)
- Feature extraction - Self-organizing maps
- Recommendation systems - Deep Boltzmann machines & Auto Encoders
- Computer Vision - Convolutional Neural Networks (CNN)
- Time Series analysis - Recurrent Neural Networks (RNN)

5.3.1 Types of activation function

Some popular types of activation functions are as follows-

i. Threshold Activation Function — (Binary step function)

A Binary step function is a threshold-based activation function. If the input value is above or below a certain threshold, the neuron is activated and sends the same signal to the next layer.

$$f(x) = \begin{cases} 0 \; if \; 0 > x \\ 1 \; if \; x \geq 0 \end{cases}$$

The problem with this function is for creating a binary classifier (1 or 0), but if you want multiple such neurons to be connected to bring in more classes, Class1, Class2, Class3, etc. In this case, all neurons will give 1, so cannot decide [115].

ii. Sigmoid Activation Function — (Logistic function)

A Sigmoid function is a mathematical function having a characteristic "S"-shaped curve or sigmoid curve which ranges between 0 and 1, therefore it is used for models where we need to predict the probability as an output.

$$\phi(z) = \frac{1}{1 + \; e^{-z}}$$

The Sigmoid function is differentiable, which means it can find the slope of the curve at any 2 points.

The drawback of the sigmoid activation function is that it can cause the neural network to get stuck at training time if strong negative input is provided.

iii. Hyperbolic Tangent Function — (tanh)

It is similar to Sigmoid but better in performance. It is nonlinear, so great we can stack layers. The function ranges between (-1,1).

$$f(x) = \; \tanh x$$

The main advantage of this function is that strong negative inputs will be mapped to negative output and only zero-valued inputs are mapped to near-zero outputs. So less likely to get stuck during training.

iv. Rectified Linear Units (ReLU)

The ReLU function is another non-linear activation function that has gained popularity in the deep learning domain. The abbreviation for Rectified Linear Unit (ReLU) is Rectified Linear Unit. The main advantage of using the ReLU feature over other activation functions is that it does not activate all of the neurons at the same time. The most common activation function in CNN and ANN is ReLU, which has a range of zero to infinity [0, ∞).

$$f(x) = \begin{cases} 0 \; if \; x < 0 \\ x \; if \; x \geq 0 \end{cases}$$

If x is positive, it returns 'x'; otherwise, it returns 0. It seems to have the same linear function problem as it is linear in the positive axis. ReLU is non-linear, and a ReLU mixture is non-linear as well. It's a strong approximator, and it can approximate any function with a combination of ReLU. The hyperbolic tangent function is 6 times better than ReLU. It can only be used on a neural network's hidden layers. As a result, for the output layer, use the SoftMax function for classification problems and a linear function for regression problems. One issue is that certain gradients are fragile and can die during training. It triggers a weight update, which prevents it from activating on any data point in the future. ReLU can result in the death of neurons [116]. Leaky ReLU was created to address the issue of dying neurons. As a result, Leaky ReLU adds a slight incline to keep the updates alive. The range of Leaky ReLU is - to +.

$$f(x) = \begin{cases} ax \; if \; x < 0 \\ x \; if \; x \geq 0 \end{cases}$$

v. Exponential Linear Unit (ELU)

It is a variant of ReLU such that the negative part of the function is a log curve.

$$f(x) = \begin{cases} a(e^x - 1) & if \; x < 0 \\ x & if \; x \geq 0 \end{cases}$$

vi. Swish

It is an activation function developed by researchers at Google, which is as computationally efficient as ReLU and performs better than ReLU on deeper models.

$$f(x) = \frac{x}{1 - e^{-x}}$$

This function ranges from negative infinity to infinity and is differentiable at all points. As it is helpful during the model optimization process, it outperforms ReLU. It is not monotonic i.e.; the value of the function may decrease even when the input values are increasing.

vii. SoftMax

SoftMax is formed by the combination of multiple sigmoid functions. Its value ranges from 0 to 1, which may be treated as the probability of a data point belonging to a particular class. Thus, SoftMax is prominently used for multi-class classification problems.

$$\sigma(z)_j = \frac{e^{z_j}}{\sum_{k=1}^{K} e^{z_k}} \; for \; j = 1, \ldots, K.$$

In multi-class classification problems, the output layer has as many neurons as the number of target classes. The output of the SoftMax function over the output values would be the probability of the input to be a part of the said classes.

Choosing the right Activation Function for a situation requires the help of some logic/heuristics. Depending on the type and properties of the problem, we can choose the optimal activation function –

- The sigmoid function and its combinations/subsidiaries are considered suitable for classification problems.
- Sigmoid and tanh functions are sometimes avoided because of the vanishing gradient problem.
- ReLU is a general activation function and is used extensively in most cases now. It should be used only in the hidden layers.
- In case 'dead' neurons are detected in the problem, the ReLU function should be replaced with the leaky ReLU function.
- Generally, the functionality of ReLU is tested, before moving on to other functions if ReLU doesn't give optimum results.

5.3.2 Training of ANN

The available dataset is usually split into three parts, usually in a 70:15:15 ratio [117]. The larger of the three datasets is used to train the ANN, while the smaller datasets are used to test and validate

it. The final outputs are compared to the expected values, the error is measured, and if the error exceeds the allowed limit, the output is sent back through the network with the required weight and bias changes. The feed-forward backpropagation (BP) algorithm's goal is to minimise the amount of the mean squared errors between the measured and realistic output values, and it does so use the gradient descent process. BP is one of the most effective algorithms for optimising a multi-layer supervised feed-forward network's weights and biases.

A neuron is trained by multiplying the input vector by a vector of weights, then adding a bias vector. This processing's output is then fed into the secret layer. After that, the sum of all the inputs is fed into a transfer function. The neural network's output is obtained in this way. After that, the output is compared to the corresponding experimental values. An error vector is produced as a result of the difference between the expected and realistic values. If the error value reaches the acceptable error limit, the output is propagated back through the network with sufficient weight and bias corrections until the desired values are achieved.

5.3.3 ANN modelling

In a neural network, several input variables can affect the method of operation, as well as the overall precision and processing speed of the network [118], [119]. The number of neurons in each hidden layer, hidden layers, the bias used, and the rate at which the network is trained are only a few of them. Since the number of hidden layers and nodes (neurons) in each layer is critical to the ANN's overall functioning and efficiency (as the network's primary processing entity), they are carefully chosen. Since there is no fixed formula for determining them, they are normally chosen by tentation. Increasing them does not always result in improved network efficiency in terms of speed and accuracy [120]. It raises the network's complexity, which, after a certain point, causes the network to slow down. If the rate of training is increased or decreased beyond a certain point, an unstable network may result. To avoid scattering, all of the input and output determinants are normalised. This implies that the determinants' values are separated by the highest value, resulting in a value between 0 and 1. The scattering of the determinants is reduced as a result.

5.3.4 Performance evaluation of ANN

To assess the output of any neural network, one can use a variety of statistical models [121], [122]. The Pearson coefficient of correlation (PCC) and mean relative error are two of the most common (MRE). Their equations are as follows:

$$PCC = \frac{\sum_{i=1}^{n}(f_{EXP,i} - F_{EXP})(f_{ANN,i} - F_{ANN})}{\sqrt{\sum_{i=1}^{n}((f_{EXP,i} - F_{EXP})^2(f_{ANN,i} - F_{ANN})^2)}}$$

$$MRE = \frac{1}{n}\sum_{i=1}^{n}\frac{\left|f_{ANN,i} - f_{EXP,i}\right| \times 100}{f_{EXP,i}}$$

$$F_{EXP} = \frac{1}{n}\sum_{i=1}^{n} f_{EXP,i} \ , F_{ANN} = \frac{1}{n}\sum_{i=1}^{n} f_{ANN,i}$$

where,

$f_{EXP} = Experimental\ values\ , f_{ANN} = ANN\ Predicted\ values$

$F_{EXP} = mean\ of\ experimental\ values\ , F_{ANN} = mean\ of\ ANN\ Predicted\ values$

5.4 Optimization Techniques

To find the best solution or unconstrained maxima and minima of continuous and differentiable functions, traditional optimization approaches can be used. There are mathematical methods for determining the best solution that makes use of differential calculus. The Genetic Algorithm (GA) is a genetic and natural selection-based search-based optimization technique. It's often used to find near-optimal or ideal solutions to complex problems that would otherwise take an eternity to solve. The objective function for ANN optimization is typically the mean square error function (loss/cost function). To minimise the objective function, we must find optimal neural network weights. Despite the fact that gradient-based search techniques like backpropagation are currently the most commonly used optimization techniques for training neural networks, it has been demonstrated that these gradient techniques are significantly restricted in their ability to 3 find global solutions. The use of global search techniques has been suggested as a possible solution to this problem. Also, in the aspect of MAF process optimization, Taguchi Method is used frequently which is already has been discussed in chapter 2.

5.4.1 Taguchi Method

To minimize uncertainty in a procedure, the Taguchi method employs a rigorous design of experiments. The method aims to provide a high-end product to the manufacturer at a low cost. Taguchi developed a method for conducting modelling tests to determine how different parameters affect the mean and variance of a process performance metric, which indicates how well the process is performing. His experimental architecture necessitates the organization of the mechanisms' affecting parameters and the levels at which they can be varied using orthogonal arrays. Rather than checking all possible combinations as the factorial architecture does, the Taguchi method tests pairs of combinations. This saves time and money by allowing the necessary data to be collected to determine which variables have the greatest effect on product quality with the least amount of experimentation. The Taguchi approach is the best option when there is an intermediate number of variables (3 to 50), few interactions between variables, and only a few variables contribute significantly [123].

Taguchi arrays can be computed or looked up. Deterministic algorithms can be used to create large arrays, while manual drawing can be used to create small arrays. The arrays used are determined by the number of parameters (variables) and levels (states). The data from the Taguchi design of experiments can be used to select new parameter values for analysis of variance optimization of the output characteristic. The philosophy of the Taguchi Method is as follows-

- Quality should be built into a commodity rather than inspected.
- The easiest way to achieve quality is to keep the variance from a goal as low as possible. The product should be designed to withstand uncontrollable environmental conditions.
- Quality costs should be calculated as a function of deviation from the norm, and losses should be calculated over the entire system.

5.4.2 Genetic Algorithm

Genetic algorithms are randomised search algorithms designed to mimic the mechanics of natural selection and genetics by replacing biological organisms with string structures and allowing strings to evolve using a randomised but standardised information exchange to obey the survival of the fittest law. This results in a new set of strings to generate per generation using the best members of the previous strings. Key features are:

- The algorithm does not work with the parameters themselves but with coding of the parameters set.
- The algorithm does not initiate its search from a single point, it does so from a group of points.
- The algorithm does not use derivatives, instead, it uses payoff information.
- The algorithm rejects the deterministic transition rules in favour of probabilistic ones.

A random procedure is used to generate an initial population of strings from a pre-specified code. This is followed by the use of a series of operators to use this population to produce sets of future populations, continuously improving every time due to the following operators acting on them- reproduction, crossover and mutation. Reproduction is a mechanism in which the string's objective function is used to determine the quality of the string. Thus, strings with higher fitness score have a better chance to produce offspring for the next generation. Crossover occurs in the mating pool where randomly selected members are mated resulting in offspring having elements of both members with exception of better fitness values. Mutation refers to the random deviation in value of a string location with the least probability which makes it effectively a method to walk randomly around the coded space. Mutation has the goal to prevent data stored in strings to be prematurely be misplaced.

5.5 Design of experiments

Design of experiments (DOE) is a branch of applied statistics concerned with the preparation, execution, analysis, and interpretation of controlled tests to determine the factors that influence the value of a parameter or group of parameters. DOE is a versatile "data collection and analysis method" that can be applied to a wide range of experiments [111]. It helps you to experiment with a variety of input variables to see if they affect the final result (response). DOE may detect essential connections that may be missed when dealing with one element at a time by controlling several inputs at the same time. Both possible combinations can be investigated (full factorial) or only a subset of the possible combinations can be investigated (partial factorial) (fractional factorial).

Any experimental issue has two parts: the experiment design and the statistical analysis of the results. Since the method of analysis is directly dependent on the template used, these two topics are closely related. An experiment that is carefully designed and carried out will reveal a lot about

the impact of one or more variables on a response variable. In several experiments, some variables are kept constant while the levels of another variable are changed. As opposed to adjusting factor levels concurrently, this "one factor at a time" approach to process information is inefficient. Many of today's "statistical methods" to planned experiments are based on R. A. Fisher's work from the early twentieth century. Fisher explained how taking the time to think about the design and implementation of an experiment before attempting it helped avoid common research issues. Randomization, replication, and blocking are all important principles in designing an experiment [124].

- **Randomization:** The use of statistical methods in experimental design is built on the foundation of randomization. By randomization, we say that both the experimental material distribution and the order in which the individual runs of the experiment will be performed are calculated at random. Statistical methods demand that the observations (or errors) be randomly distributed random variables with independent distributions. This assumption is generally correct due to randomization. A randomised series helps to minimise the influence of factors that are unknown or uncontrollable.
- **Replication:** A full experimental procedure is repeated.
- **Blocking:** It's a design technique for increasing the precision with which comparisons between variables of interest are made. Blocking is often used to minimise or remove uncertainty transmitted by nuisance factors, i.e., factors that may affect the experimental response but are not directly relevant to us. When randomising a factor is impractical or prohibitively expensive, blocking allows you to limit randomization by conducting all trials with one setting of the factor and then all trials with the other setting.

A well-conducted experiment can address questions like:

1. What are the most important factors in a process?
2. Under what conditions will the mechanism work satisfactorily?
3. What are the processes' primary, dominant, and interaction effects?
4. What settings will result in less performance variation?

Chapter 6

EXPERIMENTAL INVESTIGATIONS

In this chapter the basic parameters of the MAF method, as well as the workpiece material and geometry used for experimentation, are described. In addition, the response characteristics chosen for this study are described in detail. Experiments were conducted according to Taguchi's orthogonal array and non-orthogonal array. Variable parameters such as current or voltage to the electromagnet, machining gap, rotational speed, working gap, and finishing time etc with their levels were selected to optimize the parameters for the responses, such as a change in surface roughness, change in microhardness, Change in modulus of elastic indentation. Precisely, this chapter discusses experimental investigations, parameters, responses, material and testing methods.

6.1 Selection of process parameter and their ranges

To get better surface roughness produced by the MAF process, the optimal level of MAF process parameters need to be determined. Based on the literature review, process variables of the MAF process were arranged in the following three categories:

a. **The Machine based Parameters:** Machining/working gap, rotational speed/relative speed.
b. **The Magnetic Abrasive Parameters**: magnetic abrasive composition, abrasive grain size, viscosity,
c. **The Workpiece Based Parameters:** work piece material hardness, surface roughness of work piece.

6.2 Basic MAF process parameters

The process parameters listed have been selected based on the earlier studies.

6.2.1 Magnetic flux control parameter

6.2.1.1 Current

Current supplied to the electromagnet to alter the magnetic flux.

6.2.1.2 Voltage

Voltage applied to electromagnet to alter magnetic intensity.

6.2.2 Machining gap

The space between the flat workpiece and flat-faced, pole (known as working gap/machining gap) is filled with a mechanically mixed homogeneous mixture of abrasives and ferromagnetic particles (known as magnetic abrasive particles).

6.2.3 Rotational speed

The relative rotational motion between tool and workpiece. This motion provides the material removal mechanism to begin.

6.2.4 Type of magnetic abrasive

Natural abrasives, such as Diamond, Garnet, Corundum, and Quartz, can be found in the earth's crust as minerals or rocks. Artificial or synthetic abrasives are made from a variety of materials and have very high hardness. Carborundum, Aluminum Oxide, Silicon Carbide, and other artificial abrasives are examples. When these abrasives are mixed with ferromagnetic material they form magnetic abrasives. There are two types of abrasives: Unbonded Abrasives or loose magnetic abrasives and Bonded or Synthetic used as per the requirement of level of material removal or level of surface roughness.

6.2.5 Abrasive composition

The ratio of the mixture of the abrasive and ferromagnetic particle. Since ferromagnetic material is used for magnetic abrasive to get influenced on the magnetic field which ultimately gets forced onto the target surface by magnetic pressure. Whereas the abrasive particle used for abrasion. Therefore, it is very obvious that their ratio will affect the MAF process.

6.2.6 Time of finishing

Finishing time for an individual experimental run.

6.3 Workpiece material

Ti-6Al-4V/Titanium (Grade-5) was the workpiece material for the study to obtain the MAF performance over it. The elemental composition (wt.%) of the workpiece material was obtained

using the XRF (X-ray fluorescence) test, which comes under the prescribed limit of the grade-5 category of Titanium and shown in Table 6.1 Also, the Vickers Hardness test was done on the workpiece, and it was found around 387.

Table 6.1 The weight percent of the Material composition

Elements	**Ti**	**V**	**Al**	**Fe**	**Mn**	**Zn**	**Mo**
Wt.%	92.04	4.43	3.01	0.33	0.19	0.031	0.026

6.4 Response characteristics

6.4.1 Change in surface roughness

In the ultrasonic cleaner, the workpieces are cleaned. At the end of each experiment, the fixture and workpiece are taken out from the MAF setup. After cleaning, the change in surface roughness value (Ra) is measured by using a Taylor Hobson Precision Surtronic 3+ surface roughness tester to measure Ra (centre line average value) before and after magnetic abrasive finishing at three different points from the centre of the workpiece. Ra refers to the difference between these two Ra values (before and after MAF) at the same place. The measurement was carried out by moving the stylus in the same place, perpendicular to the lays obtained during the procedure.

For the Change in Surface Roughness (ΔR_a) in "µm".

$$\mathbf{\Delta R_a\ (\mu m) = R_{a\ (initial)} - R_{a\ (final)}}$$

6.4.2 Change in microhardness

Instrumented indentation measurements were used to derive the F-d-curves and the material's indentation hardness. The experiments were carried out on the Micro Hardness Testing HM 2000 S, which was fitted with a Damper system: 4 damper pads on a stone plate, specimen size: min. 6 mm, hardness measurement range: 0.001 - 120 000 N/mm^2 near diamond hardness, test load range: 0.1 - 2000 mN, hardness measurement range: 0.001 - 120 000 N/mm2 near diamond hardness. To characterise the indentation size effect and find the indentation load value, which will result in a reliable hardness value, indentation measurements of the before and after polished sample with differing maximum loads were carried out in the first stage.

Here in this study Change in the microhardness (ΔHV) in Vickers hardness taken as one of the response parameters during MAF processing, which is calculated as below-

$$\mathbf{\Delta HV = HV_{(initial)} - HV_{(final)}}$$

6.4.3 Change in modulus of elastic indentation

The Fischer-scope HM2000 S is a high-tech nanoindentation gauging tool that can also be used to determine the indentation modulus. This Fischer-scope HM2000 S is tested as per the ISO 14577-1 and ASTM E 2546 standards. It also analyses factors in the micro and nanometre scale. It comes with an HT2000 measuring head that houses the test load generator, indenter, and position measurement unit for measuring indentation depth. Variable factors influenced changes in the Modulus of Elastic Indentation (EIT) in GPa in this research study.

Where,

$$\mathbf{\Delta EIT\ (GPa) = EIT_{(initial)} - EIT_{(final)}}$$

6.5 Testing and Characterization

- Taylor Hobson Precision Surtronic 3+ surface roughness tester for workpiece before and after conditions.
- Micrographs of surface texture were taken using a sipcon multi-sensor CNC inspection system (SVI-5300-CNC-VT).
- For Scanning Electron Microscopy, Carl Zeiss EVO MA 18 model was used, which was upgraded with Energy dispersive spectrum (EDS-Oxford INCA x-act) facility.
- X-ray diffractometer (XRD), Brukar 8D advanced system having CuKα (λ~1.54 Å) source of radiation.
- Asylum Research MFP3D-SA model was used for atomic force microscopy.
- The strength of magnetic flux in the working gap was measured by EMF-PORTABLE digital gaussmeter having a measuring range of '0 T - 2.0 T'.
- Microhardness and modulus of elastic indentation were measured using Micro Hardness Testing HM 2000 S, the tester is shown in Figure

Figure 6.1 Taylor Hobson Precision Surtronic 3+

Figure 6.2 Sipcon multi sensor CNC inspection system

Figure 6.3 EMF-PORTABLE digital gaussmeter

Figure 6.4 Micro Hardness Testing HM 2000 S

6.6 Phases of experiments

This research work is distributed in Phases, discussed as following-

6.6.1 Phase 1

For the confirmation of the performance of developed SMA, the MAF process has been performed on Ti-6Al-4V. The parameters chosen according to the literature survey [4, 19, 30] was- current to electromagnet= 1.6 A, rotational speed= 300 rpm, working gap= 1.5 mm, and finishing time = 15 min for experiment, Control factors, value and units is shown in Table 6.2. Surface roughness profiles were determined with the help of Taylor Hobson Precision Surtronic 3+ surface roughness tester for workpiece before and after conditions. Micrographs of surface texture were taken using a sipcon multi-sensor CNC inspection system (SVI-5300-CNC-VT). For Scanning Electron Microscopy, Carl Zeiss EVO MA 18 model was used, which was upgraded with Energy dispersive spectrum (EDS-Oxford INCA x-act) facility. The diffraction patterns of SMA were obtained from X-ray diffractometer (XRD), Brukar 8D advanced system having CuKα (λ~1.54 Å) source of radiation. Asylum Research MFP3D-SA model was used for atomic force microscopy.

Table 6.2 Control factors, value and units

Parameters	**Value**
Current to electromagnet	1.6 A
Rotational speed	300 rpm
Working gap	1.5 mm
Finishing time	15 min

6.6.2 Phase 2

The Taguchi technique is a prevailing tool for designing, arrangement, and collection of experimental data in a controlled way. It also tells us the effects of process variables over some particular variables for the design of efficient systems, and simultaneously, it reveals the effects of uncontrolled factors [2, 3].

The L_9 orthogonal array for three levels and three factors was used by Ahmad et al. [36], each row of each array (three different arrays set for three different abrasives size, for investigation of a good range of abrasive size) represents the trial situation with a combination of factors. Columns were corresponding to each control parameter or process variable in the array, and there were nine combinations as it is in the L_9 orthogonal array. The response parameter was, change in Surface Roughness (ΔR_a). This technique has been effectively utilized by numerous researchers to understand the finishing impacts during the MAF process[4-6]. Nevertheless, the satisfactory decision of the researched parameters (control factors) is fundamental.

Table 6.3 Control factors, units, definition, and levels

Control Factor	**Unit**	**Definition**	**Level 1**	**Level 2**	**Level 3**
Abrasive Size(d)	μm	The average size of abrasive particles	90	150	300
Voltage (V)	Volts	Voltage applied to electromagnet to alter magnetic intensity	6	12	18
Machining Gap (x)	mm	The gap between the electromagnetic tool and workpiece	1	1.5	2
Rotational speed (S)	rpm	The relative rotational motion between tool and workpiece	60	90	120
Time will be 20 min for each run.					

Table 6.4 Experimental Design

Exp. Run	**Abrasive Size**	**Voltage**	**Machining Gap**	**Rotational Speed**	**Experimental ΔR_a (A)**
1	90	6	1	60	0.13
2	90	6	1.5	90	0.11
3	90	6	2	120	0.11
4	90	12	1	90	0.21
5	90	12	1.5	120	0.14
6	90	12	2	60	0.11

7	90	18	1	120	0.23
8	90	18	1.5	90	0.17
9	90	18	2	60	0.15
10	150	6	1	60	0.15
11	150	6	1.5	90	0.14
12	150	6	2	120	0.13
13	150	12	1	90	0.24
14	150	12	1.5	120	0.15
15	150	12	2	60	0.13
16	150	18	1	120	0.25
17	150	18	1.5	90	0.19
18	150	18	2	60	0.18
19	300	6	1	60	0.11
20	300	6	1.5	90	0.10
21	300	6	2	120	0.12
22	300	12	1	90	0.17
23	300	12	1.5	120	0.16
24	300	12	2	60	0.10
25	300	18	1	120	0.21
26	300	18	1.5	90	0.16
27	300	18	2	60	0.14

The observations in this examination were led according to a Non-orthogonal array [28, 29] as per machining set-up restrictions. The determination of the non-orthogonal array depends on relying on the prerequisite that did not fit by the orthogonal array. Table 6.3 shows the control factors, their units, definition, and levels. It is notable that the control factors level is non-uniform for abrasive size because of sieve size restriction. The experimental data [36] presented in Table 6.4 has been used to develop the ANN model. The following observations were set in a fashion using an L_{27} non-orthogonal array with four inputs and one output. The input parameters were abrasive size, voltage, machining gap, and rotational speed. The Change in Surface Roughness (ΔR_a) was an output/response parameter, measured in microns (μm).

This current research study explains the development and application of an artificial neural network and genetic algorithm (ANN-GA) as a modelling and optimisation tool that is used to improve the performance of the magnetic abrasive finishing of SS302. In addition, the results from ANN-GA modelling and optimisation have been compared with conclusions drawn from conventionally used Taguchi-ANOVA analysis. The Taguchi-ANOVA method is used to analyse the data for comparison.

6.6.3 Phase 3

This research describes the development of an artificial neural network and genetic Algorithm (ANN-GA), a modelling and optimization tool that is used to optimize a tri-objective problem. Parametric study of DC sourced magnetic abrasive finishing process. Effect of process parameters on Microhardness, Modulus of elastic indentation along with the surface roughness has been studied. Furthermore, the effect of loosely bound SiC-based magnetic abrasive media and its composition on the performance of the finishing quality on Ti-6Al-4V has been studied.

Ti-6Al-4V/Titanium (Grade-5) was the workpiece material for the study to obtain the MAF performance over it. The elemental composition (wt.%) of the workpiece material was obtained using the XRF (X-ray fluorescence) test, which comes under the prescribed limit of the grade-5 category of Titanium. Also, the Vickers Hardness test was done on the workpiece, and it was found around 387. Silicon Carbide and Iron particles with a lubricant mix were used as magnetic abrasive media [44]. This abrasive media comprises iron powder (300 mesh, a ferromagnetic material), Silicon Carbide (400 mesh), and lubricant (5W30, engine oil) to hold them together during the finishing. The various proportion of the magnetic abrasive media in terms of abrasive composition in weight percentage according to the design of experiments employed in the present study has been mentioned in Table 6.5.

Table 6.5 Composition of Magnetic abrasive media

Constituents	**% weight concentration**				**Mesh size**
Iron powder	60	50	40	30	300
Abrasive (SiO2)	40	50	60	70	400
lubricant	10-20% of the total				-

6.6.3.1 Experimental details

In the current research study, an electromagnet with a pole end face of 34 mm diameter connected by a DC pulse source of power (for variation of current see Figure. 6.1). The electromagnet was provided a different current combination of 0.8 Amp, 1.2 Amp, 1.6, Amp, and 2.0 Amp generate a varying intensity of the magnetic field at the pole end face. The electromagnet pole were positioned in such a way that its faces targets the surface of the workpiece, after that FMAB was created by slowly introducing the abrasive magnetic media in presence of the magnetic field between the machining gaps [55], [73]. The separation between the workpiece facial portion and the electromagnetic pole or tool face is well-known as the working or machining gap [18]. Figure.6.2(a). shows the electromagnetic tool over workpiece fixtured and Figure. 6.2(b). shows the FMAB formed from the electromagnet used.

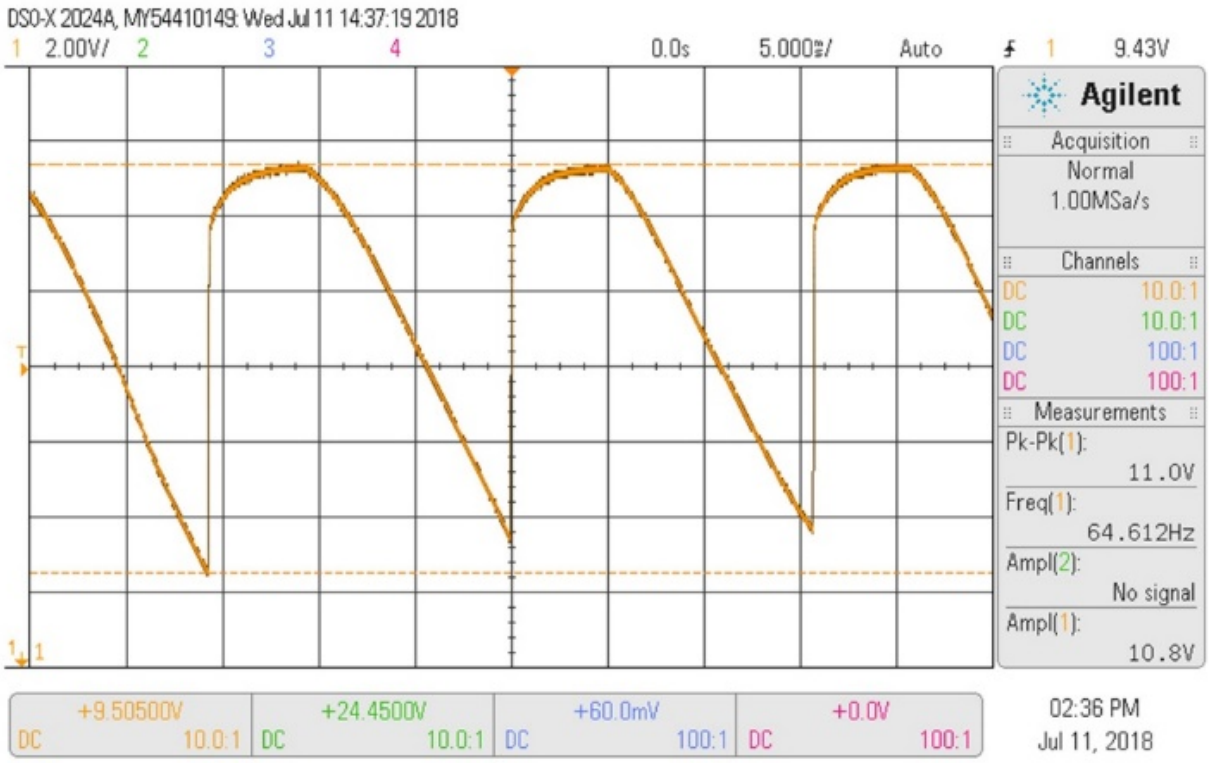

Figure 6.5 Variation of current source recorded by DSOX2024A Oscilloscope: 200 MHz, 4 Analog Channels.

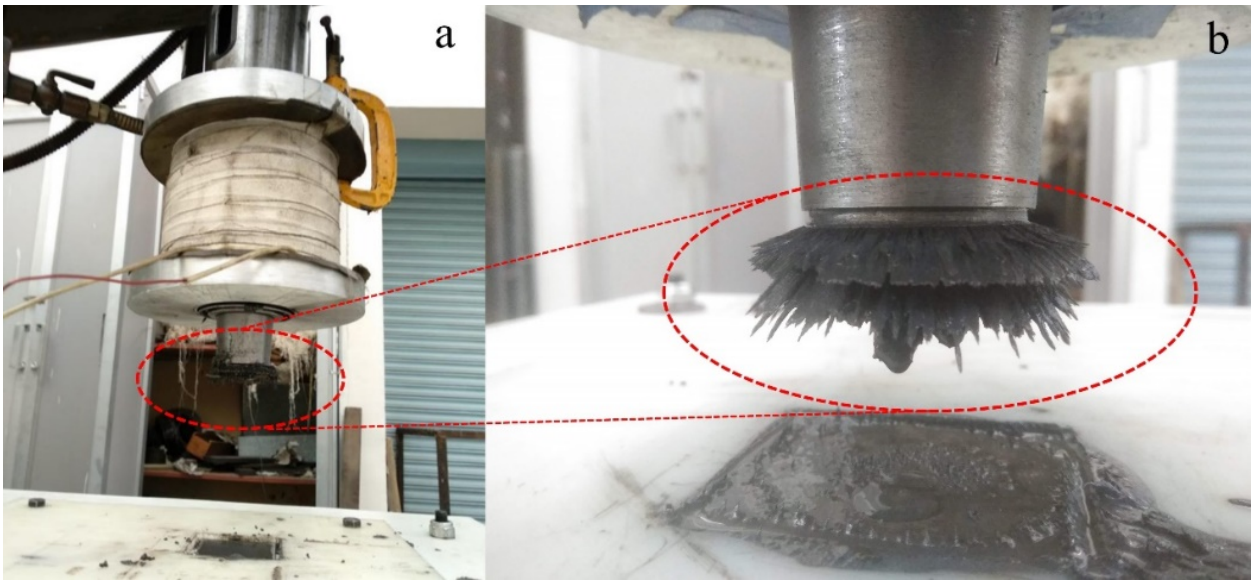

Figure 6.6 Electromagnet mounted on a radial drill and (b) enlarged view of FMAB.

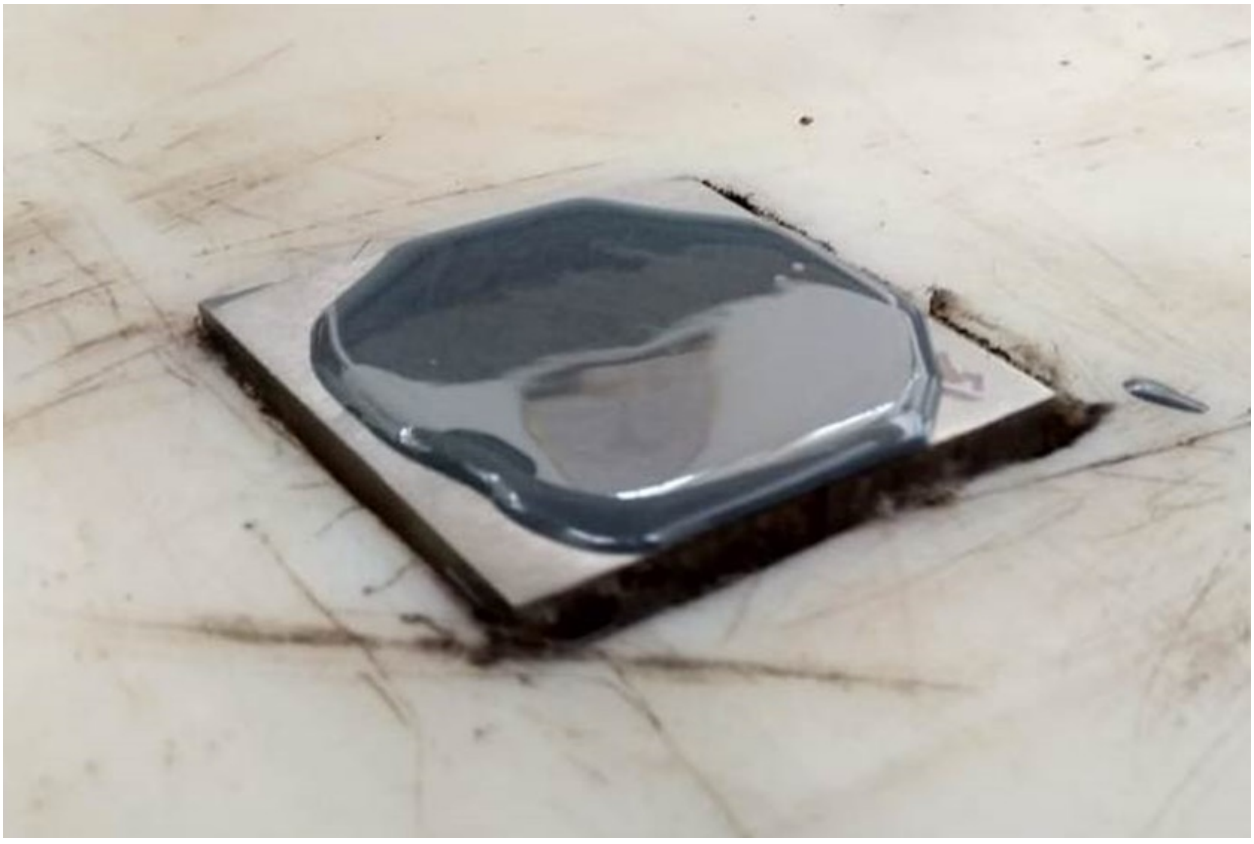

Figure 6.7 Media on the workpiece in the absence of magnetic field.

During the machining process the very fine FMAB was produced which is clearly illustrated in Figure. 6.2(b)., and the magnetic abrasive media on the workpiece in the absence of the magnetic field is shown in Figure. 6.3. The flat workpiece was kept on a flat horizontal fixture made by nylon and electromagnet spindle permitted to rotate with rotational speeds of 112 rpm, 150 rpm, 220 rpm, and 300 rpm. For the Change in Surface Roughness (ΔR_a) in "μm" change in the microhardness (ΔHV) in Vickers hardness, and change in the Modulus of Elastic Indentation (ΔEIT) in 'GPa,' were affected by variable factors i.e., and in the current MAF process, the process parameters are described in Table 6.6 and experimental design is shown in Table 6.7. During the machining process, the current, machining gap, and rotational speed, abrasive composition percentage, and finishing time were considered as the process parameter.

Table 6.6 Parameters, units, definition, and levels

Parameters	**Units**	**Definition**	**Levels**			
			1	**2**	**3**	**4**
Current (x1)	Amp	Current supplied to the electromagnet to alter the magnetic flux	0.8	1.2	1.6	2.0
Machining gap (x2)	mm	The gap between electromagnet tool and workpiece	1.5	2.0	2.5	3.0
Rotational speed (x3)	rpm	The relative rotational motion between tool and workpiece	112	150	220	300
Abrasive composition (x4)	wt. %	The mixture of the abrasive and ferromagnetic particle	40	50	60	70
Finishing time (x5)	min	Finishing time for an individual experimental run	10	20	15	20

Table 6.7 Experimental Design

S. No	Input parameters and their values					Experimental		
	x1	x2	x3	x4	x5	ΔRa (μm)	ΔHV	ΔEIT (GPa)
1	0.8	1.5	112	40	10	0.076	56.97	12.14
2	0.8	2	150	50	15	0.066	51.63	11.27
3	0.8	2.5	220	60	20	0.065	50.73	11.08
4	0.8	3	300	70	25	0.065	51.18	11.18
5	1.2	1.5	150	60	25	0.118	89.29	19.50
6	1.2	2	112	70	20	0.078	52.96	11.56
7	1.2	2.5	300	40	15	0.090	80.71	17.26
8	1.2	3	220	50	10	0.050	38.50	08.42
9	1.6	1.5	220	70	15	0.109	83.18	18.17
10	1.6	2	300	60	10	0.095	79.58	17.38
11	1.6	2.5	112	50	25	0.106	79.68	17.39
12	1.6	3	150	40	20	0.087	70.14	15.12
13	2	1.5	300	50	20	0.160	133.59	29.15
14	2	2	220	40	25	0.157	128.13	27.70
15	2	2.5	150	70	10	0.072	50.58	11.07
16	2	3	112	60	15	0.073	51.05	11.15

Chapter 7

MODELLING AND FINITE ELEMENT ANALYSIS

This chapter discusses finite element analysis of the designed electromagnet using the magnetostatic module of ANSYS 2020 workbench, to predict the capacity of production of magnetic field density.

7.1 Introduction

Magnetic abrasive particles (MAPs) are a combination of iron and abrasive particles that fill the void between the magnetic poles and the workpiece. The workpiece and pairs of magnetic poles are used in the Magnetic Abrasive Finishing method. The MAPs align along the magnetic field lines into the machining gap after the magnetic field is applied, creating the versatile magnetic abrasive brush. For finishing operations, this brush acts as a multi-point cutting tool.

The objective of this chapter is to develop a Finite element-based model and to simulate the effects of magnetic field on the interface surface of FMAB and workpiece in the MAF process. The present study focuses on magnetic field analysis of interface surface of workpiece and FMAB in MAF process using Ti-6Al-4V workpiece because less research is made in this direction. In this research work, Finite element-based modelling and simulation of magnetic flux distribution and surface temperature distribution are done using the WORKBENCH module of ANSYS 16 software. A simulated value of magnetic flux density is used to derive magnetic pressure which affects the surface roughness.

7.2 Theoretical background

Maxwell's Equations and EM Waves are the governing equations for electromagnetic field problems that consist of four sets of equations [127] are as follows:

1. Gauss' Law for electric field:

$$\Phi_E = \oint_S \boldsymbol{E} \cdot d\boldsymbol{A} = \frac{q_{\text{enc}}}{\varepsilon_0} \quad \text{or} \quad \nabla \cdot \boldsymbol{E} = \frac{\rho}{\varepsilon_0}$$

2. Gauss' Law for magnetic field:

$$\Phi_B = \oint_S \boldsymbol{B} \cdot d\boldsymbol{A} = 0 \quad \text{or} \quad \nabla \cdot \boldsymbol{B} = 0 \text{ (no magnetic monopole charges)}$$

3. Faraday's Law of Induction:

$$\oint_C \boldsymbol{E} \cdot d\boldsymbol{s} = -\frac{\partial}{\partial t}\int_S \boldsymbol{B} \cdot d\boldsymbol{A} \quad \text{or} \qquad \nabla \times \boldsymbol{E} = -\frac{\partial \boldsymbol{B}}{\partial t}$$

4. Ampere's Law and Maxwell's Law of Induction:

$$\oint_C \boldsymbol{B} \cdot d\boldsymbol{s} = \mu_0 \varepsilon_0 \frac{d}{dt}\int_S \boldsymbol{E} \cdot d\boldsymbol{A} + \mu_0 i_{enc} \quad \text{or} \quad \nabla \times \boldsymbol{B} = \mu_0 \varepsilon_0 \frac{\partial \boldsymbol{E}}{\partial t} + \mu_0 \boldsymbol{J}$$

Where E represents electric field intensity (V/m), μ_0 represents relative magnetic permeability in vacuum (Wb/(A-m)), ε_0 represents vacuum permittivity (F/m), ρ is charge density(A/m^2), B represents magnetic flux density (T), J represents electric current density (A/m^2) and magnetic scalar potential formulation is used to solve time-independent magnetic field problems (magnetostatic problems). For magnetostatic problems, this reduces Maxwell's equations to:

$$\nabla \cdot \boldsymbol{B} = 0$$

$$\nabla \cdot \boldsymbol{B} = \mu_0 \boldsymbol{J}$$

The above equations of the magnetic field, are dissolved into constitutive relation to describe the electromagnetic behaviour of materials. Following constitutive relation is considered for magnetic saturation of non-permanent magnetic materials [74].

$$B = \mu H$$

Where μ and H represent the magnetic permeability of the medium and magnetic field strength respectively.

Ferromagnetic materials get magnetised when they are exposed to an external magnetic field. As magnetic abrasive particles (in this case, a mixture of Fe and SiC abrasives) is mounted in the gap between the magnet poles and the workpiece, the Fe particles in the mixture become magnetised and aligned along the magnetic field lines, resulting in a flexible magnetic abrasive brush (FMAB). Magnetic energy is stored in the magnetic field between magnet poles and the workpiece gap filled with magnetic particles. The accumulated energy on magnetic abrasive particles generates magnetic pressure.

In the MAF process, magnetic abrasive particles placed into the working gap lies between the electromagnetic tool and workpiece. Due to the presence of an external magnetic field produced by the electromagnet, ferromagnetic particles in MAPs get magnetize and assembles in the forms of FMAB. The magnetic force acting on FMAB can be divided into two types: tangential

and normal magnetic forces. The normal magnetic force is responsible for magnetic pressure on MAPs. The magnetic pressure (P_m) on MAPs is specified by the following equation [55], [74], [88].

$$P_m = \frac{B_{avg}^2}{4\mu_0} \times \frac{3\pi(\mu_{FP}-1)\alpha}{3(2+\mu_{FP})+\pi(\mu_{FP}-1)\alpha} \quad \text{Equation 1}$$

Magnetic pressure exerts pressure on iron particles, which forces abrasive particles into the workpiece's surface, resulting in indentation. When tangential cutting force is created by the FMAB which was formed and moved due to the rotation of an electromagnetic tool, the material is extracted in the form of microchips.

7.3 Implementation procedure

The development of the FMAB and its contact with the workpiece surface is a complex phenomenon. Hence, to simplify the study of its effect during processing and to solve the 3D magnetostatic problem using FEM, the following assumptions are made:

a. Workpiece material is homogeneous and isotropic.
b. Eddy current and core losses are ignored.
c. The size of ferromagnetic and abrasive particles is consistent in the FMAB.
d. The ferromagnetic particle chains in FMAB are continuous and unaffected by the existence of non-magnetic abrasive particles.
e. The magnetic flux density is evenly distributed.
f. During the process, the properties of UMAPs do not alter. Since MAF has a low MRR, the removed content combined with magnetic abrasive has a slight consequence on the FMAB's properties.
g. The FMAB is made up of abrasive and ferromagnetic particles that are free of voids. The association with FMAB does not affect the material properties of the workpiece.
h. The workpiece material is completely plastic, and no bump occurs as a result of ploughing.
i. Active abrasive particles are a small percentage of overall abrasive particles that participate in finishing.
j.

ANSYS programme was used to implement the finite element problem, various steps are-

1. Solid 3-D Modelling of the electromagnetic tool, FMAB, and workpiece.
2. Electromagnet core with coils around them, magnet centre, workpiece, and the working void filled with magnetic abrasive particles make up the 3-D model. The dimensioning of different parts.
3. Since different materials are used in different areas of the MAF setup, Hence, the materials must be meshed correctly for the whole field.
4. In the MAF configuration, the new coil was mesh with SOURC36 elements, while the rest of the setup was mesh with SOLID117 elements. ASNYS software elements SOURC36 and SOILD117 are also ASNYS software elements. The form and position of current sources are represented by SOURC36. SOURC36 is a primitive that is used to provide magnetic field problems with current source results. Present density values were derived directly from the current source SOURC36 [128].
5. The ANSYS command set includes the macro-RACE, which allows the user to build a racetrack conductor using SOURC36. Figure 7.1(d) depicts a “racetrack” current source, which can also be seen in Figure 7.2 (see specified local y-coordinate at model's centre) and is suitable for 3-D magnetic field analysis using a scalar potential formulation [128]. Concerning the working plane, the current flows in a counter-clockwise direction. The properties of the SOURC36 element are given in Figure 7.1(c) [128].
6. As a load, the current magnitude and the number of turns in the coil were fed to SOURC36. Table 7.2 lists the current, number of coils, and magnetic field measurement parameters used in this study.
7. Magnetic scalar rigid finite element in three dimensions Modeling 3-D magnetic fields is possible with SOLID117. SOLID117 part was used to mesh the workpiece, working gap, and magnet core.

7.4 Simulation of the magnetic field

Finite element analysis of Magnetic flux distribution of interface of the workpiece- FMAB in MAF process is simulated by MAGNETOSTATIC analysis in ANSYS 2020 R1, WORKBENCH module. The primary step for finite element analysis is to create a 3D physical model. 3D Physical model consists of an electromagnet tool having copper winding around a mild steel core, flexible

magnetic abrasive brush (FMAB) and workpiece that are shown (Figure 7.1a,7.1b and 7.2). Furthermore, physical parts are surrounded by an air pocket (see Figure 7.2) to achieve magnetic effect in magneto-static simulation. The dimension of parts of 3D physical model are given in Table 7.1. The next step for finite element analysis is to assign material properties to different parts of the physical model. For achieving effective magnetic flux density simulation, the proper value of magnetic permeability and BH curve must be assigned to different parts of 3D physical model. The value of relative magnetic permeability of different parts of physical model is listed in Table 7.2. Important physical properties are mentioned in Table 5.

Table 7.1 Dimensions of various parts of 3-D Model.

Length of magnet poles	218 mm
Diameter of magnet core	34 mm
Working gap	1.5 mm
Diameter of workpiece	50 mm
Thickness of workpiece	5 mm

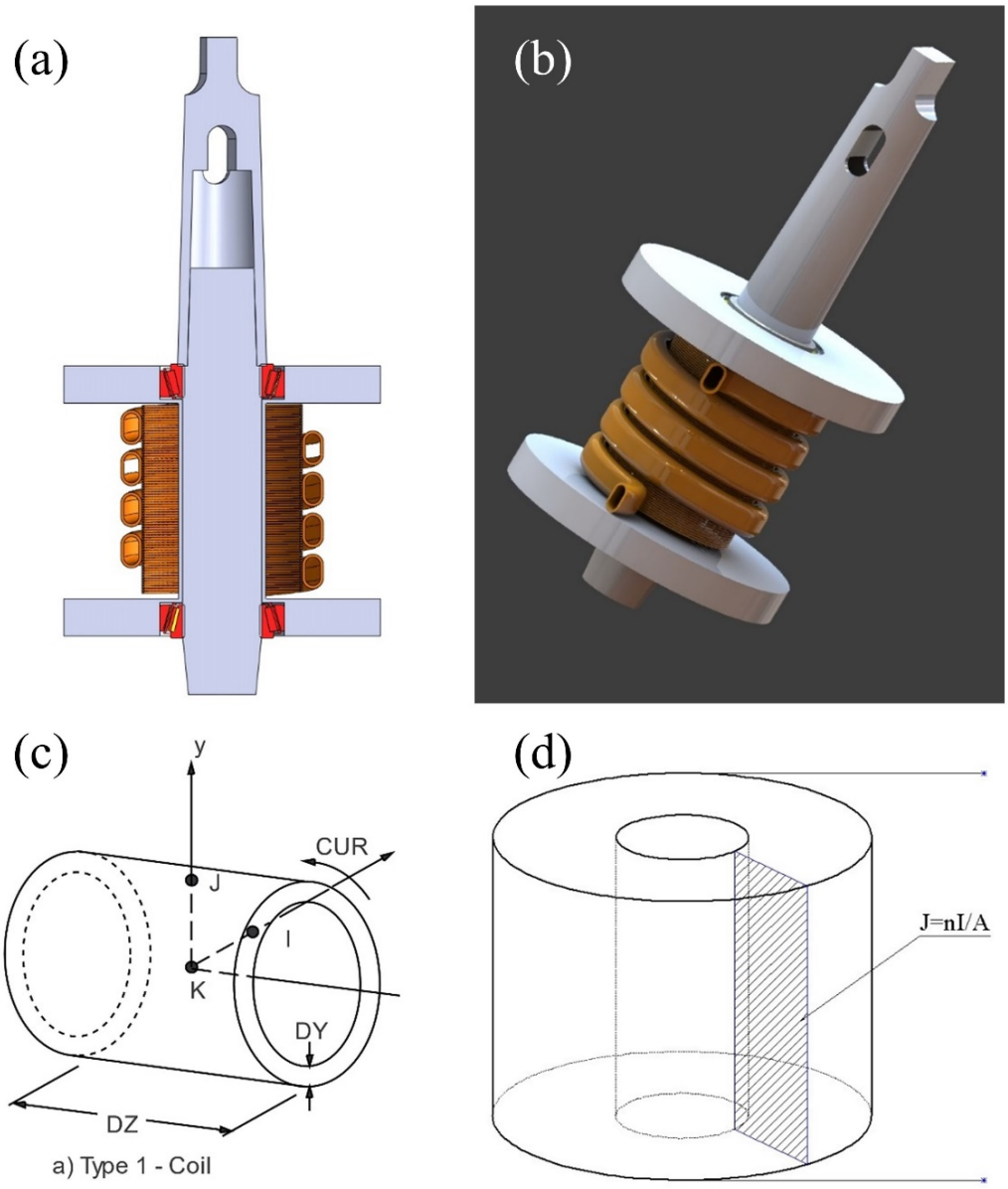

Figure 7.1 Properties of SOURC36 element *[128]*

Table 7.2 Magnetic properties of materials.

Relative magnetic permeability of Ti-6Al-4V	1 (non-magnetic)
Relative magnetic permeability of pure iron	5000
Relative magnetic permeability of air	1
Relative magnetic permeability of SiC	1 (non-magnetic)

Table 7.3 Magnetic loads and parameters.

Current in the coil (Ampere)	0.8–2.0
Number of turns in the coil	2000
Machining gap (mm)	1.5
the ratio of iron in FMAB	40-60

For the simulation of magnetic flux density, a 3D physical model and assigned material properties are fed into the magneto-static module. The meshing of the physical model is done by 2mm mesh element i.e., shown in Figure 7.3. The meshing of the 2mm element has opted after the convergence study and at 2 mm mesh element, it gave the best-simulated result. Meshing is done with the help of the Meshing tool to make them suitable for numerical evaluation and result. Accuracy obtains from FEA is directly related to the meshing method used.

SOLID117 element is used to mesh the Air pocket, FMAB, electromagnetic core and workpiece. SOLID117 element is suitable for meshing low-frequency magneto-static analysis, SOLID117 is a 20-node brick shape element and its 12 side nodes carry the edge flux, DOF, AZ. The AZ represents the edge-flux degree of freedom.

The next step is to assign the boundary condition of the magnetic flux density analysis and flux parallel applied on the surface of the Air pocket. The magnetic field generated by applying current to the coils of the electromagnet.

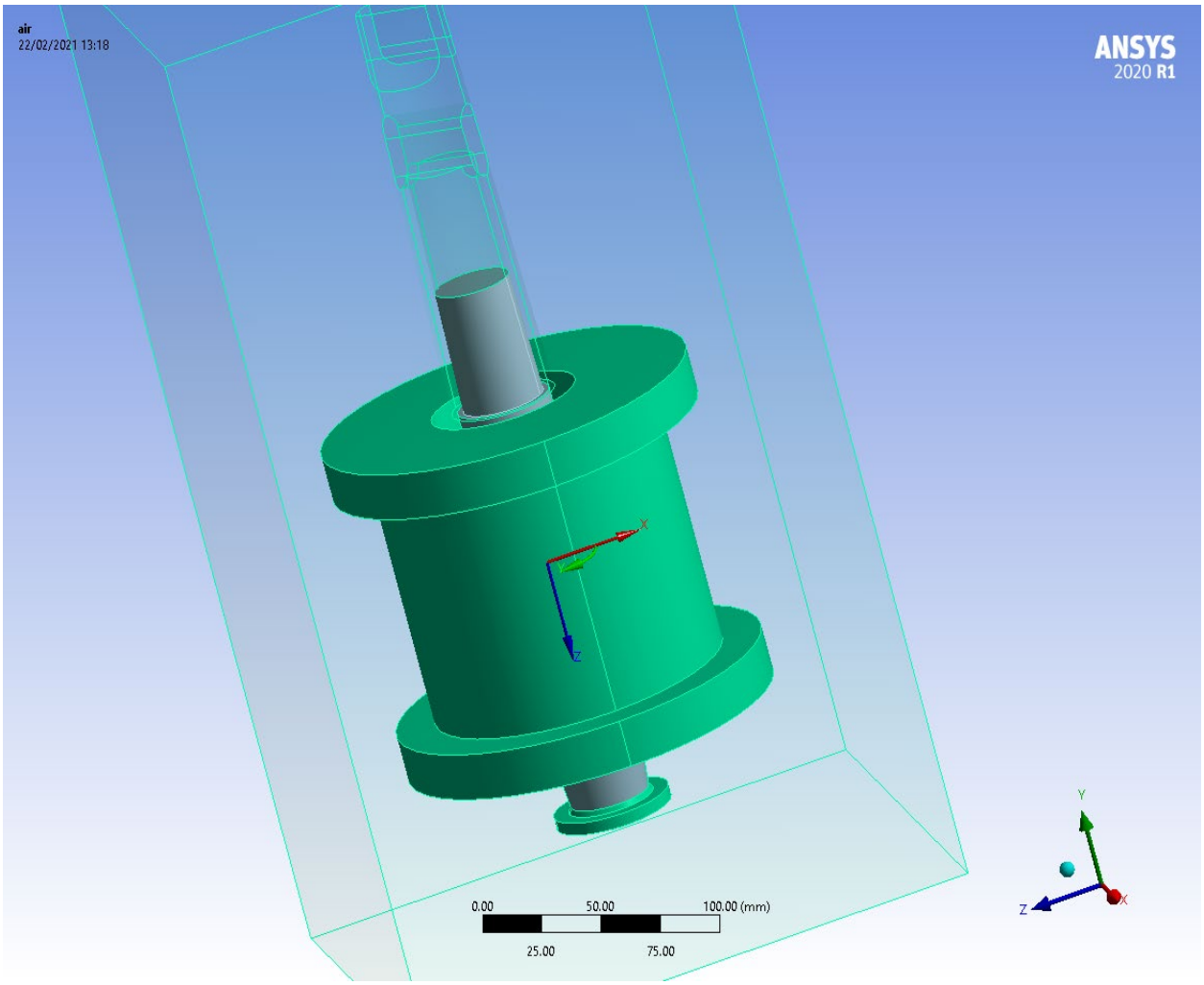

Figure 7.2 Physical model of electromagnet.

The density of magnetic flux depends on the current magnitude and number of turns in coil. Load in the form of current (A) is applied on the electromagnetic tool coil for the simulation of magnetic flux distribution. Value of current (0.8 A–2.0 A) fed to the magneto-static 3D model and number of turns in coil is 2000, working gap is 1.5 mm, volume ratio of iron in FMAB is 40:60. Table 7.3, shows magnetic loads and parameters.

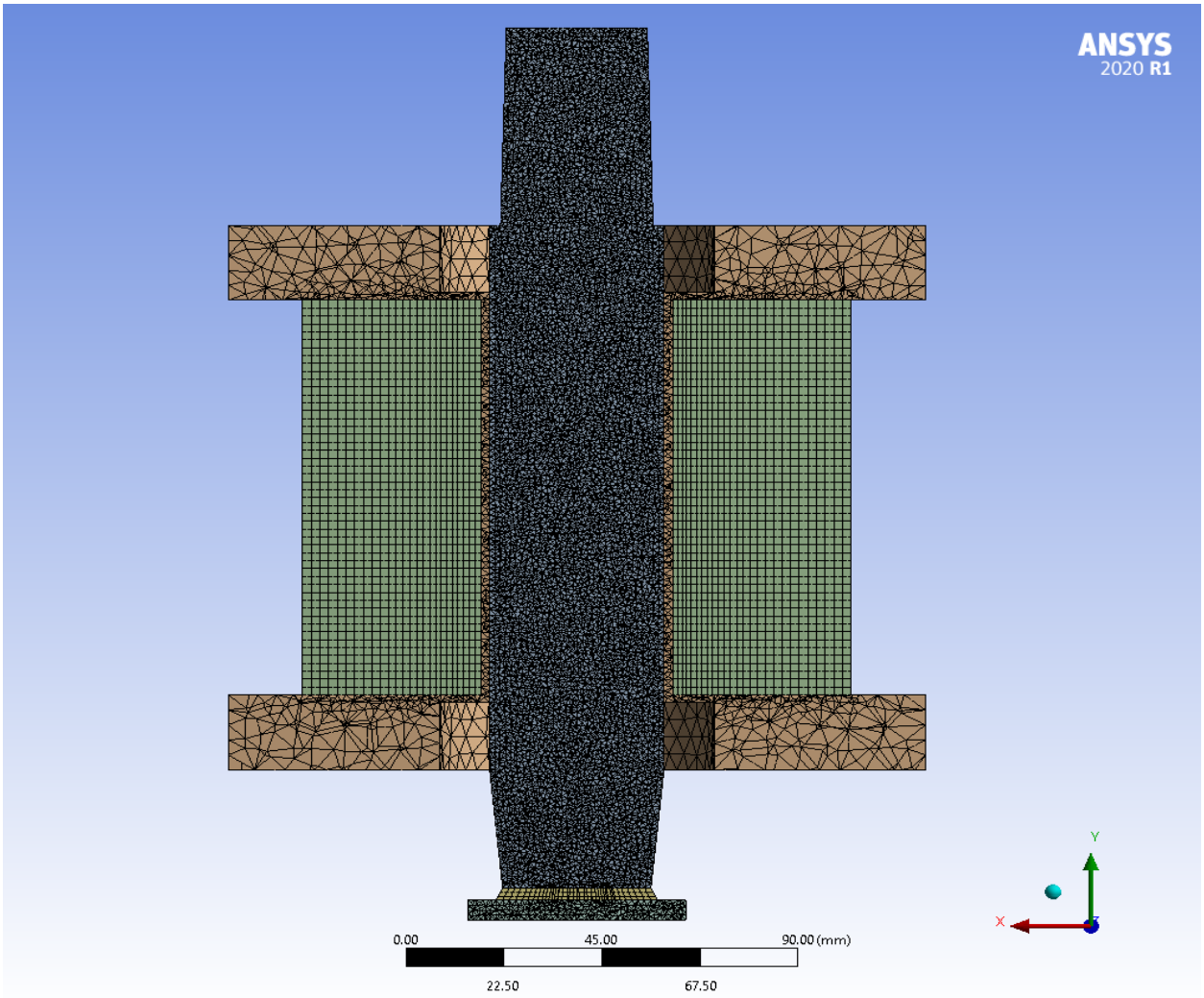

Figure 7.3 Meshing of physical electromagnet model of MAF process.

7.5 Results and discussion

The magnetic field distribution in the MAF mechanism was modelled and simulated using ANSYS 2020 R1, which was validated by comparing simulation results to experimental findings.

Figure 7.6 depicts the difference in magnetic flux density on the work-brush inter-face with various current values. As shown by the surface plots, the magnetic flux density is maximum at the corners of poles, where the distance across magnetic poles is minimal. Due to the extreme high concentration of magnetic lines of force, it occurs. The average magnetic field was obtained by integrating along a circular path around the centre of the workpiece.The following equation was used to calculate the value of B_{avg} (r).

$$B_{avg}(r) = \frac{\oint B(\theta) d\theta}{2\pi}$$

where $B(\theta)$ is magnetic field intensity at any radius.

Figure 7.7 shows the average magnetic field derived from the FEA and the experimental magnetic field measured from the set-up using a gaussmeter. The figure depicts how the average magnetic flux density calculated using FEA varies with radial distance (from the centre of the magnet's core), the pattern follows the same in the case of the experimental magnetic field vs radial distance. The magnetic flux density was found to be highest at 1.6 mm radial distance from the centre of the magnet in simulations as it was the location of the edge of the magnetic core and the magnetic flux density was also found to be maximum at the same radial distance from the centre of the electromagnet in experimental results (refer Figure 7.6).

7.5.1 Prediction of magnetic flux density

The magnetic flux density in the working gap obtained by FEM simulation and magnetic flux density obtained by experimentation is compared in Figure 7.6 (a, b). The figure shows that magnetic flux density found through simulation varies the same as in experimental magnetic flux density at the central and outer metallic poles. The simulated magnetic flux density (0.4 T) is found to be extreme at 1.6 mm from the centre of electromagnet as it was found in experimentation (0.35 T). Magnetic flux density is greater in simulated results than the experimental value at both magnetic poles. But simulated magnetic flux density at the bottom of the electromagnet coil is much higher than the experimental value of magnetic flux density which was low. Simulation of magnetic flux density was done to visualize magnetic behaviour in the FMAB present in the working gap. Simulation reveals that the density of magnetic flux is not equally distributed in FMAB which is shown in Figure 7.5, and Figure 7.6. The magnetic flux is shown in Figure 7.5, and Figure 7.6 shows between the workpiece-FMAB interface. The Contour plots display that magnetic flux density is highest at the edge of the centre pole and lower at the outer pole. This happens due to greater presence of magnetic lines of forces in central metallic core. The magnetic lines generate from the central metallic core and move toward the outer metallic pole. Figure 7.7 displays the variation in magnetic flux density when current is fed to the electromagnet and the maximum magnetic flux density generated is 0.4 Tesla. Similarly. Distribution of magnetic flux is predominant in the electromagnetic core and FMAB. At the same time, the distribution of magnetic

flux is negligible in coil and workpiece as they are non-magnetic material. Figure 7.4 shows distribution of magnetic flux (cross-section sideways).

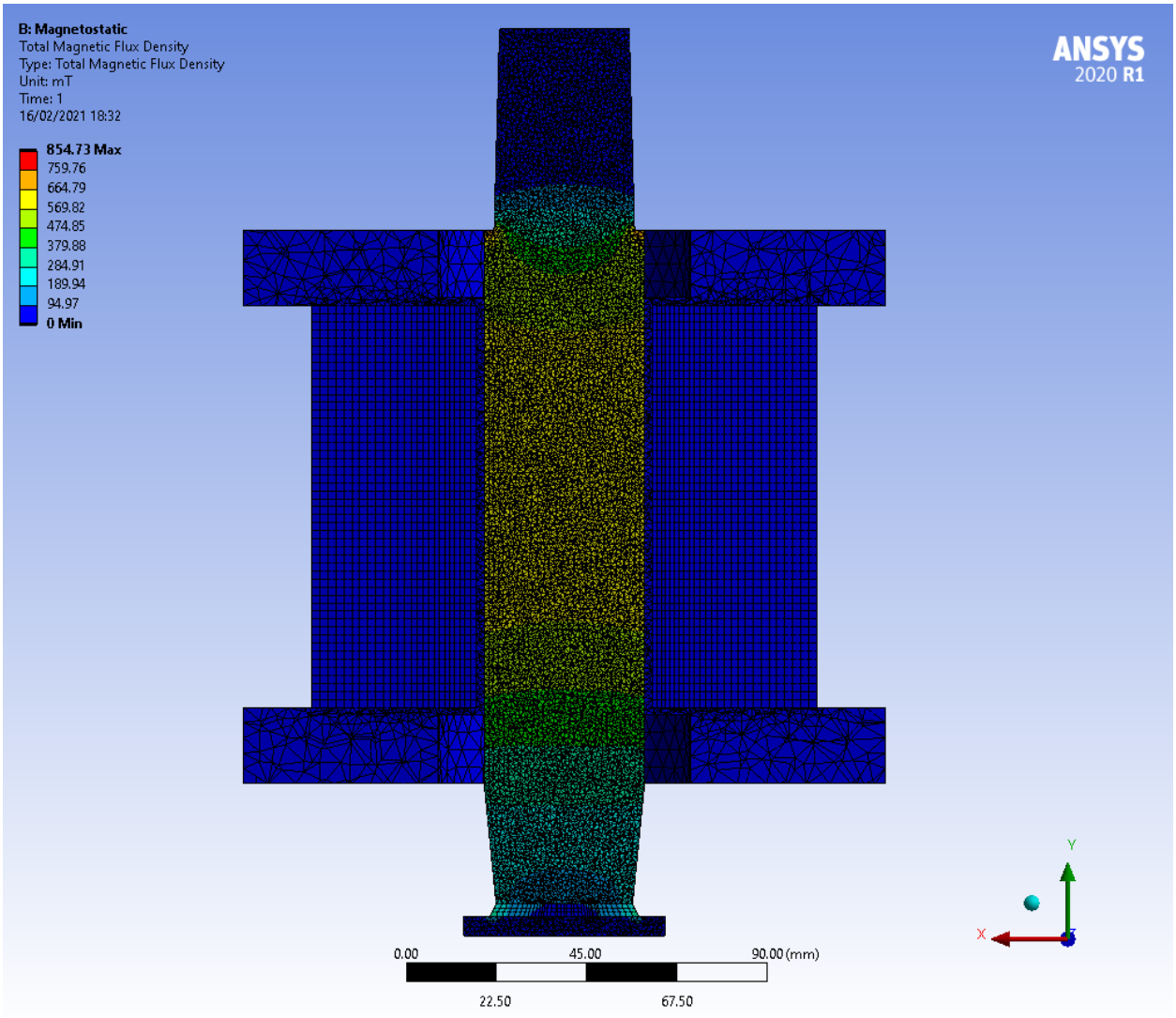

Figure 7.4 Distribution of magnetic flux (cross-section sideways).

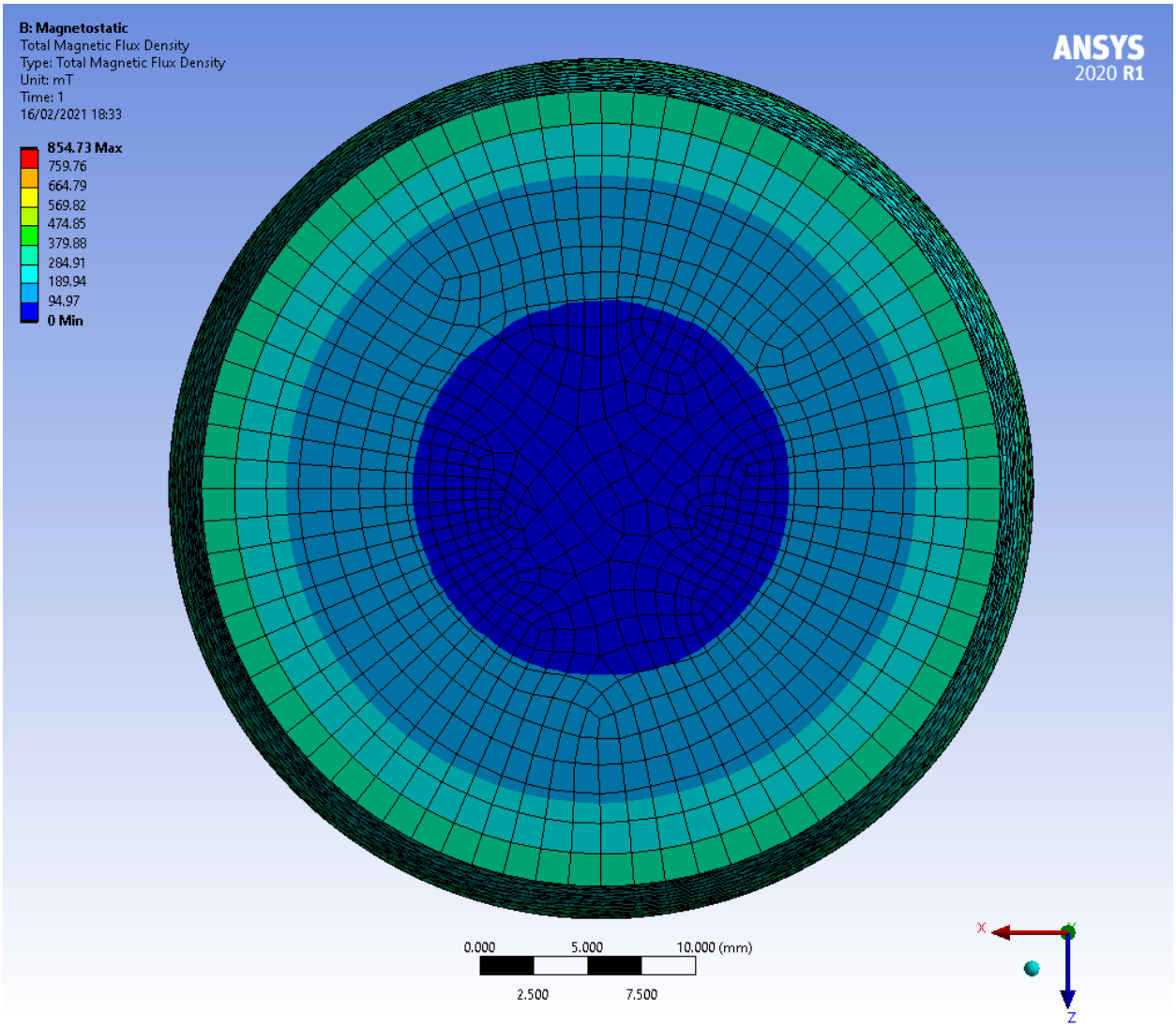

Figure 7.5 Total magnetic flux density on face of workpiece surface.

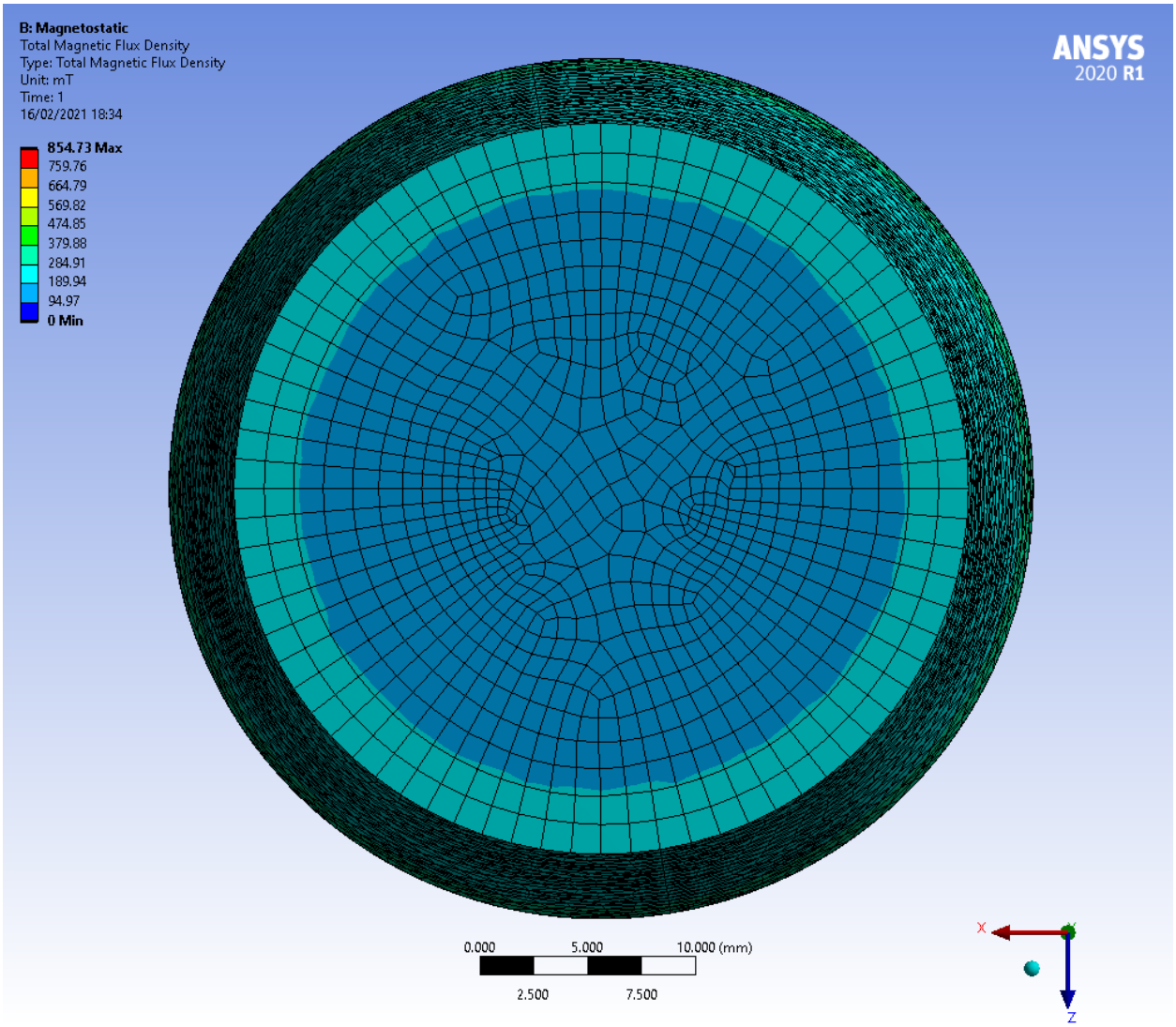

Figure 7.6 Total magnetic flux density on face of workpiece surface.

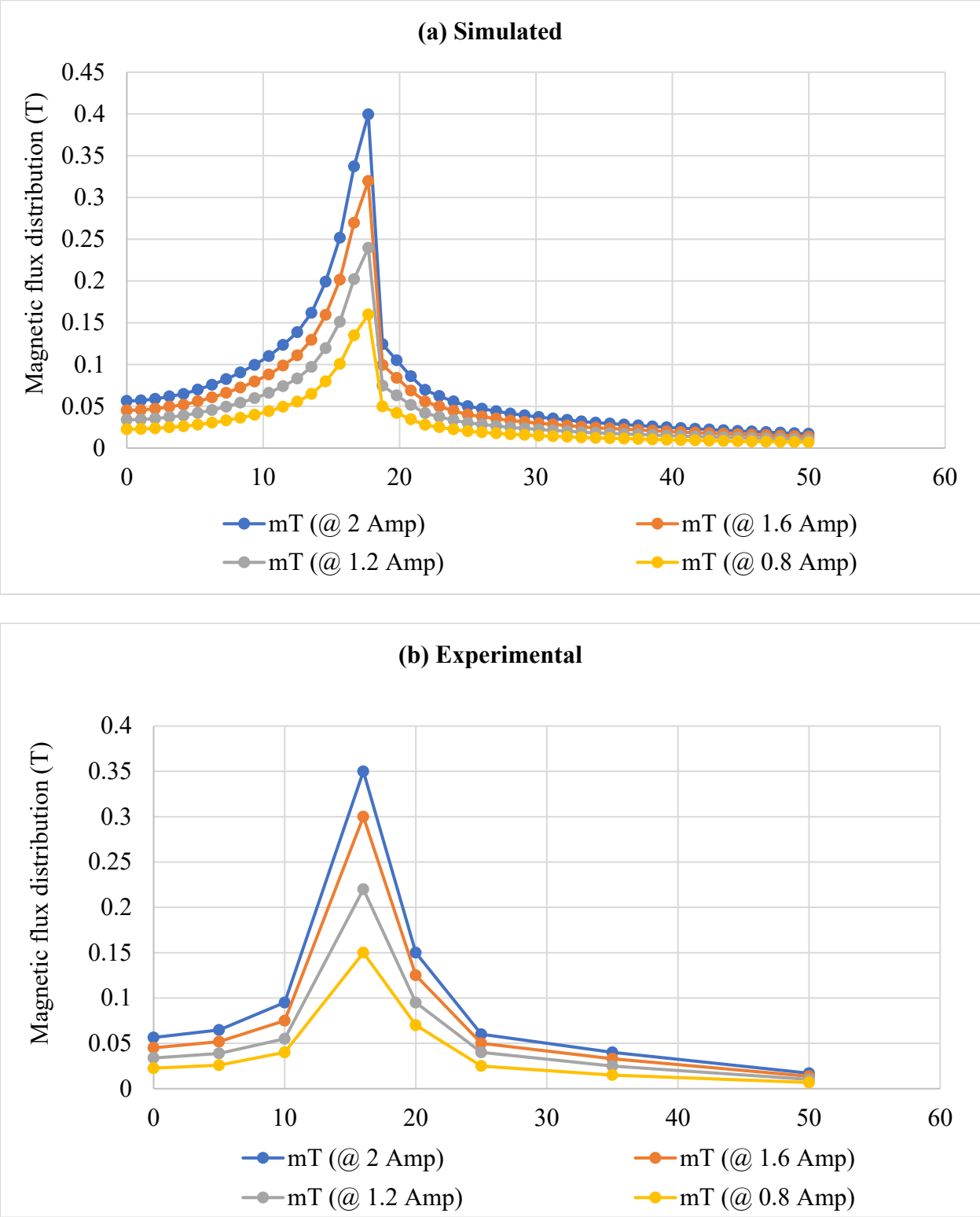

Figure 7.7 Comparison of magnetic flux density generated in working gap (a) simulated (b) experimental.

7.5.2 Variation of pressure distribution

The magnetic pressure has been calculated using Equation (1). Figure 7.8 depicts the different values of magnetic pressure at various locations with a corresponding value of current. The maximum magnetic pressure is found at the same location as the highest magnetic flux density. Number of turns of coil and surface area is remained constant as the charge density of current depend on them. Figure 7.8 shows the simulated distribution of magnetic flux density in the 3D physical model of the electromagnet. Magnetic pressure can be used to calculate heat flux, surface roughness, microhardness etc., generated as a result of rubbing between the FMAB and the workpiece's surface. Magnetic pressure at the workpiece- FMAB interface is calculated by using Equation (1). Magnetic pressure is derived by putting the simulated value of magnetic flux density in Equation (1). Figure 7.8 shows the different values of magnetic pressure at various locations with a corresponding value of current. It is found that the value of magnetic pressure is highest at a point located 1.6 mm radially outer from the centre of the magnet and lower at other location.

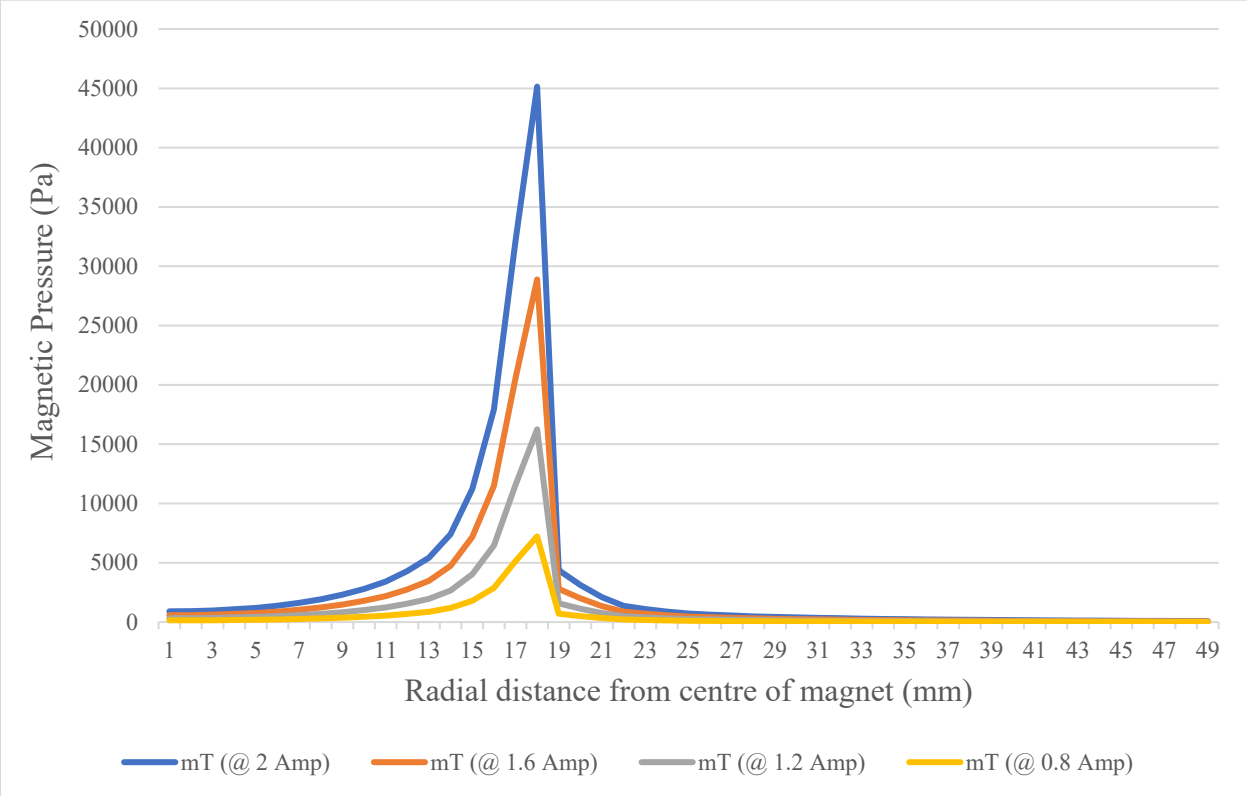

Figure 7.8 Different values of magnetic pressure at various locations with a corresponding value of current.

Chapter 8

RESULTS AND DISCUSSION

This chapter contains the important results of the study during the present investigation. It includes the morphology study of the sintered magnetic abrasive and its performance during magnetic abrasive finishing. It also, includes ANN-GA, modelling and optimisation tool to scrutinise and improve the performance of the magnetic abrasive finishing. Further the best combination of the parameters was found to improve the process efficiency. At last, the surface topography has been analysed to study the microstructure of the sample using Scanning Electron Microscope.

8.1 Results and discussion for Phase 1 experiment

In this section, the confirmation of the performance of developed SMA is done by the MAF process on Ti-6Al-4V. The parameters chosen according to the literature survey [4, 19, 30] was- current to electromagnet= 1.6 A, rotational speed= 300 rpm, working gap= 1.5 mm, and finishing time = 15 min for each experiment. Surface roughness profiles were determined with the help of Taylor Hobson Precision Surtronic 3+ surface roughness tester for workpiece before and after conditions. Micrographs of surface texture were taken using a Sipcon multi-sensor CNC inspection system (SVI-5300-CNC-VT). For Scanning Electron Microscopy, Carl Zeiss EVO MA 18 model was used, which was upgraded with Energy dispersive spectrum (EDS-Oxford INCA x-act) facility. The diffraction patterns of SMA were obtained from X-ray diffractometer (XRD), Brukar 8D advanced system having CuKα (λ~1.54 Å) source of radiation. Asylum Research MFP3D-SA model was used for atomic force microscopy.

Shadab Ahmad, Ranganath M. Singari & R.S. Mishra (2021) Tri-objective constrained optimization of pulsating DC sourced magnetic abrasive finishing process parameters using artificial neural network and genetic algorithm, Materials and Manufacturing Processes, DOI: 10.1080/10426914.2020.1866196 (Impact Factor- 3.046)

S. Ahmad, R. M. Singari & R.S. Mishra (2020) Modelling and optimisation of magnetic abrasive finishing process based on a non-orthogonal array with ANN-GA approach, Transactions of the IMF, 98:4, 186-198, DOI: 10.1080/00202967.2020.1776966 (Impact Factor- 1.052)

8.1.1 Surface Texture Study

The overall minimum to peak height was observed, and that was decreased significantly from the average surface roughness (Ra) value of 1.14 to 0.85 μm in the initial 15 minutes of finishing operation time using the produced sintered magnetic abrasive micrographs of the surface before and after magnetic abrasive finishing is shown in Figure. 8.1 and Surface roughness profiles have been clearly shown in Figure.8.2. The profile generated after surface finishing operation with the MAF process is illustrated in Fig. 8.2b and it has some deep valleys (1.6-1.8 mm and 2.8-3 mm overstretch of 3.8 mm roughness measurement) because of the higher confined normal pressure to a small area by the abrasives present in the flexible magnetic abrasive brush on the surface of the Ti-6Al-4V workpiece.

Independently, the surface roughness profiles were not sufficient to explain the shearing action by the abrasive cutting edges from the workpiece during the MAF process. Therefore, tests of atomic force microscopy (AFM) were performed. The surface obtained by the process on the Ti-6Al-4V workpiece plate has some finishing marks, and deep scratches were found to be in random order due to irregular magnetic abrasive brush forces, as shown in the AFM images in Figure. 8.3. These marks may be eliminated by means of the higher mesh number of SMA or vibrationally aided finishing [9-11]. Results from the experiment indicate that developed SMA is feasible for hard workpiece materials such as Ti-6Al-4V. Surface roughness and topography of the workpiece reveals that after the MAF process, the massive difference in peaks and valleys of the surface turns out to be smooth, and the specimen becomes flat, which is shown in Figure. 8.3b. These peaks were sheared and drawn out by the normal force applied to the surface of the workpiece by SMA. Also, the finishing torque given by the relative rotational motion between the workpiece and electromagnet during the MAF process helps in the shearing of the peaks from the workpiece surface [12-14]. The alumina-silica abrasives removed the material in the form of microchips from the Ti-6Al-4V workpiece. Fine scratch marks generated on the workpiece surface were due to FMAB, and the use of abrasives with a higher mesh number will reduce this.

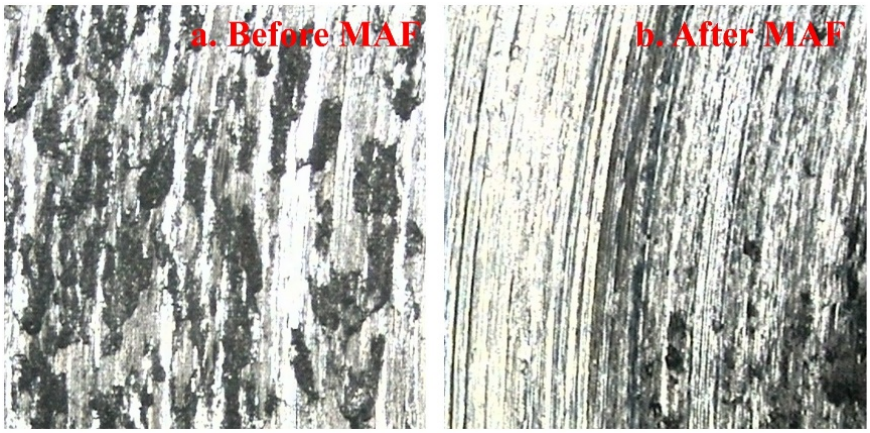

Figure 8.1 Micrographs of Ti-6Al-4V surface before and after magnetic abrasive finishing.

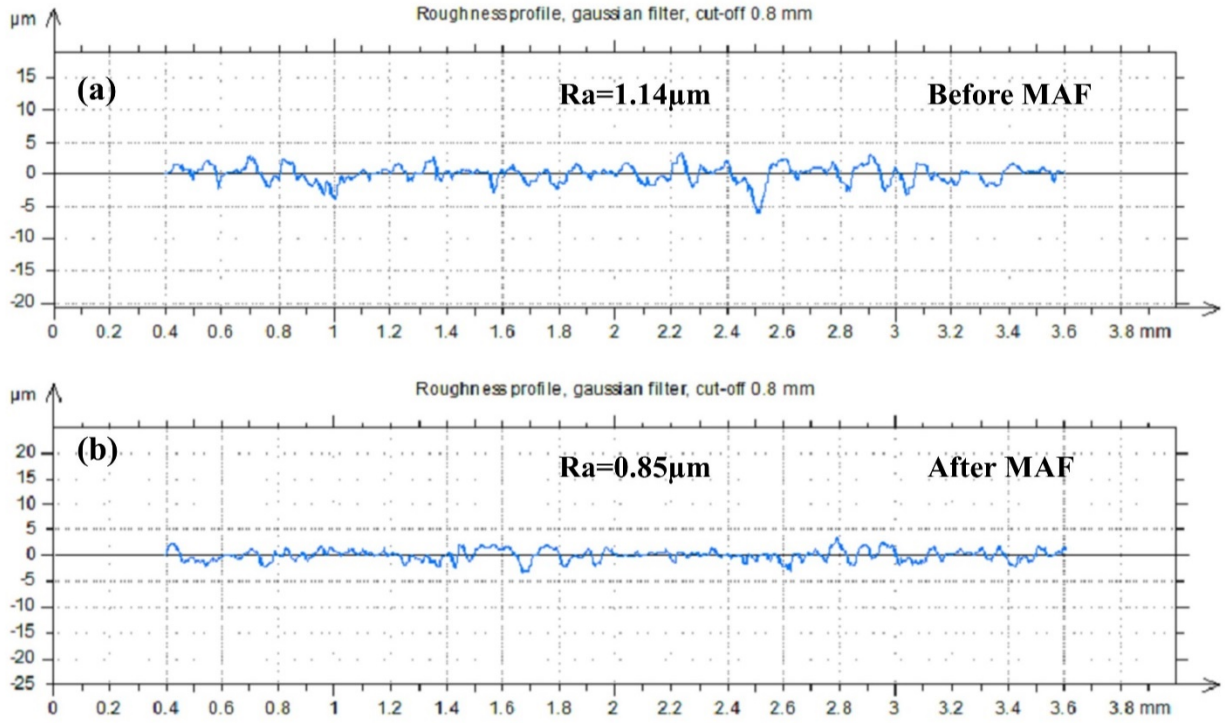

Figure 8.2 Surface roughness profile of Ti-6Al-4V workpiece **a**, **b** = before and after finishing respectively, (at current to electromagnet= 1.6 A, rotational speed 300 rpm, working gap= 1.5 mm and finishing time = 15 min for each experiment).

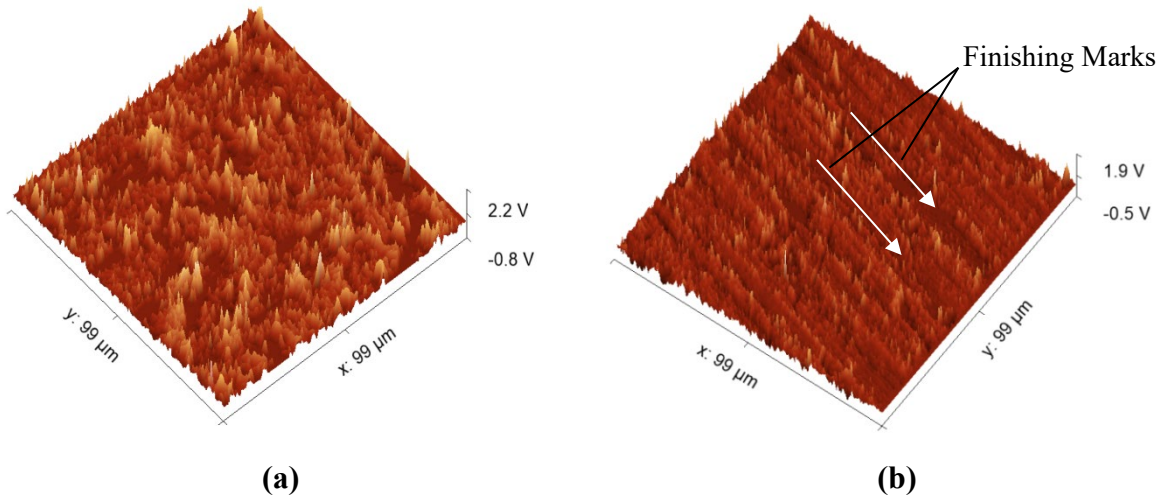

(a) **(b)**

Figure 8.3 AFM images of Ti-6Al-4V workpiece plate (a) 3D image before finishing (b) 3D image after finishing with MAF process (at current to electromagnet= 1.6 A, rotational speed 300 rpm, working gap= 1.5 mm and finishing time = 15 min for each experiment).

8.2 Results and discussion for Phase 2 experiment

The Taguchi technique is a prevailing tool for designing, arrangement, and collection of experimental data in a controlled way. It also tells us the effects of process variables over some particular variables for the design of efficient systems, and simultaneously, it reveals the effects of uncontrolled factors [2, 3].

The L_9 orthogonal array for three levels and three factors was used by Ahmad et al. [36], each row of each array (three different arrays set for three different abrasives size, for investigation of a good range of abrasive size) represents the trial situation with a combination of factors. Columns were corresponding to each control parameter or process variable in the array, and there were nine combinations as it is in the L_9 orthogonal array. The response parameter was, change in Surface Roughness (ΔR_a). This technique has been effectively utilized by numerous researchers to understand the finishing impacts during the MAF process[4-6]. Nevertheless, the satisfactory decision of the researched parameters (control factors) is fundamental.

The observations in this examination were led according to a Non-orthogonal array [28, 29] as per machining set-up restrictions. The determination of the non-orthogonal array depends on relying on the prerequisite that did not fit by the orthogonal array. Table 6.3 shows the control factors, their units, definition, and levels. It is notable that the control factors level is non-uniform for abrasive size because of sieve size restriction. The experimental data [36] presented in Table

6.4 has been used to develop the ANN model. The following observations were set in a fashion using an L_{27} non-orthogonal array with four inputs and one output. The input parameters were abrasive size, voltage, machining gap, and rotational speed. The Change in Surface Roughness (ΔR_a) was an output/response parameter, measured in microns (μm).

In the Taguchi method, the signal-to-noise (S/N) ratio response has been formed corresponding to each observation, and 'larger-the-better' quality characteristic was targeted in this assessment, as more difference in surface roughness required. The control factors and the process response were taken as inputs to calculate the S/N ratio. Moreover, ANOVA analysis was carried out to scrutinize which controlling factor was statistically significant, so the best combination of the control factors, i.e., optimal combination, can be forecasted [123]. The S/N ratio (larger the better quality) for the change of surface roughness given by Taguchi method is given below:

$$S/N = -10 \log \frac{1}{n} \left(\frac{1}{y_1^2} + \frac{1}{y_2^2} + \cdots + \frac{1}{y_n^2} \right)$$

Where y_1, y_2, ..., y_n are the responses of the change of surface roughness and n is the number of observations. For each level, the average of selected characteristics of the factor has been shown in Table 8.1 (see S/N ratio). The response, S/N ratio, merges the reiterations, and the impact of noise levels into one whole coherent information. ANOVA for the S/N ratio was carried out for the classification of the significant factor [129]. The Mean-response graphs were plotted, whereas the percentage contribution of factors was resolved by ANOVA.

The prime motive of this study was to calculate the maximum Change in Surface Roughness $(\triangle R_a)_{max}$ and optimal values of factors correspondingly that have the most significant influence. Experimental data, as shown in Table 8.1, which connects the influence of abrasive size, voltage, machining gap, and rotational speed. These factors have a vital impact on the MAF process.

Table 8.1 Experimental Design

Exp. Run	Abrasive Size	Voltage	Machining Gap	Rotational Speed	Experimental ΔR_a (A)	S/N ratio	ANN Predicted ΔR_a (B)	% Error (|A-B|/A*100)
1	90	6	1	60	0.13	-17.7211	0.1300	0
2	90	6	1.5	90	0.11	-19.1721	0.1099	0.0909
3	90	6	2	120	0.11	-19.1721	0.1101	0.0909

4	90	12	1	90	0.21	-13.5556	0.2103	0.1428
5	90	12	1.5	120	0.14	-17.0774	0.1396	0.2857
6	90	12	2	60	0.11	-19.1721	0.1097	0.2727
7	90	18	1	120	0.23	-12.7654	0.2300	0
8	90	18	1.5	90	0.17	-15.3910	0.1702	0.1176
9	90	18	2	60	0.15	-16.4782	0.1508	0.5333
10	150	6	1	60	0.15	-16.4782	0.1498	0.1333
11	150	6	1.5	90	0.14	-17.0774	0.1401	0.0714
12	150	6	2	120	0.13	-17.7211	0.1294	0.4615
13	150	12	1	90	0.24	-12.3958	0.2397	0.1250
14	150	12	1.5	120	0.15	-16.4782	0.1494	0.4000
15	150	12	2	60	0.13	-17.7211	0.1300	0
16	150	18	1	120	0.25	-12.0412	0.2497	0.1200
17	150	18	1.5	90	0.19	-14.4249	0.1900	0
18	150	18	2	60	0.18	-14.8945	0.1791	0.5000
19	300	6	1	60	0.11	-19.1721	0.1073	2.4540
20	300	6	1.5	90	0.10	-20.0000	0.1002	0.2000
21	300	6	2	120	0.12	-18.4164	0.1198	0.1666
22	300	12	1	90	0.17	-15.3910	0.1707	0.4117
23	300	12	1.5	120	0.16	-15.9176	0.1654	3.3750
24	300	12	2	60	0.10	-20.0000	0.1015	1.5000
25	300	18	1	120	0.21	-13.5556	0.2097	0.1428

26	300	18	1.5	90	0.16	-15.9176	0.1597	0.1875
27	300	18	2	60	0.14	-17.0774	0.1402	0.1428

8.2.1 Analysis of variance (ANOVA)

For the computation of the process quality and its characteristics, the experimental data has been converted into S/N ratio. Based on S/N ratio, a ranking of control factors has been shown in Table 8.2. It is clear from Table 8.2; the prevailing factor that affects the ΔR_a is voltage and then machining gap, followed by abrasive size and rotational speed, respectively. Also, the variations in S/N ratio is shown in main effects plot (Figure. 8.4) where the most optimum result by Taguchi analysis is observed as abrasive size, voltage, machining gap, and rotational speed are 150µm, 18V, 1mm, and 90rpm respectively.

Table 8.2 Response Table for S/N Ratios- Larger is better

Level	**Abrasive Size**	**Voltage**	**Machining Gap**	**Rotational Speed**
1	-16.72	-18.33	-14.79	-17.63
2	-15.47	-16.41	-16.83	-15.93
3	-17.27	-14.73	-17.85	-15.91
Delta	1.80	3.60	3.06	1.73
Rank	3	1	2	4

The analysis of the experimental data was carried out using ANOVA. The ANOVA analyses of the ΔR_a for all the analysed factors have been shown in Table 8.3. The factors, having P-value less than 0.05 shows a statistically considerable effect on the process performance. Also, Table 8.3 shows the percentage contribution of all factors in the overall result.

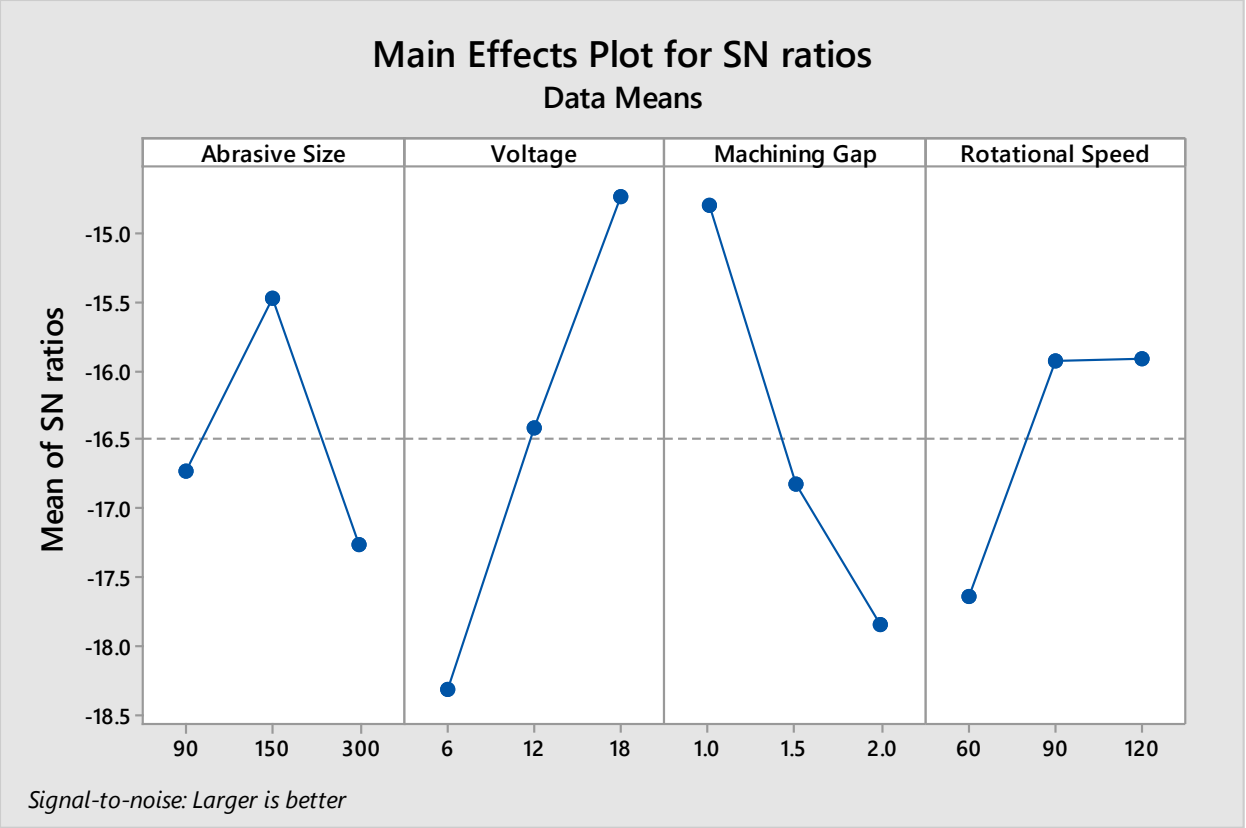

Figure 8.4 Main effects plot for S/N Ratio for ΔR_a

Table 8.3 Analysis of Variance for S/N ratio for Change in Surface Roughness

Source	DF	Adj SS	Adj MS	F-Value	P-Value	% contribution
Abrasive Size	2	15.350	7.6748	14.44	0.000	10.95
Voltage	2	58.344	29.1718	54.88	0.000	41.60
Machining Gap	2	39.225	19.6126	36.89	0.000	27.98
Rotational Speed	2	13.165	6.5826	12.38	0.000	9.39
Error	18	9.569	0.5316			6.80
Total	26	140.238				

By scrutinizing the results from Table 8.3, it can be noticed that voltage has the utmost weight on ΔR_a (% contribution = 41.60%), so exclusively, this factor should be the center of attention. Besides voltage, the change in surface roughness is also affected by machining gap ((% contribution = 27.98%), abrasive size (% contribution = 10.95%), and rotational speed (% contribution = 9.39 %).

The calculated S/N ratio was satisfactory because of the points on the normal probability plot in Figure. 8.5 shows the approximate linear pattern with normal distribution having small disintegration [19, 20]. Also, frequency versus residual plot Figure. 8.5 confirms finer the data variation as there were no outliers, and the negatively skewed histogram shows the initial observed S/N ratio has more impacts on results. The plot of residuals versus fitted value shows a random pattern (illustrated in Figure. 8.5), which means residuals have approximately constant variance, and residuals versus order plot show that the data collected can be used to find the non-random error.

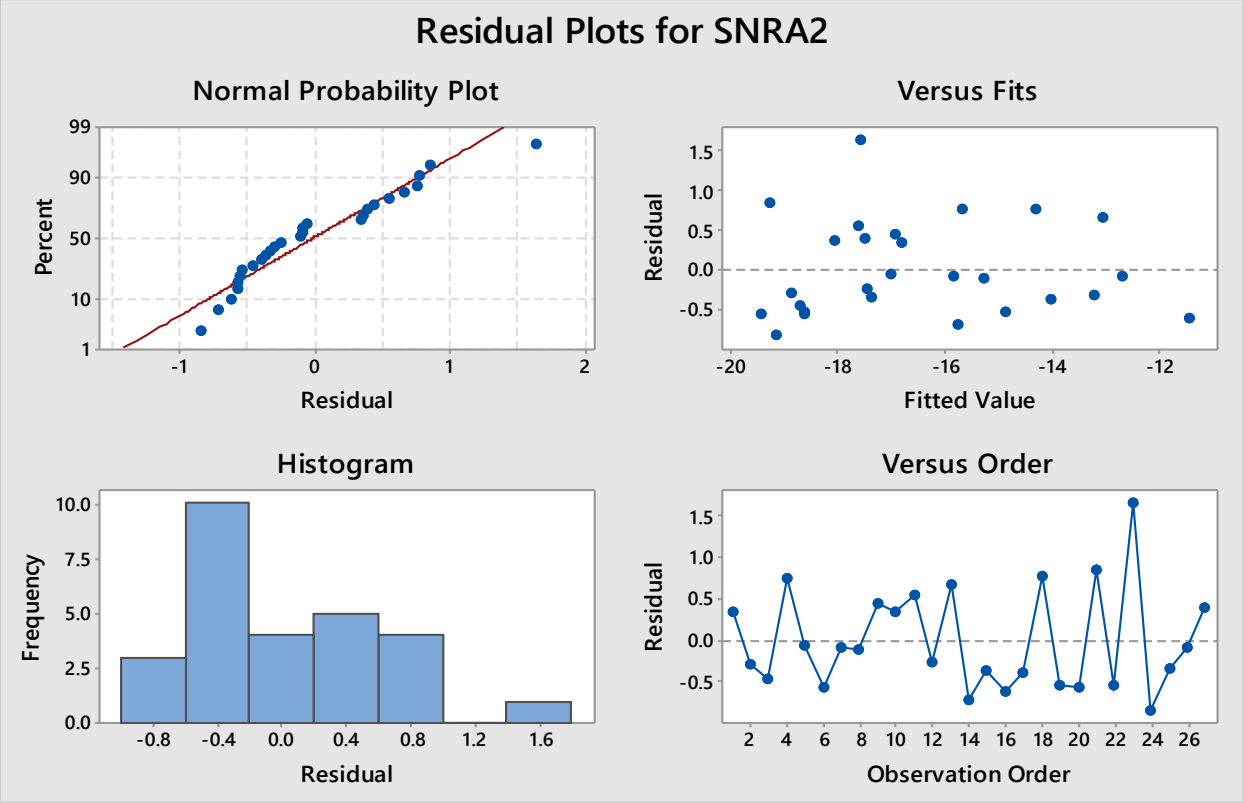

Figure 8.5 Residual plot for S/N Ratio for the change of Surface Roughness (ΔR_a)

8.2.2 Interaction plot and the effect of factors on the change in Surface Roughness

The effect of the various process factors (Data means) on ΔR_a has been shown in Figure. 8.6. Factors of Horizontal line show, insignificant effect, whereas factors correspond to the highest inclined line have the most significant effect. The most effective factor on ΔRa was Voltage as its increment was highest, while the other factors show a lesser impact. ΔRa increases with the increase of Voltage and Rotational Speed. Simultaneously ΔRa decreases with the increase of

Machining Gap and Abrasive size. The Highest ΔRa was found for the highest Voltage and the highest Rotational Speed.

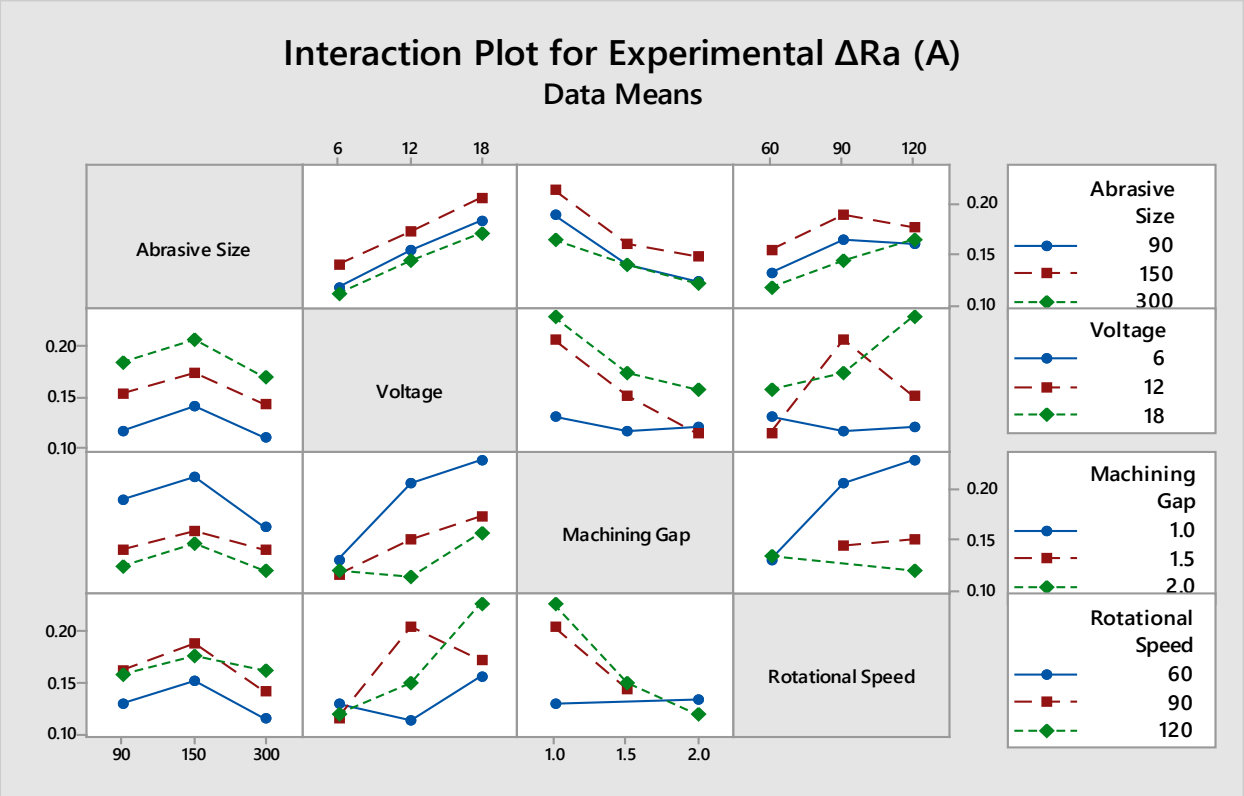

Figure 8.6 Interaction plot for ΔR_a

8.2.3 Linear regression model

The linear dependence between the value of controlling factors (Abrasive size, voltage, machining gap, and rotational speed) and ΔR_a was obtained. Using MINITAB 17 software, the linear regression equation was derived from set values of abrasive size, voltage, machining gap, and rotational speed and ANOVA. However, a linear regression model was obtained as following to predict ΔRa. A linear dependence between parameters and the unknown quantity provided by the developed model.

Experimental ΔR_a (A) = 0.1511 - 0.000080d + 0.005370 V - 0.0549x + 0.000403S (1)

ΔR_a= 0.23938 (at d=150µm, X_1=18V, X_2=1mm, X_3 =90rpm)

The developed linear regression equation with the help of MINITAB 15 for the ΔRa (particularly for 150-micron size Abrasive particle) is by Eq. 1 [36].

$\Delta R_a = 0.1850 + 0.00556X1 - 0.0646X2 + 0.00021X3$ (2)

ΔR_a = 0.21713 (at d=150µm, X_1=18V, X_2=1mm, X_3 =90rpm)

Based on the above equations 1 and 2, a difference has been shown between non-orthogonal array and an orthogonal array, and it applied for the opted controlling factors and their values. However, from Equations. 1 and 2, coefficients showed that each factor has an individual impact, on ΔR_a were dissimilar. The ΔRa increase with increasing Voltage and Rotational Speed, and decrease with increasing Machining Gap and Abrasive Size. The models formulated for prediction of ΔRa, represented by Equations. 1 was satisfactory because of the points on the normal probability plot in Figure. 8.7 shows the approximate linear pattern with normal distribution having small disintegration [19, 20]. In Figure. 8.7 the plot of residuals versus fitted value shows a random pattern, which suggests that residuals have approximately constant variance, and residuals versus order plot show that the data collected can be used to find the non-random error. Also, the frequency versus residual plot in Figure. 8.7 confirms the finer data variation as there were no outliers; however, the histogram is negatively skewed shows that the initial observations have more weight on overall results.

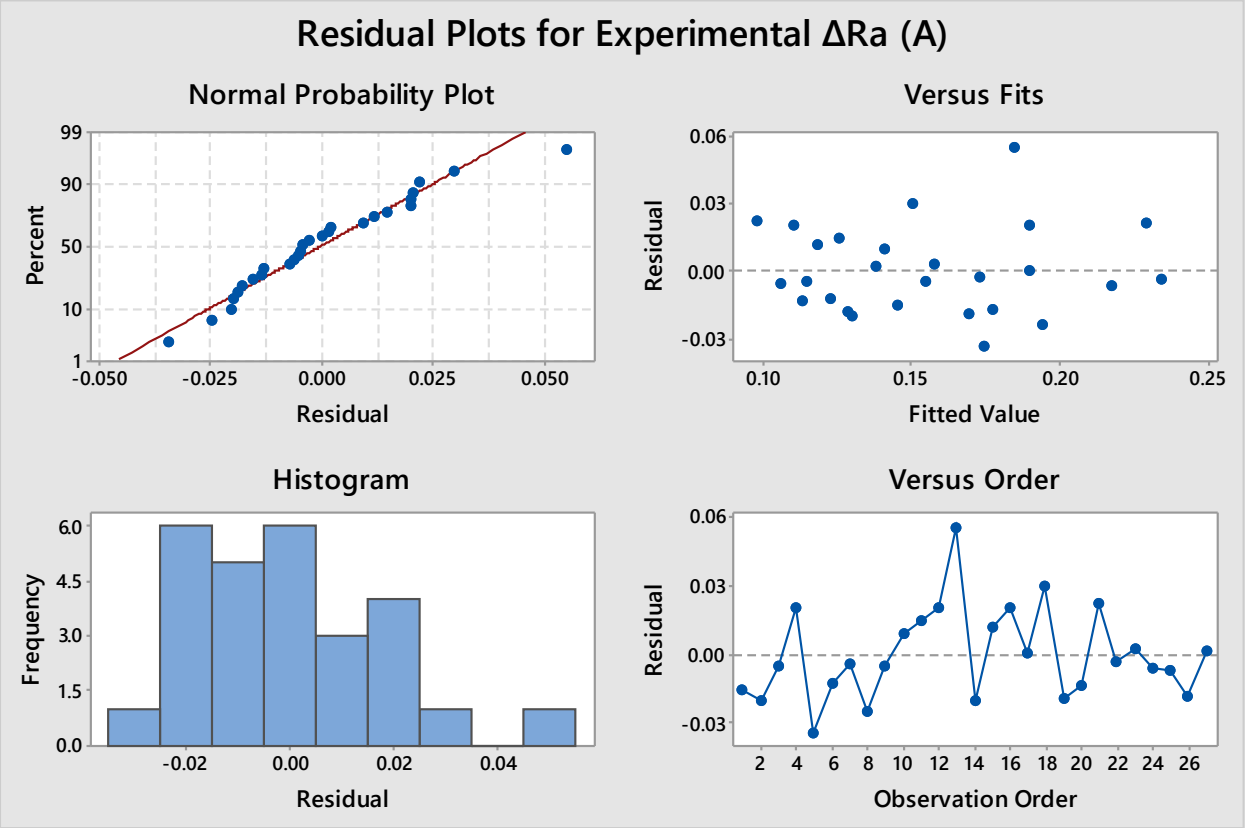

Figure 8.7 Residual plot for the change of Surface Roughness (ΔR_a)

8.2.4 Artificial neural network (ANN)

Artificial Neural Networks (ANN), normally referred to as Neural Networks, are analogous to biological neural networks. These networks were used to approximate a function (in mathematical model form) that depends on the huge number of inputs. Since much complex nature of calculations involved during the development of the network, so the software is used usually [21, 22]. For the data training and testing, MATLAB R2015a software is used in this work.

Neural network contains an input layer which is composed of neurons corresponding to the various process parameters. The experimental or real-time data (x_i) related to these parameters is subsequently fed into the neurons of input layer. Input data are transferred to the hidden layer and output layer by multiplying weights (w_{ij}) between two neurons and adding using summation function as shown Eq. (3). The feed-forward ANN model developed for modeling of ΔR_a (response or output) contains 4 different inputs layers of neurons equals to four input parameters (for this case abrasive size, voltage, machining gap, and rotational speed). The developed ANN architecture was 4-10-8-1, i.e., four inputs, two hidden layers (10 and 8 neurons, respectively), and one output, as illustrated in Figure. 8.8. This ANN architecture (4-10-8-1) has been found more appropriate for the modelling of data for which error is nearly zero as shown in Figure 8.9(c). For the present data, the ANN training algorithm was "*trainlm"* (trainlm is often the fastest backpropagation algorithm in the toolbox). The activation transfer functions (mathematical function that converts and process the input data of each layer to outputs) "*logarithmic sigmoid logsig)"* and the linear transfer function "*purelin"* were used as they offer better predictions [32], [33]. This training algorithm updates weights and biases in pursuance of "*Levenberg–Marquardt*" optimization (used to solve non-linear least squares problems). For the training, testing and validation of ANN, 70%, 15%, and 15% data is used, respectively. Regression coefficients were acquired for the training, validation, and testing after ANN training [46].

$$\text{Output} = f\left(\sum_{i=1}^{n} b + x_i w_i\right) \qquad (3)$$

where, b is bias, experimental or realtime data (x_i), corresponding weights (w_{ij}), and f is activation function.

The trained ANN performance has been shown in Figure. 8.9(a), which tells the rationally good performance of trained ANN because the validation and test curves are perfectly on line, error histogram also confirms this fact in Figure. 8.9(c). It cannot be ignored that the best validation performance has attained zero epoch (shows number of passes the ANN training has performed

over entire training dataset) with the value of 6.4892*10-7, where the training persists until the 4th epoch, Figure. 8.9(b), shows best validation performance. Figure. 8.9(d) shows the training state of ANN, where the gradient coefficient's final value is $2.14*10^{-9}$, approximately zero at the 4th epoch. Also, a diminishing value of gradient can be seen with the increase of epochs number. From Figure. 8.10, it is visible that the ANN predicted and experimental values of ΔR_a between initial, and final states conform with each other to a very high degree, with the maximum error equal to 3.43%, and the other errors are negligible Figure. 8.11 shows the percentage error plot. Hence, it is certain that the developed ANN model has effectively learned the relationship between the input values and ΔR_a values, and thus can be used for maximizing the change in surface roughness.

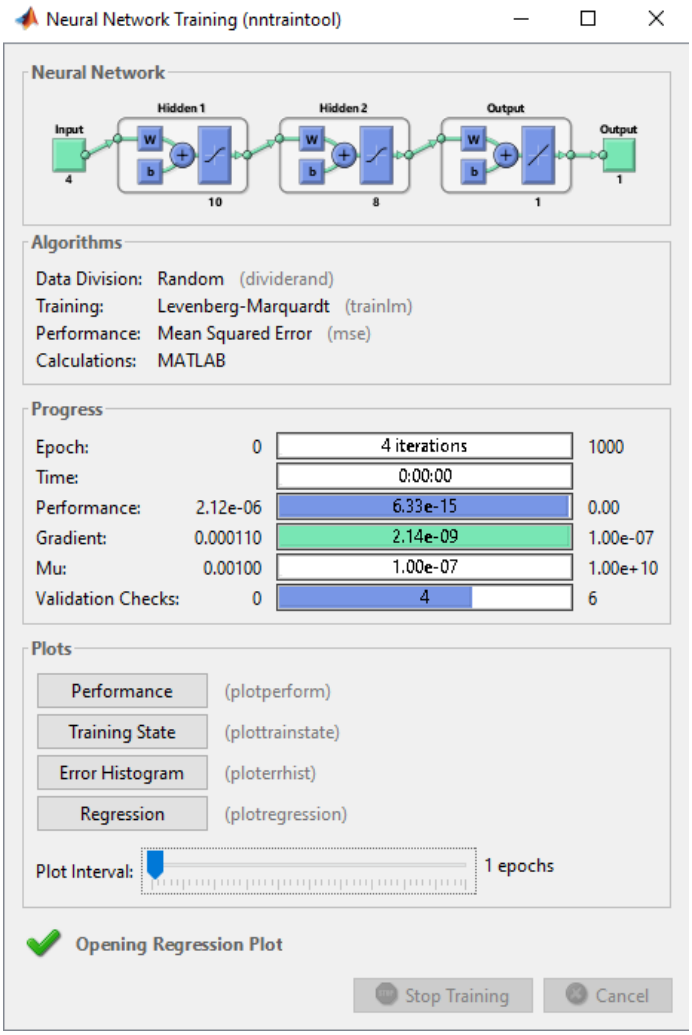

Figure 8.8 Neural network training.

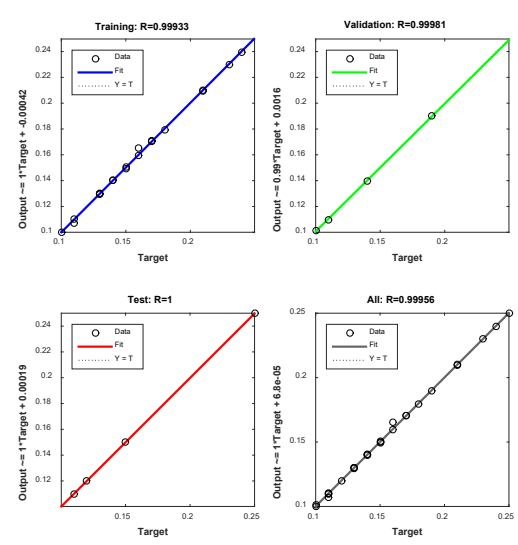

(a)

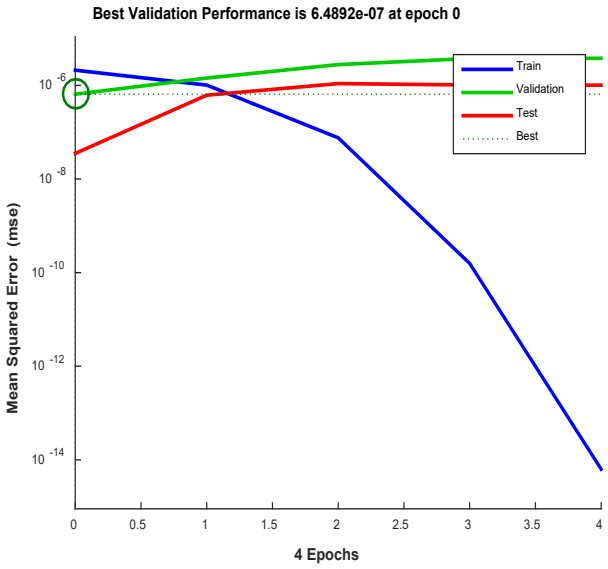

(b)

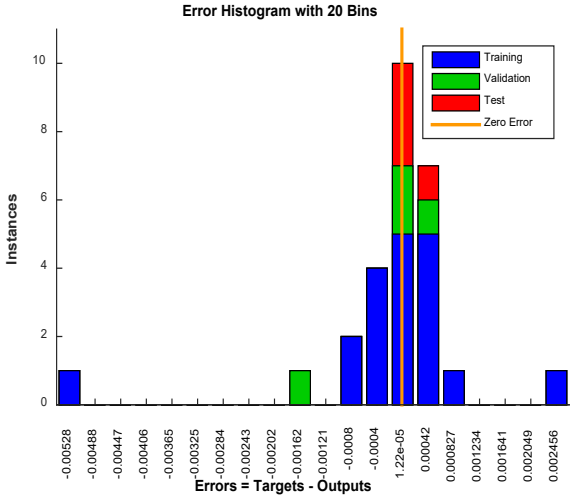

(c)

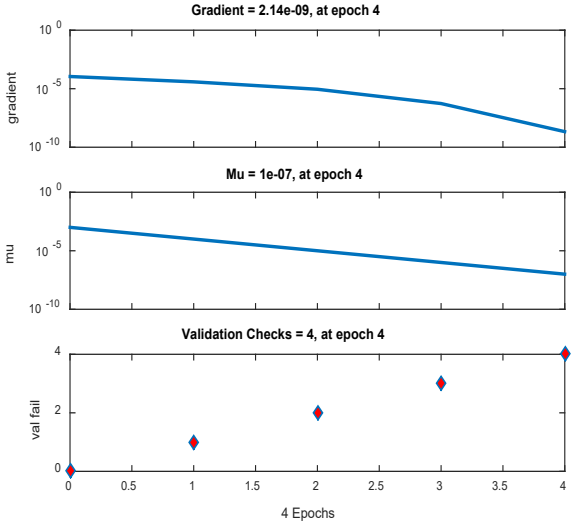

(d)

Figure 8.9 Training plots of neural network for ΔR_a: (a) Regression Performance for trained ANN (b) Variation of error with epochs (c) Error histogram plot (d) training state of ANN.

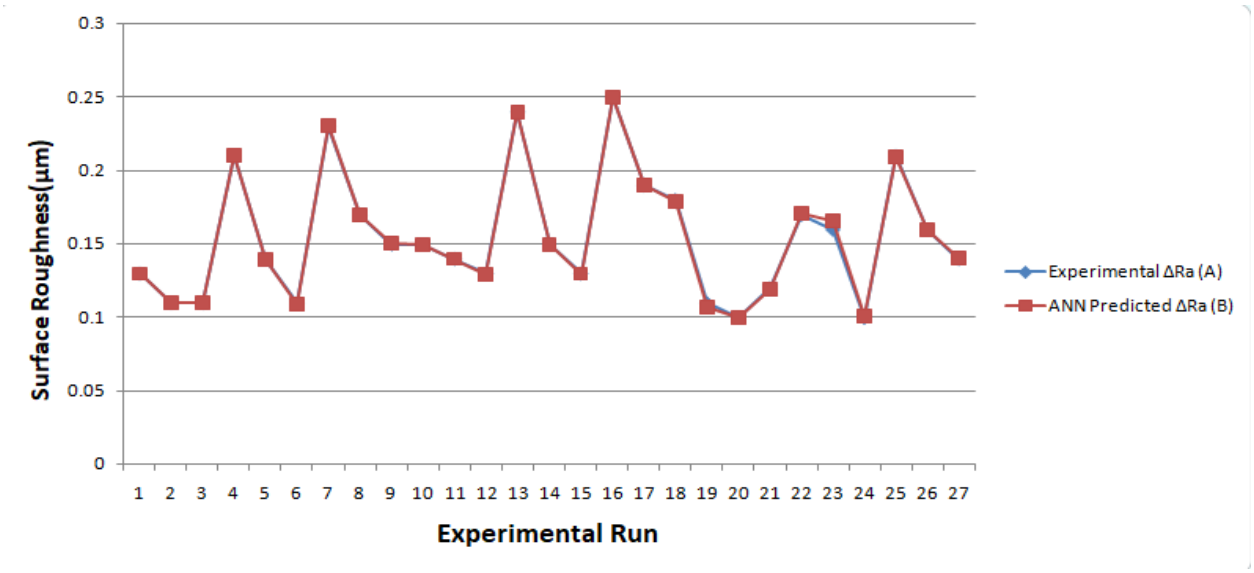

Figure 8.10 Comparison for Surface Roughness

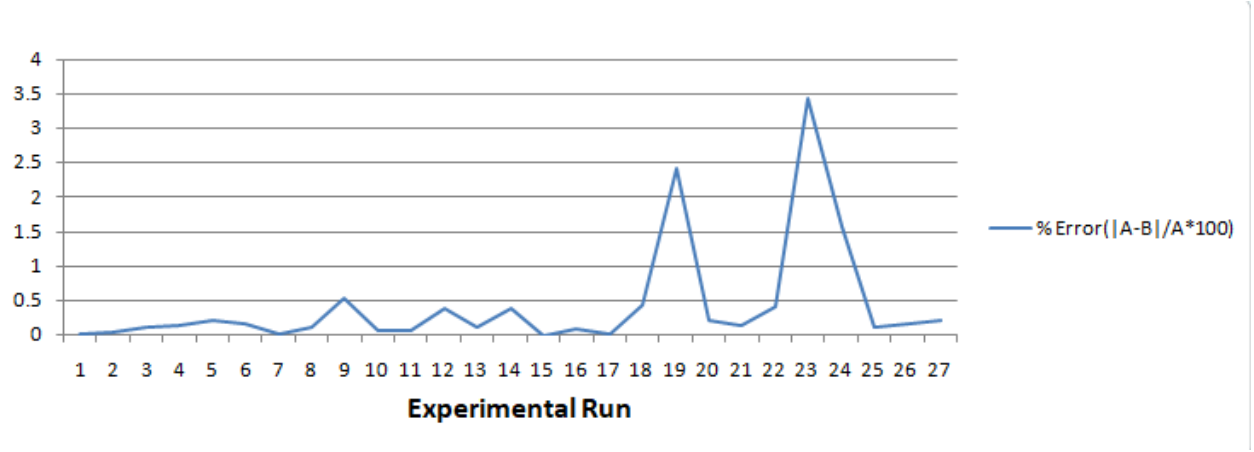

Figure 8.11 percentage error plot between Experimental and ANN predicted result

8.2.5 The individual effect of process parameters predicted by ANN Training

ANN training has predicted the relationship between the ΔR_a with controlling factors by varying the value of one factor, keeping constant value of other factors.

A Relationship between the ΔR_a with abrasive size is shown in Figure. 8.12(a), Initially, the trend is increasing until a certain limit, then it decreases. Due to the weaker magnetic bond formation on the edge of irregularity [133], the abrasive particles which are tinier than the peaks of irregularities get detached and cannot perform the shearing action satisfactorily. The increasing size of the abrasive particles improves shearing action and starts removing irregularities. The bigger particle size than irregularities shear-off the irregularities of the surface with ploughing action. These ploughing actions further cause higher surface roughness by removing the material from the root [106].

Since, voltage increase causes an increase in the strength and contact area of the magnetic brush with the target surface, which escalates the normal magnetic force (F_n); consequently, the cutting force (F_c) increases [61]. This increased F_c helps the magnetic abrasive particles to remove irregularities of the surface more efficiently. Hence, the increase in voltage causes an increase in ΔR_a and the same trend has been predicted by ANN as illustrated in Figure. 8.12(b).

When the face of electromagnet comes closer to the targeted surface, then dense electromagnetic flux causes a higher magnetic force which controls the magnetic abrasive particles to perform more intensely and vice-versa. Thus, ΔR_a decreases when the machining gap increases, the relationship illustrated in Figure.8.12(c).

Figure. 8.12(d) shows an increase in ΔR_a when rotational speed in most of the ranges increases, initially it decreases a bit because the normal magnetic force marginally decreases with increase in speed [20, 38].

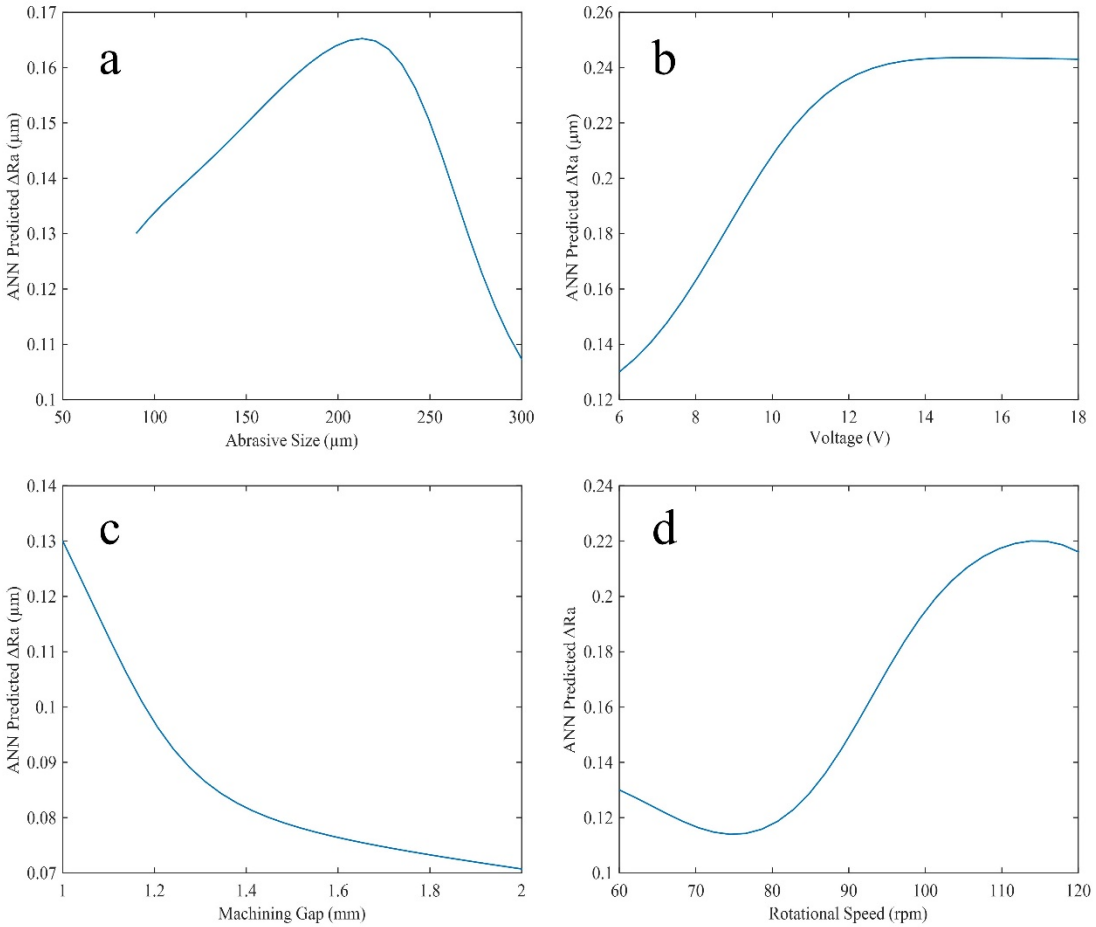

Figure 8.12 ANN predicted the individual effect of process variables (a) Effect of abrasive size on ΔR_a (b) Effect of voltage on ΔR_a (c) Effect of machining gap on ΔR_a (d) Effect of rotational speed on ΔR_a.

8.2.6 Optimization

The optimal selection of parameters has been done to increase the utility and commercial viability of manufacturing processes. Genetic Algorithms (GAs) solves optimization problems that depend on several variables. Using an input-output pattern of data from the MAF process, by combining the capability of ANN and GA to solve both the modelling and the optimization problems [131].

The basic optimization problem for this ANN-GA approach as following Eq. (4) [134]:

Optimize $y = f(x, w)$ (4)

where y represents the response or outcome of GA iteration, such as a change in surface roughness; x is a variable (instantaneous process factor during iteration) in the neural network, and w is weights that evolve in the network training process. f(.) is a fitness function that depends on the nature of input-output relation.

For the accomplishment of the target, a two-phase process has been applied. These two phases are modelling phase and optimization phase. Conventionally, the standard optimization problem is to be defined as an objective function. In this surface finishing operation, the difference between the initial and final roughness has to be maximum to achieve minimum surface roughness. Thus, the present problem is the maximization of $\triangle R_a$ and the objective function can be expressed as:

Find values of: (V, x, S, d) for which, $\triangle R_a$ is maximum.

Subjected to range of magnetic abrasive finishing parameters:

$$\left.\begin{array}{l} 6\ \text{Volts} \le V \le 18\text{Volts} \\ 1\text{mm} \le x \le 2\text{mm} \\ 90\text{rpm} \le S \le 120\text{rpm} \\ 90\mu\text{m} \le d \le 300\mu\text{m} \end{array}\right\} \quad (5)$$

where, $\triangle R_a$ is change in the surface roughness, 'V' is voltage, 'x' is machining gap, 'S' is rotational speed and 'd' is abrasive size. $\triangle R_a$ is a function of the affecting parameters which is trained by neural network.

An effective global optimization method genetic algorithm (GA), used to solve the optimization problem expressed by Eq. (4). GA is a search algorithm, analogous to the process of natural

selection that belongs to the class of evolutionary algorithms (EA). Genetic algorithms optimize the problems using methods motivated by the phenomenon of reproduction, mutation, crossover (recombination), and selection [135]. Manufacturing problems that contain data set as information and defining a continuous and smooth mathematical formula is not possible for 'optimization objective function,' can be modelled by ANN and optimized by GA. Figure. 8.13. shows a methodology for the ANN-GA operation.

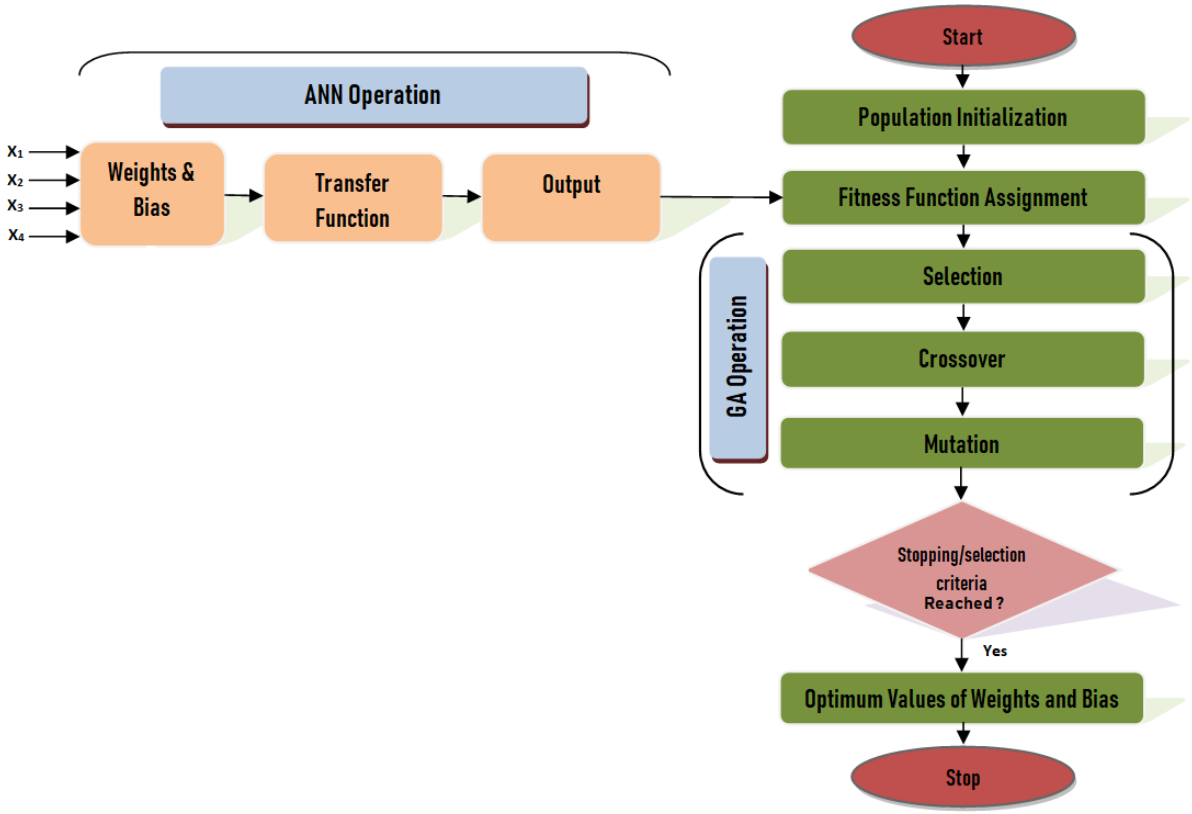

Figure 8.13 Flow chart of ANN-GA model

The decisive parameters of GA optimization operations are the population size, Crossover Fraction mutation rate, iterations number (i.e., generations). The opted initial population size was 50, the crossover rate of 0.8, the mutation rate of 0.1, and the number of iterations of 191 were utilized, and the optimization has been terminated, and optimization history plot up to 191 iterations has been shown in Figure. 8.14. Parameters of selection for GA operation have been illustrated in Table 8.4.

Table 8.4 Parameters of selection

Population Size	Population Type	Crossover Fraction	Mutation Rate	Max. Generations	Initial Population	Initial Scores
50	Double vector	0.8	0.01	191	50	50

The optimization problem in Eq. (4) has been solved with the constraint (lower and upper limits of controlling factors) to search the optimum values of finishing parameters. The contribution of the optimization process in maximizing the ΔR_a is evident when compared with Taguchi-ANOVA optimized result. From Table 8.5, ANN-GA shows $(\Delta R_a)_{max}$ of 0.256 µm, whereas Taguchi and ANOVA analysis find $(\Delta R_a)_{max}$ of 0.239µm.

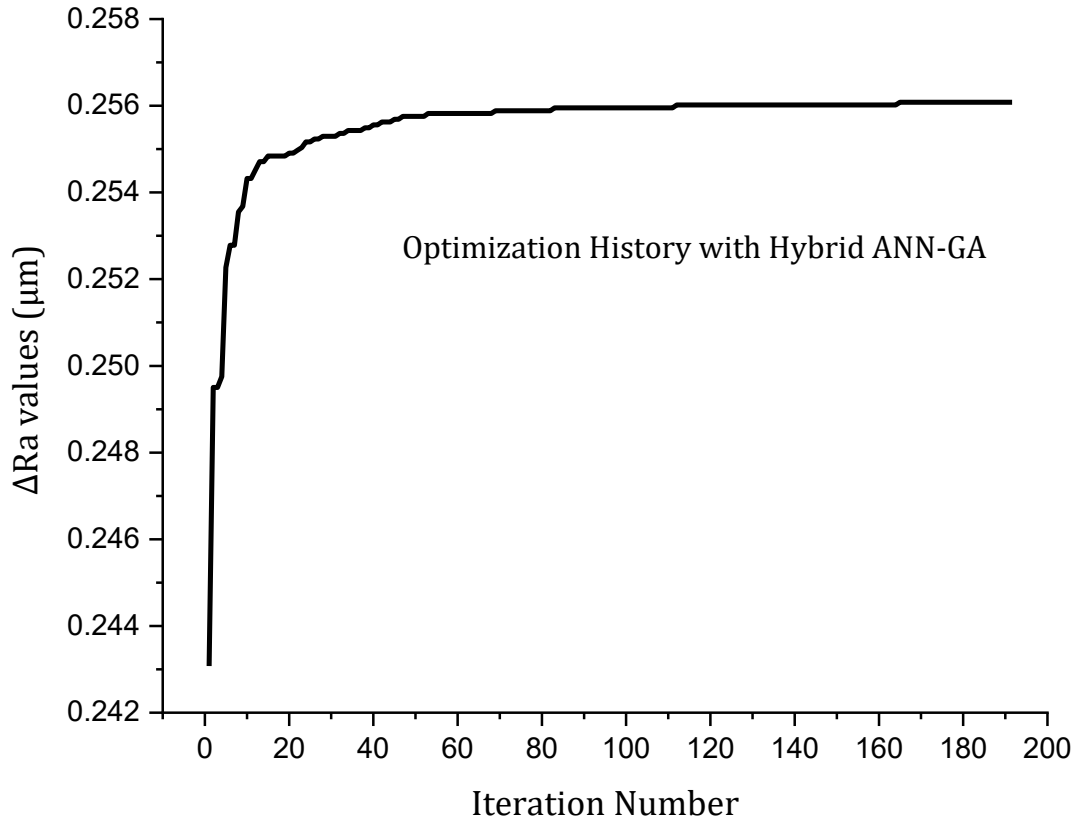

Figure 8.14 Optimization History plot

Table 8.5 Comparison of results obtained from the Taguchi method and ANN-GA Optimization

Control Factor	Taguchi Predicted	ANN-GA Predicted
Abrasive Size (μm)	150	105.158
Voltage (V)	18	17.999
Machining Gap (mm)	1	1.001
Rotational Speed (rpm)	90	91.890
Change in Surface Roughness (μm)	0.239	0.256

8.3 Results and discussion for Phase 3 (Magnetic abrasive finishing using loose magnetic abrasive and multi-objective optimization)

Air traveling became popular from the 1980s, and since then, rising demand for commercial aircraft has never ended; because of this market need, more aircraft were to be manufactured, but rising fuel prices was the parallel issue [136]. Now the manufacturing industry is compelled to reduce the weight of aircraft, but with lives were at stake; thus, compromisation with the factor of safety could never be accepted. High heat hardness, fracture toughness, corrosion resistance, high strength-to-weight ratio are few mechanical properties of mechanical parts that are expected by the aerospace, aircraft, and automotive industries [25], [137]. Ultimately more focus on research and development had to go with different materials, alloys and composites, e.g., aluminum, steel, composite, and carbon fiber, glass [138], [139]. Material industries can develop and produce the above discussed advanced engineering materials enriched with novel properties that enable them to work in the corrosion-prone environment and under high temperature, high-stress application [17], [140], [141]. Aluminum alloy and carbon fiber were suitable for the high strength-to-weight ratio [25]. Apart from the structural part, the engine's components such as discs, blades, shafts, and casings for the front fan to the rear end of the engine manufactured using Titanium and its alloys are widely used for aircraft as a replacement having lighter weight (density approx. 60% that of steel), high hardness, high strength, and excellent corrosion resistance replaced steel [49], [139], [142]. These Titanium-based engine parts must have few checks before deploying into engine assembly for the durable and safe functioning. Components should have a micro-cracks free

surface, the fine-textured surface, along with dimensional conformity [32], [143]. Also, finishing of Titanium in close tolerance without any residual stress is not suitable by conventional grinding and polishing operation due to its hardness approximately four times greater than steel [142], [144].

Magnetic abrasive finishing(MAF) is an advanced machining process in which magnetic abrasive particles work under the influence of the magnetic field, and the cutting forces produced are too less that plowing action is absent; thus, the defect-free surface is obtained [36], [44]. MAF Set-up is a low cost because it needs no special designing considerations, rigidity, vibration-free structure, etc. [49], [52], [145]]. Many researchers investigated MAF process aiming Mechanics of process, effects of process factor, nature and quality of surface produced, material removal rate (MRR), hybridization of the process to improve MRR [41], [45], [59], [61]. Hence MAF process can be a better alternative for finishing Ti-6Al-4V/Titanium (Grade 5) [47], [146].

In the literature survey, various attempts have been made by the researchers to achieve desired outputs based on surface integrity, surface finish, minor surface defects such as microcracks, etc., and various attempts have been made to improve the process efficiency with the help of different abrasive media, hybridization of MAF process, and manipulating the magnetic source and its intensity and period. Those few attempts are discussed here, e.g., Yan et al. (2004) Investigated that the MAF process can improve the quality of surfaces effectively using unbonded magnetic abrasives (UMA) and MAF process, as well as micro-crack, can be avoided by applying the same method [147]. Ahmad et al. (2017), studied the behaviour of bonded magnetic abrasives produced by sintering process to inspect the effects of process factors of the MAF process on Stainless Steel 202. Surface finish improvement was the prime motive of the study for which the magnetic abrasive particle size significantly affects [36]. Amineh et al. (2013) Reported that MAF could be a better choice for removal of the recast layer, which is hard residues generated after WECDM. The most important highlight for this particular study was the subtraction of the recast layer and micro-cracks improved by an increase of grit size [91]. Ching-Tien Lin et al. (2007) that how the MAF process affected and behaved during abrasion action on free-form surfaces of Stainless SUS304. Change of roughness was about 2.5 microns, and the 10^{th} part of microns was the order of finish achieved. It was the order similar to mirror-like surfaces [69]. Yamaguchi et al., 2012 worked on Uncoated carbide cutting tools for Titanium (Grade 5) alloy machining. They had finished uncoated carbide tool rake and flank with magnetic abrasive finishing [148]. Wang et al.

(2009) performed MAF with a new abrasive media based on silicone gel, which was mixed with Silicon Carbide (SiC) abrasive particles with ferromagnetic particles and concluded that small mesh of particles produced a high MRR. Still, at the same time, the excellent surface finish was attained by the larger mesh number particles [57]. Jain et al. (2008) studied the performance of pulsating current to make abrasive brush into a flexible one so that orientation keeps on changing for the use of the newer edge of abrasive. During static mode of current, i.e., the Direct Current supplied to electromagnet provided static brush for all time when machining was done, due to this abrasive particle face dullness in the absence of orientation change, resulting in a low rate of finishing. Performance enhancement in the process was concluded because of the regular orientation change of Flexible Magnetic Abrasive Brush (FMAB) during the switching mode of the pulsating power supply [60]. Lee et al. (2013) improved the efficiency of the MAF process by vibrational motion to change the lay of the micro-machining mark. These marks were removed by altering the set-up to vibration-assisted magnetic abrasive finishing (VAMAF) set up [50]. Li et al. have developed a Mathematical model in which MRR was a function of pressure and velocity. Their main focuses were the finishing media performance on finishing effects and efficiency. The conclusions made were, for maximum flux density, the angle between poles should be at the right angle. Also, there is a relation between ferromagnetic particles and abrasive composition with the efficiency of the process [56].

Conventional finishing methods such as grinding, honing are not capable to produce defect free surfaces and it allows high wear during the operation of the machine parts; it also results in reduced component performance and life span [149]. Therefore, the use of an unconventional method like magnetic abrasive finishing is becoming popular, and its parametric optimization is even more crucial for the reduction of processing time and cost. There are different techniques used to optimize manufacturing process parameters, such as Taguchi 's methodology, surface response methodology, fuzzy logic, gray relations techniques, etc. Also, in terms of convergence time, precision of tests, and so on, they have obvious disadvantages. The key issue connected with the modern Taguchi approach , for example, is that it cannot be used to simplify multi-objective problems [34–37]. Hence, the process parameters of the MAF process were attempted to be optimized with iterative algorithms during the finishing of the Ti-6Al-4V. The major advantages of these algorithms are that they can be used easily for any type of constrained or unconstrained problems. Genetic algorithms (GAs) can perform a global search, optimization, and generalization

[34, 35]. Also, Artificial neural networks (ANNs) have solved various parametric based problems in manufacturing processes, like pattern finding and learning in any set of data, develop the ability of pattern classification, forecasting, clustering, or modelling [31-33]. Here the feasibility of integration ANN modelling with GA optimization was implemented to predict optimum MAF parameter conditions.

This research describes the development of an artificial neural network and genetic Algorithm (ANN-GA), a modelling and optimization tool that is used to optimize a tri-objective problem. Parametric study of DC sourced magnetic abrasive finishing process. Effect of process parameters on Microhardness, Modulus of elastic indentation along with the surface roughness has been studied. Furthermore, the effect of loosely bound SiC-based magnetic abrasive media and its composition on the performance of the finishing quality on Ti-6Al-4V has been studied.

8.3.1 Artificial Neural Network (ANN)

The change in Surface roughness values (ΔR_a), change in the Microhardness (ΔHV), and change in the Modulus of Elastic Indentation (ΔEIT) between the initial and final surfaces are modelled with the help of the artificial neural network. The ANN models are developed individually for modelling ΔR_a, ΔHV, and ΔEIT.

In this work, modelling for the MAF process using ANN architecture with a backpropagation algorithm was used precisely its output concerning input parameters. Modelling the ANN works in stages: training, testing, and validation [42], [97]. The program codes were written for that purpose in MATLAB. Experimental data was trained in the ANN architecture, which is shown in Table 8.7. The neural network contains three different layers of neurons, out of which the first layer includes neurons corresponding to input parameters [153], [154]. The 1st layer being the input layer, contains '5' neurons corresponding to each of the input variables; the 2nd layer is called the hidden layer. It has 10-8, 12-10, and 12-10 neurons, respectively, for (ΔR_a) (ΔHV) and (ΔEIT), as shown in Table 8.6. The 3rd layer has '1' neuron corresponding to the single output value. For the present data outputs, the Levenberg-Marquardt training method was used for quick supervised learning is easy, safe, and computationally less expensive because of its adoptive learning and no-line search technique [155]. The transfer function selected for the hidden layer and output layer was Log-sigmoid and Tan-sigmoid, respectively, which were calculated as given by Equation (1) and Equation (2) [156]–[158].

$$tansig\ (n) = \frac{2}{(1+e^{-2n})} - 1 \qquad (1)$$

$$logsig\ (n) = \frac{1}{(1+e^{-n})} \qquad (2)$$

Where n is input for the function.

The ANN predicted, and experimental values ΔR_a, ΔHV, and ΔEIT conform with each other to a very high degree, and it is visible from Figure. 8.16, Figure. 8.17, and Figure. 8.18. The maximum error comes out between ANN predicted and experimental values for ΔR_a, ΔHV, and ΔEIT equal to 0.1388 %, 0.4387% 0.0353%, respectively. The weight and bias of the developed network are stored after confirming with this high degree of maximum error. ANN architecture presented in Table 8.6 and the developed Neural Network architecture can be seen in Fig. 8.15. The number of the hidden layers and the number of neurons in each hidden layer were chosen based on the network output following exhaustive trails Network efficiency was calculated by percentage error [132], [159]. The percentage error was measured as Equation (3)., and the values determined are shown in Table 8.7. Hence it is assured that the developed ANN model has effectively learned the relationship between the input and the output values. Thus, it can be used for the optimization of the process.

$$Percentage\ error = \frac{(Experimental\ value - ANN\ predicted\ value)\times 100}{Experimental\ value} \qquad (3)$$

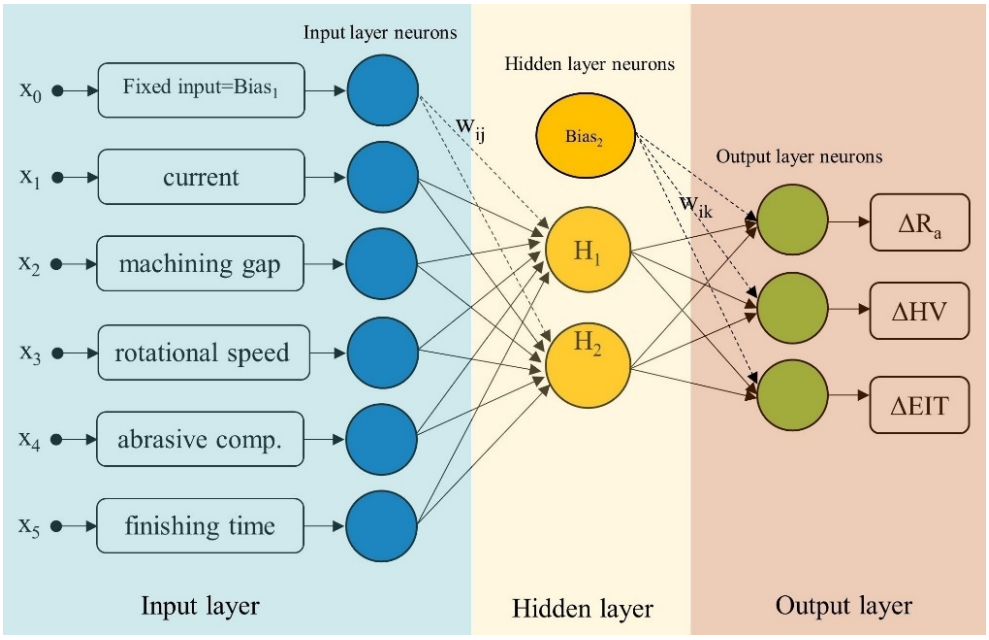

Figure 8.15 ANN architecture.

Table 8.6 ANN architecture for input to output modelling

Input	Output	ANN architecture
x_1, x_2, x_3, x_4, x_5	ΔR_a	5-10-8-1
x_1, x_2, x_3, x_4, x_5	ΔHV	5-12-10-1
x_1, x_2, x_3, x_4, x_5	ΔEIT	5-12-10-1

Table 8.7 Experimental and ANN predicted Results corresponding to L16 orthogonal array

S. No.	Input parameters and their values					Experimental			ANN Predicted			error %		
	x_1	x_2	x_3	x_4	x_5	ΔR_a (µm)	ΔHV	ΔEIT (GPa)	ΔR_a (µm)	ΔHV	ΔEIT (GPa)	ΔR_a (µm)	ΔHV	ΔEIT (GPa)
1	0.8	1.5	112	40	10	0.076	56.97	12.14	0.0759	56.9700	12.1400	0.1315	0	0
2	0.8	2	150	50	15	0.066	51.63	11.27	0.0660	51.6300	11.2699	0	0	0.0008
3	0.8	2.5	220	60	20	0.065	50.73	11.08	0.0650	50.7300	11.0800	0	0	0
4	0.8	3	300	70	25	0.065	51.18	11.18	0.0650	51.1800	11.1799	0	0	0.0008
5	1.2	1.5	150	60	25	0.118	89.29	19.50	0.1179	89.2900	19.4994	0.0847	0	0.0030
6	1.2	2	112	70	20	0.078	52.96	11.56	0.0779	52.9893	11.5600	0.1282	0.0553	0
7	1.2	2.5	300	40	15	0.090	80.71	17.26	0.0900	80.7004	17.2661	0	0.0118	0.0353
8	1.2	3	220	50	10	0.050	38.50	08.42	0.0499	38.5000	08.4199	0.2000	0	0.0011
9	1.6	1.5	220	70	15	0.109	83.18	18.17	0.1090	83.1800	18.1699	0	0	0.0005
10	1.6	2	300	60	10	0.095	79.58	17.38	0.0949	79.5800	17.3801	0.1052	0	0.0005
11	1.6	2.5	112	50	25	0.106	79.68	17.39	0.1060	79.6800	17.3900	0	0	0
12	1.6	3	150	40	20	0.087	70.14	15.12	0.0870	70.1400	15.1199	0	0	0.0006
13	2	1.5	300	50	20	0.160	133.59	29.15	0.1599	133.5900	29.1499	0.0625	0	0.0003
14	2	2	220	40	25	0.157	128.13	27.70	0.1570	128.1300	27.6999	0	0	0.0003
15	2	2.5	150	70	10	0.072	50.58	11.07	0.0719	50.3581	11.0716	0.1388	0.4387	0.0144
16	2	3	112	60	15	0.073	51.05	11.15	0.0729	51.0500	11.1500	0.1369	0	0

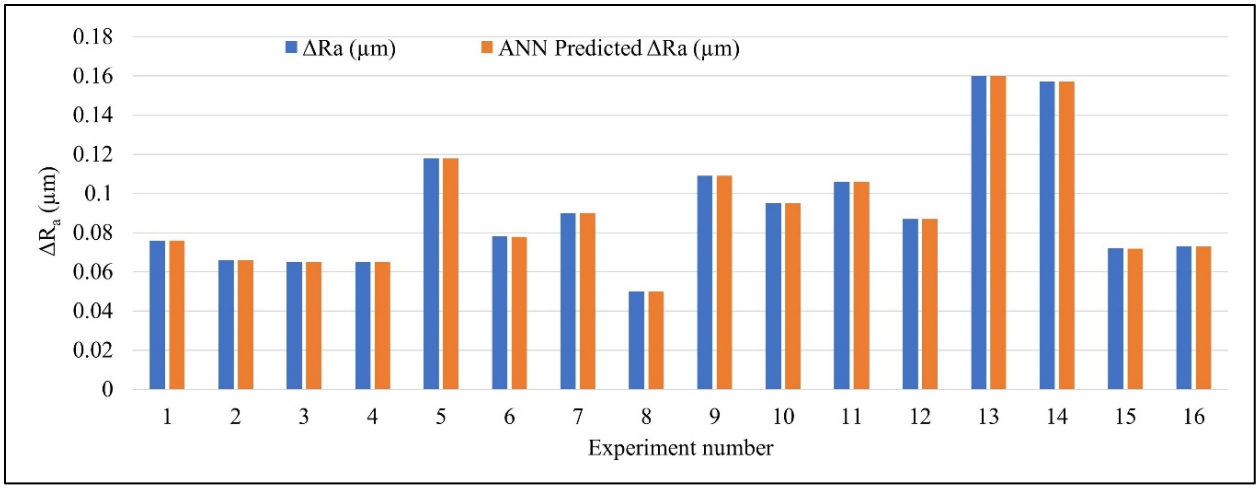

Figure 8.16 Comparison between experimental and ANN predicted ΔR_a

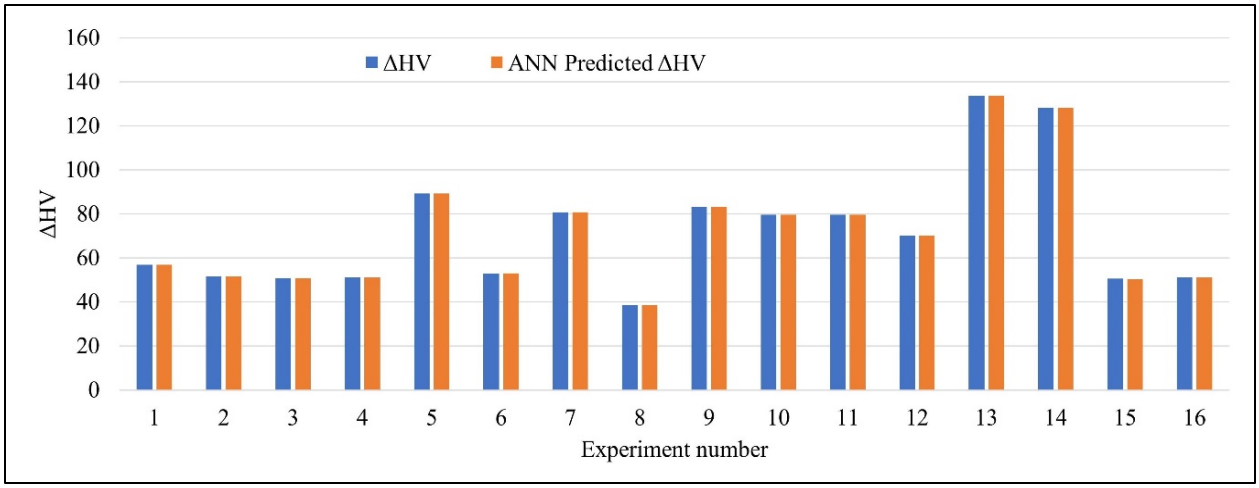

Figure 8.17 Comparison between experimental and ANN predicted ΔHV

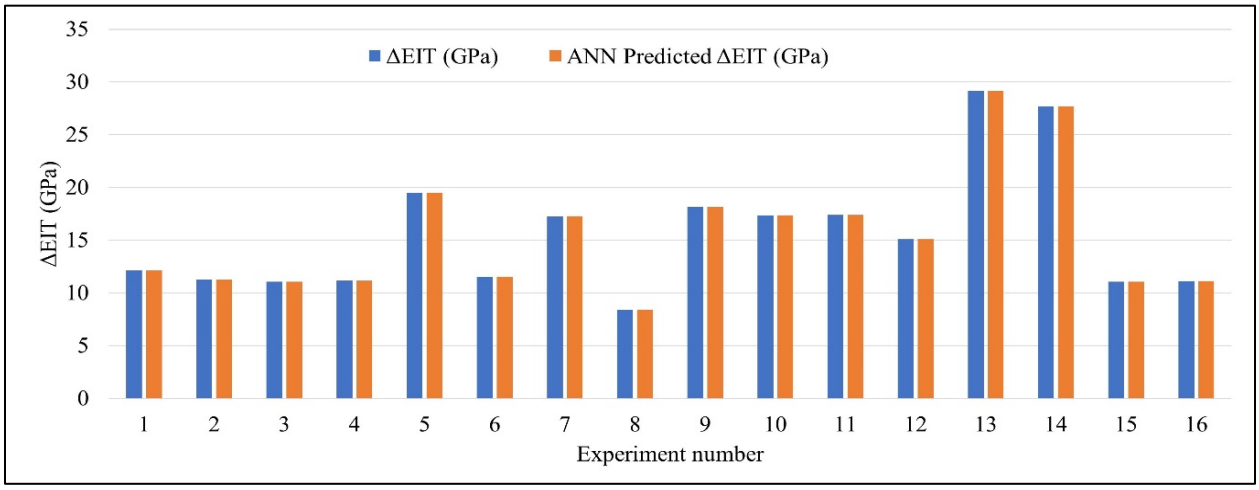

Figure 8.18 Comparison between experimental and ANN predicted ΔEIT

8.3.2 Genetic Algorithm (GA) and process optimization

It is observed from the ANN models developed and from the literature that the output responses [160], such as the ΔR_a, ΔH, and ΔEIT, are concurrent and harmonious nature. Therefore, the multi-optimal combination of process parameters would satisfy the objectives [99], [150], [159]. The Genetic Algorithm is able to offer better performance compared to traditional optimization techniques Because of its robustness, independence of gradient knowledge, and usage of intrinsic parallelism in design space searches [33], [152].

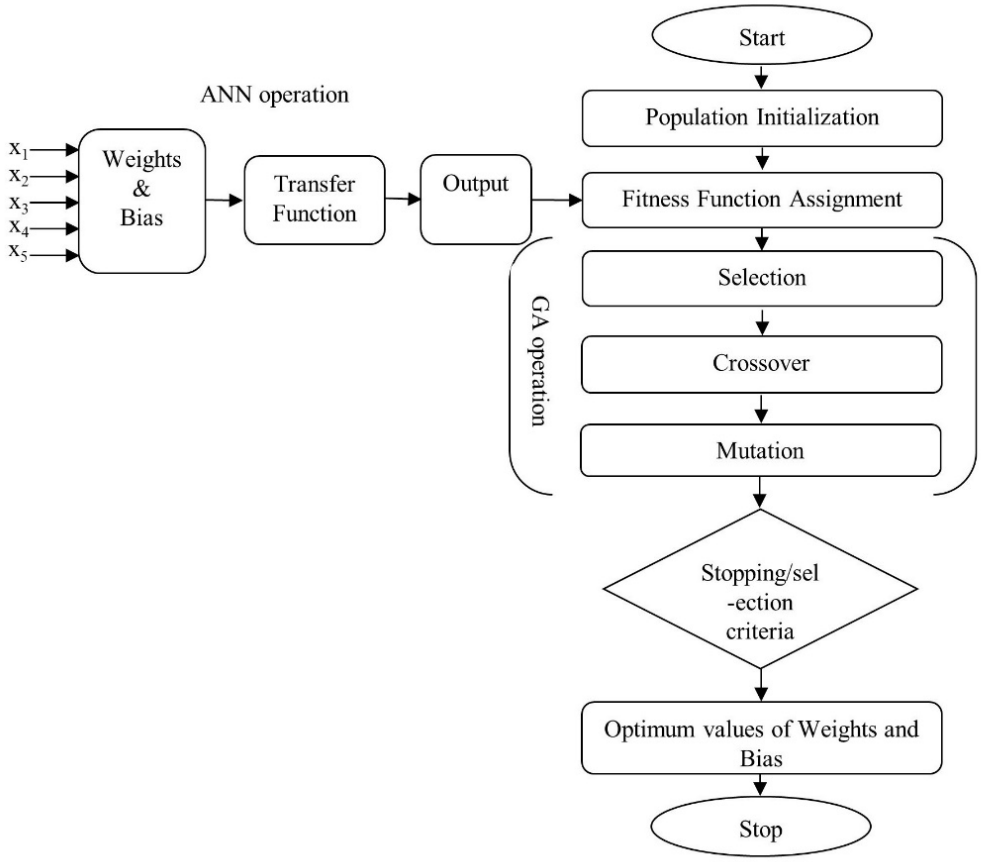

Figure 8.19 Flow chart of ANN-GA model

Genetic Algorithm is a commercially viable, less complicated, and quicker for multi-objective optimization [32,44]. An effective global optimization method, GA, is used to solve the optimization problem. GA is a search algorithm, analogous to the natural selection process which belongs to the class of evolutionary algorithms. GA optimize the problems using methods motivated by the phenomenon of reproduction, mutation, crossover (recombination), and selection

[135], [161]. Manufacturing problems that contain data set as information and defining a continuous and smooth mathematical formula is not possible for 'optimization objective function,' can be modelled by ANN and optimized by GA. To this intend, the ANN models developed in MATLAB were coupled with GA. The various steps to be implemented for operation with ANN-GA are described in Figure. 8.19. Initially, a random population of size '50' was taken by (5-10-8-1), (5-12-10-1), and (5-12-10-1) ANN models.

8.3.3 Results and Discussion

The experimental results conducted during the investigation are further used to develop a model of the MAF process using artificial neural networks. The values of the output parameters obtained after carrying out each experiment in the design of the experiment table are given in Table 8.7. The ANN models developed were used to predict the output for various input sets, and keeping other input parameters constant the influence of the input parameter on the output is observed, in section 6.1 the parametric analysis is summarized, whereas the findings of optimization and related discussion are outlined in the next article 6.2.

8.3.3.1 Parametric analysis using ANN models

In this section, the developed (5-10-8-1), (5-12-10-1), and (5-12-10-1) ANN model for ΔR_a, ΔHV, and ΔEIT respectively are used to understand the consequence of input or process parameters. These parameters such as current, machining gap, rotational speed, abrasive composition, and finishing time on output parameters ΔR_a, ΔHV, and ΔEIT on the Ti-6Al-4V workpiece.

8.3.3.2 Effect of current

Figure. 8.20, illustrates the effect of current on ΔR_a, ΔHV, and ΔEIT. It is observed that on increasing the current the outputs ΔR_a, ΔHV, and ΔEIT increases. An increase in current increases the magnetic field intensity, which helps in forming a stronger FMAB so that metal removing action by magnetic abrasive media becomes more active. A curve of the dome structure appears at 1.5 Amp in HV. This is because abrasive media are continually rubbing and flushing the removed material. Precisely a heat treatment process is taking place [55], [73]. At higher pressure (due to higher normal magnetic force), The workpiece interacts with a large number of abrasive particles,

which results in heat generation. At the same time, the heated abrasive media increasingly carried out the heat produced.

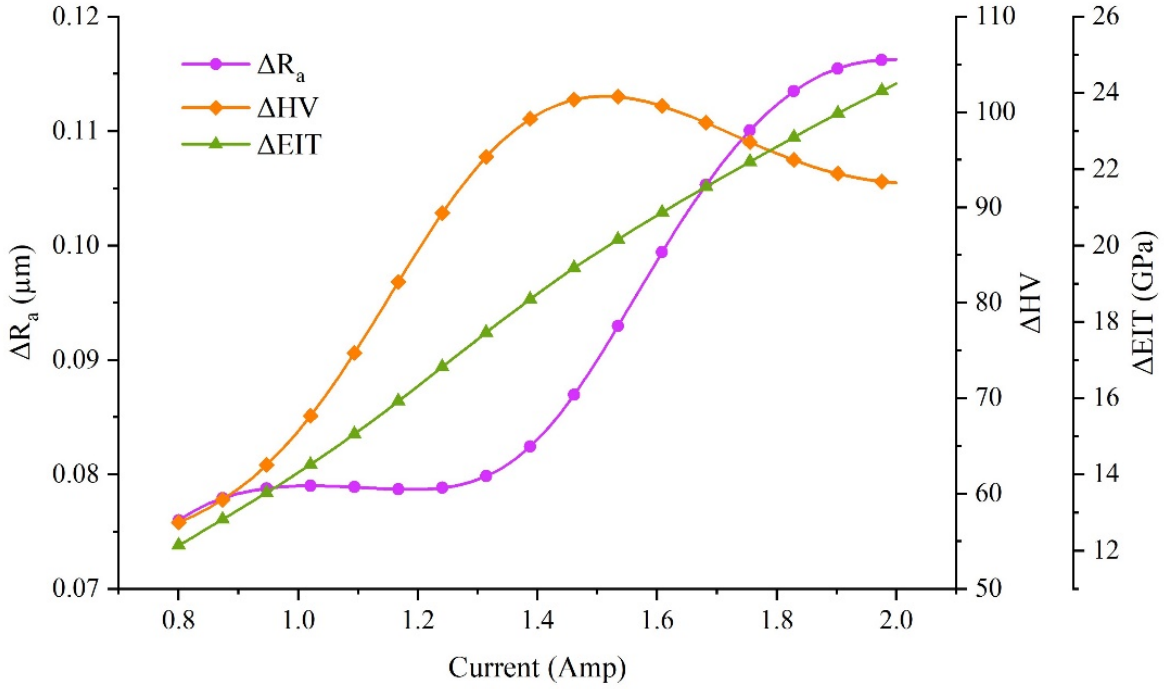

Figure 8.20 Effect of current on ΔR_a, ΔHV, and ΔEIT

8.3.3.3 Effect of the machining gap

A relationship between the machining gap with ΔR_a, ΔHV, and ΔEIT is represented in Figure. 8.21. It can be observed that output parameters are inversely proportional to the machining gap, i.e., it decreases with the increase in the machining gap, and this trend is similar for all the output parameters. Their magnitude increases with the decline in the machining gap. The reason for this observation is that on reducing the machining gap, the magnetic field intensity amplifies, which further results in the rise of the normal magnetic force and intensify the control over FMAB. Thus, improving the finishing action. Since ΔHV and ΔEIT are harmonious to ΔRa, the same effect has been observed on them, too [162].

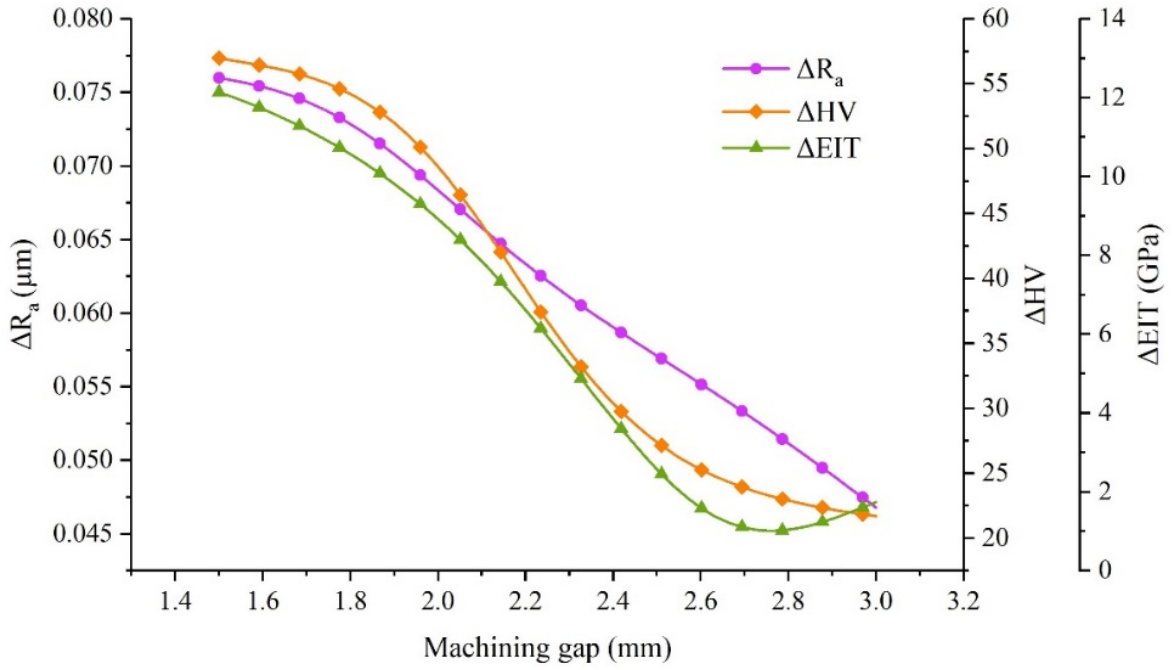

Figure 8.21 Effect of machining gap on ΔR_a, ΔHV, and ΔEIT

8.3.3.4 Effect of rotational speed

The effect of rotational speed on ΔR_a, ΔHV, and ΔEIT, is illustrated in Figure. 8.22. It is observed that a notable rise in ΔRa with a minute decrease at a lower rotational speed with the increase in the rotational speed. An increase in the rotational speed indicates an improvement in machining efficiency. Moreover, it also signifies the removal of machined particles in the form of microchips, which intern results in the decline of surface roughness value, i.e., an increase in the magnitude of ΔRa. With the help of the trends, it can also be concluded that the value of ΔHV and ΔEIT intensifies with the rotational speed only up to 210 rpm, post that their value starts decreasing with an increase in the rotational speed. It is also observed that the rate of decrement of ΔEIT is greater than ΔHV.

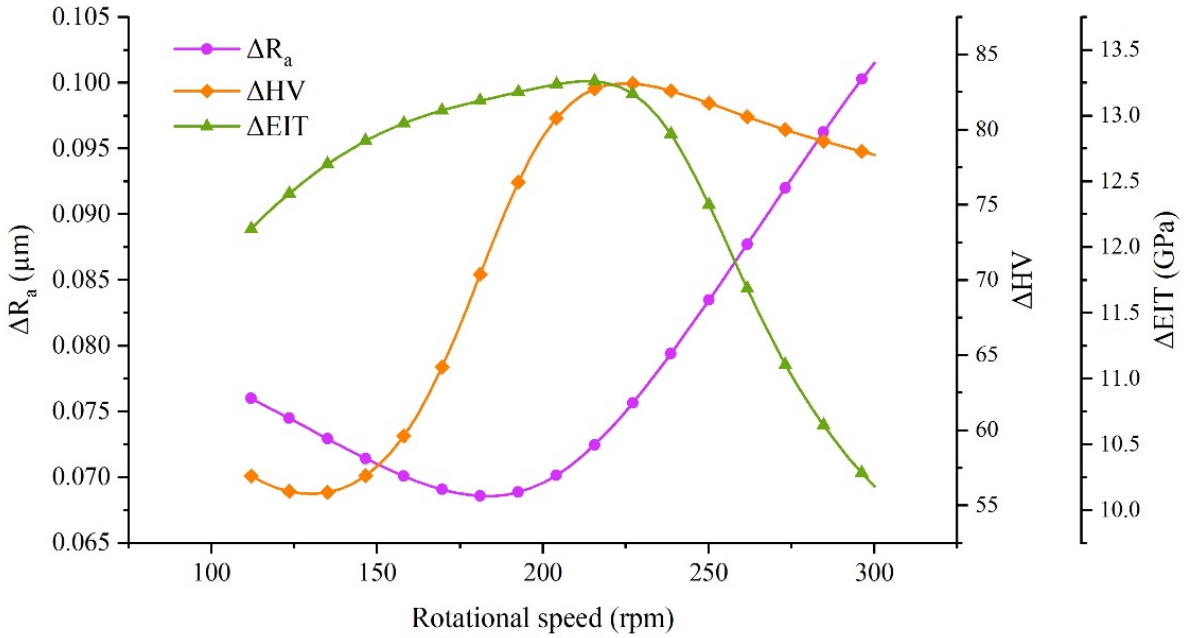

Figure 8.22 Effect of the abrasive composition

8.3.3.5 Effect of abrasive composition

The effect of the abrasive composition on ΔR_a, ΔHV, and ΔEIT is shown in Figure. 8.23.

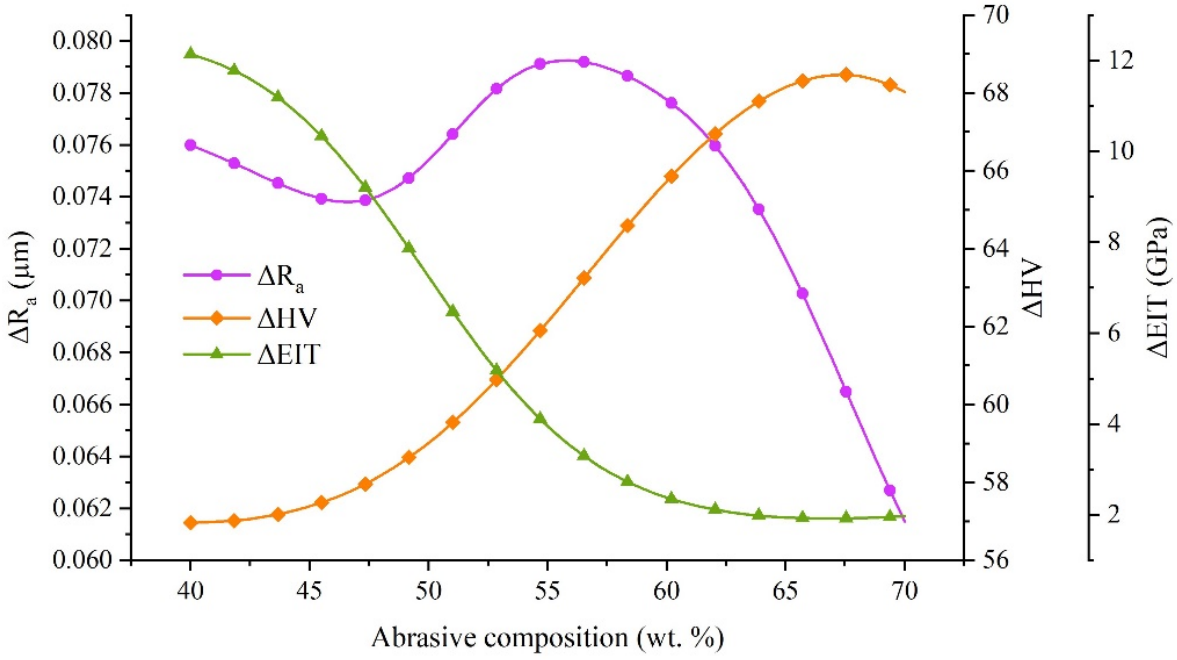

Figure 8.23 Effect of abrasive composition on ΔR_a, ΔHV, and ΔEIT

It is observed that ΔR_a attained its maximum value in the range 55-58 abrasive composition and later decreased on the increase in abrasive composition with a slight decrease in lower values of abrasive compositions. For ΔHV, it is noticed that on increasing abrasive composition, ΔHV value rises. ΔEIT decreases on increasing the abrasive composition.

8.3.3.6 Effect of finishing time

The effect of finishing time on ΔR_a, ΔHV, and ΔEIT is illustrated in Figure. 8.24. It is noted that with the increase of finishing time, ΔR_a increases. Also, it is found that after 16 minutes of finishing time, the ΔR_a decreases abruptly because of higher grinding efficiency that leads to significant material removal rates in confined zones, which further formed more profound valleys. Also ΔHV, and ΔEIT showed increasing pattern with finishing time, where a slight decrease in ΔEIT initially on the lower side of finishing time [38].

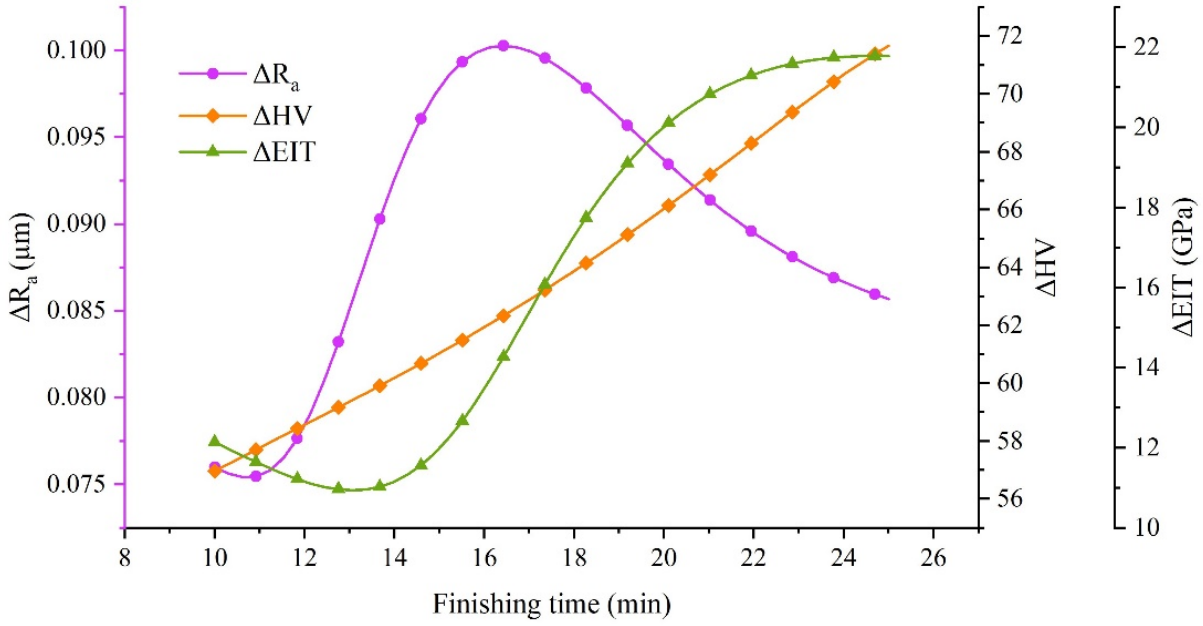

Figure 8.24 Multi-objective optimization using ANN-GA

To optimize (maximize) the change in surface roughness, change in microhardness, and change in the modulus of elastic indentation, the developed ANN models are fed to a genetic algorithm program that calculates the value of each input parameter corresponding to the maximum output value achievable. This required goal was framed as objective functions, for optimizing the MAF process using GA. Furthermore, the developed ANN models were linked with GA, for the present

tri-objective optimization. For this purpose, a GA program in MATLAB-15a is written as per objective. The goals of the present research are to optimize change in surface roughness, change in microhardness, and change in elastic indentation modulus. The objectives are as shown below-

$$\text{Objective 1} = \text{Minimize } (1/\ \Delta Ra)$$

$$\text{Objective 2} = \text{Minimize } (1/\ \Delta HV)$$

$$\text{Objective 3} = \text{Minimize } (1/\ \Delta EIT)$$

The program code is written in MATLAB for the GA based optimization of the ANN model as per objectives. During this optimization, GA was applied to the trained (5-10-8-1, 5-12-10-1, and 5-12-10-1) ANN models for the determination of the objectives function. The ANN component is responsible for deciding the objective functions in the process of combined optimization by the ANN-GA model, while the GA aspect is responsible for ranking and sorting the ANN-based solution. The developed ANN models provide the initial population of size 50 in the first iteration of optimization, and it is used in the subsequent iteration to measure the outputs viz. ΔRa, ΔHV, and ΔEIT for new offspring. During optimization process it is found that after 148 iterations, the optimum data is obtained. No noticeable improvement in process parameters was observed after that if the iterations reached 148 iterations. The Pareto fronts hence obtained were extracted for further analysis, and the optimal front of these 18 non-dominated solutions are illustrated in Figure.8.25. None of the other solutions was found to dominate the non-dominated solutions. It may hence be concluded that the preference of one solution over another solely depends on the product specifications and the predilection of the process engineer. Therefore, all the data collected was solutions. These 18 solutions have been presented in Table 8.8.

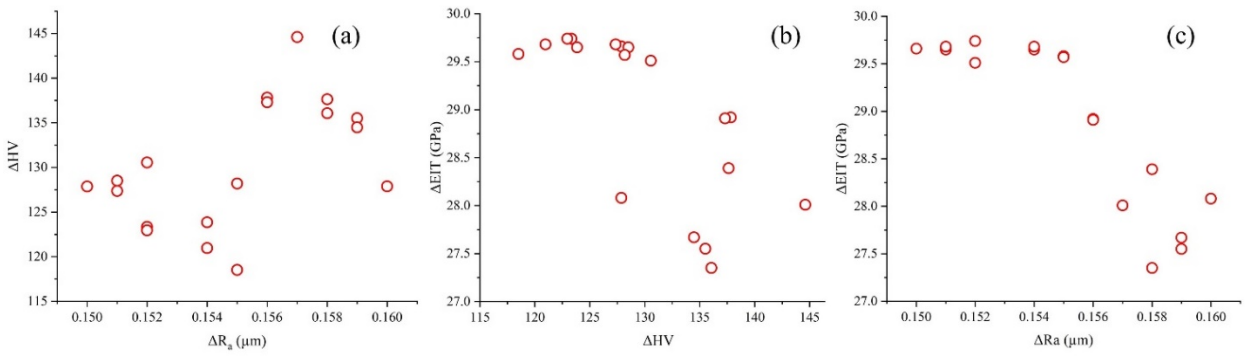

Figure 8.25 Comparison of experimental and optimal ΔRa

8.3.3.7 Comparison of experimental and optimal ΔRa

Upon comparison of experimental ΔR_a values with the values found from Pareto optimal solution, it is noted the maximum value of experimental ΔR_a is 0.160 μm at current = 2 A, machining gap = 1.5 mm, rotational speed = 300 rpm, abrasive composition = 50% and finishing time = 20 min, as shown in experiment number 13 in Table 8.7. Whereas, the maximum ΔR_a obtained from optimal solution is 0.160 μm at current = 1.99 A, machining gap = 1.51 mm, rotational speed = 223.55 rpm, abrasive composition = 53.65% and finishing time = 20.77 min, as illustrated in Table 8.8 (S. No 2). It can be concluded from these results that though the current, machining gap and finishing time are almost the same, there has been a significant drop (25.48%) in the rotational speed upon the change of the rotational speed from 300rpm to 223.55rpm. Due to this, the abrasive composition has increased from 50% to 53.65% in the optimal solution, even though the ΔR_a obtained from the optimal solution is the same. This proves that a calculated selection of process parameters can provide huge savings in energy consumption as rotational speed is decreased for the same output and effective abrasive composition. Furthermore, it can be seen that the combination of high current, less machining gap, moderate rotational speed, and abrasive composition, and sufficient finishing time is more suitable for achieving a higher ΔR_a. It can be clearly noted from Table 8.7 (Exp. 8) that a lower experimental value of ΔR_a (=0.050 μm) can be attributed to a current = 1.2 A, machining gap = 3 mm, rotational speed = 220 rpm, abrasive composition = 50% and finishing time = 10 min, while the lower ΔR_a obtained from non-dominated solution set is 0.150 μm at current = 1.99 A, machining gap = 1.51 mm, rotational speed = 223.18 rpm, abrasive composition = 44.66% and finishing time = 16.86 min (Table 8.8, S. No 4). The results show that this value of lower ΔR_a corresponding to the optimal solution is significantly higher (nearly three times) than the experimental value. This is because of the formation of a strong, flexible magnetic abrasive brush with a higher current and lower machining gap. Also, an increase in rotational speed improved the metal removal action, and 6.86 min more finishing time.

8.3.3.8 Comparison of experimental and optimal ΔHV

During the comparison of experimental ΔHV with Pareto optimal solution, the maximum value of experimental ΔHV was 133.59 at current 2 A, machining gap 1.5 mm, rotational speed 300 rpm, abrasive composition 50% and finishing time 20 min, corresponding to the experiment number 13

in Table 8.7. Furthermore, the maximum ΔHV obtained from the optimal solution was 144.61 at 1.99 A current, 1.53 mm machining gap with 224.00 rpm rotational speed, and 42.25% abrasive composition taking a finishing time of 16.68 minutes as demonstrated in Table 8.8. It is to be observed that with the same current and machining gap, a decrease of 25.34% in rotational speed (from 300.00 rpm to 224.00 rpm) and a marginal decrease in abrasive composition from 50.00% to 42.25% was there. However, the finishing time was higher during the optimal solution (24.60 minutes) as compared to the experimental one (20.00 minutes). A Prime indication is that a careful selection of process parameters can improve the ΔHV by 8.24 %. The combination of high current, machining gap, and finishing time, with moderate rotational speed, and low abrasive composition has been found to be more appropriate for attaining higher ΔHV. In Table 8.7 (Exp. 8), it has been demonstrated that the minimum experimental value of ΔHV was 38.50 at a current of 1.2 A, machining gap of 3.00 mm along with 220.00 rpm rotational speed and 50.00% abrasive composition taking the finishing time 10.00 minutes. Moreover, it is shown in Table 8.8 (S.No. 15) that the minimum value of ΔHV found from the non-dominated solution set was 120.97 at a current of 1.99 A, machining gap of 1.51 mm with the rotational speed of 222.90 rpm and 48.89% abrasive composition taking a finishing time of 16.68 minutes. Based on the data obtained, it can be concluded that the minimum value of ΔHV from the optimal solutions is around three times higher than its experimental value.

8.3.3.9 Comparison of experimental and optimal ΔEIT

On comparing the experimental ΔEIT and non-dominated solution from the Pareto Front. The maximum experimental ΔEIT value from Table 8.7 (Exp. 13) is 29.15 GPa at current = 2 A, machining gap = 1.5 mm, rotational speed = 300 rpm, abrasive composition = 50% and finishing time = 20 min, On the other hand, the maximum ΔEIT obtained from optimal solution is 29.74 GPa at current = 1.99 A, machining gap = 1.51 mm, rotational speed = 224.17 rpm, abrasive composition and finishing time is 47.02% and 16.46 min or 47.27% and 16.38 min respectively, as shown in Table 8.8 (S.No 3 and 18). By comparing the optimal solution with experimental values, it is noted that the current, machining gap, are almost the same. Still, the rotational speed is almost 25% less (from 300 rpm to 224.17 rpm), abrasive composition and finishing time are slightly lower (from 50% to 47% and 20 min to 16 min respectively). The ΔEIT obtained from the optimal solution is much higher. Thus, it concludes that the right selection of process parameters

will save enormously on energy consumption as rotational speed is decreased for the same output and effective abrasive composition [36]. In Table 8.7 (Exp. 15), the lowest experimental value of ΔHV is 11.07 GPa at current = 2 A, machining gap = 2.5 mm, rotational speed = 150 rpm, abrasive composition = 70% and finishing time = 10 min, whereas the lowest ΔEIT value obtained from non-dominated solution set is 27.35 GPa at current = 1.99 A, machining gap = 1.52 mm, rotational speed = 223.66 rpm, abrasive composition = 51.99% and finishing time = 23.95 min as shown in Table 8.8 (S.No. 5). The results show that the lowest ΔEIT obtained from the optimal solution is significantly higher (about 2.5 times) than the experimental value. This significantly better result may be attributed to a slight increase in rotational speed and 6.86 min longer finishing time, which improved metal removal [61].

Table 8.8 Optimal solution set and corresponding inputs-outputs

S. No.	ΔR_a (µm)	ΔHV	ΔEIT (GPa)	Current (Amp.)	Machining gap (mm)	Rotational speed (rpm)	Abrasive Composition (wt. %)	Finishing time (min)
1	0.157	144.61	28.01	1.99	1.53	224.00	42.25	24.60
2	0.160	127.88	28.08	1.99	1.51	223.55	53.65	20.77
3	0.152	123.33	29.74	1.99	1.51	224.17	47.02	16.46
4	0.150	127.86	29.66	1.99	1.51	223.18	44.66	16.86
5	0.158	136.07	27.35	1.99	1.52	223.66	51.99	23.95
6	0.156	137.82	28.92	1.99	1.51	223.99	44.23	20.33
7	0.159	135.52	27.55	1.99	1.52	223.36	51.92	23.35
8	0.154	123.85	29.65	1.99	1.51	222.96	48.43	17.34
9	0.151	128.51	29.65	1.99	1.51	223.49	44.77	17.13
10	0.155	118.51	29.58	1.99	1.51	223.17	50.37	16.66
11	0.152	130.55	29.51	1.99	1.52	223.58	44.61	17.92
12	0.156	137.30	28.91	1.99	1.51	223.90	44.86	20.39
13	0.159	134.48	27.67	1.99	1.51	223.21	52.13	22.76

14	0.158	137.64	28.39	1.99	1.51	223.78	47.78	21.84
15	0.154	120.97	29.68	1.99	1.51	222.90	48.89	16.68
16	0.155	128.19	29.57	1.99	1.51	223.59	47.30	18.13
17	0.151	127.36	29.68	1.99	1.51	223.12	45.43	17.07
18	0.152	122.95	29.74	1.99	1.51	224.17	47.27	16.38

8.3.4 Surface morphology and roughness

To comprehend the surface wear pattern at the micro-nano level, the Scanning electron microscopy and Atomic force microscopy of the workpiece surface checked on various experimental conditions of the MAF process and shown in Figures. 8.26(a–c) and in Figures. 8.27(a–c) respectively.

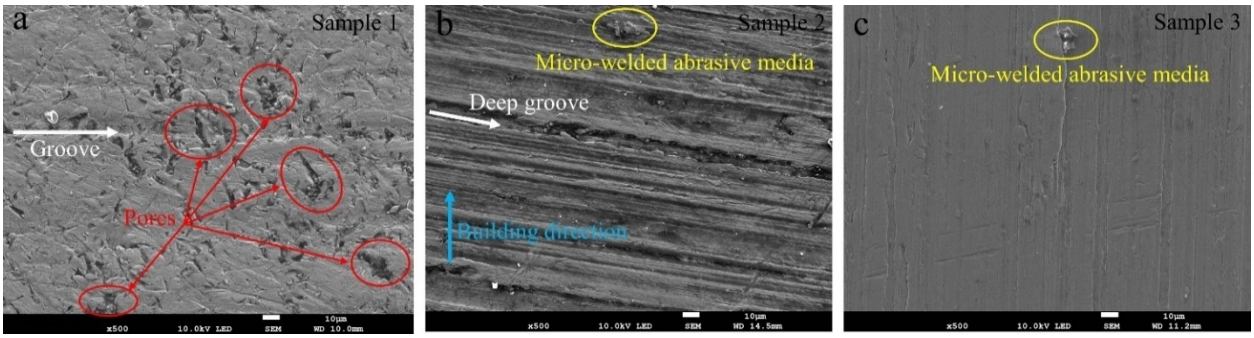

Figure 8.26 SEM images in various experimental conditions (a) voltage=0.8V; machining gap=1.5 mm; rotational speed =112 rpm; abrasive composition. =40; time=10 min; (b) voltage= 1.6V; machining gap =1.5 mm; rotational speed =220 rpm; abrasive composition. =70; time=15 min; (c) voltage=2.0V; machining gap =1.5 mm; rotational speed =300 rpm; abrasive composition= 50; time= 20 min.

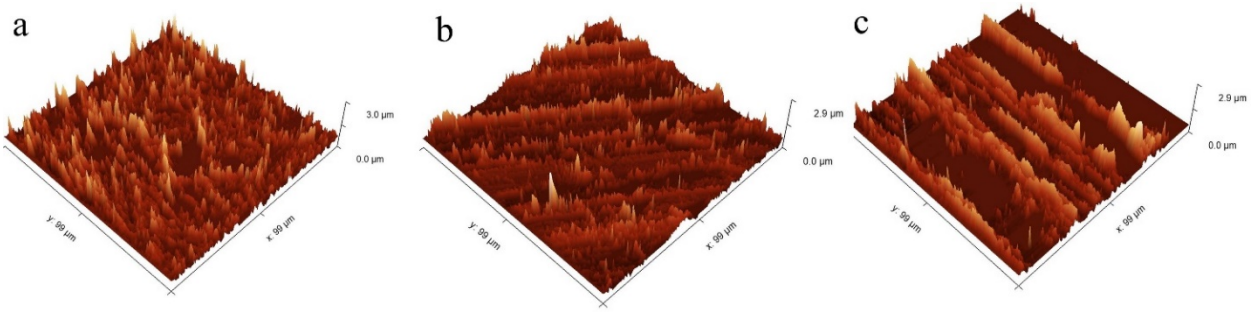

Figure 8.27 AFM images of workpiece in various experimental conditions (a) voltage=0.8V; machining gap=1.5 mm; rotational speed =112 rpm; abrasive composition= 40; time= 10 min; (b) voltage= 1.6V; machining gap= 1.5 mm; rotational speed = 220 rpm; abrasive composition= 70; time= 15 min; (c) voltage= 2.0V; machining gap= 1.5 mm; rotational speed = 300 rpm; abrasive composition= 50; time= 20 min.

The FMAB has substantially sheared off the peaks of the pre-processed ground workpiece, as can be seen in Figure. 8.26b and Figure. 8.26c. The behaviour of the FMAB fluctuates more at lower current and less abrasive composition. Hence some pores and deep scratches that damaged the finished surface are also observed in Sample 1 at voltage=0.8V, abrasive composition= 40 (Figures. 8.26a), it can also be seen in same the figure that a groove begins to form because of the bulge of magnetic abrasive media in a confined area. The reason for the formation of the bulge is concentrated magnetic flux, which is either because of nonuniform coil winding or non-homogeneous electromagnet core material. The surface texture obtained, as shown in (Figures. 8.26b–8.26c), is flatter with less groove depth resulting in a low Ra (finished surface) value. Owing to the variable intensity of FMAB and abrasive material contact with workpiece surface points, the peak heights are nonuniform. It can be seen in Figure. 8.26(b) that the potential finishing mechanism for Ti-6Al-4V is the formation of microchips by shearing and also, to some degree, a brittle fracture. From Figures. (8.26b–8.26c) it can be seen that there are leftover magnetic abrasive media that is micro-welded. The reason for such leftover micro-welded magnetic abrasive media is the generation of enough heat in concentrated regions at higher rotational speeds [55], [73]. Figure. 8.28. Shows an improvement in surface roughnesses at various stages.

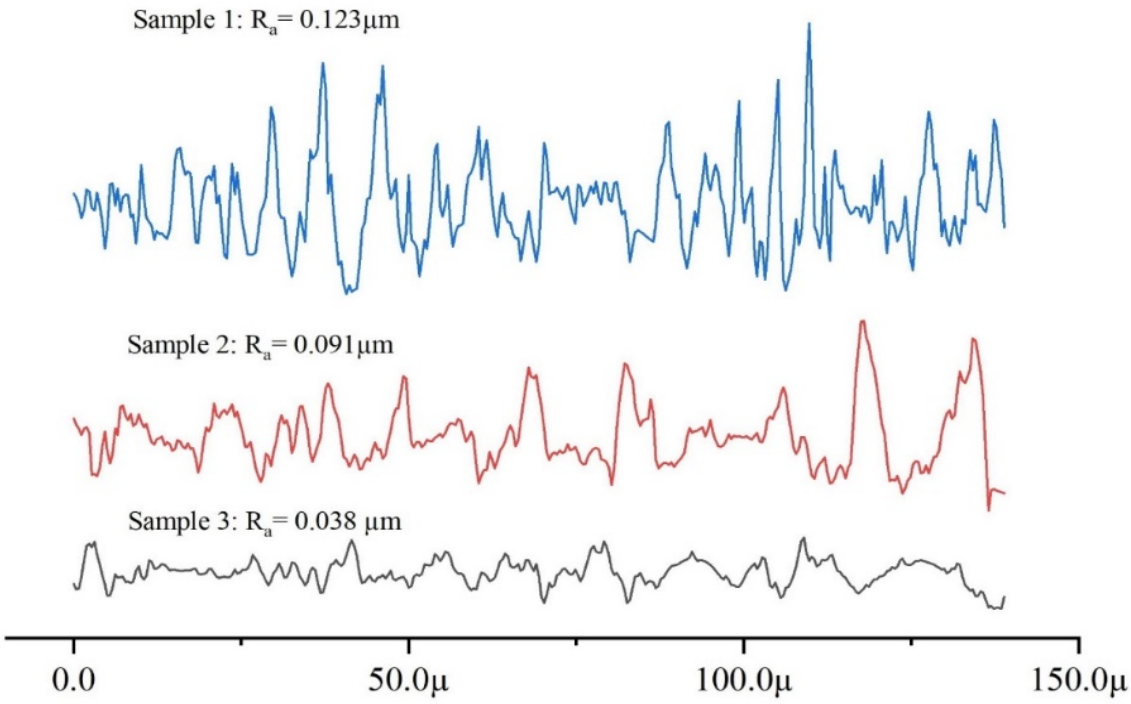

Figure 8.28 Comparison between surface roughnesses.

Chapter 9
CONCLUSIONS

This chapter contains salient conclusions. Important conclusions of the investigation regarding modelling along with selection of optimum process parameters have been presented. Significant findings have been drawn from performed experimentation.

9.1 Development of Magnetic abrasive

Based on the above results and discussion, the following conclusion can be drawn-

1. The Al_2O_3-SiO_2 based magnetic abrasive by sintering method i.e., sintered magnetic abrasive (SMA) has a fine structure, and the abrasive particles, which were distributed uniformly and densely on the carbonyl iron powder grain. These were tightly embedded into the Ferrous phase with the excellent soft magnetic property that consists of hematite and magnetite, the carbonyl iron particles.
2. It has been observed that the sintering process that combines high-pressure compaction, crushing, and sieving is a more straightforward, cheaper, least complicated, and accessible method for the large-scale commercialization of magnetic abrasives.

9.2 MAF Performance of Sintered magnetic abrasive on Ti-6Al-4V

1. The study proved that the surface produced by the magnetic abrasive finishing process on the Ti-6Al-4V workpiece plate has very excellent finishing results. Atomic force microscopy (AFM), surface micrograph, and surface roughness profiles (surface roughness from Ra = 1.14μm to Ra = 0.85μm) confirmed the effectiveness of developed magnetic abrasive for finishing of Ti-6Al-4V.

9.3 ANN-GA performance over Taguchi method for MAF process optimisation

Based upon the above results and discussion following conclusions can be made-

1. ANN-GA is robust modeling and optimization tool for any sort of data set (orthogonal array design or non-orthogonal array design) appropriate to scrutinize the finishing of SS302, and it was noticed that the parametric design used in this study provides a

straightforward, methodical, and proficient method of modeling and optimization of change of surface roughness or finishing behavior during the MAF process.

2. Modeling and optimization done with ANN-GA show a maximum value of $(\Delta R_a)_{max}$ equals to 0.25610 μm, which is 7% better than the result obtained from Taguchi-ANOVA analysis.
3. From the regression analysis, ΔR_a increases with the increase of Voltage and Rotational Speed and decrease with increasing Machining Gap and Abrasive Size, whereas from the ANN modeling predicts the same results except for the behavior of abrasive size, i.e., increases then decreases over the range, and this argument is justified by the optimum value of abrasive size (between the lower and upper limits) obtained from both the optimization techniques.
4. Voltage has the utmost influence on ΔR_a, i.e., 41.60%, followed by Machining Gap (27.98%), while Abrasive Size (10.95%) and Rotational Speed (9.39 %) shows almost four times lower effect.
5. An ANN model for predicting ΔR_a was developed, and a linear regression equation was developed, where ΔR_a depends on abrasive size, voltage, machining gap, and rotational speed at a confidence level of 99.5%. By comparing the results obtained from ANN methods, and ANOVA, it can be concluded that the ANN model is capable of predicting with very high accuracy and is more efficient.

9.4 Pulsating DC sourced magnetic abrasive finishing on Ti-6Al-4V

In this research work, the ANN-GA approach has been used for tri-objective optimization of the pulsating DC sourced magnetic abrasive finishing process parameters. After a critical observation of the results obtained, the following conclusions can be drawn:

1. The ANN model, which has been developed, can predict ΔR_a, ΔHV, and ΔEIT with the maximum error equal to 0.1388%, 0.4387% 0.0353%, respectively.
2. ΔR_a is directly proportional to current and inversely proportional to the machining gap. It is noticed that although ΔRa increases significantly on increasing the rotational speed, ΔRa at lower rotational speed, however, decreases slightly. Also, it has been seen that ΔR_a attains its maximum value in the range of 55-58 abrasive composition and later decreases when the abrasive composition was increased with a slight decrease in lower values of abrasive compositions. Moreover, ΔR_a increases with an increase in the finishing

time, and on the further increase, after 16 minutes of finishing time, the ΔR_a value decreases abruptly.

3. ΔHV increases with an increment in the current and decreases with an increase in the machining gap. Furthermore, the magnitude of all the output parameters is more when the machining gap is lower. It is observed that ΔHV and ΔEIT values increase with the rotational speed (up to 210 rpm), and then it starts to decrease with a further increase in the rotational speed. For ΔHV, it is noticed that on increasing the percentage of abrasive in the mixture, ΔHV value rises. It has been noted that ΔR_a increases with the increase of finishing time. Also, ΔHV showed an increasing trend with finishing time.
4. ΔEIT increases with increasing value of current and decreases with increasing machining gap. In addition to this, the magnitude of all the output parameters is more when the machining gap is lower. It is observed that ΔEIT value increases with the rotational speed (up to 210 rpm) and then begins to decrease as the rotational speed value increases further. Furthermore, if the abrasive composition is increased, the ΔEIT decreases. It has been found that, with the rise in finishing time, ΔEIT increases. ΔEIT showed an increasing trend with finishing time, where there was initially a slight decrease in ΔEIT on the lower side of finishing time, but a constant upwards trend was observed thereafter.
5. It was observed that the ANN models could predict the behavior of the output parameters with very high accuracy and efficiency. Upon further optimization with GA, the obtained ANN models were highly optimized and provided a better approach for the prediction of higher values of ΔRa, ΔHV, and ΔEIT than their experimental. ANN-GA based modeling and optimization suggest a direct relation between choosing process parameters correctly and enhancing machining performance.
6. Loosely bound SiC-based magnetic abrasive media is found to be a reasonable abrasive media for the finishing of Ti-6Al-4V by the MAF process. The composition of ferromagnetic material and abrasive particles in the media is found to be a very critical factor for the performance of the finishing quality.
7. Pareto's optimal front offers a non-dominated set of optimal solutions (presented in Table 8.8). The table acts as a convenient solution for/facilitates a process engineer for the selection of the optimum values of control parameters depending on the product requirements.

References

[1] S. Kalpakjian, *Manufacturing engineering and technology*. India: Pearson Education, 2001.

[2] T. Muthuramalingam, "A review on influence of electrical process parameters in EDM process," p. 8, 2014.

[3] L. Yang, L. Wang, Q. Liu, and X. Tian, "Grinding performance of a new micro-crystalline corundum wheel when form-grinding automobile gears," *Int. J. Adv. Manuf. Technol.*, vol. 96, no. 1–4, pp. 857–870, Apr. 2018, doi: 10.1007/s00170-017-1514-4.

[4] Z. W. Zhong, "Recent Advances in Polishing of Advanced Materials," *Mater. Manuf. Process.*, vol. 23, no. 5, pp. 449–456, Jun. 2008, doi: 10.1080/10426910802103486.

[5] R. I. King and R. S. Hahn, *Handbook of Modern Grinding Technology*. Boston, MA: Springer US, 1987. doi: 10.1007/978-1-4613-1965-8.

[6] G. Burkhard, F. Rehsteiner, and B. Schumacher, "High Efficiency Abrasive Tool for Honing," *CIRP Ann.*, vol. 51, no. 1, pp. 271–274, 2002, doi: 10.1016/S0007-8506(07)61515-7.

[7] V. K. Jain, S. K. Choudhury, and K. M. Ramesh, "On the machining of alumina and glass," *Int. J. Mach. Tools Manuf.*, vol. 42, no. 11, pp. 1269–1276, Sep. 2002, doi: 10.1016/S0032-3861(02)00241-0.

[8] J. H. Shaikh, N. K. Jain, and V. C. Venkatesh, "Precision Finishing of Bevel Gears by Electrochemical Honing," *Mater. Manuf. Process.*, vol. 28, no. 10, pp. 1117–1123, Oct. 2013, doi: 10.1080/10426914.2013.811737.

[9] V. K. Jain, *Nanofinishing science and technology: basic and advanced finishing and polishing processes*. CRC Press, 2016.

[10] H. S. Lim, K. Fathima, A. Senthil Kumar, and M. Rahman, "A fundamental study on the mechanism of electrolytic in-process dressing (ELID) grinding," *Int. J. Mach. Tools Manuf.*, vol. 42, no. 8, pp. 935–943, Jun. 2002, doi: 10.1016/S0890-6955(02)00023-8.

[11] V. Yadava, V. K. Jain, and P. M. Dixit, "Temperature Distribution During Electro-Discharge Abrasive Grinding," *Mach. Sci. Technol.*, vol. 6, no. 1, pp. 97–127, May 2002, doi: 10.1081/MST-120003188.

[12] R. Levinger and S. Malkin, "Electrochemical Grinding of WC-Co Cemented Carbides," *J. Eng. Ind.*, vol. 101, no. 3, pp. 285–294, Aug. 1979, doi: 10.1115/1.3439509.

[13] N. S. Qu, Q. L. Zhang, X. L. Fang, E. K. Ye, and D. Zhu, “Experimental Investigation on Electrochemical Grinding of Inconel 718,” *Procedia CIRP*, vol. 35, pp. 16–19, 2015, doi: 10.1016/j.procir.2015.08.055.

[14] P. G. Benardos and G.-C. Vosniakos, “Predicting surface roughness in machining: a review,” *Int. J. Mach. Tools Manuf.*, vol. 43, no. 8, pp. 833–844, Jun. 2003, doi: 10.1016/S0890-6955(03)00059-2.

[15] K. J. Kubiak, T. W. Liskiewicz, and T. G. Mathia, “Surface morphology in engineering applications: Influence of roughness on sliding and wear in dry fretting,” *Tribol. Int.*, vol. 44, no. 11, pp. 1427–1432, Oct. 2011, doi: 10.1016/j.triboint.2011.04.020.

[16] M. Mosavat and A. Rahimi, “Numerical-experimental study on polishing of silicon wafer using magnetic abrasive finishing process,” *Wear*, vol. 424–425, pp. 143–150, Apr. 2019, doi: 10.1016/j.wear.2019.02.007.

[17] V. K. Jain, *Advanced machining processes*. New Delhi: Allied Publishers, 2013.

[18] F. Klocke, *Manufacturing Processes 2*. Berlin, Heidelberg: Springer Berlin Heidelberg, 2009. doi: 10.1007/978-3-540-92259-9.

[19] N. Taniguchi, “Current Status in, and Future Trends of, Ultraprecision Machining and Ultrafine Materials Processing,” *CIRP Ann.*, vol. 32, no. 2, pp. 573–582, 1983, doi: 10.1016/S0007-8506(07)60185-1.

[20] M. Papanikolaou and K. Salonitis, “Fractal roughness effects on nanoscale grinding,” *Appl. Surf. Sci.*, vol. 467–468, pp. 309–319, Feb. 2019, doi: 10.1016/j.apsusc.2018.10.144.

[21] P. Ali, R. S. Walia, Q. Murtaza, and M. S. Ranganath, “Modeling and analysis of developed Thermal additive Centrifugal Abrasive Flow Machining process,” *Surf. Topogr. Metrol. Prop.*, vol. 8, no. 3, p. 035013, 2020.

[22] S. Jha and V. K. Jain, “Nanofinishing Techniques,” in *Micromanufacturing and Nanotechnology*, Berlin/Heidelberg: Springer-Verlag, 2006, pp. 171–195. doi: 10.1007/3-540-29339-6_8.

[23] D. M. Allen *et al.*, “Ion beam, focused ion beam, and plasma discharge machining,” *CIRP Ann.*, vol. 58, no. 2, pp. 647–662, 2009, doi: 10.1016/j.cirp.2009.09.007.

[24] M. Kanaoka *et al.*, “Processing efficiency of elastic emission machining for low-thermal-expansion material,” *Surf. Interface Anal.*, vol. 40, no. 6–7, pp. 1002–1006, Jun. 2008, doi: 10.1002/sia.2818.

[25] T. Dursun and C. Soutis, “Recent developments in advanced aircraft aluminium alloys,” *Mater. Des. 1980-2015*, vol. 56, pp. 862–871, Apr. 2014, doi: 10.1016/j.matdes.2013.12.002.

[26] D. Yin, X. Niu, K. Zhang, J. Wang, and Y. Cui, “Preparation of MgO doped colloidal SiO2 abrasive and their chemical mechanical polishing performance on c-, r- and a-plane sapphire substrate,” *Ceram. Int.*, vol. 44, no. 12, pp. 14631–14637, Aug. 2018, doi: 10.1016/j.ceramint.2018.05.087.

[27] S. A. Sirwal and A. K. Singh, “Analysis of the surface roughness for novel magnetorheological finishing of a typical blind hole workpiece,” *Proc. Inst. Mech. Eng. Part C J. Mech. Eng. Sci.*, vol. 233, no. 5, pp. 1541–1561, Mar. 2019, doi: 10.1177/0954406218776036.

[28] S. Ahmad, R. M. Singari, and R. S. Mishra, “Tri-objective constrained optimization of pulsating DC sourced magnetic abrasive finishing process parameters using artificial neural network and genetic algorithm,” *Mater. Manuf. Process.*, pp. 1–15, Feb. 2021, doi: 10.1080/10426914.2020.1866196.

[29] Z. Zhang, L. Liao, X. Wang, W. Xie, and D. Guo, “Development of a novel chemical mechanical polishing slurry and its polishing mechanisms on a nickel alloy,” *Appl. Surf. Sci.*, vol. 506, p. 144670, Mar. 2020, doi: 10.1016/j.apsusc.2019.144670.

[30] S. R. Bhagavatula and R. Komanduri, “On chemomechanical polishing of Si3N4 with Cr2O3,” *Philos. Mag. A*, vol. 74, no. 4, pp. 1003–1017, Oct. 1996, doi: 10.1080/01418619608242173.

[31] H. A. Youssef, *Machining of Stainless Steels and Super Alloys: Traditional and Nontraditional Techniques*. Chichester, UK: John Wiley & Sons, Ltd, 2015. doi: 10.1002/9781118919514.

[32] Y. Fu, H. Gao, X. Wang, and D. Guo, “Machining the Integral Impeller and Blisk of Aero-Engines: A Review of Surface Finishing and Strengthening Technologies,” *Chin. J. Mech. Eng.*, vol. 30, no. 3, pp. 528–543, May 2017, doi: 10.1007/s10033-017-0123-3.

[33] M. Ali-Tavoli, N. Nariman-Zadeh, A. Khakhali, and M. Mehran, “Multi-objective optimization of abrasive flow machining processes using polynomial neural networks and genetic algorithms,” *Mach. Sci. Technol.*, vol. 10, no. 4, pp. 491–510, Dec. 2006, doi: 10.1080/10910340600996126.

[34] W. I. Kordonski and D. Golini, “Fundamentals of Magnetorheological Fluid Utilization in High Precision Finishing,” *J. Intell. Mater. Syst. Struct.*, vol. 10, no. 9, pp. 683–689, Sep. 1999, doi: 10.1106/011M-CJ25-64QC-F3A6.

[35] C. Kumari and S. K. Chak, “A review on magnetically assisted abrasive finishing and their critical process parameters,” *Manuf. Rev.*, vol. 5, p. 13, 2018, doi: 10.1051/mfreview/2018010.

[36] S. Ahmad, S. Gangwar, P. C. Yadav, and D. K. Singh, “Optimization of process parameters affecting surface roughness in magnetic abrasive finishing process,” *Mater. Manuf. Process.*, vol. 32, no. 15, pp. 1723–1729, Nov. 2017, doi: 10.1080/10426914.2017.1279307.

[37] D. K. Singh, V. K. Jain, V. Raghuram, and R. Komanduri, “Analysis of surface texture generated by a flexible magnetic abrasive brush,” *Wear*, vol. 259, no. 7–12, pp. 1254–1261, Jul. 2005, doi: 10.1016/j.wear.2005.02.030.

[38] X. Teng, G. Zhang, Y. Zhao, Y. Cui, L. Li, and L. Jiang, “Study on magnetic abrasive finishing of AlSi10Mg alloy prepared by selective laser melting,” *Int. J. Adv. Manuf. Technol.*, vol. 105, no. 5–6, pp. 2513–2521, Dec. 2019, doi: 10.1007/s00170-019-04485-5.

[39] S. Yang and W. Li, *Surface Finishing Theory and New Technology*. Berlin, Heidelberg: Springer Berlin Heidelberg, 2018. doi: 10.1007/978-3-662-54133-3.

[40] R. K. Singh, D. K. Singh, and S. Gangwar, “Advances in Magnetic Abrasive Finishing for Futuristic Requirements - A Review,” *Mater. Today Proc.*, vol. 5, no. 9, pp. 20455–20463, 2018, doi: 10.1016/j.matpr.2018.06.422.

[41] A. Chaurasia, N. Rattan, and R. S. Mulik, “Magnetic abrasive finishing of AZ91 magnesium alloy using electromagnet,” *J. Braz. Soc. Mech. Sci. Eng.*, vol. 40, no. 10, p. 482, Oct. 2018, doi: 10.1007/s40430-018-1399-7.

[42] S. Ahmad, R. M. Singari, and R. S. Mishra, “Modelling and optimisation of magnetic abrasive finishing process based on a non-orthogonal array with ANN-GA approach,” *Trans. IMF*, vol. 98, no. 4, pp. 186–198, Jul. 2020, doi: 10.1080/00202967.2020.1776966.

[43] G. Z. Kremen, E. A. Elsayed, and J. L. Ribeiro, “Machining time estimation for magnetic abrasive processes,” *Int. J. Prod. Res.*, vol. 32, no. 12, pp. 2817–2825, Dec. 1994, doi: 10.1080/00207549408957102.

[44] D. K. Singh, V. K. Jain, and V. Raghuram, “On the performance analysis of flexible magnetic abrasive brush,” *Mach. Sci. Technol.*, vol. 9, no. 4, pp. 601–619, Dec. 2005, doi: 10.1080/10910340500398217.

[45] G.-W. Chang, B.-H. Yan, and R.-T. Hsu, “Study on cylindrical magnetic abrasive finishing using unbonded magnetic abrasives,” *Int. J. Mach. Tools Manuf.*, vol. 42, no. 5, pp. 575–583, Apr. 2002, doi: 10.1016/S0890-6955(01)00153-5.

[46] G. C. Verma, P. Kala, and P. M. Pandey, “Experimental investigations into internal magnetic abrasive finishing of pipes,” *Int. J. Adv. Manuf. Technol.*, vol. 88, no. 5–8, pp. 1657–1668, Feb. 2017, doi: 10.1007/s00170-016-8881-0.

[47] A. Srivastava, H. Kumar, and S. Singh, “Investigations into Internal Surface Finishing of Titanium (Grade 2) Pipe with Extended Magnetic Tool,” *Procedia Manuf.*, vol. 26, pp. 181–189, 2018, doi: 10.1016/j.promfg.2018.07.025.

[48] J. Guo, K. Liu, Z. Wang, and G. L. Tnay, “Magnetic field-assisted finishing of a mold insert with curved microstructures for injection molding of microfluidic chips,” *Tribol. Int.*, vol. 114, pp. 306–314, Oct. 2017, doi: 10.1016/j.triboint.2017.04.019.

[49] J. Guo *et al.*, “Novel rotating-vibrating magnetic abrasive polishing method for double-layered internal surface finishing,” *J. Mater. Process. Technol.*, vol. 264, pp. 422–437, Feb. 2019, doi: 10.1016/j.jmatprotec.2018.09.024.

[50] Y.-H. Lee, K.-L. Wu, J.-H. Jhou, Y.-H. Tsai, and B.-H. Yan, “Two-dimensional vibration-assisted magnetic abrasive finishing of stainless steel SUS304,” *Int. J. Adv. Manuf. Technol.*, vol. 69, no. 9–12, pp. 2723–2733, Dec. 2013, doi: 10.1007/s00170-013-5242-0.

[51] P. Kala, S. Kumar, and P. M. Pandey, “Polishing of Copper Alloy Using Double Disk Ultrasonic Assisted Magnetic Abrasive Polishing,” *Mater. Manuf. Process.*, vol. 28, no. 2, pp. 200–206, Feb. 2013, doi: 10.1080/10426914.2012.746704.

[52] M. Fox, K. Agrawal, T. Shinmura, and R. Komanduri, “Magnetic Abrasive Finishing of Rollers,” *CIRP Ann.*, vol. 43, no. 1, pp. 181–184, 1994, doi: 10.1016/S0007-8506(07)62191-X.

[53] V. Jain, U. Dixit, C. Paul, and A. Kumar, “Micromanufacturing: A review—part II,” *Proc. Inst. Mech. Eng. Part B J. Eng. Manuf.*, vol. 228, no. 9, pp. 995–1014, Sep. 2014, doi: 10.1177/0954405414539492.

[54] V. Jain, A. Sidpara, R. Balasubramaniam, G. Lodha, V. Dhamgaye, and R. Shukla, "Micromanufacturing: A review—Part I," *Proc. Inst. Mech. Eng. Part B J. Eng. Manuf.*, vol. 228, no. 9, pp. 973–994, Sep. 2014, doi: 10.1177/0954405414539487.

[55] V. Mishra, H. Goel, R. S. Mulik, and P. M. Pandey, "Determining work-brush interface temperature in magnetic abrasive finishing process," *J. Manuf. Process.*, vol. 16, no. 2, pp. 248–256, Apr. 2014, doi: 10.1016/j.jmapro.2013.10.004.

[56] W. Li, X. Li, S. Yang, and W. Li, "A newly developed media for magnetic abrasive finishing process: Material removal behavior and finishing performance," *J. Mater. Process. Technol.*, vol. 260, pp. 20–29, Oct. 2018, doi: 10.1016/j.jmatprotec.2018.05.007.

[57] A. C. Wang and S. J. Lee, "Study the characteristics of magnetic finishing with gel abrasive," *Int. J. Mach. Tools Manuf.*, vol. 49, no. 14, pp. 1063–1069, Nov. 2009, doi: 10.1016/j.ijmachtools.2009.07.009.

[58] G. Zhang, Y. Zhao, D. Zhao, F. Yin, and Z. Zhao, "Preparation of white alumina spherical composite magnetic abrasive by gas atomization and rapid solidification," *Scr. Mater.*, vol. 65, no. 5, pp. 416–419, Sep. 2011, doi: 10.1016/j.scriptamat.2011.05.021.

[59] V. K. Jain, P. Kumar, P. K. Behera, and S. C. Jayswal, "Effect of working gap and circumferential speed on the performance of magnetic abrasive finishing process," *Wear*, vol. 250, no. 1–12, pp. 384–390, Oct. 2001, doi: 10.1016/S0043-1648(01)00642-1.

[60] V. K. Jain, D. K. Singh, and V. Raghuram, "Analysis of performance of pulsating flexible magnetic abrasive brush (P-FMAB)," *Mach. Sci. Technol.*, vol. 12, no. 1, pp. 53–76, Mar. 2008, doi: 10.1080/10910340701883538.

[61] D. K. Singh, V. K. Jain, and V. Raghuram, "Parametric study of magnetic abrasive finishing process," *J. Mater. Process. Technol.*, vol. 149, no. 1–3, pp. 22–29, Jun. 2004, doi: 10.1016/j.jmatprotec.2003.10.030.

[62] C. Yin, R. Wang, J. Kim, S. Lee, and S. Mun, "Ultra-High-Speed Magnetic Abrasive Surface Micro-Machining of AISI 304 Cylindrical Bar," *Metals*, vol. 9, no. 5, p. 489, Apr. 2019, doi: 10.3390/met9050489.

[63] R. S. Mulik, V. Srivastava, and P. M. Pandey, "Experimental investigations and modeling of temperature in the work-brush interface during ultrasonic assisted magnetic abrasive finishing process," *Mater. Manuf. Process.*, vol. 27, no. 1, pp. 1–9, 2012, doi: 10.1080/10426914.2010.515647.

[64] P. Kala and P. M. Pandey, “Experimental Study on Finishing Forces in Double Disk Magnetic Abrasive Finishing Process While Finishing Paramagnetic Workpiece,” *Procedia Mater. Sci.*, vol. 5, pp. 1677–1684, 2014, doi: 10.1016/j.mspro.2014.07.356.

[65] P. Kala, P. M. Pandey, G. C. Verma, and V. Sharma, “Understanding flexible abrasive brush behavior for double disk magnetic abrasive finishing based on force signature,” *J. Manuf. Process.*, vol. 28, pp. 442–448, Aug. 2017, doi: 10.1016/j.jmapro.2017.04.010.

[66] P. Singh, L. Singh, and A. Kaushik, “Parametric Optimization of Magnetic Abrasive Finishing Using Adhesive Magnetic Abrasive Particles:,” *Int. J. Surf. Eng. Interdiscip. Mater. Sci.*, vol. 7, no. 2, pp. 34–47, Jul. 2019, doi: 10.4018/IJSEIMS.2019070103.

[67] J.-S. Kwak, “Enhanced magnetic abrasive polishing of non-ferrous metals utilizing a permanent magnet,” *Int. J. Mach. Tools Manuf.*, vol. 49, no. 7–8, pp. 613–618, Jun. 2009, doi: 10.1016/j.ijmachtools.2009.01.013.

[68] H. Yamaguchi and K. Hanada, “Development of Spherical Magnetic Abrasive Made by Plasma Spray,” *J. Manuf. Sci. Eng.*, vol. 130, no. 3, pp. 031107-1-031107–9, Jun. 2008.

[69] C.-T. Lin, L.-D. Yang, and H.-M. Chow, “Study of magnetic abrasive finishing in free-form surface operations using the Taguchi method,” *Int. J. Adv. Manuf. Technol.*, vol. 34, no. 1–2, pp. 122–130, Jul. 2007, doi: 10.1007/s00170-006-0573-8.

[70] S. C. Jayswal, V. K. Jain, and P. M. Dixit, “Modeling and simulation of magnetic abrasive finishing process,” *Int. J. Adv. Manuf. Technol.*, vol. 26, no. 5–6, pp. 477–490, Sep. 2005, doi: 10.1007/s00170-004-2180-x.

[71] J.-D. Kim and M.-S. Choi, “Development and Finite Element Analysis of the Finishing System using Rotating Magnetic Field,” *Int. J. Mach. Tools Manuf.*, vol. 36, no. 2, pp. 245–253, 1996, doi: 10.1016/0890-6955(95)98764-X.

[72] V. K. Jain, S. C. Jayswal, and P. M. Dixit, “Modeling and Simulation of Surface Roughness in Magnetic Abrasive Finishing Using Non-Uniform Surface Profiles,” *Mater. Manuf. Process.*, vol. 22, no. 2, pp. 256–270, Feb. 2007, doi: 10.1080/10426910601134096.

[73] R. K. Singh, S. Gangwar, and D. K. Singh, “Experimental investigation on temperature-affected magnetic abrasive finishing of aluminum 6060,” *Mater. Manuf. Process.*, vol. 34, no. 11, pp. 1274–1285, Aug. 2019, doi: 10.1080/10426914.2019.1628263.

[74] J.-D. Kim and M.-S. Choi, “Simulation for the prediction of surface-accuracy in magnetic abrasive machining,” *J. Mater. Process. Technol.*, vol. 53, no. 3–4, pp. 630–642, Sep. 1995, doi: 10.1016/0924-0136(94)01753-N.

[75] R. S. Mulik and P. M. Pandey, “Mechanism of Surface Finishing in Ultrasonic-Assisted Magnetic Abrasive Finishing Process,” *Mater. Manuf. Process.*, vol. 25, no. 12, pp. 1418–1427, Dec. 2010, doi: 10.1080/10426914.2010.499580.

[76] R. S. Mulik and P. M. Pandey, “Ultrasonic assisted magnetic abrasive finishing of hardened AISI 52100 steel using unbonded SiC abrasives,” *Int. J. Refract. Met. Hard Mater.*, vol. 29, no. 1, pp. 68–77, Jan. 2011, doi: 10.1016/j.ijrmhm.2010.08.002.

[77] G. Kumar and V. Yadav, “Temperature distribution in the workpiece due to plane magnetic abrasive finishing using FEM,” *Int. J. Adv. Manuf. Technol.*, vol. 41, no. 11–12, pp. 1051–1058, 2009, doi: 10.1007/s00170-008-1557-7.

[78] R. S. Mulik, V. Srivastava, and P. M. Pandey, “Experimental Investigations and Modeling of Temperature in the Work-Brush Interface during Ultrasonic Assisted Magnetic Abrasive Finishing Process,” *Mater. Manuf. Process.*, vol. 27, no. 1, pp. 1–9, Jan. 2012, doi: 10.1080/10426914.2010.515647.

[79] K. B. Judal, V. Yadava, and D. Pathak, “Experimental Investigation of Vibration Assisted Cylindrical–Magnetic Abrasive Finishing of Aluminum Workpiece,” *Mater. Manuf. Process.*, vol. 28, no. 11, pp. 1196–1202, Nov. 2013, doi: 10.1080/10426914.2013.811725.

[80] S. Yin and T. Shinmura, “Vertical vibration-assisted magnetic abrasive finishing and deburring for magnesium alloy,” *Int. J. Mach. Tools Manuf.*, vol. 44, no. 12–13, pp. 1297–1303, Oct. 2004, doi: 10.1016/j.ijmachtools.2004.04.023.

[81] R. S. Mulik, V. Srivastava, and P. M. Pandey, “Experimental Investigations and Modeling of Temperature in the Work-Brush Interface during Ultrasonic Assisted Magnetic Abrasive Finishing Process,” *Mater. Manuf. Process.*, vol. 27, no. 1, pp. 1–9, Jan. 2012, doi: 10.1080/10426914.2010.515647.

[82] J. Wu, Y. Zou, and H. Sugiyama, “Study on ultra-precision magnetic abrasive finishing process using low frequency alternating magnetic field,” *J. Magn. Magn. Mater.*, vol. 386, pp. 50–59, Jul. 2015, doi: 10.1016/j.jmmm.2015.03.041.

[83] J.-D. Kim and M.-S. Choi, “Development of the magneto-electrolytic-abrasive polishing system (MEAPS) and finishing characteristics of a Cr-coated roller,” *Int. J. Mach. Tools Manuf.*, vol. 37, no. 7, pp. 997–1006, Jul. 1997, doi: 10.1016/S0890-6955(96)00057-0.

[84] K. B. Judal and V. Yadava, “Cylindrical Electrochemical Magnetic Abrasive Machining of AISI-304 Stainless Steel,” *Mater. Manuf. Process.*, vol. 28, no. 4, pp. 449–456, Apr. 2013, doi: 10.1080/10426914.2012.736653.

[85] T. A. El-Taweel, “Modelling and analysis of hybrid electrochemical turning-magnetic abrasive finishing of 6061 Al/Al2O3 composite,” *Int. J. Adv. Manuf. Technol.*, vol. 37, no. 7–8, pp. 705–714, Jun. 2008, doi: 10.1007/s00170-007-1019-7.

[86] G. Y. Liu, Z. N. Guo, S. Z. Jiang, N. S. Qu, and Y. B. Li, “A Study of Processing Al 6061 with Electrochemical Magnetic Abrasive Finishing,” *Procedia CIRP*, vol. 14, pp. 234–238, 2014, doi: 10.1016/j.procir.2014.03.052.

[87] N. Sihag, P. Kala, and P. M. Pandey, “Chemo Assisted Magnetic Abrasive Finishing: Experimental Investigations,” *Procedia CIRP*, vol. 26, pp. 539–543, 2015, doi: 10.1016/j.procir.2014.07.067.

[88] A. Misra, P. M. Pandey, and U. S. Dixit, “Modeling of material removal in ultrasonic assisted magnetic abrasive finishing process,” *Int. J. Mech. Sci.*, vol. 131–132, pp. 853–867, Oct. 2017, doi: 10.1016/j.ijmecsci.2017.07.023.

[89] H. Yamaguchi, A. K. Srivastava, M. A. Tan, R. E. Riveros, and F. Hashimoto, “Magnetic abrasive finishing of cutting tools for machining of titanium alloys,” *CIRP Ann.*, vol. 61, no. 1, pp. 311–314, 2012, doi: 10.1016/j.cirp.2012.03.066.

[90] H. Yamaguchi, A. K. Srivastava, M. Tan, and F. Hashimoto, “Magnetic Abrasive Finishing of cutting tools for high-speed machining of titanium alloys,” *CIRP J. Manuf. Sci. Technol.*, vol. 7, no. 4, pp. 299–304, 2014, doi: 10.1016/j.cirpj.2014.08.002.

[91] S. Khalaj Amineh, A. Fadaei Tehrani, and A. Mohammadi, “Improving the surface quality in wire electrical discharge machined specimens by removing the recast layer using magnetic abrasive finishing method,” *Int. J. Adv. Manuf. Technol.*, vol. 66, no. 9–12, pp. 1793–1803, Aug. 2012, doi: 10.1007/s00170-012-4459-7.

[92] S. K. Amnieh, P. Mosaddegh, and Tehrani, Alireza Fadaei, “Study on magnetic abrasive finishing of spiral grooves inside of aluminum cylinders,” *Int J Adv Manuf Technol*, vol. 91, pp. 2885–2894, 2017, doi: https://doi.org/10.1007/s00170-016-9970-9.

[93] J. Guo, J. Bai, K. Liu, and J. Wei, “Surface quality improvement of selective laser sintered polyamide 12 by precision grinding and magnetic field-assisted finishing,” *Mater. Des.*, vol. 138, pp. 39–45, Jan. 2018, doi: 10.1016/j.matdes.2017.10.048.

[94] J. Guo, H. Wang, M. Goh, and K. Liu, “Investigation on Surface Integrity of Rapidly Solidified Aluminum RSA 905 by Magnetic Field-Assisted Finishing,” *Micromachines*, vol. 9, no. 4, p. 146, Mar. 2018, doi: 10.3390/mi9040146.

[95] Y. Gao, Y. Zhao, G. Zhang, G. Zhang, and F. Yin, “Polishing of paramagnetic materials using atomized magnetic abrasive powder,” *Mater. Manuf. Process.*, vol. 34, no. 6, pp. 604–611, Apr. 2019, doi: 10.1080/10426914.2018.1532087.

[96] T. C. Kanish, P. Kuppan, S. Narayanan, and S. D. Ashok, “A Fuzzy Logic based Model to Predict the Improvement in Surface Roughness in Magnetic Field Assisted Abrasive Finishing,” *Procedia Eng.*, vol. 97, pp. 1948–1956, 2014, doi: 10.1016/j.proeng.2014.12.349.

[97] R. K. Singh, S. Gangwar, D. K. Singh, and V. K. Pathak, “A novel hybridization of artificial neural network and moth-flame optimization (ANN–MFO) for multi-objective optimization in magnetic abrasive finishing of aluminium 6060,” *J. Braz. Soc. Mech. Sci. Eng.*, vol. 41, no. 6, p. 270, Jun. 2019, doi: 10.1007/s40430-019-1778-8.

[98] M. Vahdati and S. Rasouli, “Evaluation of Parameters Affecting Magnetic Abrasive Finishing on Concave Freeform Surface of Al Alloy via RSM Method,” *Adv. Mater. Sci. Eng.*, vol. 2016, pp. 1–14, 2016, doi: 10.1155/2016/5256347.

[99] S. H. R. Pasandideh and S. T. A. Niaki, “Multi-response simulation optimization using genetic algorithm within desirability function framework,” *Appl. Math. Comput.*, vol. 175, no. 1, pp. 366–382, Apr. 2006, doi: 10.1016/j.amc.2005.07.023.

[100] A. A. Moosa, “Utilizing a Magnetic Abrasive Finishing Technique (MAF) Via Adaptive Nero Fuzzy (ANFIS),” *Am. J. Mater. Eng. Technol.*, p. 5.

[101] A. C. Wang, L. Tsai, C. H. Liu, K. Z. Liang, and S. J. Lee, “Elucidating the Optimal Parameters in Magnetic Finishing with Gel Abrasive,” *Mater. Manuf. Process.*, vol. 26, no. 5, pp. 786–791, May 2011, doi: 10.1080/10426914.2010.505620.

[102] N. Sihag, P. Kala, and P. M. Pandey, “Analysis of Surface Finish Improvement during Ultrasonic Assisted Magnetic Abrasive Finishing on Chemically treated Tungsten Substrate,” *Procedia Manuf.*, vol. 10, pp. 136–146, 2017, doi: 10.1016/j.promfg.2017.07.040.

[103] F. Y. Cheung, Z. F. Zhou, A. Geddam, and K. Y. Li, “Cutting edge preparation using magnetic polishing and its influence on the performance of high-speed steel drills,” *J. Mater. Process. Technol.*, vol. 208, no. 1–3, pp. 196–204, Nov. 2008, doi: 10.1016/j.jmatprotec.2007.12.108.

[104] V. K. Jain, “Magnetic field assisted abrasive based micro-/nano-finishing,” *J. Mater. Process. Technol.*, vol. 209, no. 20, pp. 6022–6038, Nov. 2009, doi: 10.1016/j.jmatprotec.2009.08.015.

[105] R. S. Mulik and P. M. Pandey, “Experimental Investigations and Modeling of Finishing Force and Torque in Ultrasonic Assisted Magnetic Abrasive Finishing,” *J. Manuf. Sci. Eng.*, vol. 134, no. 5, p. 051008, 2012, doi: 10.1115/1.4007131.

[106] V. C. Shukla, P. M. Pandey, U. S. Dixit, A. Roy, and V. Silberschmidt, “Modeling of normal force and finishing torque considering shearing and ploughing effects in ultrasonic assisted magnetic abrasive finishing process with sintered magnetic abrasive powder,” *Wear*, vol. 390–391, pp. 11–22, Nov. 2017, doi: 10.1016/j.wear.2017.06.017.

[107] Y. Gao, Y. Zhao, and G. Zhang, “Preparation of Al2O3 magnetic abrasives by gas-solid two-phase double-stage atomization and rapid solidification,” *Mater. Lett.*, vol. 215, pp. 300–304, Mar. 2018, doi: 10.1016/j.matlet.2017.12.124.

[108] S. Singh, P. Singh, and H. S. Shan, “Comparative Evaluation of Mechanically Alloyed and Sintered Magnetic Abrasives for Fine Finishing,” p. 6, 2014.

[109] J. Guo, H. Wang, M. Goh, and K. Liu, “Investigation on Surface Integrity of Rapidly Solidified Aluminum RSA 905 by Magnetic Field-Assisted Finishing,” *Micromachines*, vol. 9, no. 4, p. 146, Mar. 2018, doi: 10.3390/mi9040146.

[110] J. Guo, Z. E. Tan, K. H. Au, and K. Liu, “Experimental investigation into the effect of abrasive and force conditions in magnetic field-assisted finishing,” *Int. J. Adv. Manuf. Technol.*, vol. 90, no. 5–8, pp. 1881–1888, May 2017, doi: 10.1007/s00170-016-9491-6.

[111] H. J. C. de Souza *et al.*, “Robust Design and Taguchi Method Application,” in *Design of Experiments - Applications*, M. Borges Silva, Ed. InTech, 2013. doi: 10.5772/56580.

[112] M. T. Hagan, H. B. Demuth, and M. H. Beale, *Neural Network Design*. Campus Pub. Service, University of Colorado Bookstore, 2002. [Online]. Available: https://books.google.co.in/books?id=bUNJAAAACAAJ

[113] N. D. Ghetiya and K. M. Patel, “Prediction of Tensile Strength in Friction Stir Welded Aluminium Alloy Using Artificial Neural Network,” *Procedia Technol.*, vol. 14, pp. 274–281, Jan. 2014, doi: 10.1016/j.protcy.2014.08.036.

[114] N. S. Chauhan, “Introduction to Artificial Neural Networks(ANN),” *Medium*, Oct. 10, 2019. https://towardsdatascience.com/introduction-to-artificial-neural-networks-ann-1aea15775ef9 (accessed Jun. 09, 2020).

[115] C. Nwankpa, W. Ijomah, A. Gachagan, and S. Marshall, “Activation Functions: Comparison of trends in Practice and Research for Deep Learning,” *ArXiv181103378 Cs*, Nov. 2018, Accessed: Jun. 10, 2020. [Online]. Available: http://arxiv.org/abs/1811.03378

[116] J. Feng and S. Lu, “Performance Analysis of Various Activation Functions in Artificial Neural Networks,” *J. Phys. Conf. Ser.*, vol. 1237, p. 022030, Jun. 2019, doi: 10.1088/1742-6596/1237/2/022030.

[117] N. Marjan and E. M. A. Masud, “ESTIMATION OF PRODUCTS FINAL PRICE USING BAYESIAN ANALYSIS GENERALIZED POISSON MODEL AND ARTIFICIAL NEURAL NETWORKS,” vol. 2, no. 2, pp. 55–60, Jan. 2009.

[118] E. Maleki and K. Sherafatnia, “Investigation of single and dual step shot peening effects on mechanical and metallurgical properties of 18CrNiMo7-6 steel using artificial neural network,” *Int. J. Mater. Mech. Manuf.*, vol. 4, pp. 100–105, Jan. 2016, doi: 10.7763/IJMMM.2016.V4.233.

[119] K. S. Sangwan, S. Saxena, and G. Kant, “Optimization of Machining Parameters to Minimize Surface Roughness using Integrated ANN-GA Approach,” *Procedia CIRP*, vol. 29, pp. 305–310, Jan. 2015, doi: 10.1016/j.procir.2015.02.002.

[120] O. B. Nakhjavani and M. Ghoreishi, “Multi Criteria Optimization of Laser Percussion Drilling Process Using Artificial Neural Network Model Combined with Genetic Algorithm,” *Mater. Manuf. Process.*, vol. 21, no. 1, pp. 11–18, Jan. 2006, doi: 10.1081/AMP-200060402.

[121] B. P. Nasution and A. Agah, “Currency Exchange Rate Forecasting with Neural Networks,” *J. Intell. Syst.*, vol. 10, no. 3, Jan. 2000, doi: 10.1515/JISYS.2000.10.3.219.

[122] “(PDF) Prediction of Friction Stir Welding Characteristic Using Neural Network.” https://www.researchgate.net/publication/215588726_Prediction_of_Friction_Stir_Welding_Characteristic_Using_Neural_Network (accessed Jun. 10, 2020).

[123] R. K. Roy, *A primer on the Taguchi method*, 2nd ed. Dearborn, MI: Society of Manufacturing Engineers, 2010.

[124] D. C. Montgomery, "Design and Analysis of Experiments," p. 748, 2017.

[125] C.-X. Ma, K.-T. Fang, and E. Liski, "A new approach in constructing orthogonal and nearly orthogonal arrays," *Metrika*, vol. 50, no. 3, pp. 255–268, Apr. 2000, doi: 10.1007/s001840050049.

[126] R. Mead, "The Non-Orthogonal Design of Experiments," *J. R. Stat. Soc. Ser. A Stat. Soc.*, vol. 153, no. 2, pp. 151–201, 1990.

[127] W. E. Schiesser and G. W. Griffiths, "A compendium of partial differential equation models: method of lines analysis with Matlab," *Choice Rev. Online*, vol. 47, no. 04, pp. 47-2062-47–2062, 2009, doi: 10.5860/CHOICE.47-2062.

[128] "ANSYS LS-DYNA 11. User's Guide." ANSYS Corporation Inc., 2009.

[129] C. M. Judd, G. H. McClelland, and C. S. Ryan, *Data analysis: a model comparison approach to regression, ANOVA, and beyond*, Third Edition. New York: Routledge, Taylor & Francis Group, 2017.

[130] H. Oktem, T. Erzurumlu, and F. Erzincanli, "Prediction of minimum surface roughness in end milling mold parts using neural network and genetic algorithm," *Mater. Des.*, vol. 27, no. 9, pp. 735–744, Jan. 2006, doi: 10.1016/j.matdes.2005.01.010.

[131] K. Wang, H. L. Gelgele, Y. Wang, Q. Yuan, and M. Fang, "A hybrid intelligent method for modelling the EDM process," *Int. J. Mach. Tools Manuf.*, vol. 43, no. 10, pp. 995–999, Aug. 2003, doi: 10.1016/S0890-6955(03)00102-0.

[132] B. Stojanović, A. Vencl, I. Bobić, S. Miladinović, and J. Skerlić, "Experimental optimisation of the tribological behaviour of Al/SiC/Gr hybrid composites based on Taguchi's method and artificial neural network," *J. Braz. Soc. Mech. Sci. Eng.*, vol. 40, no. 6, p. 311, Jun. 2018, doi: 10.1007/s40430-018-1237-y.

[133] T. Mori, K. Hirota, and Y. Kawashima, "Clarification of magnetic abrasive finishing mechanism," *J. Mater. Process. Technol.*, vol. 143–144, pp. 682–686, Dec. 2003, doi: 10.1016/S0924-0136(03)00410-2.

[134] K. Wang, G. L. Kovacs, M. Wozny, and M. Fang, Eds., *Knowledge Enterprise: Intelligent Strategies in Product Design, Manufacturing, and Management: Proceedings of*

PROLAMAT 2006, IFIP TC5 International Conference, June 15–17, 2006, Shanghai, China, vol. 207. Boston, MA: Springer US, 2006. doi: 10.1007/0-387-34403-9.

[135] A. Ghosh and S. Tsutsui, *Advances in Evolutionary Computing Theory and Applications*. Berlin: Springer Berlin, 2013.

[136] T. M. Pollock, "Alloy design for aircraft engines," *Nat. Mater.*, vol. 15, no. 8, pp. 809–815, 2016, doi: 10.1038/nmat4709.

[137] M. S. El-Eskandarany, *Mechanical alloying for fabrication of advanced engineering materials*. Norwich, N.Y: Noyes Publications, 2001.

[138] F. Barthelat, "Architectured materials in engineering and biology: fabrication, structure, mechanics and performance," *Int. Mater. Rev.*, vol. 60, no. 8, pp. 413–430, Nov. 2015, doi: 10.1179/1743280415Y.0000000008.

[139] G. Srinivasu, Y. Natraj, A. Bhattacharjee, T. K. Nandy, and G. V. S. Nageswara Rao, "Tensile and fracture toughness of high strength β Titanium alloy, Ti–10V–2Fe–3Al, as a function of rolling and solution treatment temperatures," *Mater. Des.*, vol. 47, pp. 323–330, May 2013, doi: 10.1016/j.matdes.2012.11.053.

[140] S. Kovaliova *et al.*, "Mechanosynthesis of composites in chemically non-reacting and exothermically reacting systems for magnetic abrasive media," *J. Mater. Sci.*, vol. 53, no. 19, pp. 13560–13572, Oct. 2018, doi: 10.1007/s10853-018-2463-5.

[141] S. Mozammil, J. Karloopia, R. Verma, and P. K. Jha, "Effect of varying TiB2 reinforcement and its ageing behaviour on tensile and hardness properties of in-situ Al-4.5%Cu-xTiB2 composite," *J. Alloys Compd.*, vol. 793, pp. 454–466, Jul. 2019, doi: 10.1016/j.jallcom.2019.04.137.

[142] M. Kotobi and M. Honarpisheh, "Through-depth residual stress measurement of laser bent steel–titanium bimetal sheets," *J. Strain Anal. Eng. Des.*, vol. 53, no. 3, pp. 130–140, Apr. 2018, doi: 10.1177/0309324717753212.

[143] T. J. Carter, "Common failures in gas turbine blades," *Eng. Fail. Anal.*, vol. 12, no. 2, pp. 237–247, Apr. 2005, doi: 10.1016/j.engfailanal.2004.07.004.

[144] I. Yadroitsev and I. Yadroitsava, "Evaluation of residual stress in stainless steel 316L and Ti6Al4V samples produced by selective laser melting," *Virtual Phys. Prototyp.*, vol. 10, no. 2, pp. 67–76, Apr. 2015, doi: 10.1080/17452759.2015.1026045.

[145] A. Barman and M. Das, “Design and fabrication of a novel polishing tool for finishing freeform surfaces in magnetic field assisted finishing (MFAF) process,” *Precis. Eng.*, vol. 49, pp. 61–68, Jul. 2017, doi: 10.1016/j.precisioneng.2017.01.010.

[146] K. Zhou, Y. Chen, Z. W. Du, and F. L. Niu, “Surface integrity of titanium part by ultrasonic magnetic abrasive finishing,” *Int. J. Adv. Manuf. Technol.*, vol. 80, no. 5–8, pp. 997–1005, Sep. 2015, doi: 10.1007/s00170-015-7028-z.

[147] B.-H. Yan, G.-W. Chang, J.-H. Chang, and R.-T. Hsu, “Improving Electrical Discharge Machined Surfaces Using Magnetic Abrasive Finishing,” *Mach. Sci. Technol.*, vol. 8, no. 1, pp. 103–118, Dec. 2004, doi: 10.1081/MST-120034246.

[148] H. Yamaguchi, A. K. Srivastava, M. A. Tan, R. E. Riveros, and F. Hashimoto, “Magnetic abrasive finishing of cutting tools for machining of titanium alloys,” *CIRP Ann.*, vol. 61, no. 1, pp. 311–314, 2012, doi: 10.1016/j.cirp.2012.03.066.

[149] Y. Zhu, X. Chen, J. Zou, and H. Yang, “A study on the influence of surface topography on the low-speed tribological performance of port plates in axial piston pumps,” *Wear*, vol. 338–339, pp. 406–417, Sep. 2015, doi: 10.1016/j.wear.2015.07.016.

[150] S. Ajith Arul Daniel, R. Pugazhenthi, R. Kumar, and S. Vijayananth, “Multi objective prediction and optimization of control parameters in the milling of aluminium hybrid metal matrix composites using ANN and Taguchi -grey relational analysis,” *Def. Technol.*, vol. 15, no. 4, pp. 545–556, Aug. 2019, doi: 10.1016/j.dt.2019.01.001.

[151] G. Candan and H. R. Yazgan, “Genetic algorithm parameter optimisation using Taguchi method for a flexible manufacturing system scheduling problem,” *Int. J. Prod. Res.*, vol. 53, no. 3, pp. 897–915, Feb. 2015, doi: 10.1080/00207543.2014.939244.

[152] S. Datta, C. Garai, and C. Das, “Efficient Genetic Algorithm On Linear Programming Problem For Fittest Chromosomes,” *J. Glob. Res. Comput. Sci.*, vol. 3, no. 6, p. 8, 2012.

[153] E. Deniz, O. Aydogmus, and Z. Aydogmus, “Implementation of ANN-based Selective Harmonic Elimination PWM using Hybrid Genetic Algorithm-based optimization,” *Measurement*, vol. 85, pp. 32–42, May 2016, doi: 10.1016/j.measurement.2016.02.012.

[154] C. M. Bishop, “Neural Networks for Pattern Recognition,” p. 251.

[155] M. K. Transtrum, B. B. Machta, and J. P. Sethna, “Geometry of nonlinear least squares with applications to sloppy models and optimization,” *Phys. Rev. E*, vol. 83, no. 3, p. 036701, Mar. 2011, doi: 10.1103/PhysRevE.83.036701.

[156] M. A. Gluck and C. E. Myers, *Gateway to memory: an introduction to neural network modeling of the hippocampus and learning*. Cambridge, Mass: MIT Press, 2001.

[157] S. Shanmuganathan and S. Samarasinghe, Eds., *Artificial Neural Network Modelling*, vol. 628. Cham: Springer International Publishing, 2016. doi: 10.1007/978-3-319-28495-8.

[158] C. E. Rasmussen and C. K. I. Williams, *Gaussian processes for machine learning*. Cambridge, Mass: MIT Press, 2006.

[159] R. N. Yadav, V. Yadava, and G. K. Singh, "Multi-objective optimization of process parameters in Electro-Discharge Diamond Face Grinding based on ANN-NSGA-II hybrid technique," *Front. Mech. Eng.*, vol. 8, no. 3, pp. 319–332, Sep. 2013, doi: 10.1007/s11465-013-0269-3.

[160] L. Chen, A. Ahadi, J. Zhou, and J.-E. Ståhl, "Modeling Effect of Surface Roughness on Nanoindentation Tests," *Procedia CIRP*, vol. 8, pp. 334–339, 2013, doi: 10.1016/j.procir.2013.06.112.

[161] K. Deb, "Multi-Objective Optimization using Evolutionary Algorithms," p. 8.

[162] P. Puranto *et al.*, "Indentation modulus and hardness investigation of crystalline silicon surfaces treated by inductively coupled plasma reactive ion etching," *J. Phys. Conf. Ser.*, vol. 1319, p. 012008, Sep. 2019, doi: 10.1088/1742-6596/1319/1/012008.

Research Publications

ARTICLES PUBLISHED IN SCIENTIFIC JOURNALS

1. **Shadab Ahmad,** Ranganath M. Singari & R.S. Mishra (2021) Tri-objective constrained optimization of pulsating DC sourced magnetic abrasive finishing process parameters using artificial neural network and genetic algorithm, **Materials and Manufacturing Processes,** DOI: 10.1080/10426914.2020.1866196 (**Impact Factor- 3.046**)
2. **S. Ahmad,** R. M. Singari & R.S. Mishra (2021) Development of Al2O3-SiO2 based magnetic abrasive by sintering method and its performance on Ti-6Al-4V during magnetic abrasive finishing, Transactions of the IMF, 99:2, 94-101, DOI: 10.1080/00202967.2021.1865644 (**Impact Factor- 1.052**)
3. **S. Ahmad,** R. M. Singari & R.S. Mishra (2020) Modelling and optimisation of magnetic abrasive finishing process based on a non-orthogonal array with ANN-GA approach, **Transactions of the IMF**, 98:4, 186-198, DOI: 10.1080/00202967.2020.1776966 (**Impact Factor- 1.052**)
4. **Shadab Ahmad**, Swati Gangwar, Prabhat Chand Yadav & D. K. Singh (2017) Optimization of process parameters affecting surface roughness in magnetic abrasive finishing process, **Materials and Manufacturing Processes**, 32:15, 1723-1729, DOI: 10.1080/10426914.2017.1279307 (**Impact Factor- 3.046**)
5. **S. Ahmad,** R. M. Singari & R.S. Mishra (2020), Experimental Investigations of Magnetic Abrasive Finishing on Titanium, **International Journal of Advanced Production and Industrial Engineering**, Vol. 4 (2), 2019, pp. 30-34. (Peer Reviewed Journal)., 98:4, 186-198, DOI: 10.35121/ijapie201904236

CONFERENCE PRESENTATIONS

1. **Shadab Ahmad,** Rajneesh Kumar Singh, Ranganath M. Singari, R. S. Mishra, 'On the relationship between surface microhardness and roughness produced by MAF process, 4th International Conference on Processing and Characterization of Materials (CPCM-2020), at NIT Rourkela, 18-20 December 2020. Paper ID: CPCM-0004

2. **Shadab Ahmad,** Ranganath M. Singari, R. S. Mishra, 'Preparation of alumina-silica based bonded magnetic abrasive by sintering method, 4th International Conference on Advanced Production and Industrial Engineering (ICAPIE 2019), at DTU, Delhi, 5-6 October 2019. Paper ID: ICAPIE-2019-PE MT 251
3. Rajneesh Singh, Swati Gangwar, D. K. Singh, **Shadab Ahmad**, 'Multi-Objective optimization of Magnetic Abrasive Finishing by Desirability Function coupled with Genetic Algorithm', 3rd International Conference on Advanced Production and Industrial Engineering, October 5-6, 2018, organized by Center for advanced production and Industrial Engineering Research (CAPIER), Delhi Technological University, New Delhi, India.
4. Md Jamil Akhtar, Navendu Sharma, Ramu Yadav, **Shadab Ahmad,** Ranganath M. Singari, R. S. Mishra, 'Experimental Investigations and parametric studies on CNC milling operation, 2nd International Conference on Advanced Production and Industrial Engineering (ICAPIE 2018), at DTU, Delhi, 5-6 October 2018. Paper ID: ICAPIE-2018-PE MT 251

Resume

SHADAB AHMAD

Research fellow in Mechanical Engineering,
Delhi Technological University, Delhi 110042
Email: shadab.gkp09@gmail.com
ORCiD: 0000-0001-7468-8686
https://www.linkedin.com/in/shadab-ahmad-501896b4/

RESEARCH INTERESTS

Advanced manufacturing processes, Magnetic assisted finishing, Composite material, Electro-Magneto-Thermo-Mechanics, Finite Element Analysis, Optimization, Soft computing.

EDUCATION

Doctor of Philosophy in Mechanical Engineering — **2016 onwards**
Delhi Technological University, Delhi, India.
Thesis: Experimental investigations on Magnetic Abrasive Finishing process.

Master of Technology in Mechanical Engineering — **2013 - 2015**
Madan Mohan Malviya University of Technology, Gorakhpur, India.
Dissertation: Analysis and optimization of parameters affecting surface roughness in magnetic abrasive finishing process

Bachelor of Technology in Mechanical Engineering — **2009 - 2013**
Uttar Pradesh Technical University, Lucknow, India.
Project: Portable bridge to support the Indian Army for rough terrains movements (Design and fabrication)

SOFTWARE PROFICIENCY

1) **Programming languages:** MATLAB, Python
2) **CAD:** AutoCAD, CATIA, Unigraphics, SolidWorks, FreeCAD
3) **CAE:** HyperMesh, ANSYS

HONOURS AND AWARDS

- 2018 - 2021: Senior research fellowship for PhD from CSIR-HRDG India.
- 2016 - 2018: Junior research fellowship for PhD from CSIR-HRDG India.
- 2013 - 2015: Scholarship for master's degree from Ministry of Human Resource Development, Government of India.